A Contribution to Computational Contact Procedures in Flexible Multibody Systems

Von der Fakultät Maschinenbau der Universität Stuttgart
zur Erlangung der Würde eines Doktor-Ingenieurs (Dr.-Ing.)
genehmigte Abhandlung

by

Saeed Ebrahimi

geboren in Schiraz (Iran)

Hauptberichter:	Prof. Dr.–Ing. Peter Eberhard
Mitberichter:	Prof. Dr.–Ing. Wolfgang Seemann

Tag der Einreichung:	11. November 2006
Tag der mündlichen Prüfung:	6. Juli 2007

Institut für Technische und Numerische Mechanik
Universität Stuttgart

2007

A Contribution to Computational Contact Procedures in Flexible Multibody Systems

With the Department of Mechanical Engineering
at the University of Stuttgart for the achievement
of a Doctor's Degree of Engineering (Dr.-Ing.)
submitted treatise

by

Saeed Ebrahimi

born in Shiraz (Iran)

First reviewer:	Prof. Dr.–Ing. Peter Eberhard
Second reviewer:	Prof. Dr.–Ing. Wolfgang Seemann

Date of Submission:	11. November 2006
Date of Oral Exam:	6. July 2007

Institute of Engineering and Computational Mechanics
University of Stuttgart

2007

Preface

The presented work in hand is the result of my study and research during three years at the Institute of Engineering and Computational Mechanics (Institut für Technische und Numerische Mechanik), formerly named as the Institute B of Mechanics, University of Stuttgart in the frame of a grant received from the government of the Islamic Republic of Iran for pursuing high educational studies in abroad. In this period, I have used the support of many people who have shared their experiences with me and here, I would like to thank all of them.

At first, I would like to express my deepest appreciation to my suervisor Prof. Dr.-Ing. Peter Eberhard for all his supports and encouragements during my study. He supported me kindly and provided me many disscussions in spite of his engagement with different projects. In addition, my special thanks goes also to Prof. Dr.-Ing. Wolfgang Seemann from University of Karlsruhe for the review of this thesis and Prof. Dr.-Ing. Prof.E.h. Dr.h.c. Werner Schiehlen for his useful comments.

Furthermore, I really appreciate my friend Dr.-Ing. Gerhard Hippmann, Intec GmbH for providing me the source code of the Polygonal Contact Model and giving me the opportunity to have many disscussions. I want also to acknowledge the support and encouragement of Dr.-Ing. Lutz Mauer, Intec GmbH who provided me the source code of the rigid gear wheel module of SIMPACK and who gave in many discussions indispensable advice and assistance. My investigations related to the extension of contact modeling to flexible multibody systems and contact of gear wheels would not have been possible without their valuable suggestions and kindly supports. Also, I want to acknowledge the support of my colleague Pascal Ziegler. He provided me the FEM model, gave very important comments and shared with me his deep knowledge about such systems.

Finally, I would like to thank my colleagues at the Institute of Engineering and Computational Mechanics, in particular Michael Lehner for his support about flexible multibody systems, Robert Seifried for his comments about contact and impact phenomena, Basileios Mavroudakis and Alexandra Ast for their support about SIMPACK, Beate Muth and Florian Fleissner for their hints about programming, my roomates Marko Ackermann and Hashem Alkhaldi for making a nice environment for research and study and in general the other members of the institute. At this point, I would like to thank my parents and my family in Iran for their encouragement and support during my life.

Stuttgart, July 2007 Saeed Ebrahimi

To my parents,
who always have their best wishes for me

Contents

Zusammenfassung

Mit der zunehmenden Bedeutung von Mehrkörpersimulationen in der Industrie und Ingenieurwissenschaft steigt auch die Zahl der Anwendungen, in denen Kontaktprobleme zu bewältigen sind, was die Bedeutsamkeit dieses Teilbereichs der Mehrkörperdynamik unterstreicht. Aus diesem Grund konzentrieren sich vermehrt Forschungstätigkeiten auf dieses Thema und viele theoretische und mathematische Methoden werden dazu entwickelt. Die Modellierung des Kontaktvorgangs bei der dynamischen Simulation von Mehrkörpersystemen ist eine schwierige Aufgabe, der dieses Forschungsthema gewidmet ist. Vor allem mit der Berücksichtigung elastischer Körper nimmt diese Schwierigkeit zu, da es hierbei zu einem erheblich erhöhten Rechenaufwand kommt. Aufgrund der Flexibilität der Körper wird die Kontakterkennung erschwert die zu jedem Zeitschritt der Simulation durchgeführt werden muss.

Kontaktprobleme zwischen elastischen Körpern spielen in der Technik eine wichtige Rolle, weshalb dieses Thema bereits mit erheblichem Aufwand untersucht wurde. Obgleich in der Mehrkörperdynamik viele Kontaktprobleme als Starrkörperkontakt betrachtet werden können, gibt es dennoch eine beträchtliche Zahl an Kontaktproblemen, bei denen die Elastizität der kontaktierenden Körper nicht vernachlässigt werden kann und daher eine Modellierung als Starrkörper nicht in Frage kommt. Dies macht eine elastische Kontaktmodellierung notwendig.

In Kapitel 1 wird die Einleitung zu Kontaktproblemen in Mehrkörpersystemen vorgestellt. Kapitel 2 enthält dann einige grundlegende Konzepte der flexiblen Mehrkörperdynamik, unter anderem zur Herleitung der Bewegungsgleichungen und zu Lösungsalgorithmen. Als Grundlage werden die Kinematik und die Kinetik starrer Körper zusammengefasst, die als Basis weiterer Betrachtungen der flexiblen Mehrkörpersysteme dienen. Im Folgenden werden verschiedene Modellierungsansätze im Kontext der flexiblen Mehrkörpersysteme erklärt, die sich in Basismodelle, überlagerte Bewegungen (moving frame of reference) und absolute Knotenkoordinaten Formulierungen (absolute nodal coordinates) einteilen lassen. Zusätzlich werden Schwierigkeiten bei der Modellierung und getroffene Annahmen kurz erklärt. Die zur Herleitung der Bewegungsgleichung im Rahmen dieser Arbeit verwendete Methode der überlagerten Bewegungen wird in Abschnitt 2.3 umfangreich beschrieben. Dieser Ansatz ist die am weitesten verbreitete Methode, bei der zwei verschiedene Ko-

ordinatenbeschreibungen zur Darstellung von Körperreferenzbewegungen und elastischen Deformationen verwendet werden. Zur weiteren Veranschaulichung der Konzepte, die diesem Ansatz zugrundeliegen, werden die Eigenschaften, Vorteile und Beschränkungen dieser Methode, sowie die Darstellung der elastischen Deformationen erklärt. Darüber hinaus wird auf die Kinematik und Kinetik flexibler Körper eingegangen. Dabei werden alle Komponenten der Massenmatrix und der verallgemeinerten Kräfte bestimmt und schliesslich werden mit Hilfe des Prinzips der virtuellen Arbeit die Bewegungsgleichungen in Form von differential-algebraischen Gleichungen aufgestellt. Zusätzlich werden andere Strategien vorgestellt, um die Bewegungsgleichungen für reale Anwendungen in symbolischer sowie numerischer Form aufzustellen. Das Kapitel schliesst mit der Beschreibung einiger numerischer Integratoren, welche zur Lösung von Bewegungsgleichungen verwendet werden können.

In Kapitel 3 werden einige bekannte Formulierungen aus der Mehrkörperdynamik kurz beschrieben, welche benötigt werden, um die Kontaktbedingungen in die Bewegungsgleichungen des starren bzw. elastischen Systems einzubinden. Aus einer Vielzahl von möglichen, bereits existierenden Methoden werden hier die Penalty Methode, die Methode der Lagrange-Multiplikatoren, die Linearen Komplementaritätsprobleme (LCPs) und die sogenannte Proximal Point Formulierung herausgegriffen und erläutert.

Zur Modellierung von Kontakten gibt es zahlreiche Methoden, die häufig von Forschern und Ingenieuren angewandt werden. Ein häufig gebräuchlicher Ansatz ist, den kontinuierlichen Kontakt bzw. Stoß in komplementärer Form zu formulieren, was zu einem Komplementaritätsproblem führt. Diese Ansätze liefern exakte Lösungen sowohl für andauernde Kontakte (auf Kraft-Beschleunigungsebene) als auch für Stöße (auf Impuls-Geschwindigkeitsebene). Indem solche Methoden verwendet werden, kann auch Reibung angemessen betrachtet werden.

Für Anwendungsfälle, in denen die Flexibilität der kontaktierenden Körper nicht vernachlässigt werden kann, ist es nicht mehr möglich diese Starrkörperkontaktmethoden zu verwenden und es muss die Verformbarkeit der kontaktierenden Körper berücksichtigt werden. Aus diesem Grund wird in Kapitel 4 versucht, diese Methode so zu formulieren, dass Verformungen der sich berührenden Körper berücksichtigt werden können. Bei dieser Formulierung werden verformbare Körper auf der Basis bewegter Bezugssysteme mit Modalkoordinaten modelliert. Die linearen Komplementaritätsgleichungen können mit einem LCP-Löser wie Lemke's Algorithmus [25] gelöst werden um die Kontaktkräfte zu berechnen.

In Kapitel 5 wird zuerst ein Ansatz für reibungsfreie Stöße verformbarer, ebener Körper präsentiert sowie die Formulierung eines LCPs auf Lageebene ohne Verwendung einer Stoßzahl, welche als Energieverlustmechanismus dient. Dieser Ansatz basiert auf der Einhaltung der Signorini-Bedingungen für Stoßprobleme von Kontinua. Dabei wird zuerst der Körper mit FEM diskretisiert und dann mit einer finiten Anzahl von Eigenmoden

reduziert. Die Bewegungsgleichungen des verformbaren Körpers werden mit dem Ansatz des bewegten Bezugssystems erstellt. Dann werden die Normalabstände zwischen den stoßenden Körpern in Abhängigkeit der verallgemeinerten Koordinaten bestimmt. Im nächsten Schritt werden unter Verwendung verschiedener Integrationsmethoden, wie die explizite Euler und die explizite und implizite Runge-Kutta Methode, die verallgemeinerten Beschleunigungen aus der Integration der Bewegungsgleichungen bestimmt, um einen Zusammenhang mit den verallgemeinerten Koordinaten zu erstellen. Schliesslich werden die verallgemeinerten Koordinaten in die Beziehung der Normalabstände eingesetzt und das Stoßproblem wird als LCP formuliert. Dies führt zur Lösung des Stoßproblems unter Berücksichtigung von Stoßkräften und Normalabständen. Darüberhinaus wird der Ansatz auf Reibstöße erweitert. Die Idee hinter diesem Ansatz folgt aus der Tatsache, dass im Fall verformbarer Körper das Stoßverhalten in tangentialer Richtung ähnlich zu einem kontinuierlichen Kontakt ist. Jedoch ist es offensichtlich, dass diese Annahme nur gültig ist für die Stoßuntersuchung verformbarer Körper. Im Falle von Stößen starrer Körper müssen diese zwei Vorgänge unterschieden werden. Zusätzlich werden einige Formulierungen, basierend auf LCPs auf Geschwindigkeitsebene vorgestellt und die Ergebnisse mit denen auf Lageebene verglichen.

Für den allgemeinen Fall der Kontaktmodellierung räumlicher Systeme ist das *surface compliance model* eine sehr geeignete Methode. Das Polygonale-Kontakt-Modell (PCM) [67] gehört zu dieser Sorte von Kontaktmodellierungsmethoden und ist ein Mehrkörperdynamikalgorithmus zur Kontaktmodellierung von Starrkörpern, die durch polygonale Oberflächen beschrieben werden. Aus der Sicht der Mehrkörperdynamik verhält sich PCM wie ein Kraftelement, welches als benutzerdefinierte Routine in den kommerziellen MKS Code SIMPACK [129] eingebaut werden kann.

Für die Kontaktmodellierung zwischen flexiblen räumlichen Systemen bietet es sich an PCM zu erweitern. Die Ausgangslage für die Untersuchungen in Kapitel 6 bildet der ursprüngliche Code [67], welcher auf starre Körper beschränkt ist. Dieser wurde sukzessive erweitert und angepasst, so dass auch Kontaktvorgänge bei räumlichen flexiblen Systemen gerechnet werden können.

Kapitel 7 wird der Anwendung der Kontaktmodellierung der Zahnrädergetriebe in den Mehrkörpersystemen gewidmet. In vielen Anwendungen des Maschinenbaus werden Zahnräder dazu benutzt, um Leistung zwischen sich drehenden Wellen zu übertragen. Daher gewinnt die Fähigkeit diese in Mehrkörpersystemen zu integrieren und deren dynamisches Verhalten zu simulieren immer mehr an Bedeutung.

Das Mehrkörpersimulationsprogramm SIMPACK mit seinem Modul SIMPACK/Engine bietet dazu ein Kraftelement, um den Kontakt zwischen starren Zahnrädern zu simulieren. Aus der Geometrie und dem kinematischen Zustand der kämmenden Zahnräder ermittelt das Kraftelement die auf die Räder wirkenden Kräfte und Momente.

Da Zahnräder in Wirklichkeit nicht starres, sondern besonders bei Kontaktvorgängen elastisches Verhalten aufweisen, muss bei der Modellierung des Zahnradkontakts diese Elastizität mit berücksichtigt werden. Die FEM ist sicherlich einer der leistungsfähigsten Ansätze zur Modellierung von Kontaktvorgängen. Allerdings führt der speziell bei der Simulation des Zahnradkontakts sehr grosse Rechenaufwand zu Schwierigkeiten in der praktischen Anwendung der FEM. Aus diesem Grund werden im Rahmen des Kapitels 7 elastische Elemente zwischen den Zähnen und dem Körper der Zahnräder verwendet. Dieser Ansatz scheint vor allem für Mehrkörpersysteme geeignet, da er einen Kompromiss zwischen dem starren und dem elastischen Modell darstellt. Die Zähne und der Körper der Zahnräder sind zwar immer noch starr, sind jedoch durch elastische Elemente verbunden. Hierzu wird ein präziser Algorithmus verwendet, der sowohl gleichzeitigen Kontakt mehrerer Zahnpaare als auch den Einfluss von Flankenspiel, sowie links- und rechtsseitigen Kontakt berechnet.

In Kapitel 8 wird die Arbeit zusammengefasst und einen Ausblick zu weiteren interessanten Themen gegeben.

Chapter 1

Introduction

The field of *Multibody System Dynamics* (MBS) has its root in classical and analytical methods of dynamics to meet the growing demands in modeling and simulation of complex and advanced mechanical systems in industry and engineering.

The definition of multibody systems contains basically mechanical systems consisting of rigid and/or flexible bodies interconnected with mechanical joints or force elements. Examples of such systems can be found in automotive, railway, aerospace, robotics and other mechanical industries. In general, the bodies in multibody systems may experience large rigid body motions and small elastic deformations. There exist several classifications of multibody systems based on different viewpoints. One may distinguish between unconstrained and constrained systems. In an unconstrained system, the bodies are free to move without constraint or prescribed motion. In contrast, in a constrained system the motion of bodies is restricted by constraints. The second classification covers the definitions of open loop and closed loop systems. In open loop systems, starting from the base of the system the arrangement of the bodies does not complete a closed loop. On the other hand, a closed loop system consists of one or more closed loops built from the connection of bodies. A four bar linkage can be a simple example of this type. In a third classification, a multibody system may consist of only rigid bodies or rigid and flexible bodies.

Computational mechanics is concerned with computer-aided techniques developed for generating mathematical models associated with mechanical systems. Simulation of multibody systems is performed by describing the multibody system with an equivalent mathematical model, which captures, e.g., properties of different parts of the system including bodies, mechanical joints or elastic elements. Realistic understanding of the system based on the kinematics and kinetics of the system is an inevitable task. The mathematical model is finally represented by either a set of ordinary differential equations (ODE) or a set of differential algebraic equations (DAE).

It may be possible to represent a physical model with quite different mathematical models depending on the utilized modeling strategy. It is the experience of the analyst to choose the most suitable strategy for constructing the mathematical model. However, in some applications it is not a trivial task to decide which model will provide best results with least effort. Some of such difficulties will be demonstrated in Chapter 2.

Modeling and simulation of multibody systems are suffering from difficulties arising in three main parts. As the first step, identification of the system parameters makes some difficulties. The second part contains difficulties arising in the mechanical and mathematical modeling. The third group is concerned with implementation of numerical algorithms.

Multibody dynamics was first developed for systems with rigid bodies having constant geometries. The state-of-the-art and perspectives of rigid multibody system dynamics together with historical remarks on classical mechanics and its departure to multibody dynamics concept have been well documented in [116]. The first international symposium on this topic was very successful [90]. The first text book in this context was written in [150], see [116]. Later on, the computer-aided formulation of rigid multibody systems was documented, e.g., in [98] and [61].

Although the concept of rigid multibody dynamics is applicable to a large variety of systems, the subject of flexible multibody dynamics became increasingly important. Among all, light weight structures, robot manipulators and precision mechanical systems are common examples of such systems. Shabana formulated the general form of equations of motion of flexible multibody systems in [124]. Later he provided a review of the past and recent developments in the dynamics of flexible multibody systems [121]. In addition, some basic approaches used in the kinematic and dynamic analysis of flexible mechanical systems were presented. The work on this subject was further continued by other researchers, e.g. [4, 17, 52, 72], with different formulations focusing on different features of multibody dynamics.

In addition to constraints such as various types of mechanical joints and elements with imposing prescribed motions, the motion of bodies in multibody systems can be affected by contact constraints. This type of constraints needs special attention since the position of contact points of contacting bodies is not known in advance and additionally the amount of contact forces in both normal and tangential direction has to be found based on some contact force laws. These two points in particular and many other difficulties arising in the formulation and solution of contact problems in general have made the handling of contact a most challenging problem in modeling and simulation of multibody systems. In the following sections, some basics of contact in multibody systems and the corresponding computational procedures for its handling are given. Finally, this introduction chapter ends with an outline of the thesis.

1.1 Contact Problems in Multibody Systems

Classical contact is an old subject in engineering which begins from 1882 with the work of Hertz [65]. Although his theory was based on the frictionless contact for linear elastic bodies, it caused a rapid development in this field and led to the establishment of many further researches. Since the contact behavior is highly dependent on the material properties of two contacting surfaces, the nature of the contact problem and the magnitude of resultant contact forces, the investigation of contact behavior is one of the most challenging topics in engineering.

Contact events can frequently happen in multibody systems and in many cases the function of mechanical systems is based on them, see Figure 1.1. In the simulation of multibody systems in industry and engineering, there are many applications which deal with contact problems. Therefore, the development of numerical procedures for solving such problems accurately and efficiently has become the subject of many researches.

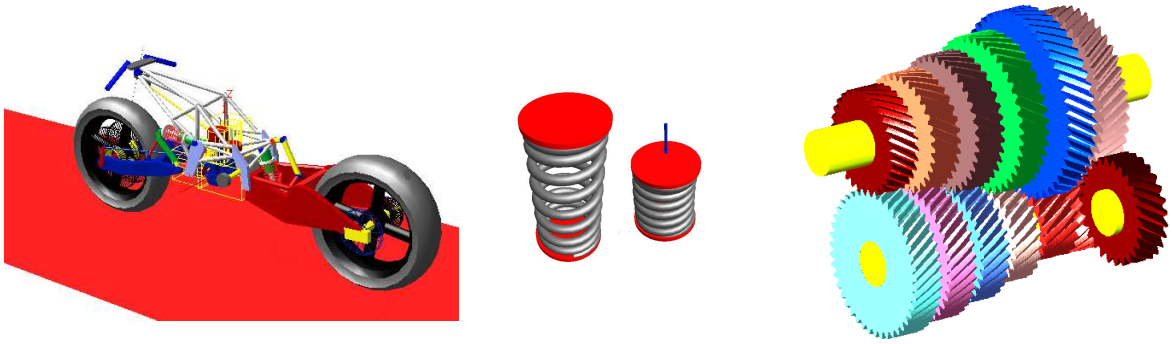

contact between tire and road, from [92] | contact between coils of a compressed spring | contact in geared systems

Figure 1.1: Contact in multibody systems

Contact between tire and road in motorbikes and automobiles, wheel and rail in railway vehicles, contact in robotics and grasping machines, power transmission systems like geared systems, cam and follower, chain and gear, contact in granular media etc. are common examples. In granular media, the motion of many bodies is investigated but usually no consideration of flexibility is taken into account see e.g. [95]. In addition, computation times are very high and typically no joints can be considered between colliding bodies. The contact formulation is based on simple models in order to keep the computational times within a feasible range.

As another aspect of contact application, gear wheels are used to transmit power between rotating shafts and, therefore, the ability to incorporate them into multibody systems has become an essential topic. Contact modeling of gear wheels has some special difficulties which arise from, e.g., the nonlinear behavior of the tooth stiffness, backlash, gear geometric parameters, see e.g. [75, 76].

1.2 Computational Procedures

The dynamic characteristics of multibody systems are usually represented by formulating the governing system of equations of motion and calculating the corresponding kinematic and kinetic quantities. For this purpose, all necessary factors affecting the dynamic behavior of multibody systems have to be considered correctly.

Before the appearance of digital computers, the solutions in contact dynamics were limited to analytical solutions which utilized linear elasticity. Such analytical solutions were hardly applicable to contact problems of bodies with complicated surfaces. After the work by Hertz [65] about frictionless contact of linear elastic bodies with simple geometries, Signorini [125] proposed the solution to the general problem of linear elastic body in the case of frictionless contact with a rigid foundation. Fichera [43] contributed the Signorini problem of the boundary value problems in the case of unilateral constraints. The concept of contact mechanics was extended further by Galin [49] for the case of three dimensional contact without friction. Gladwell [54], Johnson [74], Kalker [77] and others dealt with the theoretical and engineering aspects of contact.

Later, special attention was paid to the numerical investigation of contact problems. Nowadays, numerical techniques are frequently used to analyze contact problems with all complications involved. However, there are still challenging parts in design and implementation of computational methods which are efficient and reliable.

The numerical approaches which are being used widely in contact analysis can be divided into several groups: first, Finite Element Methods (FEM), see e.g. [29, 153, 154, 155] and second, approaches based on multibody dynamics (MBS) e.g. [29, 33, 55, 67, 106]. Additionally, approaches based on boundary elements, finite differences and finite volume schemes in this context may be mentioned. Finite element methods [136, 24] were introduced to deal with problems of structural analysis. The FEM is without doubt the most powerful numerical method in the field of contact. Although it is well suited for particularly high accuracy requirements, its very high computational effort causes practical difficulties such as very long simulation times. In such situations, MBS can often efficiently model the contact with acceptable accuracy and considerably less computational effort compared to the FEM. In contrast to the FEM, approaches based on multibody dynamics can deal with the effect of contact forces on the overall motion of the system for long simulation times.

The subject of contact dynamics and its applications in multibody systems had not been developed until the last couple of decades. In general, contact modeling in multibody systems consists of some major steps: a) detecting the collision between moving bodies, b) constructing contact regions, and c) computing contact forces, see e.g. [33, 66, 67]. The resultant contact forces have to be determined based on the contact regions, geometric and material properties, and relative velocity of contacting bodies. From the modeling

methodology point of view, several different methods have been introduced. As a rough classification, they may be divided into contact force based methods and methods based on geometrical constraints. Although there are extensive researches addressed in the literature about contact problems in rigid multibody systems, much fewer of publications were specifically developed for flexible multibody systems. In the majority of the approaches used for contact of flexible bodies, the same procedure of contact modeling as for rigid bodies with some small modifications has been used. Contact modeling is highly dependent on the properties and geometries of contacting bodies. One of these considerations is about the rigidity or elasticity of the contacting bodies. In the nature no body is absolutely rigid but in many applications they might be considered as rigid to simplify the problem and reduce the cost of numerical computations.

As an effective method in contact analysis between complex objects with multiple contacts, the surface compliance method uses a penalty formulation, see e.g. [12, 26, 33, 57, 81, 85, 130]. It is assumed that each contact region is covered with some spring-damper elements scattered over the body surfaces. The normal force including the elastic and damping shares prevents penetration, i.e., no explicit kinematic constraint is considered. The magnitudes of stiffness and deflection of the spring-damper elements are computed based on the penetration, material properties and surface geometries of the colliding bodies, see e.g. [81, 85]. In [81] the required parameters for representing contact force laws are obtained based on the energy balance during contact. This formulation uses a force-displacement law that involves determination of material stiffness and damping coefficients. In [85] two continuous contact force models are presented for which unknown parameters are evaluated analytically. In the first model, internal damping of bodies represents the energy dissipation at low impact velocities. However, in the second model local plasticity of the surfaces in contact becomes the dominant source of energy dissipation. Dias and Pereira [26] described the contact law using a continuous force model based on the Hertz contact law with hysteresis damping. The effect and importance of structural damping schemes in flexible bodies were also considered. A contact model with hysteresis damping is also presented in [84]. Hunt and Grossley [70] obtained also a model for computing the stiffness coefficient from the energy balance relations. In their approach, the damping force is a linear function of the elastic penetration which is estimated from the energy dissipated during impact.

The effect of friction in this approach is often taken into consideration by using a regularized Coulomb friction model. An overview of different models of friction together with fundamentals can be found, e.g., in [40, 101].

In spite of the fact that the approaches based on the penalty formulation are usually simple to be implemented, they have some restrictions and are not always applicable due to the problems arising from selection of high values of penalty factor for imposing non-penetration conditions which results in stiff systems with ill-conditioned numerical

problems. There are some proposed approaches from which a proper penalty factor for normal contact may be obtained, see e.g. [74, 100].

For treatment of jump discontinuities in the system velocities and contact forces, impulse-momentum approaches have been used. They introduce a coefficient of restitution as a measure of energy loss during impact of flexible bodies. In general, when dealing with contact of flexible bodies, no coefficient of restitution should be used since the energy dissipation can be treated by material damping and the effects of deformations. Simple energy dissipation interpretation of this coefficient used for rigid bodies impact analysis may no longer be valid for flexible bodies. Based on the momentum balance relations before and after impact and using the coefficient of restitution, the velocity jumps are treated from either the Newton's or the Poisson's laws [106]. In the Newton's law, coefficient of restitution relates the velocities immediately before and after impact while in the Poisson's law a relation between impulse forces during compression and expansion phases of impact is used. There exist some numerical and experimental researches for evaluation of coefficient of restitution. Among all, in [119] the loss of kinetic energy due to initiation of waves and plastic deformation of colliding bodies has been investigated.

This approach was first applied to constrained rigid mechanical systems [148] and was further extended to include flexible bodies [79, 80]. In this context, Pereira and Nikravesh [105] present a formulation for impact analysis of mechanical systems with friction using joint coordinates. The impulse-momentum approaches are mainly divided into the global and the local methods. In the global version, the impulse-momentum equations are written for generalized coordinates of impacting bodies. Among all, the works presented in [8, 39, 79, 80, 112, 161] may be referred which belong to this category. These approaches can deliver only an approximation of impulses and may be suitable for impact problems of stiff flexible bodies. They cannot achieve acceptable results in situations where the effect of local deformations becomes important. In the local impulse-momentum approach the method is applied for local nodes encountered in impact [144, 145]. So, the impact problem is more considered as a local phenomenon in which only the motion of the impacting nodes is directly affected by impact whereas the motion of the rest of the impacting bodies will further be affected through internal forces and wave propagation. The conservation of momentum and restitution equations were used as local velocity constraints to determine the post-impact velocities of the impacting nodes in impact of flexible bodies. Two coefficients of restitution have been used, one for normal direction and the other for considering friction in the tangential direction.

The impulse momentum approaches may not be used to model accurately the contact between objects with complicated geometries. Also, in the case of multiple contacts and constrained multibody systems using them is not recommended. In addition, the treatment of impact has some differences when dealing with finite and infinite dimensional flexible bodies [39].

In some other approaches, the attention is put on using a so-called constraint addition-deletion technique, see e.g. [60, 156, 157, 158]. This technique is based on the Lagrange multiplier method. The augmented Lagrange multiplier technique was further developed in which a combination of both the penalty and the Lagrange multipliers method is used to gain their advantages, see e.g. [10, 22].

Linear Complementarity Problems (LCPs) are the result of other methods which mathematically give the exact solution to the contact problem. These formulations are basically arising from the complementarity relations and unilateral contact constraints. In addition to the exact solution of contact problems, other advantages of these formulations are that they do not result in stiff equations of motion and they show a lower effort for time integration compared to applying a brute force Lagrange multipliers method. These methods are often time consuming compared to the penalty approaches and their relation to microscopic deformation is unclear. Other disadvantages that can be mentioned are the neglection of the contact patch deflection, extreme simplification of complex physical phenomena and open problems in frictional impact theory. There are extensive researches addressed in the literature about investigation of frictionless and frictional contact of rigid bodies initiated from the idea of complementarity [107]. These approaches have been well established and frequently used in the context of dealing with rigid bodies. As a result, some algorithms were developed based on unilateral contact constraints [55, 82, 83, 89, 103, 106]. Initially, only planar contact kinematics was considered which led to an LCP and then, this algorithm was extended for the case of spatial contact for which a Nonlinear Complementarity Problem (NCP) has to be formulated, see [134, 152]. However, for the case of dealing with flexible bodies there is a very limited number of publications devoted to this subject which attempt to get rid of difficulties in such cases. In such treatments, the formulations of rigid contact model are extended with some modifications needed for dealing with flexible bodies, see e.g. [31, 33, 34, 36, 37].

There exist approaches which are based on the same mathematical concept as those yielding LCPs but are formulated differently. In these approaches, complementarity relations denoting the contact/impact laws are transformed to variational inequalities and finally are solved in an iterative process as a proximal point formulation, see e.g. [86, 151].

In the presence of impulsive forces as well as the presence of friction, the problem of discontinuities may frequently occur. As a common way, the time-stepping methods have been developed to overcome these difficulties, see e.g. [5, 6, 130, 133]. In this framework, the integration process is combined with the equations of motion in order to reach a discretized formulation of equations of motion. Various time-stepping methods differ in the integration methods used to discretize the equations of motion. However, following different discretization schemes, time-stepping methods with different properties can be achieved. Unfortunately, most of the developed time-stepping approaches use the Euler integration method and normally require choosing a very small time step size. Addi-

tionally, they are not suitable for handling impact problems of stiff multibody systems including flexible bodies. However, there are number of researches which have focused on their implementation for stiff multibody systems, see e.g. [6, 48].

1.3 Outline of the Thesis

This thesis aims first to give a short overview of some already developed methods which are widely used in the context of contact modeling of planar and spatial flexible multibody systems. Further, some formulations of continual contact and impact obtained from different strategies will be given.

Chapter 2 provides some basic concepts of flexible multibody dynamics including solution algorithms. First kinematics and kinetics of rigid bodies in multibody systems are explained. Then, in flexible multibody dynamics different modeling strategies which are grouped as basic, superimposed motion and absolute nodal coordinates approaches together with difficulties and assumptions will be briefly explained. As the main procedure in this work, the floating frame of reference serves to generate equations of motion. This approach introduces two kinds of variables for rigid body reference motion and elastic deformations. In order to demonstrate the basic concepts of this approach, some notes will be given about properties, advantages and restrictions together with some remarks for representing elastic deformations. Furthermore, a detailed explanation of kinematics and kinetics of flexible bodies is provided. In this step, all components of the inertia mass matrix and generalized forces are derived and finally, based on the virtual work principle in dynamics, equations of motion in the form of differential algebraic equations are written. This chapter ends with introducing some numerical integration approaches for solving systems of equations.

In Chapter 3 some frequently-used formulations to incorporate contact constraints into governing equations of rigid and flexible systems are introduced briefly. Herein the penalty technique, the Lagrange multipliers method, procedures yielding LCPs and finally proximal point formulations are explained.

Chapter 4 is devoted to continual contact of planar flexible bodies in multibody systems. Kinematic relations are formulated in such a way that they consider the effect of deformations. They are taken into account starting from relative velocity of contact points in the normal direction of contact and then, the relative acceleration of contact points is introduced. The complementarity relations are formulated following the same procedure as for rigid bodies contact. The main change of this algorithm compared to the rigid body case is in the formulation of kinematics of contact.

In Chapter 5, a linear complementarity problem on position level for frictional impact of planar flexible bodies is presented without introducing any coefficient of restitution

as a measure of energy loss. This approach is based on Signorini's conditions for impact problems of continua. Normal gaps between the two impacting bodies are written in terms of the generalized coordinates. In the next step, by following different integration methods, such as the explicit Euler and the explicit and implicit Runge-Kutta approaches, the generalized acceleration vector will be integrated. By substituting the generalized coordinates in the relationship of normal gaps, the impact problem is formulated as a linear complementarity problem. Consideration of friction is done in the same way as was followed for the continual contact.

Contact of spatial flexible multibody systems is considered in Chapter 6. The approach devoted to this subject uses a polygonal contact model contributed by Hippmann [66, 67, 68]. In the course of this work, this algorithm for rigid bodies was modified and extended, so that flexible bodies may be considered, too.

In Chapter 7 as an application of contact modeling in industry, the subject of gear wheel systems is chosen. This chapter starts with a brief explanation of an approach for contact modeling of meshing rigid gear wheels which is implemented as a force element in the commercial MBS code SIMPACK. Then, an extension of this algorithm by introducing some elastic elements between the teeth and the gear body will be described to consider partially elasticities. This approach is a compromise between a totally rigid model and a fully elastic model allowing the simulation of large motions with many revolutions. The teeth and the body of each gear wheel are still modelled as being rigid but they are connected to each other by elastic elements. In doing so, an efficient algorithm is described and implemented in order to find the effect of multi-tooth contact as well as backlash and left and right hand side contact of the meshing teeth. Some examples compare the simulation results of rigid, partially elastic and fully elastic models.

Finally, this thesis ends in Chapter 8 with a summary of the presented work and an outlook to further interesting topics.

Chapter 2

Flexible Multibody Dynamics

Flexible Multibody Dynamics (EMBS) is the subject of intensive research. The objective is to introduce flexible objects in rigid body simulations.

Sometimes deformations have a significant effect on the system behavior and, therefore, flexibility of objects cannot be ignored. Examples are light weight structures, robot manipulators, precision mechanical systems, ground and space vehicles, biomechanical systems, mechanisms etc. . Here, some of the most widely-used methods for analysis of EMBS are reviewed briefly. Before that, some basics of rigid multibody dynamics are presented.

2.1 Basics of Rigid Multibody Dynamics

In this section some basic concepts of rigid multibody dynamics are described. Equations of motion of flexible bodies are generated in this work using an approach which is based on the extension of MBS to EMBS in a natural way. Therefore, in order to provide a better understanding of the approach, the general procedure to reach the equations of motion of rigid multibody systems is explained shortly.

Multibody dynamics has been the main subject of many researches, see the references cited in [116, 146]. In order to facilitate the process of dynamic modeling and analysis of multibody systems, many software tools for both research and commercial tasks have been developed. A survey of some important ones can be found e.g. in [115, 142].

2.1.1 Kinematics of Rigid Bodies

The rigid body assumption in multibody dynamics is based on a simple model of continuum mechanics. It states that a rigid body is a collection of material points whose relative

positions remain constant. A wide range of real applications can be modeled efficiently with this assumption.

The position and orientation of each rigid body is completely defined through a body fixed coordinate system with respect to the inertial frame. Figure 2.1 shows a rigid body, on which a reference coordinate system is rigidly attached at point O^R. The position of any arbitrary point p^i on the body is described by a vector $\mathbf{u}^i$ whose magnitude remains constant during the motion of the body. The global position and orientation of the body reference coordinate system given in the inertial coordinate system are defined here with three components of the vector $\mathbf{R}^i$ and four Euler parameters $\boldsymbol{\theta}^i = (\theta_0, \theta_1, \theta_2, \theta_3)^i$, respectively.

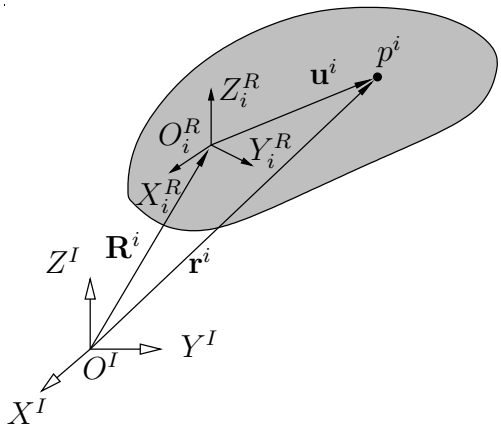

Figure 2.1: Rigid body kinematics

The position of the arbitrary point p^i given in the inertial coordinate system reads as

$$\mathbf{r}^i = \mathbf{R}^i + \mathbf{u}^i = \mathbf{R}^i + \mathbf{A}^i \cdot \bar{\mathbf{u}}^i \ , \tag{2.1}$$

where $\bar{\mathbf{u}}^i$ is the position of point p^i given in coordinates of the body reference coordinate system and $\mathbf{A}^i$ is the transformation matrix between the body reference and the inertial coordinate systems

$$\mathbf{A}^i = \begin{bmatrix} 2((\theta_0)^2 + (\theta_1)^2) - 1 & 2(\theta_1\theta_2 - \theta_0\theta_3) & 2(\theta_1\theta_3 + \theta_0\theta_2) \\ 2(\theta_1\theta_2 + \theta_0\theta_3) & 2((\theta_0)^2 + (\theta_2)^2) - 1 & 2(\theta_2\theta_3 - \theta_0\theta_1) \\ 2(\theta_1\theta_3 - \theta_0\theta_2) & 2(\theta_2\theta_3 + \theta_0\theta_1) & 2((\theta_0)^2 + (\theta_3)^2) - 1 \end{bmatrix}^i . \tag{2.2}$$

We denote the angular velocity vector of the reference coordinate system of body i defined in the inertial coordinate system by $\boldsymbol{\omega}^i$ and differentiate Eq. (2.1) with respect to time to obtain

$$\dot{\mathbf{r}}^i = \dot{\mathbf{R}}^i + \mathbf{A}^i \cdot \dot{\bar{\mathbf{u}}}^i + \widetilde{\boldsymbol{\omega}}^i \cdot \mathbf{A}^i \cdot \bar{\mathbf{u}}^i \ , \tag{2.3}$$

in which $\widetilde{\boldsymbol{\omega}}^i$ denotes the skew symmetric matrix of $\boldsymbol{\omega}^i$. The second derivative of the position vector with respect to time leads to

$$\ddot{\mathbf{r}}^i = \ddot{\mathbf{R}}^i + \mathbf{A}^i \cdot \ddot{\mathbf{u}}^i + 2\widetilde{\boldsymbol{\omega}}^i \cdot \mathbf{A}^i \cdot \dot{\mathbf{u}}^i + \widetilde{\dot{\boldsymbol{\omega}}}^i \cdot \mathbf{u}^i + \widetilde{\boldsymbol{\omega}}^i \cdot \widetilde{\boldsymbol{\omega}}^i \cdot \mathbf{u}^i \ . \tag{2.4}$$

As it can be seen, the global acceleration of the arbitrary point p^i contains the translational acceleration of the origin of the body reference coordinate system $\ddot{\mathbf{R}}^i$, the acceleration of point p^i relative to the body reference coordinate system $\mathbf{A}^i \cdot \ddot{\mathbf{u}}^i$, the Coriolis acceleration $2\widetilde{\boldsymbol{\omega}}^i \cdot \mathbf{A}^i \cdot \dot{\mathbf{u}}^i$, the tangential acceleration $\widetilde{\dot{\boldsymbol{\omega}}}^i \cdot \mathbf{u}^i$ and the centrifugal acceleration $\widetilde{\boldsymbol{\omega}}^i \cdot \widetilde{\boldsymbol{\omega}}^i \cdot \mathbf{u}^i$.

2.1.2 Kinetics of Rigid Bodies

There are different approaches resulting in *Differential Algebraic Equations* (DAE) or *Ordinary Differential Equations* (ODE) when generating equations of motion in multibody systems. In the former case, as one possibility, the implicit constraints $\boldsymbol{\Phi}(\mathbf{R}^i, \boldsymbol{\theta}^i, t) = \mathbf{0}$ can be differentiated twice and added to the Newton-Euler equations. In the latter approach, one can eliminate the constraint forces using the orthogonality of generalized motions and constraints. In this way, a minimal set of equations is generated [30]. The formulation presented here follows the first approach.

The general form of equations of motion of rigid multibody systems obtained from the *principle of virtual work in dynamics*, also known as *d'Alembert's principle*, is presented here. The main issue stated by this principle expresses the equilibrium condition of the virtual works done by inertia forces, constraint forces and external forces

$$\delta W_I^i = \delta W_C^i + \delta W_E^i \ . \tag{2.5}$$

The derivation of equations of motion is basically followed by stating either the kinetic energy or the virtual work of the inertia forces of the system based on the kinematics of bodies to obtain the mass matrix of the bodies. Here, the procedure is not presented and only the final relations are mentioned. The detailed procedure can be found, e.g., in [61, 124].

The virtual work of the generalized inertia forces of body i with the generalized coordinates $\mathbf{q}^i = (\mathbf{R}^{iT},\ \boldsymbol{\theta}^{iT})^T$ yields

$$\delta W_I^i = [\ddot{\mathbf{q}}^{iT} \cdot \mathbf{M}^i - \mathbf{Q}_Q^{iT}] \cdot \delta \mathbf{q}^i \ . \tag{2.6}$$

Here, the mass matrix $\mathbf{M}^i$ reads as

$$\mathbf{M}^i = \begin{bmatrix} \mathbf{m}_{RR}^i & \mathbf{m}_{R\theta}^i \\ \text{symmetric} & \mathbf{m}_{\theta\theta}^i \end{bmatrix} \ . \tag{2.7}$$

Its components are defined as integrals over the volume V^i of body i with density ρ^i

$$\mathbf{m}^i_{RR} = \int_{V^i} (\rho^i \mathbf{I}) dV^i \ , \qquad \mathbf{m}^i_{R\theta} = -\int_{V^i} (\rho^i \mathbf{A}^i \cdot \tilde{\bar{\mathbf{u}}}^i \cdot \mathbf{G}^i) dV^i \ ,$$
$$\mathbf{m}^i_{\theta\theta} = \int_{V^i} (\rho^i \mathbf{G}^{iT} \cdot \tilde{\bar{\mathbf{u}}}^{iT} \cdot \tilde{\bar{\mathbf{u}}}^i \cdot \mathbf{G}^i) dV^i \ , \tag{2.8}$$

where $\mathbf{I}$ is the 3×3 identity matrix, $\tilde{\bar{\mathbf{u}}}^i$ denotes the skew symmetric matrix of $\bar{\mathbf{u}}^i$ and

$$\mathbf{G}^i = 2 \begin{bmatrix} -\theta^i_1 & \theta^i_0 & \theta^i_3 & -\theta^i_2 \\ -\theta^i_2 & -\theta^i_3 & \theta^i_0 & \theta^i_1 \\ -\theta^i_3 & \theta^i_2 & -\theta^i_1 & \theta^i_0 \end{bmatrix} \tag{2.9}$$

with the property of

$$\bar{\boldsymbol{\omega}}^i = \mathbf{G}^i \cdot \dot{\boldsymbol{\theta}}^i \ , \tag{2.10}$$

where $\bar{\boldsymbol{\omega}}^i$ is the angular velocity vector of the reference coordinate system of body i defined also in that coordinate system. It may be important to mention that $\mathbf{m}^i_{R\theta}$ is a null matrix when the origin of the body reference coordinate system is attached to the mass center of the body.

The vector of Coriolis forces $\mathbf{Q}^i_Q$ that contains the quadratic terms in velocities can be stated as

$$\mathbf{Q}^i_Q = \begin{bmatrix} (\mathbf{Q}^i_Q)_R \\ (\mathbf{Q}^i_Q)_\theta \end{bmatrix} = \begin{bmatrix} -\mathbf{A}^i \cdot \int_{V^i} \rho^i [(\tilde{\bar{\boldsymbol{\omega}}}^i)^2 \cdot \bar{\mathbf{u}}^i - \tilde{\bar{\mathbf{u}}}^i \cdot \dot{\mathbf{G}}^i \cdot \dot{\boldsymbol{\theta}}^i] dV^i \\ \mathbf{G}^{iT} \cdot \int_{V^i} \rho^i [\tilde{\bar{\mathbf{u}}}^{iT} \cdot (\tilde{\bar{\boldsymbol{\omega}}}^i)^2 \cdot \bar{\mathbf{u}}^i - \tilde{\bar{\mathbf{u}}}^{iT} \cdot \tilde{\bar{\mathbf{u}}}^i \cdot \dot{\mathbf{G}}^i \cdot \dot{\boldsymbol{\theta}}^i] dV^i \end{bmatrix} \ , \tag{2.11}$$

in which $\bar{\boldsymbol{\omega}}^i$ represents the angular velocity of body i defined in the body reference coordinate system. In the same way, the virtual work of the constraint and external forces has to be calculated and substituted in the general form of the virtual work principle in Eq. (2.5), see [124]. Finally, the general form of equations of motion of body i is expressed in the following form

$$\mathbf{M}^i \cdot \ddot{\mathbf{q}}^i + \boldsymbol{\Phi}^T_{\mathbf{q}^i} \cdot \boldsymbol{\lambda}_C = \mathbf{h}^i \ , \tag{2.12}$$

where $\boldsymbol{\Phi}^T_{\mathbf{q}^i}$ is a part of the system constraints Jacobian matrix corresponding to the coordinates $\mathbf{q}^i$, the Lagrange multipliers vector $\boldsymbol{\lambda}_C$ contains all constraint forces of the system and $\mathbf{h}^i$ collects all the external and Coriolis forces exerted on body i. It is clear that there will not be any contribution from other constraints that do not involve body i and the components of $\boldsymbol{\Phi}^T_{\mathbf{q}^i}$ associated with other constraints have zero values. Equation (2.12) can simply be extended for n_b bodies of the system and rewritten as follows

$$\mathbf{M} \cdot \ddot{\mathbf{q}} + \boldsymbol{\Phi}^T_{\mathbf{q}} \cdot \boldsymbol{\lambda}_C = \mathbf{h} \ , \tag{2.13}$$

where

$$\mathbf{M} = \begin{bmatrix} \mathbf{M}^1 & & & \\ & \mathbf{M}^2 & & \mathbf{0} \\ & & \ddots & \\ \mathbf{0} & & & \mathbf{M}^{n_b} \end{bmatrix}, \ \ddot{\mathbf{q}} = \begin{bmatrix} \ddot{\mathbf{q}}^1 \\ \ddot{\mathbf{q}}^2 \\ \vdots \\ \ddot{\mathbf{q}}^{n_b} \end{bmatrix}, \ \mathbf{\Phi}_{\mathbf{q}}^T = \begin{bmatrix} \mathbf{\Phi}_{\mathbf{q}^1}^T \\ \mathbf{\Phi}_{\mathbf{q}^2}^T \\ \vdots \\ \mathbf{\Phi}_{\mathbf{q}^{n_b}}^T \end{bmatrix}, \ \mathbf{h} = \begin{bmatrix} \mathbf{h}^1 \\ \mathbf{h}^2 \\ \vdots \\ \mathbf{h}^{n_b} \end{bmatrix} . \quad (2.14)$$

The equations in this form cannot be solved since the number of unknowns $\ddot{\mathbf{q}}^i$ and $\boldsymbol{\lambda}_C$ exceeds the number of equations. As one possibility, the implicit constraints $\mathbf{\Phi}(\mathbf{q}, t) = \mathbf{0}$ are differentiated twice and added to Eq. (2.13)

$$\mathbf{\Phi}(\mathbf{q}, t) = \mathbf{0} \qquad \rightarrow \qquad \mathbf{\Phi}_{\mathbf{q}} \cdot \ddot{\mathbf{q}} = -\mathbf{\Phi}_{tt} - (\mathbf{\Phi}_{\mathbf{q}} \cdot \dot{\mathbf{q}})_{\mathbf{q}} \cdot \dot{\mathbf{q}} - 2\mathbf{\Phi}_{\mathbf{q}t} \cdot \dot{\mathbf{q}} = \boldsymbol{\gamma} \ , \quad (2.15)$$

which leads to

$$\begin{bmatrix} \mathbf{M} & \mathbf{\Phi}_{\mathbf{q}}^T \\ \mathbf{\Phi}_{\mathbf{q}} & \mathbf{0} \end{bmatrix} \cdot \begin{bmatrix} \ddot{\mathbf{q}} \\ \boldsymbol{\lambda}_C \end{bmatrix} = \begin{bmatrix} \mathbf{h} \\ \boldsymbol{\gamma} \end{bmatrix} . \quad (2.16)$$

This relation represents the general form of equations of motion of constrained rigid multibody systems and can be solved by using standard DAE solvers [38].

2.2 Modeling Strategies

As the result of researches in modeling of flexible multibody systems, quite different strategies have been followed to consider the effect of deformations as exact as possible and still preserve computation effort within an acceptable range. As a general classification, the available methods for analysis of EMBS may be divided into several groups: a) the motion of a flexible body is represented by superimposing a rigid body motion and a relative flexible motion, and b) an absolute representation of movement including large displacements and deformations with respect to an inertial frame is considered. Here, a very short overview of the popular procedures in this context is given. A more detailed description can be found in review papers [121, 146] and the references cited therein.

2.2.1 Superimposed Motion Approaches

The primary approaches were basically simple extensions of the methods used for rigid multibody systems. The key issue behind such approaches is to reach an extended formulation which preserves large rigid body motions with some relatively small elastic deformations.

In this framework, the *elasto-dynamic method* decouples the overall motion of flexible bodies into uncoupled rigid and elastic motions [149]. In this way, the effect of deformations is considered separately assuming that they have no influence on the rigid body

motion. Such an assumption cannot be adopted in general and the effect of deformations on the rigid body motion must be taken into consideration yielding acceptable results.

Another class of this group includes nonlinear coupling terms between rigid body motion and deformations and, therefore, provides a better approximation to the real behavior of EMBS when compared to the elasto-dynamics technique. This approach is known as *floating* or *moving frame of reference* and is currently the most widely-used method in the analysis of EMBS. Examples of contributions devoted to this subject are quite numerous and can be found in the references cited in [121, 146]. As the main procedure for simulation of EMBS in this work, this approach serves to generate equations of motion. Two kinds of variables are utilized to formulate EMBS based on this approach. The first set describes position and rotation of the body reference coordinate system with respect to an inertial frame. This set of coordinates is actually the rigid body motion of the flexible body. The second set which contains elastic coordinates is used to express the deformations of each flexible body with respect to the corresponding floating frame. However, the assumption of relatively small deformations is required in order to allow linear elasticity for consideration of deformations [124].

For treatment of the restrictions involved with the floating frame of reference, the *corotational frame* approach which is known also as *convected coordinate system* was used, see e.g. [14, 108]. In this approach, the incremental finite element formulation is used to solve large deformation and rotation problems. For this purpose, each flexible body is discretized in finite elements on which a corotational frame is attached. The overall motion of each finite element is divided into a rigid body motion in terms of nodal variables in the inertial frame and natural deformation modes. In this way, rigid body variables do not appear explicitly and equations of motion are written with respect to the inertial frame. A drawback of this approach compared to the floating frame of reference is that it does not lead to the exact description of the rigid body motion.

2.2.2 Absolute Motion Approaches

The motivation of this group of methods was to embed nonlinear finite elements into the multibody formalism and to remedy the problem encountered in flexible multibody systems undergoing large deformations and rotations [128]. The absolute representation of motion including deformations in the inertial frame eases the process of generating equations of motion since all coordinates are described in the inertial frame and no moving frame has to be defined.

As the most widely-used approach in this framework the *absolute nodal coordinate* method proposed in [120, 122] attempts to cover a large variety of applications. Definition of global position vectors makes use of the element nodal coordinates together with the element global shape function. The formulation proposed in [120, 122] has been used extensively

by many researchers, see e.g. [159].

There exist some other approaches which are not as popular as the absolute nodal coordinate method. Among all, the *large rotation vectors* formulation [50, 121] may be mentioned which employs finite rotation angles instead of infinitesimal ones and consequently, represents correctly the rigid body motion. However, it suffers from some limitations like the coordinate redundancy and high nonlinearities of equations of motion.

2.3 Floating Frame of Reference

Some basics of the floating frame of reference approach are first introduced and then, using this approach the equations of motion of a flexible body are derived.

2.3.1 Properties, Advantages and Restrictions

A major advantage of the floating frame of reference is that it extends rigid multibody dynamics to flexible multibody systems in a natural way. In contrast to some other methods, it leads to the exact rigid body dynamics when the deformations vanish. It makes use of the linear finite element method to introduce either the nodal variables or the mode shapes.

The most important limitations of the floating frame of reference is that it cannot deal with systems with large deformations. Additionally, it fails to consider the rotational stiffening effects that appear for high rotational speeds of flexible bodies, see [78]. For such situations, one of the corotational frame and the absolute nodal coordinates approaches may be used.

In addition to the already mentioned assumptions, the following points are considered when formulating the floating frame of reference:

1. Elastic coordinates may be defined using the component mode method, the finite element method or experimental identification techniques.

2. Selection of the deformation shapes and the body reference coordinate system may not be considered as two independent issues.

3. The accuracy of the results will significantly depend on the selected modal basis.

4. Modal reduction may be used for bodies undergoing slow rotation or uniform angular velocity. However, for bodies undergoing fast nonuniform angular velocity, nonlinear modal reduction must be used to include the centrifugal stiffening effect [111].

2.3.2 Displacement Fields, Model Reduction and Choice of Shape Functions

The rigid and elastic motions of flexible bodies are coupled through the inertia coupling terms of the mass matrix. Therefore, the deformations can have a significant effect on the system behavior. This fact, however, leads to the problem of model reduction which means that to find a reduced-order model of the original model which results in a lower number of degrees of freedom and still preserves the most important features of the original model. By doing so, the system size and consequently computational cost will be considerably reduced.

In this context, one may mention the techniques which are based on the optimization of the reduced-order model considering a given criteria, see e.g. [7]. On the other hand, some techniques attempt to preserve exactly a predefined selection of parameters of the original model. The selected parameters can be the dominant eigenfrequencies. In this framework, the projection methods have been widely used. The basic idea behind these approaches is to generate a reduced-order model by approximating the solutions in a low-dimensional subspace and imposing some pre-specified conditions in the original space. A detailed description devoted to this subject can be found, e.g., in [58, 137].

One of the well-established procedures which makes use of the projection methods is based on the *Rayleigh-Ritz* approximation functions. From this approach, the displacement field due to the deformation is approximated by a combination of space dependent shape functions and time dependent elastic coordinates

$$\bar{\mathbf{u}}_e(\mathbf{r}, t) = \mathbf{S}(\mathbf{r}) \cdot \mathbf{q}_e(t) \ , \tag{2.17}$$

where the shape functions matrix $\mathbf{S}(\mathbf{r})$ contains the modal eigenvectors and $\mathbf{r}$ is a point mass position vector. The accuracy of the displacement field vector $\bar{\mathbf{u}}_e(\mathbf{r}, t)$ is directly affected by the considered shape functions. The shape functions may be represented by interpolation functions used in a finite element model of the flexible body.

The Ritz method requires selection of the shape functions whose choice is affected by the definition of the body reference frame [117, 118]. Different sets of shape functions and body reference frames result in different magnitudes of the reference and elastic coordinates. The correct representation of the body deformation using various sets of shape functions requires that the shape functions form a complete set of functions, mainly known as admissible functions, which satisfy the geometric boundary conditions. This goal has been improved by use of the so-called quasi-comparison functions which can be suitable static deformation modes, see e.g. [93].

There are mainly two different approaches from which the shape functions are obtained. In the first technique, a nodal approach based on the finite element method is utilized, where local polynomial functions are weighted with nodal deformations. The second technique

makes use of the global eigenfunctions as weighting functions and so is called modal approach. In this way, it leads to the smaller number of degrees of freedom but instead, requires the proper selection of the shape functions since it affects the accuracy and quality of the obtained results. As a general rule, appropriate selection of the displacement fields requires experience and judgment of the analyst. A discussion about methods for straightforward selection of the mode shapes together with approximation models for the displacement fields is presented in [27].

2.3.3 Selection of Reference Frame

The selection of the body reference frame is an issue of major importance when formulating the floating frame of reference. This fact is corporated with the choice of shape functions. Additionally, further simplifications and linearizations of equations of motion compel small deformations with respect to this frame. As another important point, the requirement for weak decoupling between reference and elastic coordinates may be mentioned.

There exist two general concepts which have been followed for the selection of reference frame namely kinematic and dynamic concepts. The former leads to the geometric boundary conditions while the latter attempts to minimize linear and angular momentum due to body deformations.

In the kinematic approach, the origin of the reference frame $\{O^i, \mathbf{e}_1^i, \mathbf{e}_2^i, \mathbf{e}_3^i\}$ may rigidly be attached to an arbitrary point k^1 on the flexible body. Then, after considering two other points k^2 and k^3 on the body, the first axes $\mathbf{e}_1^i$ of the reference frame is aligned from k^1 to k^2. The axes $\mathbf{e}_3^i$ is oriented from k^1 perpendicular to the plane which passes through three points. Finally, the axes $\mathbf{e}_2^i$ is specified so that to build a right hand coordinate system together with $\mathbf{e}_1^i$ and $\mathbf{e}_3^i$ which means that $\mathbf{e}_2^i = \mathbf{e}_3^i \times \mathbf{e}_1^i$, for more details see [117, 118].

Examples of the most well known approaches based on the dynamic concept can be mentioned as the *principle axes frame*, the *mean axes frame* (known also as the *Tisserand frame* or *Gylden frame*) and the *Buckens frame*. In these approaches, the origin of the reference frame is basically attached at the instantaneous center of mass. However, in the principle axes frame approach, the corresponding axes of the frame coincide with the current principle axes of inertia about the origin of the frame. As a result, it minimizes the inertia coupling between the generalized reference coordinates and the elastic coordinates which results in less complex systems of equations of motion. In the mean axes frame approach the reference frame follows a mean displacement of the flexible body [1]. This condition minimizes the relative kinetic energy arising from the deformations when observed from the body reference frame. The axes of the reference frame are oriented in such way that the angular momentum vector in the actual configuration becomes zero. Finally, the Buckens frame [20] is the frame to which the sum of the squares of the dis-

placements with respect to an observer at the reference frame is minimum. This approach is based on the linearized reference conditions of the mean axes frame which leads to the smallest deformations favorable for linearization.

2.3.4 Nonlinearities and Geometric Stiffening Effect

Under the assumption of small deformations, equations of motion may be linearized for further simplifications. However, it can frequently happen that considering an improper linearization leads to ignoring the effect of *geometric stiffening* which results in wrong simulations. Therefore, this point needs special attention when using a linear modal reduction for bodies undergoing high angular velocities [78]. The effect of geometric stiffening becomes important when dealing with flexible structures with very stiff and soft mode shapes in orthogonal directions.

2.3.5 Kinematics of Flexible Bodies

Figure 2.2 shows a flexible body in undeformed and deformed configuration. The displacement of an arbitrary point p^i on the body due to deformation given in the inertial coordinate system is shown with the vector $\mathbf{u}_e^i$. In order to identify the configuration of the flexible body, two sets of reference coordinates $\mathbf{q}_r^i = (\mathbf{R}^{iT},\ \boldsymbol{\theta}^{iT})^T$ and elastic coordinates $\mathbf{q}_e^i$ are selected.

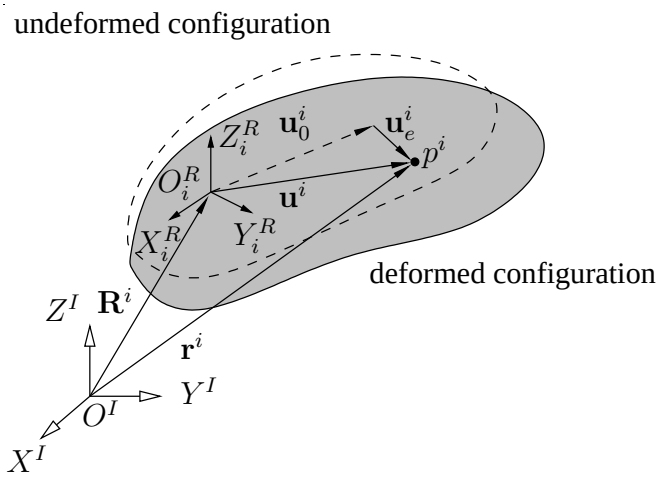

Figure 2.2: Flexible body kinematics

The reference coordinates set specifies the position and orientation of the body reference frame in the inertial frame whereas the elastic coordinates are the measures of deformation with respect to the body reference frame. In this way, the location of the arbitrary point

p^i can be described uniquely in terms of these generalized coordinates when observed from the inertial frame as

$$\mathbf{r}^i = \mathbf{R}^i + \mathbf{u}^i = \mathbf{R}^i + (\mathbf{u}_0^i + \mathbf{u}_e^i) = \mathbf{R}^i + \mathbf{A}^i \cdot (\bar{\mathbf{u}}_0^i + \bar{\mathbf{u}}_e^i) \ , \tag{2.18}$$

where both $\bar{\mathbf{u}}_0^i$ and $\bar{\mathbf{u}}_e^i$ are given in the body reference frame. One can rewrite this equation in terms of the time dependent generalized elastic coordinates by using Eq. (2.17)

$$\mathbf{r}^i = \mathbf{R}^i + \mathbf{A}^i \cdot \bar{\mathbf{u}}^i = \mathbf{R}^i + \mathbf{A}^i \cdot (\bar{\mathbf{u}}_0^i + \mathbf{S}^i \cdot \mathbf{q}_e^i) \ . \tag{2.19}$$

Maybe it is important to emphasize that the components of the shape function matrix $\mathbf{S}^i$ are dependent on the selected body reference frame and, therefore, the transformation matrix is considered. The time derivative of the position vector $\mathbf{r}^i$ yields

$$\dot{\mathbf{r}}^i = \dot{\mathbf{R}}^i + \dot{\mathbf{A}}^i \cdot \bar{\mathbf{u}}^i + \mathbf{A}^i \cdot \dot{\bar{\mathbf{u}}}^i = \dot{\mathbf{R}}^i + \dot{\mathbf{A}}^i \cdot \bar{\mathbf{u}}^i + \mathbf{A}^i \cdot \mathbf{S}^i \cdot \dot{\mathbf{q}}_e^i \ . \tag{2.20}$$

The second term on the right hand side can be written as, see [124],

$$\dot{\mathbf{A}}^i \cdot \bar{\mathbf{u}}^i = \mathbf{A}^i \cdot (\bar{\boldsymbol{\omega}}^i \times \bar{\mathbf{u}}^i) = -\mathbf{A}^i \cdot (\bar{\mathbf{u}}^i \times \bar{\boldsymbol{\omega}}^i) = -\mathbf{A}^i \cdot \tilde{\bar{\mathbf{u}}}^i \cdot \mathbf{G}^i \cdot \dot{\boldsymbol{\theta}}^i \ . \tag{2.21}$$

Consequently Eq. (2.20) is written as

$$\dot{\mathbf{r}}^i = \dot{\mathbf{R}}^i - \mathbf{A}^i \cdot \tilde{\bar{\mathbf{u}}}^i \cdot \mathbf{G}^i \cdot \dot{\boldsymbol{\theta}}^i + \mathbf{A}^i \cdot \mathbf{S}^i \cdot \dot{\mathbf{q}}_e^i \ . \tag{2.22}$$

Matrix $\mathbf{G}^i$ was previously defined in Eq. (2.9). One can write the absolute velocity vector of Eq. (2.25) in the alternative compact form

$$\dot{\mathbf{r}}^i = \left[\begin{array}{ccc} \mathbf{I} & -\mathbf{A}^i \cdot \tilde{\bar{\mathbf{u}}}^i \cdot \mathbf{G}^i & \mathbf{A}^i \cdot \mathbf{S}^i \end{array} \right] \cdot \left[\begin{array}{c} \dot{\mathbf{R}}^i \\ \dot{\boldsymbol{\theta}}^i \\ \dot{\mathbf{q}}_e^i \end{array} \right] \ \rightarrow \ \dot{\mathbf{r}}^i = \mathbf{L}^i \cdot \dot{\mathbf{q}}^i \ , \tag{2.23}$$

where $\mathbf{I}$ is the 3×3 identity matrix and the generalized velocity vector $\dot{\mathbf{q}}^i$ summarizes the reference and elastic velocities. Further differentiation of Eq. (2.23) leads to the absolute acceleration of the point p^i

$$\ddot{\mathbf{r}}^i = \dot{\mathbf{L}}^i \cdot \dot{\mathbf{q}}^i + \mathbf{L}^i \cdot \ddot{\mathbf{q}}^i \ , \tag{2.24}$$

which may be written also by differentiating Eq. (2.20). For this purpose, first Eq. (2.20) is written in the following form as

$$\dot{\mathbf{r}}^i = \dot{\mathbf{R}}^i + \mathbf{A}^i \cdot \dot{\bar{\mathbf{u}}}^i + \widetilde{\boldsymbol{\omega}}^i \cdot \mathbf{A}^i \cdot \bar{\mathbf{u}}^i \ . \tag{2.25}$$

Therefore, one obtains

$$\ddot{\mathbf{r}}^i = \ddot{\mathbf{R}}^i + \mathbf{A}^i \cdot \ddot{\bar{\mathbf{u}}}^i + \dot{\mathbf{A}}^i \cdot \dot{\bar{\mathbf{u}}}^i + \widetilde{\boldsymbol{\omega}}^i \cdot \mathbf{A}^i \cdot \dot{\bar{\mathbf{u}}}^i + \widetilde{\dot{\boldsymbol{\omega}}}^i \cdot \mathbf{A}^i \cdot \bar{\mathbf{u}}^i + \widetilde{\boldsymbol{\omega}}^i \cdot \dot{\mathbf{A}}^i \cdot \bar{\mathbf{u}}^i \ , \tag{2.26}$$

which finally is written as

$$\ddot{\mathbf{r}}^i = \ddot{\mathbf{R}}^i + \mathbf{A}^i \cdot \ddot{\bar{\mathbf{u}}}^i + 2\widetilde{\boldsymbol{\omega}}^i \cdot \mathbf{A}^i \cdot \dot{\bar{\mathbf{u}}}^i + \widetilde{\dot{\boldsymbol{\omega}}}^i \cdot \mathbf{u}^i + \widetilde{\boldsymbol{\omega}}^i \cdot \widetilde{\boldsymbol{\omega}}^i \cdot \mathbf{u}^i \ . \tag{2.27}$$

This equation has the same general form as the obtained equation for rigid bodies (2.4) but the effect of deformations is considered in the vectors $\bar{\mathbf{u}}^i$ and $\mathbf{u}^i$. Interpretation of the acceleration components can be done similarly, too.

2.3.6 Kinetics of Flexible Bodies

In this section, the equations of motion of flexible multibody systems are derived. The procedure is based on the derivation of the components of the inertia mass matrix and the generalized forces including elastic forces, external forces, inertia forces and constraint forces. The effect of contact forces is further considered in Chapter 3.

Mass Matrix

In the following, first the inertia mass matrix of the flexible body i is established and then, it is extended to include the mass matrix of the system consisting of n_b rigid and flexible bodies. The derivation may be followed by stating the kinetic energy of body i

$$T^i = \frac{1}{2}\int_{V^i} (\rho^i \dot{\mathbf{r}}^{iT} \cdot \dot{\mathbf{r}}^i) dV^i \ , \tag{2.28}$$

which can be expressed by using Eq. (2.23) as

$$T^i = \frac{1}{2}\dot{\mathbf{q}}^{iT} \cdot \left(\int_{V^i} (\rho^i \mathbf{L}^{iT} \cdot \mathbf{L}^i) dV^i \right) \cdot \dot{\mathbf{q}}^i = \frac{1}{2}\dot{\mathbf{q}}^{iT} \cdot \mathbf{M}^i \cdot \dot{\mathbf{q}}^i \tag{2.29}$$

with

$$\mathbf{M}^i = \int_{V^i} (\rho^i \mathbf{L}^{iT} \cdot \mathbf{L}^i) dV^i \ , \tag{2.30}$$

which finally by using the orthogonality of the transformation matrix, $\mathbf{A}^{iT} \cdot \mathbf{A}^i = \mathbf{I}$, leads to

$$\mathbf{M}^i = \int_{V^i} \rho^i \begin{bmatrix} \mathbf{I} & -\mathbf{A}^i \cdot \tilde{\tilde{\mathbf{u}}}^i \cdot \mathbf{G}^i & \mathbf{A}^i \cdot \mathbf{S}^i \\ & \mathbf{G}^{iT} \cdot \tilde{\tilde{\mathbf{u}}}^{iT} \cdot \tilde{\tilde{\mathbf{u}}}^i \cdot \mathbf{G}^i & -\mathbf{G}^{iT} \cdot \tilde{\tilde{\mathbf{u}}}^{iT} \cdot \mathbf{S}^i \\ \text{symmetric} & & \mathbf{S}^{iT} \cdot \mathbf{S}^i \end{bmatrix} dV^i \ . \tag{2.31}$$

Furthermore, one can write the mass matrix $\mathbf{M}^i$ in the compact form

$$\mathbf{M}^i = \begin{bmatrix} \mathbf{m}^i_{RR} & \mathbf{m}^i_{R\theta} & \mathbf{m}^i_{Re} \\ & \mathbf{m}^i_{\theta\theta} & \mathbf{m}^i_{\theta e} \\ \text{symmetric} & & \mathbf{m}^i_{ee} \end{bmatrix} \ , \tag{2.32}$$

in which

$$\mathbf{m}^i_{RR} = \int_{V^i} \rho^i \ \mathbf{I} \ dV^i, \ \mathbf{m}^i_{\theta\theta} = \int_{V^i} \rho^i \mathbf{G}^{iT} \cdot \tilde{\tilde{\mathbf{u}}}^{iT} \cdot \tilde{\tilde{\mathbf{u}}}^i \cdot \mathbf{G}^i dV^i, \ \mathbf{m}^i_{ee} = \int_{V^i} \rho^i \mathbf{S}^{iT} \cdot \mathbf{S}^i dV^i, \tag{2.33}$$

$$\mathbf{m}^i_{R\theta} = \int_{V^i} -\rho^i \mathbf{A}^i \cdot \tilde{\tilde{\mathbf{u}}}^i \cdot \mathbf{G}^i dV^i, \ \mathbf{m}^i_{Re} = \int_{V^i} \rho^i \mathbf{A}^i \cdot \mathbf{S}^i dV^i, \ \mathbf{m}^i_{\theta e} = \int_{V^i} -\rho^i \mathbf{G}^{iT} \cdot \tilde{\tilde{\mathbf{u}}}^{iT} \cdot \mathbf{S}^i dV^i.$$

It is noticeable that the mass matrix $\mathbf{M}^i$ can also be obtained from the virtual work relation of the inertia forces, see [123, 124],

$$\delta W^i_I = \int_{V^i} (\rho^i \ddot{\mathbf{r}}^{iT} \cdot \delta \mathbf{r}^i) dV^i \ . \tag{2.34}$$

Generalized Elastic Forces

The magnitude of the generalized elastic forces is strongly dependent on the amount of components of the *strain tensor* arising from deformations

$$\boldsymbol{\varepsilon}^i = \begin{bmatrix} \varepsilon^i_{11} & \varepsilon^i_{12} & \varepsilon^i_{13} \\ \varepsilon^i_{21} & \varepsilon^i_{22} & \varepsilon^i_{23} \\ \varepsilon^i_{31} & \varepsilon^i_{32} & \varepsilon^i_{33} \end{bmatrix} , \tag{2.35}$$

which is mainly defined with a so-called *strain vector* $\boldsymbol{\varepsilon}_v$ because of the symmetry of the strain tensor, see [124],

$$\boldsymbol{\varepsilon}^i_v = \begin{bmatrix} \varepsilon^i_{11} & \varepsilon^i_{22} & \varepsilon^i_{33} & \varepsilon^i_{12} & \varepsilon^i_{13} & \varepsilon^i_{23} \end{bmatrix}^T . \tag{2.36}$$

From the theory of elasticity it is known that

$$\boldsymbol{\varepsilon}^i_v = \delta\mathbf{D} \cdot \bar{\mathbf{u}}^i_e , \tag{2.37}$$

where $\bar{\mathbf{u}}_e$ denotes the displacement fields due to deformations and $\delta\mathbf{D}$ is the differential operator defined as

$$\delta\mathbf{D} = \frac{1}{2} \begin{bmatrix} 2\dfrac{\partial}{\partial x} & 0 & 0 \\ 0 & 2\dfrac{\partial}{\partial y} & 0 \\ 0 & 0 & 2\dfrac{\partial}{\partial z} \\ \dfrac{\partial}{\partial y} & \dfrac{\partial}{\partial x} & 0 \\ \dfrac{\partial}{\partial z} & 0 & \dfrac{\partial}{\partial x} \\ 0 & \dfrac{\partial}{\partial z} & \dfrac{\partial}{\partial y} \end{bmatrix} . \tag{2.38}$$

The differentiations with respect to x, y and z in this relation are done for three axes X^R_i, Y^R_i and Z^R_i of the body reference frame, see Figure 2.2.

On the other hand, one can write the virtual work of the elastic forces as

$$\delta W^i_S = -\int_{V^i} (\mathbf{E}^i \cdot \boldsymbol{\varepsilon}^i_v)^T \cdot \delta\boldsymbol{\varepsilon}^i_v \, dV^i , \tag{2.39}$$

where $\mathbf{E}^i$ is the symmetric *elastic constants matrix* of body i. By substituting the strain vector $\boldsymbol{\varepsilon}^i_v$ from Eq. (2.37) and the displacement fields vector $\bar{\mathbf{u}}^i_e$ from the Ritz approximation function Eq. (2.17) one obtains

$$\delta W^i_S = -\mathbf{q}^{i\,T}_e \int_{V^i} \left(\mathbf{S}^{iT} \cdot \mathbf{D}^{iT} \cdot \mathbf{E}^i \cdot \mathbf{D}^i \cdot \mathbf{S}^i dV^i \right) \cdot \delta\mathbf{q}^i_e . \tag{2.40}$$

Comparing this relation with the general form of virtual work of the elastic forces,

$$\delta W_S^i = -\mathbf{q}_e^{i\,T} \cdot \mathbf{k}_{ee}^i \cdot \delta \mathbf{q}_e^i \ , \tag{2.41}$$

yields a relation for the stiffness matrix $\mathbf{k}_{ee}^i$ associated with the elastic coordinates of body i

$$\mathbf{k}_{ee}^i = \int_{V^i} \mathbf{S}^{i\,T} \cdot \mathbf{D}^{i\,T} \cdot \mathbf{E}^i \cdot \mathbf{D}^i \cdot \mathbf{S}^i dV^i \ . \tag{2.42}$$

Therefore, the final relation of the elastic forces of body i reads as

$$\mathbf{h}_s^i = \mathbf{k}_{ee}^i \cdot \mathbf{q}_e^i \ . \tag{2.43}$$

Finally, the generalized elastic forces corresponding to three sets of the generalized coordinates $\mathbf{R}^i, \boldsymbol{\theta}^i$ and $\mathbf{q}_e^i$ can be written as

$$\mathbf{Q}_S^i = \begin{bmatrix} \mathbf{0} \\ \mathbf{0} \\ \mathbf{k}_{ee}^i \cdot \mathbf{q}_e^i \end{bmatrix} = \begin{bmatrix} \mathbf{0} & \mathbf{0} & \mathbf{0} \\ \mathbf{0} & \mathbf{0} & \mathbf{0} \\ \mathbf{0} & \mathbf{0} & \mathbf{k}_{ee}^i \end{bmatrix} \cdot \begin{bmatrix} \mathbf{R}^i \\ \boldsymbol{\theta}^i \\ \mathbf{q}_e^i \end{bmatrix} = \mathbf{K}^i \cdot \mathbf{q}^i \ . \tag{2.44}$$

In this relation, $\mathbf{K}^i$ and $\mathbf{q}^i$ denote the stiffness matrix and the generalized coordinates of body i, respectively.

Generalized Damping Forces

The procedure outlined in the previous subsection for the generalized elastic forces can be followed similarly for the damping forces but instead, the corresponding relations must be used. However, the problem which arises is that the corresponding material constants matrix $\mathbf{E}_v$ is often not known for damping. Therefore, the damping coefficient matrix $\mathbf{d}_{ee}$ is sometimes approximated with a so-called *proportional* or *Rayleigh damping* as a linear combination of the mass matrix $\mathbf{m}_{ee}$ and the stiffness matrix $\mathbf{k}_{ee}$, see e.g. [11, 51],

$$\mathbf{d}_{ee} = \alpha \mathbf{m}_{ee} + \beta \mathbf{k}_{ee} \ , \tag{2.45}$$

where α and β are two constant parameters, which can be determined from two given damping ratios ξ_1 and ξ_2 that correspond to two unequal frequencies ω_1 and ω_2

$$\alpha = \frac{2\omega_1\omega_2}{\omega_2^2 - \omega_1^2}(\xi_1\omega_2 - \xi_2\omega_1) \ , \tag{2.46}$$

$$\beta = \frac{2}{\omega_2^2 - \omega_1^2}(\xi_2\omega_2 - \xi_1\omega_1) \ . \tag{2.47}$$

In practice one may obtain these coefficients by performing both experiment and simulation for the same structure and fitting the results of simulation to the experimental one. One may note the mass proportional and stiffness proportional shares of the Rayleigh damping from Eq. (2.45). This fact is depicted in Figure 2.3.

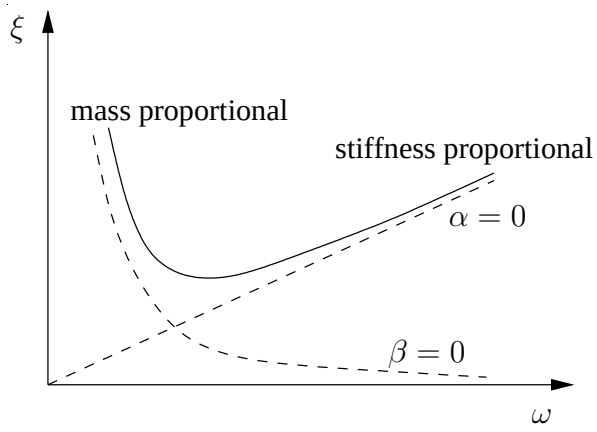

Figure 2.3: Mass proportional and stiffness proportional dampings, see [51]

After calculation of the damping coefficient matrix $\mathbf{d}^i_{ee}$, the damping forces are obtained from

$$\mathbf{h}^i_d = \mathbf{d}^i_{ee} \cdot \dot{\mathbf{q}}^i_e \ . \tag{2.48}$$

The generalized damping forces corresponding to three sets of the generalized coordinates can be written as

$$\mathbf{Q}^i_D = \begin{bmatrix} \mathbf{0} \\ \mathbf{0} \\ \mathbf{d}^i_{ee} \cdot \dot{\mathbf{q}}^i_e \end{bmatrix} = \begin{bmatrix} \mathbf{0} & \mathbf{0} & \mathbf{0} \\ \mathbf{0} & \mathbf{0} & \mathbf{0} \\ \mathbf{0} & \mathbf{0} & \mathbf{d}^i_{ee} \end{bmatrix} \cdot \begin{bmatrix} \dot{\mathbf{R}}^i \\ \dot{\boldsymbol{\theta}}^i \\ \dot{\mathbf{q}}^i_e \end{bmatrix} = \mathbf{D}^i \cdot \dot{\mathbf{q}}^i \ , \tag{2.49}$$

where $\mathbf{D}^i$ and $\dot{\mathbf{q}}^i$ denote the damping coefficient matrix and the generalized velocities vector of body i, respectively.

The Rayleigh damping can improve the numerical performance of the simulation by damping of high frequency vibrations which are not desired in the majority of mechanical systems.

Generalized External Forces

The generalized external forces include different kinds of forces like point forces $(\mathbf{Q}^i_E)_p$, point moments $(\mathbf{Q}^i_E)_m$, surface forces $(\mathbf{Q}^i_E)_s$ and volume forces $(\mathbf{Q}^i_E)_v$

$$\mathbf{Q}^i_E = (\mathbf{Q}^i_E)_p + (\mathbf{Q}^i_E)_m + (\mathbf{Q}^i_E)_s + (\mathbf{Q}^i_E)_v \ . \tag{2.50}$$

The gravity force can be considered as volume force when it is not assumed as a concentrated load at the center of gravity. The general form of the virtual work of the external forces $\mathbf{Q}^i_E$ can be written as

$$\delta W^i_E = \begin{bmatrix} (\mathbf{Q}^i_{E_R})^T & (\mathbf{Q}^i_{E_\theta})^T & (\mathbf{Q}^i_{E_e})^T \end{bmatrix} \cdot \begin{bmatrix} \delta\mathbf{R}^i \\ \delta\boldsymbol{\theta}^i \\ \delta\mathbf{q}^i_e \end{bmatrix} \ . \tag{2.51}$$

For the case of point forces, suppose that an external force $\mathbf{F}_p^i$ is acting at an arbitrary point p^i on body i with the virtual displacements vector $\delta\mathbf{r}^i$. The associated virtual work reads as

$$(\delta W_E^i)_p = \mathbf{F}_p^{i\,T} \cdot \delta\mathbf{r}^i \ , \tag{2.52}$$

where by substituting the vector $\delta\mathbf{r}^i$ from Eq. (2.19) one obtains, see also Eq. (2.25),

$$(\delta W_E^i)_p = \mathbf{F}_p^{i\,T} \cdot \left(\delta\mathbf{R}^i + (-\mathbf{A}^i \cdot \tilde{\bar{\mathbf{u}}}^i \cdot \mathbf{G}^i) \cdot \delta\boldsymbol{\theta}^i + \mathbf{A}^i \cdot \mathbf{S}^i \cdot \delta\mathbf{q}_e^i\right) \ , \tag{2.53}$$

and consequently

$$(\delta W_E^i)_p = \left[\begin{array}{ccc} \mathbf{F}_p^{i\,T} & -\mathbf{F}_p^{i\,T} \cdot \mathbf{A}^i \cdot \tilde{\bar{\mathbf{u}}}^i \cdot \mathbf{G}^i & \mathbf{F}_p^{i\,T} \cdot \mathbf{A}^i \cdot \mathbf{S}^i \end{array}\right] \cdot \left[\begin{array}{c} \delta\mathbf{R}^i \\ \delta\boldsymbol{\theta}^i \\ \delta\mathbf{q}_e^i \end{array}\right] \ . \tag{2.54}$$

By comparing this relation with the general form of Eq. (2.51) one concludes that the three components of the generalized external force associated with three sets of the generalized coordinates can be written as

$$(\mathbf{Q}_E^i)_p = \left[\begin{array}{c} \mathbf{F}_p^i \\ -\mathbf{G}^{i\,T} \cdot \tilde{\bar{\mathbf{u}}}^{i\,T} \cdot \mathbf{A}^{i\,T} \cdot \mathbf{F}_p^i \\ \mathbf{S}^{i\,T} \cdot \mathbf{A}^{i\,T} \cdot \mathbf{F}_p^i \end{array}\right] \ . \tag{2.55}$$

Similarly, consideration of a moment $\mathbf{M}_p^i$ acting at an arbitrary point p^i on body i can be done and the associated virtual work read as

$$(\delta W_E^i)_m = \mathbf{M}_p^{i\,T} \cdot \delta\boldsymbol{\theta}_e^i \ , \tag{2.56}$$

where $\delta\boldsymbol{\theta}_e^i$ is the vector of total virtual rotation angles of the body at point p^i. It can be stated as the summation of the virtual rotation angles of the body reference frame $\delta\boldsymbol{\theta}^i$ and the virtual rotation angles of the body at point p^i with respect to the body reference frame $\delta\boldsymbol{\theta}_{r/e}^i$

$$\delta\boldsymbol{\theta}_e^i = \delta\boldsymbol{\theta}^i + \delta\boldsymbol{\theta}_{r/e}^i \ , \tag{2.57}$$

where $\delta\boldsymbol{\theta}_{r/e}^i$ can be calculated from the shape functions matrix $\boldsymbol{\Psi}^i$ corresponding to the rotation angles $\delta\boldsymbol{\theta}_{r/e}^i = \mathbf{A}^i \cdot \boldsymbol{\Psi}^i \cdot \delta\mathbf{q}_e^i$ yielding, see [117],

$$\delta\boldsymbol{\theta}_e^i = \delta\boldsymbol{\theta}^i + \mathbf{A}^i \cdot \boldsymbol{\Psi}^i \cdot \delta\mathbf{q}_e^i \ . \tag{2.58}$$

This equation together with Eq. (2.56) leads to a relation for the generalized external forces arising from the point moment

$$(\mathbf{Q}_E^i)_m = \left[\begin{array}{c} \mathbf{0} \\ \mathbf{M}_p^i \\ \boldsymbol{\Psi}^{i\,T} \cdot \mathbf{A}^{i\,T} \cdot \mathbf{M}_p^i \end{array}\right] \ . \tag{2.59}$$

It is noticeable that when body i is subjected to point forces and/or point moments at different locations, their effects must be added when using Eqs. (2.55) and (2.59).

The generalized surface forces associated with a surface load $\mathbf{F}_s^i$ per unit area can be written as

$$(\mathbf{Q}_E^i)_s = \begin{bmatrix} \int_{A_a^i} \mathbf{F}_s^i dA_a^i \\ -\int_{A_a^i} \mathbf{G}^{iT} \cdot \tilde{\tilde{\mathbf{u}}}^{iT} \cdot \mathbf{A}^{iT} \cdot \mathbf{F}_s^i dA_a^i \\ \int_{A_a^i} \mathbf{S}^{iT} \cdot \mathbf{A}^{iT} \cdot \mathbf{F}_s^i dA_a^i \end{bmatrix} . \tag{2.60}$$

Here, the symbol A_a^i denotes the area and must be distinguished from transformation matrix $\mathbf{A}^i$.

Finally, the generalized volume forces which arise from a load $\mathbf{F}_v^i$ per unit volume reads as

$$(\mathbf{Q}_E^i)_v = \begin{bmatrix} \int_{V^i} \mathbf{F}_v^i dV^i \\ -\int_{V^i} \mathbf{G}^{iT} \cdot \tilde{\tilde{\mathbf{u}}}^{iT} \cdot \mathbf{A}^{iT} \cdot \mathbf{F}_v^i dV^i \\ \int_{V^i} \mathbf{S}^{iT} \cdot \mathbf{A}^{iT} \cdot \mathbf{F}_v^i dV^i \end{bmatrix} . \tag{2.61}$$

This relation can be used for the gravity force with $\mathbf{F}_v^i = \rho^i \mathbf{g}$ where $\mathbf{g}$ denotes the gravity acceleration.

Generalized Inertia Forces: Second Order Forces and Quadratic Velocity Vector

Here, the virtual work associated with the inertia forces of body i is used to reach the relation of the generalized inertia forces, see Eq. (2.34). Substituting the absolute acceleration from Eq. (2.24) into Eq. (2.34) leads to

$$\delta W_I^i = \int_{V^i} (\rho^i \ddot{\mathbf{q}}^{iT} \cdot \mathbf{L}^{iT} \cdot \mathbf{L}^i \cdot \delta \mathbf{q}^i) dV^i + \int_{V^i} (\rho^i \dot{\mathbf{q}}^{iT} \cdot \dot{\mathbf{L}}^{iT} \cdot \mathbf{L}^i \cdot \delta \mathbf{q}^i) dV^i . \tag{2.62}$$

The above equation may be rewritten by using Eq. (2.30) for the first term on the right hand side and the following abbreviation for the second term

$$\mathbf{Q}_Q^i = -\int_{V^i} (\rho^i \mathbf{L}^{iT} \cdot \dot{\mathbf{L}}^i \cdot \dot{\mathbf{q}}^i) dV^i , \tag{2.63}$$

which yields, see also Eq. (2.6),

$$\delta W_I^i = [\mathbf{M}^i \cdot \ddot{\mathbf{q}}^i - \mathbf{Q}_Q^i]^T \cdot \delta \mathbf{q}^i . \tag{2.64}$$

The first part in the bracket denotes the second order inertia forces whereas the second part collects the quadratic terms in velocities and is known as *Quadratic Velocity Vector*

denoting gyroscopic and Coriolis forces. By distinguishing between three components of the quadratic velocity vector associated with three sets of the generalized coordinates and after performing some mathematical manipulations one obtains, for details see [124],

$$\mathbf{Q}^i_{Q_R} = -\mathbf{A}^i \cdot \left((\widetilde{\boldsymbol{\omega}}^i)^2 \cdot \int_{V^i} \rho^i \bar{\mathbf{u}}^i dV^i + 2\widetilde{\boldsymbol{\omega}}^i \cdot \int_{V^i} \rho^i \mathbf{S}^i dV^i \cdot \dot{\mathbf{q}}^i_e \right) , \tag{2.65}$$

$$\mathbf{Q}^i_{Q_\theta} = -2\dot{\mathbf{G}}^{iT} \cdot \int_{V^i} (\rho^i \tilde{\bar{\mathbf{u}}}^{iT} \cdot \tilde{\bar{\mathbf{u}}}^i) dV^i \cdot \bar{\boldsymbol{\omega}}^i - 2\dot{\mathbf{G}}^{iT} \cdot \int_{V^i} (\rho^i \tilde{\bar{\mathbf{u}}}^i \cdot \mathbf{S}^i) dV^i \cdot \dot{\mathbf{q}}^i_e \tag{2.66}$$

$$- 2\mathbf{G}^{iT} \cdot \int_{V^i} (\rho^i \tilde{\bar{\mathbf{u}}}^{iT} \cdot \dot{\tilde{\bar{\mathbf{u}}}}^i) dV^i \cdot \bar{\boldsymbol{\omega}}^i,$$

$$\mathbf{Q}^i_{Q_e} = -\int_{V^i} \rho^i \mathbf{S}^{iT} \cdot \left((\widetilde{\boldsymbol{\omega}}^i)^2 \cdot \bar{\mathbf{u}}^i + 2(\widetilde{\boldsymbol{\omega}}^i) \cdot \dot{\bar{\mathbf{u}}}^i_e \right) dV^i \ . \tag{2.67}$$

The components of the quadratic velocity vector are highly nonlinear functions of the system generalized coordinates and velocities.

Generalized Constraint Forces

Multibody systems consisting of interconnected flexible and rigid bodies are basically subjected to some kinematic constraints which restrict the motion of the bodies relative to each other. In general, constraints may be classified into three main groups: mechanical joints such as revolute, prismatic and spherical joints, constraints which impose a prescribed motion such as rheonomic constraints and finally contact constraints. In this section, only the effect of the first and the second groups is considered and the treatment of contact constraints as the main subject of this work is explained in the proceeding chapters.

As a result of the constrained motion, the system coordinates used for description of the motion are not independent. Their dependency may be stated with the constraint functions in the implicit form of algebraic equations

$$\boldsymbol{\Phi}(\mathbf{q}, t) = \mathbf{0} \ . \tag{2.68}$$

Here, only the holonomic constraints expressed in the form of Eq. (2.68) are considered and the disscussion of the non-holonomic constraints will be ignored. Incorporation of the constraints in the type of Eq. (2.68) into the differential equations of motion may be carried out through different ways: the Lagrange multiplier method, the penalty method, the augmented Lagrange method, the relative coordinates method and special methods for hinge joints and internal element constraints. A partial list of publications devoted to this subject can be found in [146]. In the formulation presented in this work, the Lagrange multiplier method is used which is a widely-used method in this framework.

The procedure based on the Lagrange multiplier method replaces the constraint forces with an equivalent relation which finally leads to the system of differential algebraic

equations. Among all system constraints of Eq. (2.68), assume that body i is subjected to n_{c_i} constraints. The constraint equations that describe this condition can be written as

$$\Phi_k(\mathbf{q}, t) = 0 \ , \qquad k = 1, \cdots, n_{c_i} \ . \tag{2.69}$$

The generalized reaction forces $\mathbf{Q}_C^i$ of body i can be expressed in terms of the Lagrange multipliers $\boldsymbol{\lambda}_C$ associated with the constraints of Eq. (2.68) as

$$\mathbf{Q}_C^i = -\boldsymbol{\Phi}_{\mathbf{q}^i}^T \cdot \boldsymbol{\lambda}_C \ . \tag{2.70}$$

Based on this relation, there will not be any contribution from other constraints that do not involve body i.

Equations of Motion of Flexible Multibody Systems

In the previous subsections, the generalized forces associated with the flexible body i have been derived which include generalized elastic, damping, external, inertia and constraint forces. Now, one can derive the corresponding equations of motion for body i based on the principle of virtual work in dynamics

$$\delta W_I^i = \delta W_S^i + \delta W_D^i + \delta W_E^i + \delta W_C^i \ , \tag{2.71}$$

which states that the virtual work of the inertia forces acting on the body i (δW_I^i) is equivalent to the summation of the virtual works of the elastic forces (δW_S^i), the damping forces (δW_D^i), the external forces (δW_E^i) and the constraint forces (δW_C^i). The above equation can be written in terms of the generalized forces

$$[\mathbf{M}^i \cdot \ddot{\mathbf{q}}^i - \mathbf{Q}_Q^i]^T \cdot \delta\mathbf{q}^i = (-\mathbf{q}^{iT} \cdot \mathbf{K}^i \cdot \delta\mathbf{q}^i) + (-\dot{\mathbf{q}}^{iT} \cdot \mathbf{D}^i \cdot \delta\mathbf{q}^i) + (\mathbf{Q}_E^{iT} \cdot \delta\mathbf{q}^i) + (\mathbf{Q}_C^{iT} \cdot \delta\mathbf{q}^i) \ , \tag{2.72}$$

which finally leads to

$$\mathbf{M}^i \cdot \ddot{\mathbf{q}}^i + \mathbf{D}^i \cdot \dot{\mathbf{q}}^i + \mathbf{K}^i \cdot \mathbf{q}^i + \boldsymbol{\Phi}_{\mathbf{q}^i}^T \cdot \boldsymbol{\lambda}_C = \mathbf{Q}_E^i + \mathbf{Q}_Q^i \ , \tag{2.73}$$

where $\mathbf{Q}_E^i$ and $\mathbf{Q}_Q^i$ have to be substituted from their corresponding relations. Maybe it is important to emphasize that the constraints Jacobian matrix $\boldsymbol{\Phi}_{\mathbf{q}^i}^T$ of Eq. (2.73) is a part of the system constraints Jacobian matrix which corresponds to the generalized coordinates of body i and does not include any contribution from other constraints that do not involve body i. The Lagrange multipliers vector $\boldsymbol{\lambda}_C$ in this equation includes all constraint forces in the system. In this way, the connection of body i with the other parts of the system is considered properly.

Equation (2.73) is the extension of Eq. (2.12) to the flexible body i. The further extension to n_b bodies and corporation of the second derivatives of the constraints may be followed in the same manner as for the rigid multibody case, see Eqs. (2.13) and (2.16).

2.4 Generation of Equations of Motion

In the following, some general aspects of the procedures used for generation of equations of motion in flexible multibody systems are introduced. In general, these procedures may be divided into two main groups of symbolic and numerical approaches.

2.4.1 Symbolic Generation

One major advantage of the symbolic generation approach appears when data such as some vector components vanish for a specific application. Symbolic generation of equations of motion can speed up the solution process since by simplification of the symbolic expression of the output, the number of arithmetic operations needed for evaluation can be considerably reduced. However, the final symbolic equations are integrated numerically since the resulting differential equations are generally highly nonlinear and, therefore, it is sometimes impossible to obtain closed form solutions.

Symbolic formulation of flexible multibody systems as an extension to previously developed procedures for rigid multibody systems was first applied to open loop flexible manipulators [21] and further was extended to closed loop systems using a so-called cut-joint constraints technique, see [44, 45, 94]. In [94] a formalism for flexible multibody systems based on a minimum set of generalized coordinates and symbolic computation is proposed. The time-invariant system matrices describing the elastodynamics behavior of the flexible bodies are treated by a standardized object oriented data model. The final equations of motion are derived in a form independent of the modelling technique used.

2.4.2 Numerical Generation

Incorporating flexible multibody systems for computational contact procedures in this thesis has been done through different ways. In some simple cases, the procedure in Section 2.3 based on the floating frame of reference is directly followed and the equations of motion are derived with the help of MAPLE. In the second and the third approaches, a model of the flexible body is first created in the finite element software ANSYS. Then, by performing a modal analysis in ANSYS, the results are stored for further use. In the next step, the stored information is loaded in a SIMPACK preprocessor and transformed to another standard format which is normally referred to as Standard Input Data (SID) [140, 141, 142]. From this point, in the second approach the equations of motion are generated in MATLAB by extracting the input data. In the third approach the model is generated directly in SIMPACK. What follows, gives a brief explanation of the generation of an SID file in SIMPACK.

Standard Input Data

The multibody system software SIMPACK is a general purpose software in the field of multibody dynamics and is being used in the automotive, railway, aerospace and other general mechanical industries. Incorporation of flexible multibody systems in SIMPACK is based on a modal representation with respect to the floating reference frame. The required steps to do so are illustrated in Figure 2.4. Based on a finite element model provided by a finite element software, the finite element-multibody interface of SIMPACK (FEMBS) [41] reads the finite element model and generates a so-called Flexible Body Input (FBI) file whose format is independent of the used FE software. The FE models of flexible bodies contain usually a large number of nodal coordinates whereas FEMBS aims to generate a modal elastic body model as an SID file with a comparatively low number of modal coordinates. The following points must be included in the input FE model for FEMBS:

1. nodes information including degrees of freedom and their positions with respect to a body reference frame,

2. mass and stiffness matrices,

3. translational and rotational mode shapes and corresponding eigenfrequencies,

4. geometric stiffness matrix and load vectors if required.

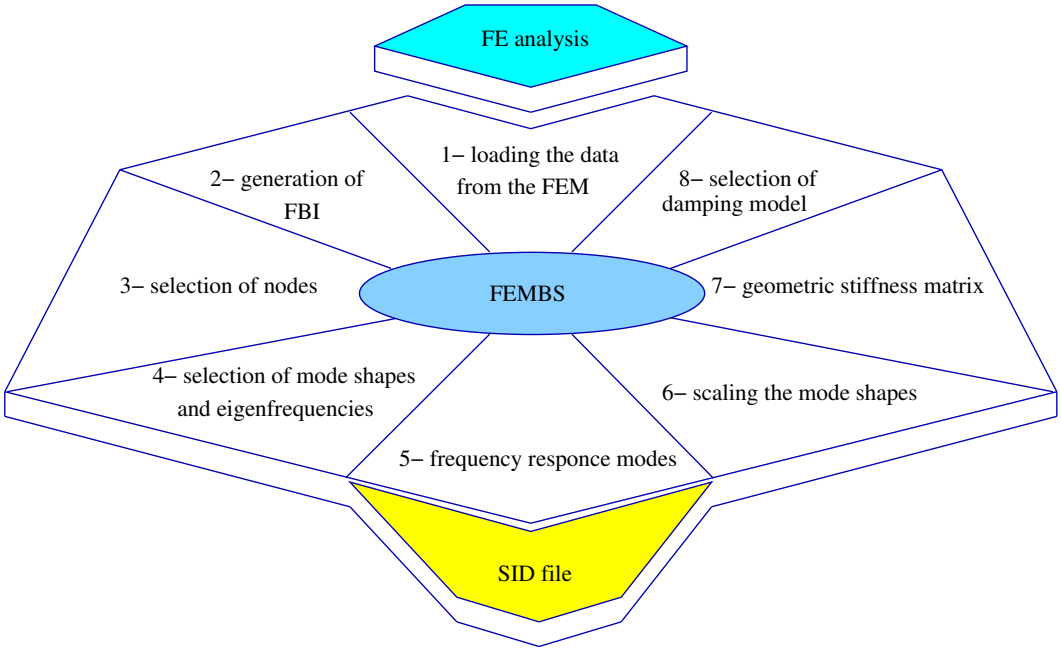

Figure 2.4: Generating the SID file from an FE analysis in SIMPACK

While using the FEMBS interface, a selection of the desired nodes and modes necessary for simulation is performed. An important issue which has a significant effect on the simulation results for some applications is the proper handling of *frequency response modes*. Therefore, the frequency response modes and their corresponding load cases are defined in FEMBS. Since the deformations due to unit loads acting at attachment points are described using so-called correction modes, FEMBS enables the analyst to use frequency response modes for this purpose. For setting up a modal representation of elastic deformations, the most significant forces within coupling elements and the corresponding load cases are to be defined. For doing so, the unit load case of each attachment node is separately defined. Finally, calculation of frequency response modes and the associated frequencies is done with providing an excitation frequency and a maximum frequency. In the next step, scaling the mode shapes is to be done to proceed to the further steps.

As another important issue, geometric stiffening effects are to be taken into consideration, see Section 2.3.4. This fact becomes important when dealing with flexible structures with very stiff and soft mode shapes in orthogonal directions. For consideration of the geometric stiffenning effect in FEMBS, the corresponding terms must be calculated in the finite element code and finally can be selected within FEMBS for further considerations.

Finally, one has to choose a damping model. FEMBS provides two damping models based on the modal and natural damping values, respectively, the stiffness and mass values of the modes, see [41]. When it is done, FEMBS writes an SID file.

An SID file contains the volume integrals needed to establish the equations of motion of a flexible multibody system. In general, an SID file is composed of the input data of a flexible body including description of the attachment points like coupling and observation points, rigid body and linear modal mass matrices, inertia coupling matrices, mode shapes, stiffness and damping matrices, geometric stiffness matrices and frequency response modes. In fact, the input data or the sub-matrices of the equations of motion are represented as functions of the system generalized coordinates in the form of Taylor series with different orders.

In order to generate the equations of motion based on the SID file concept, the required terms stored in the SID file have to be extracted in a preprocessing step and the input data are approximated with the associated Taylor series. A detailed description about the structure of an SID file can be found in [140, 141].

2.5 Numerical Integration

In addition to the difficulties involved with numerical integration of rigid multibody systems, flexible multibody systems consisting of interconnected rigid and flexible objects comprise some other difficulties and, therefore, special attention has been paid to their

simulation. Gross motion of the body reference frame corresponding to rigid body motion and small elastic deformations may have usually different time scales during numerical integration, i.e. the system equations are stiff. This problem has been addressed extensively by researchers, e.g. [19, 59, 126, 127]. In [126, 127] the behavior of numerical time integration methods in flexible multibody systems is investigated and some recommendations for their practical use are given. Different definitions for a system of stiff equations have been proposed in the literature. In [59] stiff equations are supposed as the problems for which explicit methods do not lead to a successful numerical integration. As another definition in [38] for a stiff system, the required step size is limited additionally by a stability bound which restricts the step size more than the tolerance bound.

The numerical integration approaches applied for stiff DAE are often based on approaches developed for ODE. The required conditions for which standard ODE solvers may lead to acceptable solution when applied to DAEs are presented in [18]. In addition, the DAE solvers are usually implicit and require a corrector iteration process based on e.g. Newton iteration method, see [59].

As a result of using implicit methods, the required time step can be much larger than for explicit procedures which turns out to be well suited when dealing with stiff systems. Some widely-used methods based on the implicit approach may be mentioned as the Newmark method, the implicit Runge-Kutta method and backward differentiation formulas (BDF). The Newmark family of methods were presented as single step methods for the solution of structural dynamic problems. Several methods have been contributed in this framework to improve the numerical properties of the Newmark approach by introducing numerical damping at high frequencies without degrading the order of accuracy. The generalized α method proposed by Chung and Hulbert [23] and the Hilbert-Hughes-Taylor algorithm [69] may be mentioned among all. The numerical integration RADAU5 belongs to the class of implicit Runge-Kutta methods of 5^{th} order. The RADAU5 is a single step method and is well suited for stiff DAE [59]. As another approach, the solver DASSL applies backward differentiation formulae which follows a multi step procedure [18]. It is based on interpolating the solution points instead of the derivatives in which the order of the method is set by changing the number of interpolation points.

Another class of integrators attempts to preserve invariants of the dynamic system such as energy. A so-called energy decaying scheme was proposed in [13] which guarantees unconditional stability in the nonlinear regime by dissipating the high frequencies. The proposed approach meets four requirements: nonlinear unconditional stability, treatment of both geometric and material nonlinearities, exact fulfillment of the constraints, and numerical dissipation of high frequency.

The already mentioned approaches were only some of the most important and frequently used ones in the context of flexible multibody systems.

Chapter 3

Contact Treatments in Multibody Systems

Contact introduces a dependency between coordinates of the contacting bodies and, therefore, their corresponding constraints have to be imposed in the system. First, the equations of motion including the contact forces in a matrix form are rewritten. Then, calculation of the contact forces from some widely-used approaches is explained shortly.

3.1 Contact Forces in Flexible Multibody Systems

The equations of motion of the flexible bodies derived in Chapter 2 can be extended by taking into account the effect of generalized contact forces $\mathbf{F}_C$

$$\mathbf{M} \cdot \ddot{\mathbf{q}} + \mathbf{D} \cdot \dot{\mathbf{q}} + \mathbf{K} \cdot \mathbf{q} + \mathbf{\Phi}_{\mathbf{q}}^T \cdot \boldsymbol{\lambda}_C = \mathbf{Q}_E + \mathbf{Q}_Q + \mathbf{F}_C \ . \tag{3.1}$$

When two bodies come in contact, normal and tangential contact forces arise as the result of the collision. Therefore, the contact force vector $\mathbf{F}_C$ in Eq. (3.1) for n_c contact points can be supposed to be the summation of normal and tangential forces which are written in terms of two vectors $\boldsymbol{\lambda}_N$ and $\boldsymbol{\lambda}_T$, respectively, see [106],

$$\mathbf{F}_C = \sum_{l=1}^{n_c} (\mathbf{W}_N^l \lambda_N^l + \mathbf{W}_T^l \lambda_T^l) = \mathbf{W}_N \cdot \boldsymbol{\lambda}_N + \mathbf{W}_T \cdot \boldsymbol{\lambda}_T \ , \tag{3.2}$$

where

$$\begin{aligned} \mathbf{W}_N &= \left[\begin{array}{ccc} \mathbf{W}_N^1 & \dots & \mathbf{W}_N^{n_c} \end{array} \right] , \qquad \mathbf{W}_T = \left[\begin{array}{ccc} \mathbf{W}_T^1 & \dots & \mathbf{W}_T^{n_c} \end{array} \right] , \\ \boldsymbol{\lambda}_N &= \left[\begin{array}{ccc} \lambda_N^1 & \dots & \lambda_N^{n_c} \end{array} \right]^T , \qquad \boldsymbol{\lambda}_T = \left[\begin{array}{ccc} \lambda_T^1 & \dots & \lambda_T^{n_c} \end{array} \right]^T . \end{aligned} \tag{3.3}$$

The matrices $\mathbf{W}_N$ and $\mathbf{W}_T$ project respectively the normal and tangential contact forces to the generalized directions. Equation (3.1) can be rewritten by using Eq. (3.2) and

summarizing internal, external and Coriolis forces with the symbol $\mathbf{h}$

$$\mathbf{M}\cdot\ddot{\mathbf{q}}+\mathbf{\Phi}_{\mathbf{q}}^{T}\cdot\boldsymbol{\lambda}_{C}=\mathbf{h}+\mathbf{W}_{N}\cdot\boldsymbol{\lambda}_{N}+\mathbf{W}_{T}\cdot\boldsymbol{\lambda}_{T}\ . \tag{3.4}$$

One may summarize Eq. (3.4) together with the second derivatives of the constraints, see also Eq. (2.15),

$$\mathbf{\Phi}(\mathbf{q},t)=\mathbf{0}\qquad\rightarrow\qquad\mathbf{\Phi}_{\mathbf{q}}\cdot\ddot{\mathbf{q}}=-\mathbf{\Phi}_{tt}-\left(\mathbf{\Phi}_{\mathbf{q}}\cdot\dot{\mathbf{q}}\right)_{\mathbf{q}}\cdot\dot{\mathbf{q}}-2\mathbf{\Phi}_{\mathbf{q}t}\cdot\dot{\mathbf{q}}=\boldsymbol{\gamma}\ , \tag{3.5}$$

in the compact matrix form as

$$\underbrace{\begin{bmatrix}\mathbf{M}&\mathbf{\Phi}_{q}^{T}\\ \mathbf{\Phi}_{q}&\mathbf{0}\end{bmatrix}}_{\mathbf{M}_{c}}\cdot\underbrace{\begin{bmatrix}\ddot{\mathbf{q}}\\ \boldsymbol{\lambda}_{C}\end{bmatrix}}_{\ddot{\mathbf{q}}_{c}}=\underbrace{\begin{bmatrix}\mathbf{h}\\ \boldsymbol{\gamma}\end{bmatrix}}_{\mathbf{h}_{c}}+\begin{bmatrix}\mathbf{W}_{N}&\mathbf{W}_{T}\\ \mathbf{0}&\mathbf{0}\end{bmatrix}\cdot\begin{bmatrix}\boldsymbol{\lambda}_{N}\\ \boldsymbol{\lambda}_{T}\end{bmatrix}\ . \tag{3.6}$$

3.2 Calculation of Contact Forces

Formulation of some frequently-used approaches applied to incorporate contact constraints into the governing equations on the system is given briefly. Herein the penalty technique, the Lagrange multipliers method, procedures yielding linear complementarity problems (LCPs) and finally the proximal point formulation are introduced shortly. Each approach has some advantages and some disadvantages and an appropriate procedure has to be chosen.

3.2.1 Compliance Contact Method: The Penalty Approach

In this approach contact is modeled by a continuous force-displacement law over the contact duration which is represented by material compliance and damping. For this purpose, the normal contact force law follows a penalty formulation by considering some spring-damper elements at contact region of colliding bodies

$$F_{n}^{l}=K^{l}\delta^{l}+D^{l}v_{n}^{l}\ ,\qquad l=1,\ldots,n_{c}\ , \tag{3.7}$$

where l is the contact counter, n_c is the number of contacts, K^l and D^l are the stiffness and damping coefficients, respectively, δ^l denotes penetration and v_n^l is the relative normal velocity of colliding bodies at contact point. In [81] the stiffness coefficient has been formulated based on the impulse-momentum conservation principle for impact between two bodies i and j with masses M_i and M_j

$$K=\frac{M_{i}M_{j}}{M_{i}+M_{j}}\left(\frac{v_{n_{ij}}}{\delta_{ij}}\right)^{2}\ , \tag{3.8}$$

where δ_{ij} and $v_{n_{ij}}$ are the values of maximum penetration and relative velocity of impacting bodies at the contact point just at the start of the compression. In order to guarantee that the damping force satisfies the boundary conditions at contact and separation, a linear function in the form of $D = \zeta\delta$ has been chosen in which δ is the current value of penetration and ζ is called *hysteresis damping factor* and is a function of masses M_i and M_j, stiffness coefficient K, penetration δ_{ij} and relative velocity $v_{n_{ij}}$. The normal force law in the penalty formulation may also be a nonlinear spring-damper element with a defined exponent e, see e.g. [70, 85],

$$F_n^l = K^l \delta^{l^e} + D^l v_n^l \ , \qquad \text{with} \qquad D^l = \zeta^l \delta^{l^e} \ , \qquad l = 1, \ldots, n_c \ . \tag{3.9}$$

There are some other proposed approaches which relate the stiffness coefficient with material properties of contacting bodies including Young's modulus, Poisson's ratio and a so-called elastic layer thickness, see e.g. [74].

Consideration of friction which imposes tangential forces is often done by using a regularized Coulomb friction model based on a continuous regularized function $\phi(v_t^l, v_\epsilon)$, see also Eq. (6.6),

$$F_t^l = \mu F_n^l \phi(v_t^l, v_\epsilon) \ , \tag{3.10}$$

where μ is the coefficient of friction, v_ϵ is a given limit of slip velocity and v_t^l is the relative tangential velocity of colliding bodies at contact point. Although the friction states are distinguished between sliding and sticking phases, the regularized Coulomb friction does not consider the sticking phase properly. In this model, the sticking friction force is approximated with a function dependent on the relative tangential velocity v_t^l of contacting bodies at contact point. In fact, such formulations state a variable friction coefficient which changes from zero for $v_t^l = 0$ and reaches a constant value corresponding to the sliding friction coefficient when the relative tangential velocity exceeds the limit of slip velocity $v_t^l \geq v_\epsilon$. The values of normal contact force F_n^l and tangential contact force F_t^l obtained from Eqs. (3.7) (or (3.9)) and (3.10) can be substituted in Eq. (3.2) with the values of λ_N^l and λ_T^l, respectively, to obtain the generalized contact force vector $\mathbf{F}_C$.

3.2.2 The Lagrange Multipliers Approach

In order to impose exactly contact constraints $\mathbf{\Omega} = \mathbf{0}$ in the equations of motion, one can use the *Lagrange Multipliers method* (sometimes known as the *kinematic constraint method*) [29, 155, 154]. In this approach for all contacts between bodies, contact constraint equations are derived and appended to the equations of motion, see e.g. [123]. Their treatment can be carried out in the same manner as the joint constraints. Therefore, the contact force vector in Eq. (3.1) can be written as

$$\mathbf{F}_C = \mathbf{\Omega}_\mathbf{q}^T \cdot \boldsymbol{\lambda} \ , \tag{3.11}$$

which yields

$$\mathbf{M} \cdot \ddot{\mathbf{q}} + \mathbf{D} \cdot \dot{\mathbf{q}} + \mathbf{K} \cdot \mathbf{q} + \mathbf{\Phi}_{\mathbf{q}}^T \cdot \boldsymbol{\lambda}_C + \mathbf{\Omega}_{\mathbf{q}}^T \cdot \boldsymbol{\lambda} = \mathbf{Q}_E + \mathbf{Q}_Q \ . \tag{3.12}$$

Here $\boldsymbol{\lambda}_C$ denotes the vector of constraint forces, $\boldsymbol{\lambda}$ is the vector of contact forces and $\mathbf{\Omega}_{\mathbf{q}}$ is the Jacobian matrix associated with the contact constraints $\mathbf{\Omega} = \mathbf{0}$. By using this method, the continual contact is modeled well. However, this method cannot be used easily for contact between bodies with complicated geometries and non-continuous contact due to the difficulties involved with the generation and fulfillment of the contact constraints in a systematic way.

3.2.3 Contact as Linear Complementarity Problems

In Section 1.2 the contact modeling methods yielding the linear complementarity problems were briefly introduced. In such approaches, contact constraints are represented as complementarity relations and then, the contact kinematics is formulated as a complementarity problem.

Complementarity Relations

Considering two colliding bodies in Figure 3.1, the normal contact law on position level for a potential contact pair l may be characterized by imposing complementarity condition between the normal gap distance g_N^l and contact force λ_N^l, see Figure 3.2 left,

$$g_N^l \geq 0 \ , \qquad \lambda_N^l \geq 0 \ , \qquad g_N^l \lambda_N^l = 0 \ , \tag{3.13}$$

where

$$g_N^l = \mathbf{g}_{ij}^l \cdot \mathbf{n}_i = -\mathbf{g}_{ij}^l \cdot \mathbf{n}_j \ . \tag{3.14}$$

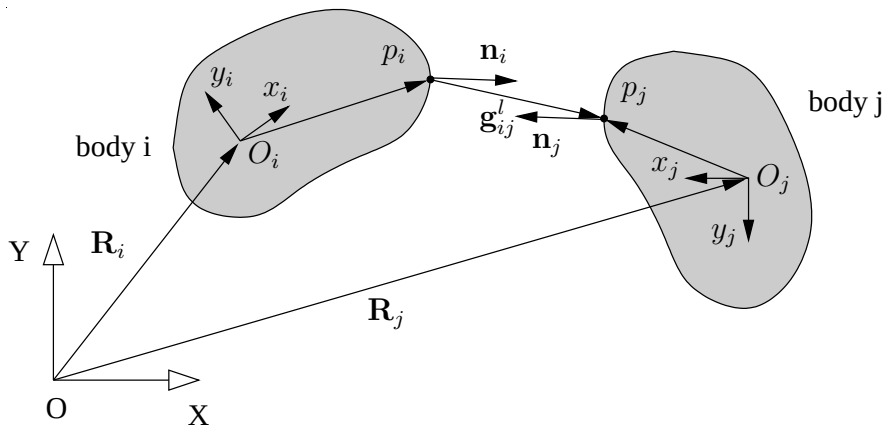

Figure 3.1: Contact kinematics

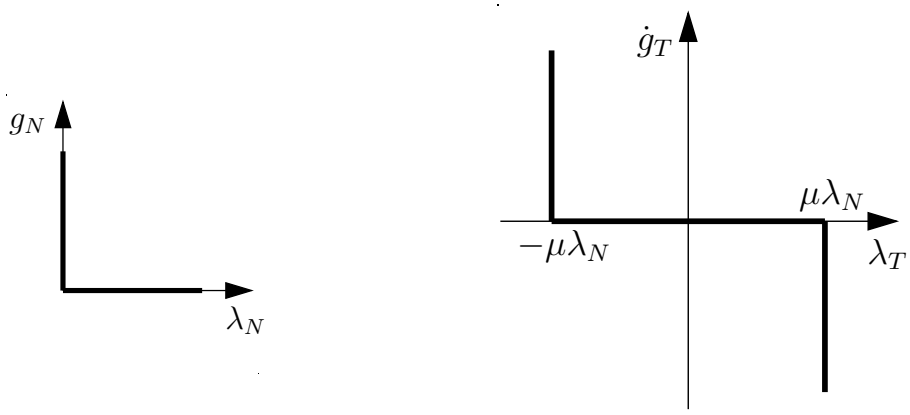

normal contact law tangential contact law

Figure 3.2: Normal and tangential contact laws, see [106]

Equation (3.13) ensures impenetrability of contact and includes all possible situations of normal contact such as separation ($g_N^l \geq 0, \lambda_N^l = 0$), transition to contact ($g_N^l = 0, \lambda_N^l \geq 0$), active contact ($g_N^l = 0, \lambda_N^l > 0$) and transition to detachment ($g_N^l \geq 0, \lambda_N^l = 0$), see e.g. [107].

One may also write the normal contact law on velocity level by considering the velocity of normal gap, $\dot{g}_N^l$, instead of the normal gap distance

$$\dot{g}_N^l \geq 0 \ , \qquad \lambda_N^l \geq 0 \ , \qquad \dot{g}_N^l \lambda_N^l = 0 \ . \tag{3.15}$$

It is noticeable that unlike the relation on position level, the formulation on velocity level is only applicable for closed contacts. It is also a common approach to express complementarity relations of Eqs. (3.13) and (3.15) in terms of impulsive force Λ_N^l instead of λ_N^l, see e.g. [134].

Both cases of complementarity relations (3.13) and (3.15) on position and velocity levels can handle normal continual contact and impact of planar flexible bodies, see Chapter 5. However, normal continual contact of planar flexible bodies may also be treated by considering complementarity relations on acceleration level [31, 34]

$$\ddot{g}_N^l \geq 0 \ , \qquad \lambda_N^l \geq 0 \ , \qquad \ddot{g}_N^l \lambda_N^l = 0 \ . \tag{3.16}$$

For tangential continual contact and impact of planar flexible bodies, complementarity relations may be written either on velocity level or on acceleration level. For this purpose, the Coulomb friction model is used which distinguishes between two cases of sticking and sliding friction, see Figure 3.2 right. Formulating tangential contact is not a trivial task. The tangential characteristic of contact has to be decomposed according to Figure 3.3. By denoting λ_T^l for tangential force, μ^l for friction coefficient and $\dot{g}_T^l$ for relative tangential velocity, the complementarity relation on velocity level for tangential contact may be

obtained as, see e.g. [134],

$$\begin{aligned} \dot{g}_T^{+l} \geq 0 \ , \qquad \lambda_{H0}^{(+)l} \geq 0 \ , \qquad \dot{g}_T^{+l} \lambda_{H0}^{(+)l} = 0 \ , \\ \dot{g}_T^{-l} \geq 0 \ , \qquad \lambda_{H0}^{(-)l} \geq 0 \ , \qquad \dot{g}_T^{-l} \lambda_{H0}^{(-)l} = 0 \ , \end{aligned} \tag{3.17}$$

where

$$\begin{aligned} \dot{g}_T^{+l} = \frac{1}{2}(|\dot{g}_T^l| + \dot{g}_T^l) \geq 0 \ , \qquad \lambda_{H0}^{(+)l} = \mu^l \lambda_N^l + \lambda_T^l \ , \\ \dot{g}_T^{-l} = \frac{1}{2}(|\dot{g}_T^l| - \dot{g}_T^l) \geq 0 \ , \qquad \lambda_{H0}^{(-)l} = \mu^l \lambda_N^l - \lambda_T^l \ . \end{aligned} \tag{3.18}$$

Following a more sophisticated strategy, one may obtain the complementarity relations on acceleration level for tangential contact, see e.g. [106]. However, formulation on velocity level is preferred since it needs less effort to formulate tangential continual contact and impact. Furthermore, it is physically more realistic.

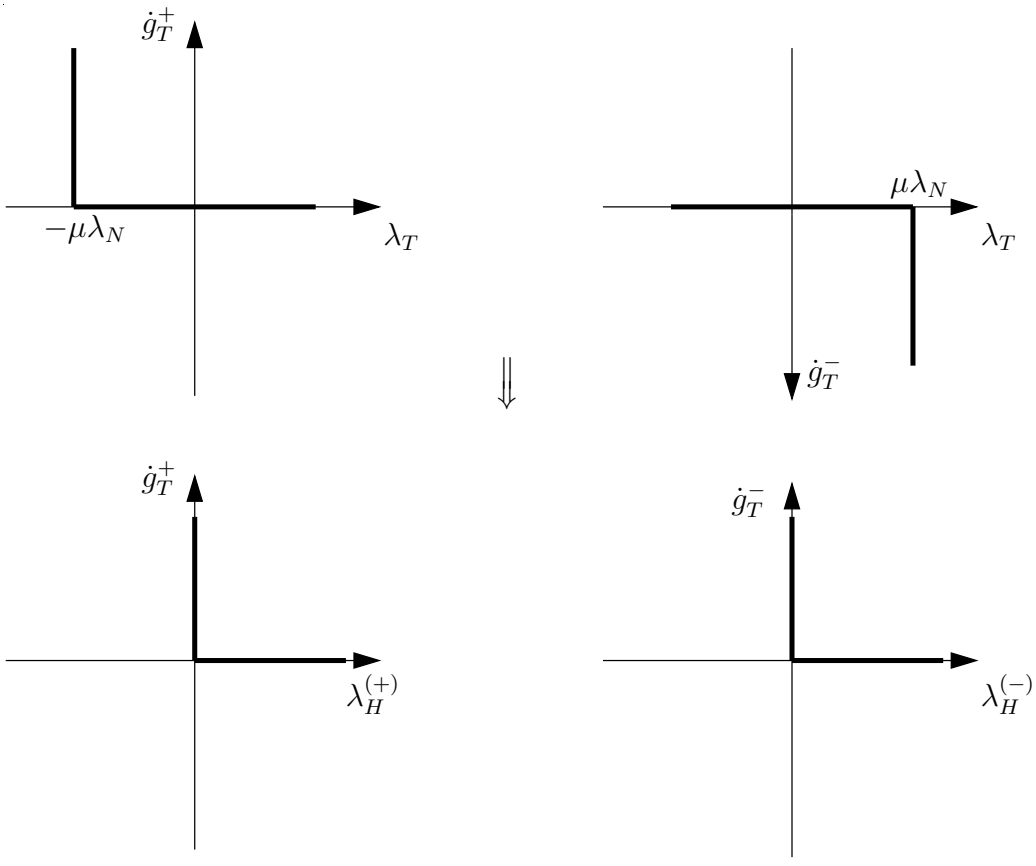

Figure 3.3: Decomposition of the friction law, see [106, 134]

Complementarity Problem

For simplicity let us consider here only the formulation on acceleration level for frictionless continual contact. Formulations on position and velocity levels including friction may also be considered with some more difficulties by keeping the same idea, see Chapters 4 and 5.

In order to formulate the contact problem, one has to find a relation between acceleration of normal gaps and normal contact forces. Obtaining such a required relation is followed in some steps. First, based on the kinematics of contact the acceleration of normal gaps are written in terms of the generalized accelerations. Then, the generalized accelerations are formulated from the equations of motion in terms of the normal contact forces. Substituting the generalized accelerations in the relation of the acceleration of normal gaps together with the complementarity relation of Eq. (3.16) written for all contacts yields to a linear complementarity problem in the general form

$$\ddot{\mathbf{g}}_N = \mathbf{a} \cdot \boldsymbol{\lambda}_N + \mathbf{b} \ , \qquad \ddot{\mathbf{g}}_N \geq \mathbf{0} \ , \qquad \boldsymbol{\lambda}_N \geq \mathbf{0} \ , \qquad \ddot{\mathbf{g}}_N \cdot \boldsymbol{\lambda}_N = 0 \ . \tag{3.19}$$

The unknown vectors $\ddot{\mathbf{g}}_N$ and $\boldsymbol{\lambda}_N$ may be calculated by a standard LCP solver like Lemke's algorithm [25]. It is noticeable that an LCP of the first or the second order can be solved analytically [29], too.

3.2.4 Proximal Point Formulation

In addition to linear complementarity problems, there exist some other formulations which are based on the same mathematical concept as LCP but are formulated differently and, therefore, follow different solution strategies. Investigation of such formulations started with the work by Alart and Curnier [2] and after a short time became a popular approach, see e.g. [47, 86, 135]. In this framework, the complementarity relations denoting contact/impact laws are transformed to variational inequalities and finally are solved in an iterative process as a proximal point formulation.

We consider the complementarity relation of Eq. (3.15) and express it in the following variational inequality for the set of all active contacts $l \in I_N$, see e.g. [55, 151],

$$-\dot{g}_N^l({\lambda_N^*}^l - \lambda_N^l) \leq 0 \ , \qquad \lambda_N^l \in C_N \ , \qquad \forall {\lambda_N^*}^l \in C_N \ , \tag{3.20}$$

where C_N is the convex set which contains all admissible contact forces $\boldsymbol{\lambda}_N^*$

$$C_N = \{\boldsymbol{\lambda}_N^* : \ \boldsymbol{\lambda}_N^* \geq \mathbf{0}\} \ . \tag{3.21}$$

In order to show that Eqs. (3.15) and (3.20) are equivalent, see also [55], first consider Eq. (3.15). By using the complementarity relation of Eq. (3.15), Eq. (3.20) is simplified to $\dot{g}_N^l {\lambda_N^*}^l \geq 0 \ , \ \forall {\lambda_N^*}^l \in C_N$ which is correct since both $\dot{g}_N^l$ and ${\lambda_N^*}^l$ are positive. Now, Eq.

(3.20) is considered for two cases: for $\lambda_N^l = 0$, it is simplified again to $\dot{g}_N^l \lambda_N^{*\,l} \geq 0$, $\forall \lambda_N^{*\,l} \in C_N$. This results in $\dot{g}_N^l \geq 0$ which is the same condition as in Eq. (3.15). On the other hand, for $\lambda_N^l > 0$ the expression $\lambda_N^{*\,l} - \lambda_N^l$, $\forall \lambda_N^{*\,l} \in C_N$ can take any arbitrary value. Therefore, for fulfillment of Eq. (3.20) one concludes that $\dot{g}_N^l = 0$ which approves again Eq. (3.15). Based on this proof, Eqs. (3.15) and (3.20) are equivalent.

One can reformulate Eq. (3.20) by multiplying an arbitrary positive factor r with the property $r \in \mathbb{R}$ and by adding and subtracting λ_N^l as

$$((\lambda_N^l - r\dot{g}_N^l) - \lambda_N^l)(\lambda_N^{*\,l} - \lambda_N^l) \leq 0 \ , \qquad \lambda_N^l \in C_N \ , \qquad \forall \lambda_N^{*\,l} \in C_N \ . \tag{3.22}$$

The factor r is used to set up a cone normal to C_N. In order to continue the formulation of this procedure, one needs to refer to the orthogonal projection operator from the convex analysis theory with the property, see e.g. [109, 110],

$$(\mathbf{y} - \mathbf{x}) \cdot (\mathbf{x}^* - \mathbf{x}) \leq 0 \ , \qquad \mathbf{x} \in C \ , \qquad \forall \mathbf{x}^* \in C \qquad \Longleftrightarrow \qquad \mathbf{x} = \mathrm{proj}_C(\mathbf{y}) \ , \tag{3.23}$$

where $\mathbf{y} \in \mathbb{R}^n$, and $C \subset \mathbb{R}^n$ is a convex set. Comparing Eqs. (3.22) and (3.23) and considering Eq. (3.22) for all contact pairs leads to the following relation for normal contact forces

$$\boldsymbol{\lambda}_N = \mathrm{proj}_{C_N}(\boldsymbol{\lambda}_N - r\dot{\mathbf{g}}_N) = (\boldsymbol{\lambda}_N - r\dot{\mathbf{g}}_N)^+ \ . \tag{3.24}$$

The symbol + in this equation simply denotes the positive components of the vector $\boldsymbol{\lambda}_N - r\dot{\mathbf{g}}_N$, i.e., it sets the negative components to zero. This fact is based on the definition of the orthogonal projection operator given in Eq. (3.23).

In the solution strategy of the proximal point method for normal contact forces, Eq. (3.24) has to be solved in an iterative process. At each integration step n of the simulation the closed contacts are found and suitable initial values for normal contact forces are chosen. For this purpose, the values of normal contact forces of the first iteration $k = 1$ are substituted from the final normal contact forces of the integration step $n - 1$. For the first integration step they might be set to zero. Using these values, the amount of $\dot{\mathbf{g}}_N$ is calculated from the kinematics of contact. Then, the normal contact forces are modified from Eq. (3.24). This process is followed in an iterative process and based on a prescribed stopping rule untill convergence. Therefore, Eq. (3.24) can be rewritten for the iteration $k + 1$ as

$$\boldsymbol{\lambda}_N^{k+1} = \mathrm{proj}_{C_N}(\boldsymbol{\lambda}_N^k - r\dot{\mathbf{g}}_N^k) = (\boldsymbol{\lambda}_N^k - r\dot{\mathbf{g}}_N^k)^+ \ . \tag{3.25}$$

The proximal point approach eliminates the necessity of generating LCP and simplifies considerably the treatment of friction. However, there are some drawbacks which can effect the efficiency and accuracy of this approach. The most important one is related to the selection of a suitable value for positive factor r in Eq. (3.25). Small values of r can increase the convergence duration while high values yield the problem of ill-conditioning and numerical instabilities. Depending on the kinematic and kinetic properties of the

system for which this approach is used, it might frequently happen that the convergence is reached after many iterations and consequently it requires higher computational effort compared to standard LCP formulation. On the other hand, the accuracy of the results in the best case will not be better than for the LCP. This point is not unexpected since the LCP formulation is based on the exact resolution of the contact/impact problem whereas the proximal point approach aims to solve the problem based on an iterative process.

Chapter 4

Contact of Planar Flexible Systems: LCP Approach

In this chapter and Chapter 5, continual contact and impact events in flexible multibody systems are distinguished from each other. In the former, the contacting bodies are already in contact and the relative acceleration of contact points remains zero for the whole duration of contact. In the latter case the colliding bodies have initially no contact and after awhile come in contact. At this time, they may separate or alternatively keep the continual contact depending on their initial conditions before impact. Although, in many researches and specially ones based on finite element methods no difference between contact and impact of flexible bodies has been taken into account and they have been treated with the same approach, see e.g. [29, 155], in these two chapters they are supposed as two different events due to the different methodologies for dealing with them.

We present first an extended formulation for continual contact of planar flexible bodies and formulation of impact is followed in Chapter 5. This procedure will start by reformulating the kinematics of contact for flexible bodies and will follow by introducing this in the complementarity form known from rigid body formulations. From this chapter, subscripts are used for referring to the parameters of a specific body since superscript l is kept for referring to a contact number.

4.1 Kinematics of Contact

In Figure 4.1 two contacting flexible bodies i and j are depicted. In order to describe position and orientation of these flexible bodies with respect to the inertial coordinate system, two sets of the generalized coordinates $\mathbf{q}_i = (\mathbf{R}_i^T,\ \boldsymbol{\theta}_i^T,\ \mathbf{q}_{e_i}^T)^T$ and $\mathbf{q}_j = (\mathbf{R}_j^T,\ \boldsymbol{\theta}_j^T,\ \mathbf{q}_{e_j}^T)^T$ are used. Here $\mathbf{q}$ is not a vector of minimal coordinates since constraints from joints must be considered by the Lagrange multipliers additionally. Considering the flexible body

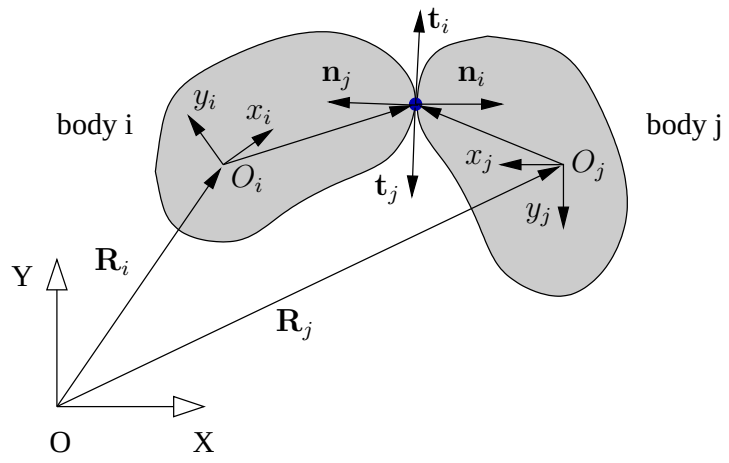

Figure 4.1: Kinematics of continual contact of two planar flexible bodies

i, one can write the velocity of the contact point on the body i associated with the l^{th} contact from Eq. (2.20). For planar bodies, the second term on the right hand side of this equation can be simplified yielding

$$\dot{\mathbf{A}}_i \cdot \bar{\mathbf{u}}_i = \frac{\partial}{\partial \boldsymbol{\theta}_i}(\mathbf{A}_i \cdot \bar{\mathbf{u}}_i^l) \cdot \dot{\boldsymbol{\theta}}_i = \underbrace{\frac{\partial}{\partial \boldsymbol{\theta}_i}(\mathbf{A}_i \cdot (\bar{\mathbf{u}}_{0i}^l + \mathbf{S}_i^l \cdot \mathbf{q}_{ei}))}_{\mathbf{B}_i^l} \cdot \dot{\boldsymbol{\theta}}_i = \mathbf{B}_i^l \cdot \dot{\boldsymbol{\theta}}_i \ , \tag{4.1}$$

where $\mathbf{B}_i^l$ is a 2×1 matrix in the case of planar flexible bodies and the vector $\bar{\mathbf{u}}_{0i}^l$ denotes the position of the l^{th} contact point on the undeformed body i given in the body reference coordinate system. By using Eq. (4.1), Eq. (2.20) can be rewritten as

$$\mathbf{v}_i^l = \dot{\mathbf{R}}_i + \mathbf{B}_i^l \cdot \dot{\boldsymbol{\theta}}_i + \mathbf{A}_i \cdot \mathbf{S}_i^l \cdot \dot{\mathbf{q}}_{ei} \ . \tag{4.2}$$

Equation (4.2) can be further rewritten in the following compact form

$$\mathbf{v}_i^l = \mathbf{L}_i^l \cdot \dot{\mathbf{q}}_i \ , \qquad \text{with} \qquad \mathbf{L}_i^l = \left[\begin{array}{ccc} \mathbf{I} & \mathbf{B}_i^l & \mathbf{A}_i \cdot \mathbf{S}_i^l \end{array} \right] \ , \tag{4.3}$$

where $\mathbf{I}$ is an identity matrix. According to Figure 4.1 and noticing that at contact point the normal vectors $\mathbf{n}_i$ and $\mathbf{n}_j$ and consequently the tangential vectors $\mathbf{t}_i$ and $\mathbf{t}_j$ are aligned with each other, the relative velocities in normal and tangential directions for the l^{th} contact point can be written as

$$\dot{g}_{N_{ij}}^l = \mathbf{n}_i^l \cdot (\mathbf{L}_i^l \cdot \dot{\mathbf{q}}_i - \mathbf{L}_j^l \cdot \dot{\mathbf{q}}_j) \ , \qquad \dot{g}_{T_{ij}}^l = \mathbf{t}_i^l \cdot (\mathbf{L}_i^l \cdot \dot{\mathbf{q}}_i - \mathbf{L}_j^l \cdot \dot{\mathbf{q}}_j) \ . \tag{4.4}$$

The relative accelerations in the normal and tangential directions for the l^{th} contact point are calculated by differentiating the relative velocities

$$\ddot{g}_{N_{ij}}^l = (\mathbf{W}_N^l)_{ij}^T \cdot \ddot{\mathbf{q}}_{ij} + (\mathbf{w}_N^l)_{ij}^T \cdot \dot{\mathbf{q}}_{ij} \ , \qquad \ddot{g}_{T_{ij}}^l = (\mathbf{W}_T^l)_{ij}^T \cdot \ddot{\mathbf{q}}_{ij} + (\mathbf{w}_T^l)_{ij}^T \cdot \dot{\mathbf{q}}_{ij} \ , \tag{4.5}$$

where

$$\dot{\mathbf{q}}_{ij} = \begin{bmatrix} \dot{\mathbf{q}}_i \\ \dot{\mathbf{q}}_j \end{bmatrix},\ \ddot{\mathbf{q}}_{ij} = \begin{bmatrix} \ddot{\mathbf{q}}_i \\ \ddot{\mathbf{q}}_j \end{bmatrix},\ (\mathbf{W}_N^l)_{ij} = \begin{bmatrix} (\mathbf{n}_i^l \cdot \mathbf{L}_i^l)^T \\ -(\mathbf{n}_i^l \cdot \mathbf{L}_j^l)^T \end{bmatrix},\ (\mathbf{W}_T^l)_{ij} = \begin{bmatrix} (\mathbf{t}_i^l \cdot \mathbf{L}_i^l)^T \\ -(\mathbf{t}_i^l \cdot \mathbf{L}_j^l)^T \end{bmatrix},$$
$$(\mathbf{w}_N^l)_{ij} = \begin{bmatrix} (\dot{\mathbf{n}}_i^l \cdot \mathbf{L}_i^l + \mathbf{n}_i^l \cdot \dot{\mathbf{L}}_i^l)^T \\ -(\dot{\mathbf{n}}_i^l \cdot \mathbf{L}_j^l + \mathbf{n}_i^l \cdot \dot{\mathbf{L}}_j^l)^T \end{bmatrix},\quad (\mathbf{w}_T^l)_{ij} = \begin{bmatrix} (\dot{\mathbf{t}}_i^l \cdot \mathbf{L}_i^l + \mathbf{t}_i^l \cdot \dot{\mathbf{L}}_i^l)^T \\ -(\dot{\mathbf{t}}_i^l \cdot \mathbf{L}_j^l + \mathbf{t}_i^l \cdot \dot{\mathbf{L}}_j^l)^T \end{bmatrix}. \quad (4.6)$$

It is clear that the effects of deformations are introduced to the kinematic relation of the relative normal and tangential accelerations ($\ddot{g}_N$ and $\ddot{g}_T$) of the l^{th} contact point through the matrices $\mathbf{L}_i^l$ and $\mathbf{L}_j^l$. Although Eq. (4.5) looks similar to the rigid body case, its evaluation is totally different. This equation which holds for the l^{th} contact point can be used to obtain the matrix form of the relative normal and tangential accelerations ($\ddot{\mathbf{g}}_N$ and $\ddot{\mathbf{g}}_T$) for all n_c contact points between bodies i and j in the form of

$$\ddot{\mathbf{g}}_{N_{ij}} = \begin{bmatrix} \ddot{g}_{N_{ij}}^1 \\ \vdots \\ \ddot{g}_{N_{ij}}^{n_c} \end{bmatrix} = \underbrace{\begin{bmatrix} (\mathbf{W}_N^1)_{ij}^T \\ \vdots \\ (\mathbf{W}_N^{n_c})_{ij}^T \end{bmatrix}}_{(\mathbf{W}_N)_{ij}^T} \cdot \ddot{\mathbf{q}}_{ij} + \underbrace{\begin{bmatrix} (\mathbf{w}_N^1)_{ij}^T \\ \vdots \\ (\mathbf{w}_N^{n_c})_{ij}^T \end{bmatrix}}_{(\mathbf{w}_N)_{ij}^T} \cdot \dot{\mathbf{q}}_{ij}\ , \quad (4.7)$$

$$\ddot{\mathbf{g}}_{T_{ij}} = \begin{bmatrix} \ddot{g}_{T_{ij}}^1 \\ \vdots \\ \ddot{g}_{T_{ij}}^{n_c} \end{bmatrix} = \underbrace{\begin{bmatrix} (\mathbf{W}_T^1)_{ij}^T \\ \vdots \\ (\mathbf{W}_T^{n_c})_{ij}^T \end{bmatrix}}_{(\mathbf{W}_T)_{ij}^T} \cdot \ddot{\mathbf{q}}_{ij} + \underbrace{\begin{bmatrix} (\mathbf{w}_T^1)_{ij}^T \\ \vdots \\ (\mathbf{w}_T^{n_c})_{ij}^T \end{bmatrix}}_{(\mathbf{w}_T)_{ij}^T} \cdot \dot{\mathbf{q}}_{ij}\ , \quad (4.8)$$

or in the compact form of

$$\ddot{\mathbf{g}}_{N_{ij}} = (\mathbf{W}_N)_{ij}^T \cdot \ddot{\mathbf{q}}_{ij} + (\mathbf{w}_N)_{ij}^T \cdot \dot{\mathbf{q}}_{ij}\ , \qquad \ddot{\mathbf{g}}_{T_{ij}} = (\mathbf{W}_T)_{ij}^T \cdot \ddot{\mathbf{q}}_{ij} + (\mathbf{w}_T)_{ij}^T \cdot \dot{\mathbf{q}}_{ij}\ . \quad (4.9)$$

Consequently, one obtains a similar relation for consideration of all active contacts between n_b bodies of the system

$$\ddot{\mathbf{g}}_N = \mathbf{W}_N^T \cdot \ddot{\mathbf{q}} + \mathbf{w}_N^T \cdot \dot{\mathbf{q}}\ , \qquad \ddot{\mathbf{g}}_T = \mathbf{W}_T^T \cdot \ddot{\mathbf{q}} + \mathbf{w}_T^T \cdot \dot{\mathbf{q}}\ , \quad (4.10)$$

where the vectors $\dot{\mathbf{q}}$ and $\ddot{\mathbf{q}}$ are the generalized velocities and accelerations of the system consisting of all n_b bodies. The other parameters of this relation are constructed based on their corresponding variables from each pair of contacting bodies. Then, the relative accelerations $\ddot{\mathbf{g}}_N$ and $\ddot{\mathbf{g}}_T$ and equations of motion of flexible bodies will be used together in order to form complementarity relationships between contact forces and relative accelerations. This procedure will be described next.

Equations of Motion

By separating the tangential contact forces $\boldsymbol{\lambda}_T$ to sliding and sticking forces, one can rewrite Eq. (3.2). The sliding share is simply calculated from the Coulomb friction law.

Therefore, the vector of generalized contact forces $\mathbf{F}_C$ in Eq. (3.2) can be obtained from

$$\mathbf{F}_C = (\mathbf{W}_N + \mathbf{W}_G \cdot \boldsymbol{\mu}_G) \cdot \boldsymbol{\lambda}_N + \mathbf{W}_H \cdot \boldsymbol{\lambda}_H \ . \tag{4.11}$$

Here, $\boldsymbol{\lambda}_H$ denotes the sticking contact forces, the matrices $\mathbf{W}_G$ and $\mathbf{W}_H$ are extracted from the matrix $\mathbf{W}_T$ and correspond to the sliding and sticking contacts, respectively, and the matrix $\boldsymbol{\mu}_G$ collects the coefficients of friction corresponding to the sliding contacts, see [55, 106]. The equations of motion (3.6) can be reformulated by substituting the contact forces from Eq. (4.11)

$$\mathbf{M}_c \cdot \ddot{\mathbf{q}}_c - \mathbf{h}_c - \underbrace{\begin{bmatrix} \mathbf{W}_N + \mathbf{W}_G \cdot \boldsymbol{\mu}_G & \mathbf{W}_H \\ \mathbf{0} & \mathbf{0} \end{bmatrix}}_{\mathbf{W}_{NH}} \cdot \underbrace{\begin{bmatrix} \boldsymbol{\lambda}_N \\ \boldsymbol{\lambda}_H \end{bmatrix}}_{\boldsymbol{\lambda}} = \mathbf{0} \ . \tag{4.12}$$

Now, the equations of motion of multibody systems including constrained and non-constrained rigid and flexible bodies in terms of contact forces which are denoted by $\boldsymbol{\lambda}_N$ and $\boldsymbol{\lambda}_H$ have been obtained. These equations will be used further to construct complementarity relations of the continual contact problem.

4.2 Construction of Complementarity Relations

In this section, a similar procedure as described in [106] to construct complementarity relations of continual contact of planar flexible bodies is used. Maybe at the first view, they seem to be similar to the rigid ones, but the effect of deformations are taken into account through kinematic quantities whose evaluations are totally different.

Starting from Eq. (4.12) and supposing that there is no dependent constraint in the system and so $\mathbf{M}_c$ is a regular matrix, one can find the vector $\ddot{\mathbf{q}}_c$ as a function of the Lagrange multipliers $\boldsymbol{\lambda}$

$$\ddot{\mathbf{q}}_c = \mathbf{M}_c^{-1} \cdot \mathbf{h}_c + \mathbf{M}_c^{-1} \cdot \mathbf{W}_{NH} \cdot \boldsymbol{\lambda} \ . \tag{4.13}$$

Then, Eq. (4.10) is rewritten for sliding and sticking contacts

$$\ddot{\mathbf{g}}_{NH} = \begin{bmatrix} \ddot{\mathbf{g}}_N \\ \ddot{\mathbf{g}}_H \end{bmatrix} = \begin{bmatrix} \mathbf{W}_N^T \\ \mathbf{W}_H^T \end{bmatrix} \cdot \ddot{\mathbf{q}} + \begin{bmatrix} \mathbf{w}_N^T \\ \mathbf{w}_H^T \end{bmatrix} \cdot \dot{\mathbf{q}} \ . \tag{4.14}$$

The matrix $\mathbf{w}_H$ is a part of the matrix $\mathbf{w}_T$ which corresponds to the sticking contact. This equation can be further extended by considering the Lagrange multipliers $\boldsymbol{\lambda}_C$ for constraint forces as the unknown variables, as it was done for generation of equations of motion (3.6),

$$\ddot{\mathbf{g}}_{NH} = \begin{bmatrix} \ddot{\mathbf{g}}_N \\ \ddot{\mathbf{g}}_H \end{bmatrix} = \underbrace{\begin{bmatrix} \mathbf{W}_N^T & \mathbf{0} \\ \mathbf{W}_H^T & \mathbf{0} \end{bmatrix}}_{\mathbf{W}^T} \cdot \underbrace{\begin{bmatrix} \ddot{\mathbf{q}} \\ \boldsymbol{\lambda}_C \end{bmatrix}}_{\ddot{\mathbf{q}}_c} + \underbrace{\begin{bmatrix} \mathbf{w}_N^T \cdot \dot{\mathbf{q}} \\ \mathbf{w}_H^T \cdot \dot{\mathbf{q}} \end{bmatrix}}_{\mathbf{w}} \ . \tag{4.15}$$

This relation is required since the unknown variables vector of Eq. (3.6) includes the generalized accelerations and constraint forces. In the next step, the vector $\ddot{\mathbf{q}}_c$ from Eq. (4.13) can be substituted in this equation

$$\ddot{\mathbf{g}}_{NH} = \mathbf{W}^T \cdot \mathbf{M}_c^{-1} \cdot \mathbf{W}_{NH} \cdot \boldsymbol{\lambda} + (\mathbf{W}^T \cdot \mathbf{M}_c^{-1} \cdot \mathbf{h}_c + \mathbf{w}) \ . \tag{4.16}$$

By following the same procedure as described in [106] and using Eq. (4.16), one can construct the required complementarity relations. In doing so and in order to handle the condition of switching between sliding and sticking contacts, the Coulomb friction law must be decomposed to reach complementarity relations of tangential contact. Thereby, frictional contact can be handled appropriately.

The final form of complementarity equations based on the introduced notation and according to the above mentioned points reads as

$$\begin{bmatrix} \ddot{\mathbf{g}} \\ \boldsymbol{\lambda}_{H_0} \end{bmatrix} = \begin{bmatrix} \mathbf{W}^T \cdot \mathbf{M}_c^{-1} \cdot \mathbf{W}_{NH} & \mathbf{I}^T \\ \mathbf{N}_H - \mathbf{I} & \mathbf{0} \end{bmatrix} \cdot \begin{bmatrix} \boldsymbol{\lambda} \\ \mathbf{z} \end{bmatrix} + \begin{bmatrix} \mathbf{W}^T \cdot \mathbf{M}_c^{-1} \cdot \mathbf{h}_c + \mathbf{w} \\ \mathbf{0} \end{bmatrix} ,$$
$$\begin{bmatrix} \ddot{\mathbf{g}} \\ \boldsymbol{\lambda}_{H_0} \end{bmatrix} \geq \mathbf{0} \ , \qquad \begin{bmatrix} \boldsymbol{\lambda} \\ \mathbf{z} \end{bmatrix} \geq \mathbf{0} \ , \qquad \begin{bmatrix} \ddot{\mathbf{g}} \\ \boldsymbol{\lambda}_{H_0} \end{bmatrix} \cdot \begin{bmatrix} \boldsymbol{\lambda} \\ \mathbf{z} \end{bmatrix} = 0 \ . \tag{4.17}$$

The parameters $\boldsymbol{\lambda}_{H_0}, \mathbf{N}_H$ and $\mathbf{z}$ were chosen in the same way as in [106] and have the same meaning. They are some dummy parameters which have arisen while decomposing the Coulomb friction law.

4.3 Comparison between Both Formulations

The presented formulation for continual contact modeling is applicable for multibody systems including constrained and non-constrained planar rigid and flexible bodies with relatively small deformations. The major difference between this formulation and the approach for rigid bodies in [106] is in the kinematics of contact. Considering rigid bodies, this formulation leads to the same results as the approach of [106]. To check this point, one compares the obtained formulation for $\ddot{\mathbf{g}}$ from both approaches. In doing so, one can start from the presented relations and reach the relations in [106] by setting the elastic coordinates to zero denoting that no deformation is available.

Considering two rigid bodies i and j, the relative normal acceleration of the l^{th} contact point is obtained from Eq. (4.5). For simplicity and without loss of generality, suppose that one of these bodies, for example body j, is ground and, therefore, its corresponding coordinates vanish from that equation. With this assumption, Eq. (4.5) is expanded as

$$\ddot{g}^l_{N_{ij}} = \mathbf{n}_i^l \cdot \mathbf{L}_i^l \cdot \ddot{\mathbf{q}}_i + (\mathbf{n}_i^l \cdot \dot{\mathbf{L}}_i^l + \dot{\mathbf{n}}_i^l \cdot \mathbf{L}_i^l) \cdot \dot{\mathbf{q}}_i \ . \tag{4.18}$$

Since body i is assumed to be rigid, all its elastic coordinates vanish and, therefore, matrix $\mathbf{B}_i^l$ in Eq. (4.1) reduces to $\mathbf{B}_i^l = \partial(\mathbf{A}_i \cdot \bar{\mathbf{u}}_{0i}^l)/\partial\boldsymbol{\theta}_i$. In the case of rigid planar systems, $\mathbf{L}_i^l$ is

a 2×3 matrix and the rotational coordinates $\boldsymbol{\theta}_i$ are replaced with the scalar θ_i. Therefore, the above equation is expanded further to

$$\ddot{g}^l_{N_{ij}} = \underbrace{\mathbf{n}^l_i \cdot (\ddot{\mathbf{R}}_i + \ddot{\theta}_i \mathbf{B}^l_i + \dot{\theta}_i \dot{\mathbf{B}}^l_i)}_{\text{part 1}} + \underbrace{\dot{\mathbf{n}}^l_i \cdot (\dot{\mathbf{R}}_i + \dot{\theta}_i \mathbf{B}^l_i)}_{\text{part 2}} = \mathbf{n}^l_i \cdot \mathbf{a}^l_i + \dot{\mathbf{n}}^l_i \cdot \mathbf{v}^l_i \ . \tag{4.19}$$

It is clear that the relative normal accelerations $\ddot{\mathbf{g}}_N$ for any contact point consists of two parts. The first part is due to the acceleration of that point in the direction of the normal vector $\mathbf{n}^l_i$ and the second part is due to the variations of the normal vector direction. This procedure can be followed exactly in the same way for the relative tangential accelerations $\ddot{\mathbf{g}}^l_T$ of the l^{th} contact point

$$\ddot{g}^l_{T_{ij}} = \mathbf{t}^l_i \cdot \mathbf{L}^l_i \cdot \ddot{\mathbf{q}}_i + (\mathbf{t}^l_i \cdot \dot{\mathbf{L}}^l_i + \dot{\mathbf{t}}^l_i \cdot \mathbf{L}^l_i) \cdot \dot{\mathbf{q}}_i = \mathbf{t}^l_i \cdot (\ddot{\mathbf{R}}_i + \ddot{\theta}_i \mathbf{B}^l_i + \dot{\theta}_i \dot{\mathbf{B}}^l_i) + \dot{\mathbf{t}}^l_i \cdot (\dot{\mathbf{R}}_i + \dot{\theta}_i \mathbf{B}^l_i) = \mathbf{t}^l_i \cdot \mathbf{a}^l_i + \dot{\mathbf{t}}^l_i \cdot \mathbf{v}^l_i \ . \tag{4.20}$$

Therefore, one can verify that the presented relations for relative accelerations result in the accelerations of rigid bodies when deformations of flexible bodies are set to zero. Compared to the continual contact of rigid bodies, the matrices $\mathbf{W}_N$, $\mathbf{W}_T$, $\mathbf{w}_N$ and $\mathbf{w}_T$ are the most important parameters which have to be reformulated in such a way to lead to a correct formulation for the continual contact of flexible bodies. The results shown in the following section confirm the validity of this procedure as well.

4.4 Numerical Examples

The formulation presented in the previous sections is implemented and examined in two examples. With due attention to the numerical results of these examples, one can verify the validity and feasibility of the described approach. In these examples, the continual contact of an elastic rectangular block on a rigid foundation is investigated. In both examples, it is supposed that the elastic rectangular block slides on the foundation and after awhile due to the effect of friction force, sliding contact changes to sticking contact. The examples differ in two important points: first, their foundations have different shapes and second, in the second example the rectangular block is restricted by a constraint which forces the center of the block to follow a certain curve. These cases are explained briefly in the corresponding sections. The shape of the rigid foundations are chosen in such a way to activate all important terms in the presented formulation.

Example 1: Continual Contact of an Elastic Rectangular Block

In Figure 4.2 an elastic rectangular block in both undeformed and deformed configurations in an arbitrary position and orientation with respect to the inertial coordinate system O is shown. The block reference coordinate system O_i is attached rigidly to node 4. The

X-axis is aligned to edge 4-1. The rigid coordinates of the block, $\mathbf{R}_i$ and θ, are calculated from position and orientation of this coordinate system. Therefore, the position of any arbitrary point on the elastic block can be calculated with respect to the coordinate system O_i through nodal coordinates. The elastic coordinates are summarized as $\mathbf{q_e} = ((q_{e_1})_x, (q_{e_2})_x, (q_{e_2})_y, (q_{e_3})_x, (q_{e_3})_y)^T$ since they have to be compatible with the rigid coordinates, see Section 2.3.2 and [118]. The rigid and elastic coordinates have to lead to a unique description of position and orientation of the elastic block. This means that node 1 can only move in the x direction with respect to the coordinate system O_i. The vector of the generalized coordinates for this example can be considered as $\mathbf{q} = (R_x, R_y, \theta, \mathbf{q_e}^T)^T$.

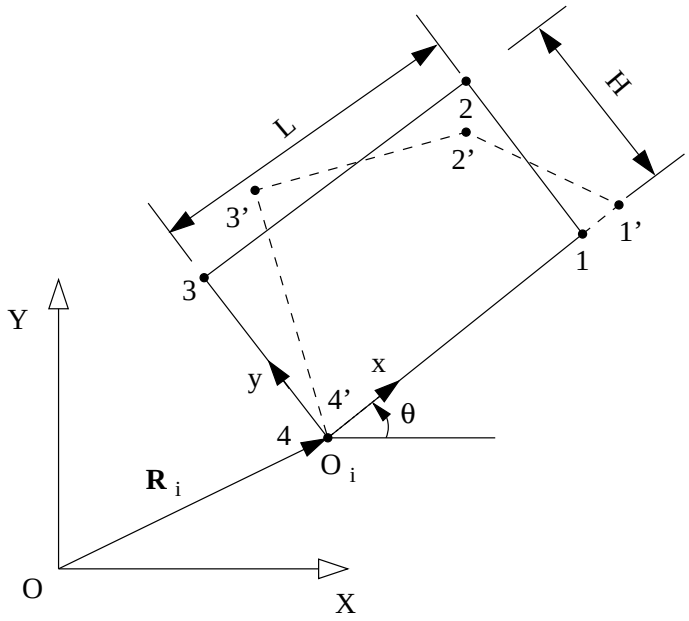

Figure 4.2: An elastic block in the undeformed and deformed configurations

The shape matrix of this elastic block is given by

$$\mathbf{S} = \begin{bmatrix} N_1 & N_2 & 0 & N_3 & 0 \\ 0 & 0 & N_2 & 0 & N_3 \end{bmatrix} , \tag{4.21}$$

where N_1, N_2 and N_3 are shape functions defined in terms of the length L and the height H of the block as follows

$$N_1 = \frac{x}{L}(1 - \frac{y}{H}) , \qquad N_2 = \frac{x}{L}\frac{y}{H} , \qquad N_3 = (1 - \frac{x}{L})\frac{y}{H} . \tag{4.22}$$

These shape functions have the usual property that they take the value one at their corresponding corner and the value zero at the other corners

$$\begin{cases} \text{at node 1:} & N_1 = 1 , \; N_2 = 0 , \; N_3 = 0 , \\ \text{at node 2:} & N_1 = 0 , \; N_2 = 1 , \; N_3 = 0 , \\ \text{at node 3:} & N_1 = 0 , \; N_2 = 0 , \; N_3 = 1 , \\ \text{at node 4:} & N_1 = 0 , \; N_2 = 0 , \; N_3 = 0 . \end{cases} \tag{4.23}$$

Based on the selected coordinates and the described shape matrix, one can construct the matrix $\mathbf{L}$ and start to generate the kinematic relations of contact. After some mathematical manipulations, the matrix $\mathbf{L}$ can be given as

$$\mathbf{L} = \begin{bmatrix} 1 & 0 & -x\sin\theta - y\cos\theta & N_1\cos\theta & N_2\cos\theta & -N_2\sin\theta & N_3\cos\theta & -N_3\sin\theta \\ 0 & 1 & x\cos\theta - y\sin\theta & N_1\sin\theta & N_2\sin\theta & N_2\cos\theta & N_3\sin\theta & N_3\cos\theta \end{bmatrix} . \tag{4.24}$$

This matrix has to be differentiated with respect to time. Afterwards, following Eq. (4.5) all necessary quantities for contact modeling between the elastic block and the rigid foundation are obtained. After formulating the kinematic relations, the equations of motion of the elastic block on the rigid foundation have to be generated. Since there is no explicit constraint in the system, the second row of the system of equations (4.12) vanishes yielding, see also Eq. (3.6),

$$\mathbf{M}\cdot\ddot{\mathbf{q}} = \mathbf{h} + (\mathbf{W}_N + \mathbf{W}_G\cdot\boldsymbol{\mu}_G)\cdot\boldsymbol{\lambda}_N + \mathbf{W}_H\cdot\boldsymbol{\lambda}_H \ . \tag{4.25}$$

The quantities in Eq. (4.25) are derived following the explained procedure in Sections 2.3.6 and 4.1. In the last step, the complementarity relations of Section 4.2 are derived and solved by the PATH solver which is an algorithm for mixed complementarity problems, see [28] and [42]. In order to overcome common problems of instability in the integration process of flexible bodies, the equations of motion are integrated using the RADAU5 code [38, 59].

For simulation of this academic test example, the following values are used:

initial conditions: $x_0 = -13.66$ m, $y_0 = -3.66$ m, $\theta_0 = -30$ Deg, $\mathbf{q}_e = \mathbf{0}$,
$\dot{x}_0 = 0$, $\dot{y}_0 = 0$, $\dot{\theta}_0 = 0$, $\dot{\mathbf{q}}_e = \mathbf{0}$,

material: $E = 1000$ N/m, $\nu = 0.3$, $\rho = 2$ kg/m^2 ,

geometry: $H = 1$ m, $L = 2$ m .

Here, E and ρ are the areal modulus of elasticity and areal density, respectively. The elastic block and the rigid foundation are depicted in Figure 4.3. According to this figure, the foundation consists of three parts: two inclined straight parts and a curved part which is an arc of a circle with radius $r = 10$ m. The length of each inclined part is 10 m and the inclination angle is $\alpha = 30$ Deg.

The simulation is done for $t_{end} = 10$ s and for two cases with different friction coefficients $\mu = 0.1$ and $\mu = 0.2$. Some results of these simulations are illustrated in Figures 5.5 and 5.6. In the first simulation ($\mu = 0.1$), as it can be seen from Figure 5.5b, the elastic block slides on the foundation, leaves the left inclined part of the path at $t = 2$ s and enters the curved part. It reaches the lowest point of the curved path at $t = 2.7$ s where $x = 0$ m, $y = -10$ m and $\theta = 0$ rad and then enters the right inclined part at $t = 3.8$ s. There, θ has a constant value 0.523 rad which is equal to the inclination angle of the right inclined part. The elastic block moves upward on the right inclined path and stops at $t = 4.2$ s

before it starts to move in opposite direction. This point can also be seen from Figure 5.5a where the x and y coordinates of node 4 have their maximum value.

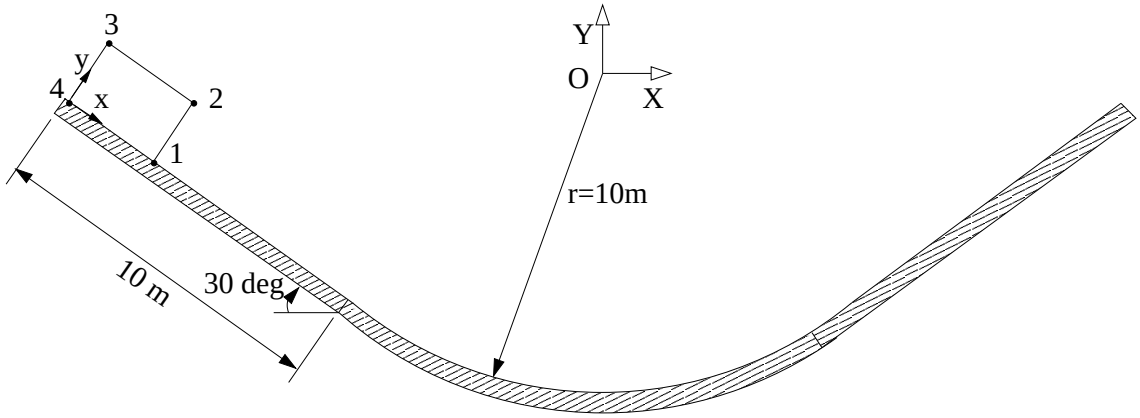

Figure 4.3: Continual contact of the non-constrained elastic block

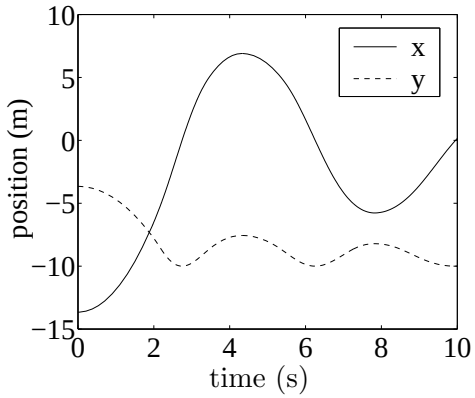

a: position of node 4

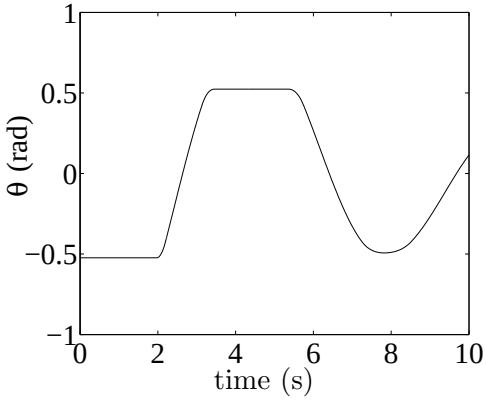

b: orientation at node 4

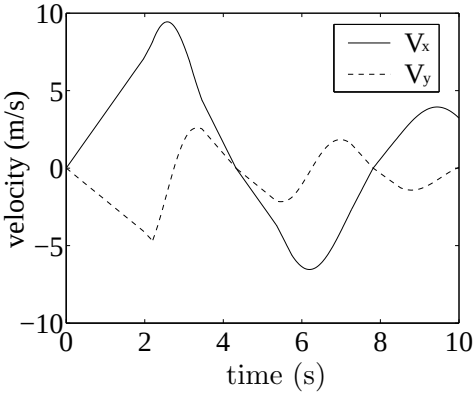

c: translational velocity of node 4

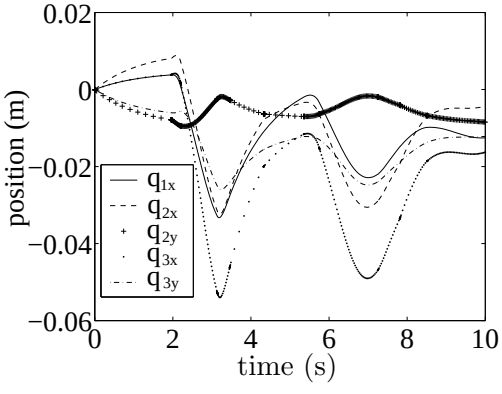

d: elastic coordinates

Figure 4.4: Contact simulation of the elastic block for $\mu = 0.1$

The elastic block enters the curved part for the second time at $t = 5.6$ s. Due to the effect of friction force it doesn't reach again the left inclined part any more and its reciprocal motion will continue in the curved part unitill the end of simulation. This time, $t = 10$ s, is not sufficient to bring the elastic block in sticking contact and, therefore, it will have sliding contact untill the end of the simulation. The translational velocity and variation of the elastic coordinates are shown in Figures 5.5c and 5.5d, respectively.

In the second simulation, one can see that due to the higher value of the friction coefficient, $\mu = 0.2$, the elastic block will come to sticking contact. As shown in Figure 5.6, due to the larger friction the elastic block reaches the curved part later than the first case, namely at $t = 2.3$ s. In this case, according to Figure 5.6b it reaches the lowest point of the curved path at $t = 3$ s but it cannot enter the right inclined part since θ doesn't reach the constant value of 0.523 rad which is the inclination angle of the right inclined part. Instead, it starts to move in the opposite direction at $t = 4$ s. This point can be seen from Figures 5.6a and 5.6b. In the end, it comes to rest somewhere on the curved part at $t = 7.6$ s and at this time sliding contact switches to sticking one.

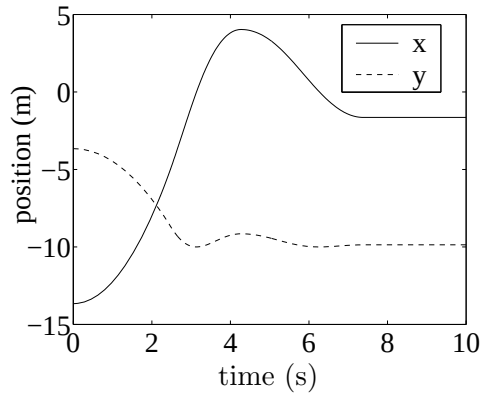

a: position of node 4

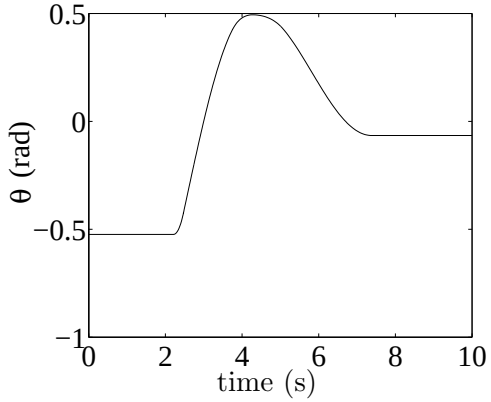

b: orientation of node 4

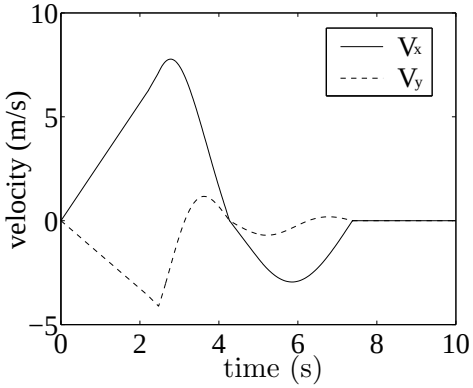

c: translational velocity of node 4

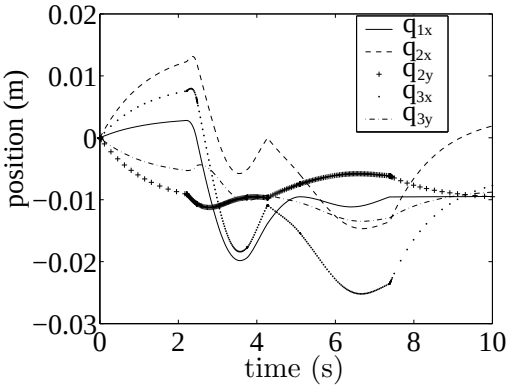

d: elastic coordinates

Figure 4.5: Contact simulation of the elastic block for $\mu = 0.2$

Example 2: Constrained Elastic Rectangular Block

In the second example depicted in Figure 4.6, contact of the constrained elastic block on a rigid half-circular foundation with radius $r = 10$ m is investigated.

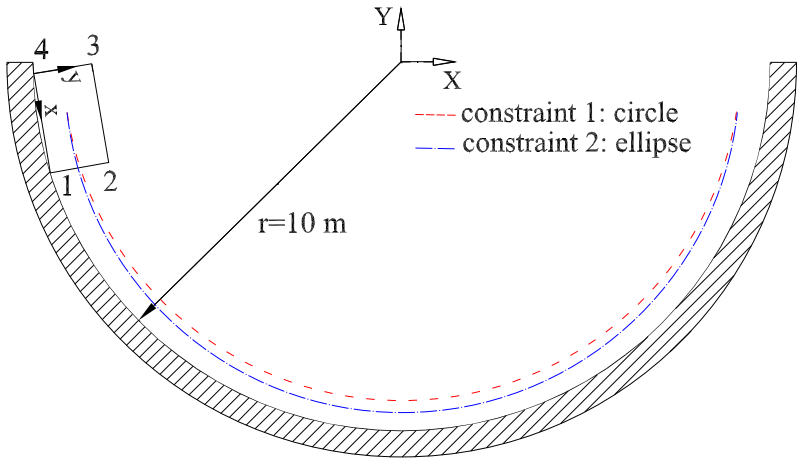

Figure 4.6: Continual contact of the constrained elastic block

This example is simulated for two different constraints. In the first simulation, the constraint is supposed to keep the center point of the elastic block in a constant distance from the center of the half-circular rigid foundation. In the second simulation, the constraint has to keep the center point of the elastic block in a half-ellipse path according to the figure. The constraint applies a constraint force which is considered in Eq. (3.6) by the parameter $\boldsymbol{\lambda}_C$. The second simulation is done in order to force the block to deform much more so that one can investigate the effect of deformations in the amount of contact forces. In other words, one can find out that how considering deformations will affect the contact forces.

The elastic block has the same material parameters as in the previous example, but the friction coefficient $\mu = 0.5$ is chosen. The simulation results for the first constraint (half-circle constraint) are shown in Figure 4.7. It can easily be seen that the block slides on the foundation until $t = 8.2$ s and at this time, sticking contact appears and the block comes to rest.

For the second constraint (half-ellipse constraint), the amount of contact force of node 1 in y direction when it passes through the lowest point of the rigid foundation (at $x = 0$ and $y = -10$ m) is illustrated in Figure 4.8 for different values of Young's modulus E. According to this figure, by increasing the value of E the contact force increases too. The slope of the variations is almost constant for soft material and decreases for the stiff material. As the rigidity of the elastic block is increased by increasing Young's modulus, the amount of contact forces approaches a constant value. Therefore, the importance and

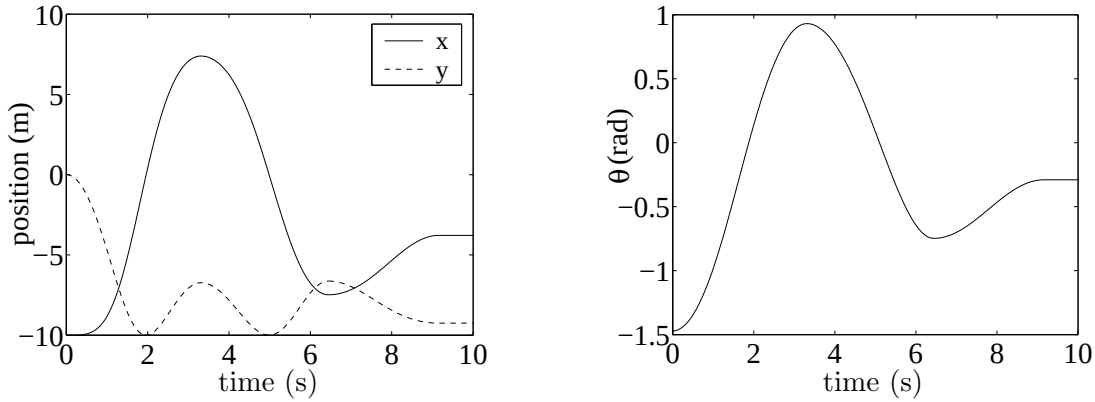

a: position of node 4 b: orientation of node 4

Figure 4.7: Simulation results for the first constraint

necessity of considering deformations becomes clear stating that for such situations, the elastic contact modeling has to be used instead of rigid contact modeling.

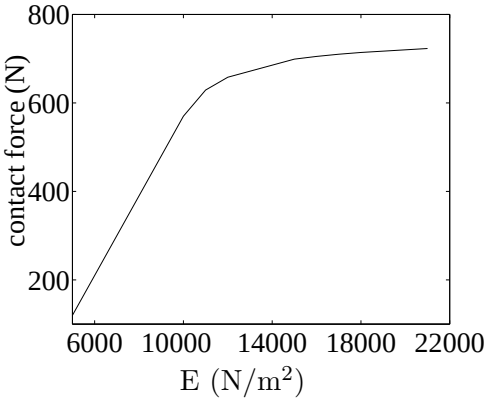

Figure 4.8: Contact force of node 1 in y direction for the second constraint

Chapter 5

Impact of Planar Flexible Systems: LCP Approach

Impact events in multibody systems may arise from different sources. The most common type happens when moving bodies collide. Clearances in joints, mass capture and mass release, intermittent motion of bodies and others may be other sources of impact [79]. Due to the nature of impact, high forces will be exerted to the impacting bodies during a very short period of time. Therefore, in order to describe the physical process correctly, considering deformations becomes often an inevitable demand.

Unlike for rigid bodies where the impact duration is infinitesimal, the impact events in flexible multibody systems take finite time due to the effect of local deformations and the excited waves propagate at finite velocities. In the treatment of impact in rigid multibody systems, coordinates of impacting bodies during impact are usually kept constant and they experience velocity jumps which theoretically lead to infinite values for accelerations and impulsive forces. This causes difficulties in the numerical solution process and equations of motion have to be reformulated in terms of velocities and impulses instead of accelerations and impact forces. Nevertheless, in approaches where a finite duration is considered for impact of rigid bodies, the equations of motion on acceleration level can still be used. In the case of dealing with impact of flexible bodies, local deformations prevent any discontinuity in velocities.

In contrast to the formulation of continual contact of planar flexible bodies in which the relative acceleration of contact points is formulated in terms of contact forces, see Chapter 4 and [31, 34], impact formulations cannot simply follow the same strategy. In continual contact, for preserving the contact the relative acceleration of contact points must be kept zero. However, for the case of impact in which bodies have initially no contact and then, come in contact, colliding bodies have a relative velocity with possibly some accelerations at contact points.

Here, an approach for impact analysis of planar flexible bodies is developed which can be formulated as linear complementarity problems on position and velocity levels, see also [36, 37]. At this point it should be emphasized that in both approaches on position and velocity levels, no coefficient of restitution has to be introduced for obtaining the impact law. Although there exist some approaches for impact modeling of flexible bodies which introduce this coefficient as a measure of energy loss during impact, no coefficient of restitution should be used here since the energy loss is taken into account by the material law of the flexible bodies

5.1 Kinematics of Impact

The key point of the approach presented here is based on Signorini's conditions [125] of impact problems which are usually described as complementarity conditions between the gap distance of colliding bodies and normal contact forces, see Eq. (3.13),

$$g \geq 0 \ , \qquad \lambda_N \geq 0 \ , \qquad g\lambda_N = 0 \ . \tag{5.1}$$

In the first step, the kinematics of impact has to be considered by obtaining a relation between gap distances and generalized coordinates of bodies. Then, the impact problem will be formulated as a linear complementarity problem by solving the kinetics of impact and inserting in the obtained relations of gap distances. In Figure 5.1 two planar flexible bodies i and j are depicted. According to this figure, p_i and p_j are two potential contact points of the l^{th} contact pair. The distance vector $\mathbf{g}_{ij}^l$ between two points is shown in this figure as well as the normal vectors $\mathbf{n}_i^l$ and $\mathbf{n}_j^l$ at the points p_i and p_j, respectively.

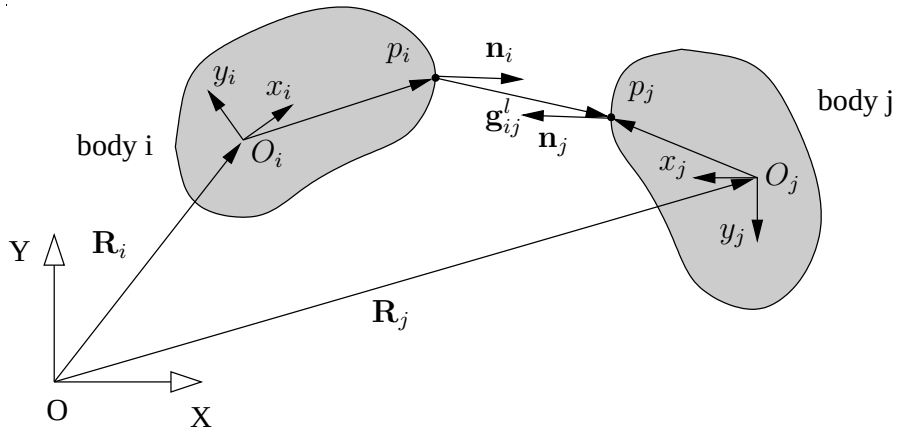

Figure 5.1: Kinematics of impact between two flexible bodies

The position and orientation of flexible bodies i and j with respect to the inertial coordinate system are described by two sets of generalized coordinates $\mathbf{q}_i = (\mathbf{R}_i^T,\ \boldsymbol{\theta}_i^T,\ \mathbf{q}_{e_i}^T)^T$ and

$\mathbf{q}_j = (\mathbf{R}_j^T,\ \boldsymbol{\theta}_j^T,\ \mathbf{q}_{e_j}^T)^T$. Now, one can write the gap distance vector $\mathbf{g}_{ij}^l$ using the quantities shown in Figure 5.1, see Eq. (2.19),

$$\mathbf{g}_{ij}^l = (\mathbf{R}_j + \mathbf{A}_j \cdot (\bar{\mathbf{u}}_{0p_j} + \mathbf{S}_j \cdot \mathbf{q}_{e_j})) - (\mathbf{R}_i + \mathbf{A}_i \cdot (\bar{\mathbf{u}}_{0p_i} + \mathbf{S}_i \cdot \mathbf{q}_{e_i}))\ . \tag{5.2}$$

In this equation, $\mathbf{A}$ is the transformation matrix, $\bar{\mathbf{u}}_{0p}$ is the position vector of point p in the undeformed configuration of its corresponding body and given in the body reference coordinate system and $\mathbf{S}$ is the shape matrix at point p. Equation (5.2) may be rearranged after expanding the transformation matrix $\mathbf{A}$

$$\mathbf{g}_{ij}^l = (\mathbf{R}_j - \mathbf{R}_i) + \begin{bmatrix} \cos\theta_j & -\sin\theta_j \\ \sin\theta_j & \cos\theta_j \end{bmatrix} \cdot (\bar{\mathbf{u}}_{0p_j} + \mathbf{S}_j \cdot \mathbf{q}_{e_j}) - \begin{bmatrix} \cos\theta_i & -\sin\theta_i \\ \sin\theta_i & \cos\theta_i \end{bmatrix} \cdot (\bar{\mathbf{u}}_{0p_i} + \mathbf{S}_i \cdot \mathbf{q}_{e_i})\ , \tag{5.3}$$

and consequently

$$\begin{aligned} \mathbf{g}_{ij}^l = (\mathbf{R}_j - \mathbf{R}_i) + \begin{bmatrix} -(\bar{u}_{0x})_i \cos\theta_i + (\bar{u}_{0y})_i \sin\theta_i \\ -(\bar{u}_{0x})_i \sin\theta_i - (\bar{u}_{0y})_i \cos\theta_i \end{bmatrix} + \begin{bmatrix} (\bar{u}_{0x})_j \cos\theta_j - (\bar{u}_{0y})_j \sin\theta_j \\ (\bar{u}_{0x})_j \sin\theta_j + (\bar{u}_{0y})_j \cos\theta_j \end{bmatrix} + \\ \begin{bmatrix} -\mathbf{S}_{i_1} \cos\theta_i + \mathbf{S}_{i_2} \sin\theta_i \\ -\mathbf{S}_{i_1} \sin\theta_i - \mathbf{S}_{i_2} \cos\theta_i \end{bmatrix} \cdot \mathbf{q}_{e_i} + \begin{bmatrix} \mathbf{S}_{j_1} \cos\theta_j - \mathbf{S}_{j_2} \sin\theta_j \\ \mathbf{S}_{j_1} \sin\theta_j + \mathbf{S}_{j_2} \cos\theta_j \end{bmatrix} \cdot \mathbf{q}_{e_j}\ , \end{aligned} \tag{5.4}$$

where $\bar{u}_{0x}$ and $\bar{u}_{0y}$ denote the x and y components of the vector $\bar{\mathbf{u}}_{0p}$, respectively. The row vectors $\mathbf{S}_{i_1}$ and $\mathbf{S}_{i_2}$ correspond to the first and the second rows of the shape matrix $\mathbf{S}_i$, respectively. The same holds for the row vectors $\mathbf{S}_{j_1}$ and $\mathbf{S}_{j_2}$ of the shape matrix $\mathbf{S}_j$. Since for planar systems one only deals with one rotational coordinate, in this equation a scalar quantity θ is used directly. Equation (5.4) contains the terms $\sin\theta$ and $\cos\theta$. However, in order to write $\mathbf{g}_{ij}^l$ in terms of the generalized coordinates in an explicit form (which is a requirement for building the LCP), one needs to have the rotational coordinate θ explicitly. Therefore, by expanding $\sin\theta$ and $\cos\theta$ in a Taylor series up to the third term and after some mathematical manipulations one can rewrite Eq. (5.4) in a matrix notation in terms of the generalized coordinate vectors $\mathbf{q}_i$ and $\mathbf{q}_j$ as

$$\mathbf{g}_{ij}^l = \underbrace{\left[\begin{array}{cccc|ccc} -\mathbf{I} & \mathbf{W}_{\theta_i} & \mathbf{W}_{\mathbf{q}_{ei}} & & \mathbf{I} & \mathbf{W}_{\theta_j} & \mathbf{W}_{\mathbf{q}_{ej}} \end{array}\right]^l}_{\mathbf{W}_{g_{ij}}^l} \cdot \underbrace{\left[\begin{array}{c} \mathbf{R}_i \\ \theta_i \\ \mathbf{q}_{e_i} \\ \hline \mathbf{R}_j \\ \theta_j \\ \mathbf{q}_{e_j} \end{array}\right]}_{\mathbf{q}_{ij}} + \bar{\mathbf{w}}_{ij}^l\ , \tag{5.5}$$

where

$$\mathbf{W}_{\theta_i} = \left[\begin{array}{c} (1 - \frac{\theta^2}{3!} + \frac{\theta^4}{5!})\bar{u}_{0y} + (\frac{\theta^2}{2!} - \frac{\theta^4}{4!})\bar{u}_{0x} \\ -(1 - \frac{\theta^2}{3!} + \frac{\theta^4}{5!})\bar{u}_{0x} + (\frac{\theta^2}{2!} - \frac{\theta^4}{4!})\bar{u}_{0y} \end{array} \right]_i , \; \mathbf{W}_{q_{e_i}} = \left[\begin{array}{c} -\mathbf{S}_1 \cos\theta + \mathbf{S}_2 \sin\theta \\ -\mathbf{S}_1 \sin\theta - \mathbf{S}_2 \cos\theta \end{array} \right]_i ,$$

$$\mathbf{W}_{\theta_j} = \left[\begin{array}{c} (-\frac{\theta^2}{2!} + \frac{\theta^4}{4!})\bar{u}_{0x} - (1 - \frac{\theta^2}{3!} + \frac{\theta^4}{5!})\bar{u}_{0y} \\ (-\frac{\theta^2}{2!} + \frac{\theta^4}{4!})\bar{u}_{0y} + (1 - \frac{\theta^2}{3!} + \frac{\theta^4}{5!})\bar{u}_{0x} \end{array} \right]_j , \; \mathbf{W}_{q_{e_j}} = \left[\begin{array}{c} \mathbf{S}_1 \cos\theta - \mathbf{S}_2 \sin\theta \\ \mathbf{S}_1 \sin\theta + \mathbf{S}_2 \cos\theta \end{array} \right]_j ,$$

$$\mathbf{I} = \left[\begin{array}{cc} 1 & 0 \\ 0 & 1 \end{array} \right] , \; \bar{\mathbf{w}}_{ij}^l = \left[\begin{array}{c} (\bar{u}_{0x})_j - (\bar{u}_{0x})_i \\ (\bar{u}_{0y})_j - (\bar{u}_{0y})_i \end{array} \right] . \tag{5.6}$$

It is noticeable that all parameters in the matrices $\mathbf{W}_{\theta_i}$ and $\mathbf{W}_{q_{e_i}}$ are evaluated for body i. The same holds also for the matrices $\mathbf{W}_{\theta_j}$ and $\mathbf{W}_{q_{e_j}}$ and body j. At this point it is important to emphasize that the Taylor series used to get Eq. (5.5) provides a good approximation only for small values of θ. Therefore, in the case of high values of θ a higher order approximation must be used instead. Also, for the case of several revolutions of bodies when θ exceeds 2π *rad*, its value may be considered between $-\pi$ and $+\pi$ to provide a better approximation for $\sin\theta$ and $\cos\theta$.

Then, from Eq. (5.5) one may derive the normal gap distance by multiplying the vector $\mathbf{g}_{ij}^l$ with either the vector $\mathbf{n}_i^l$ or $-\mathbf{n}_j^l$ yielding

$$g_{N_{ij}}^l = \mathbf{n}_i^l \cdot \mathbf{g}_{ij}^l = (\mathbf{n}_i^l \cdot \mathbf{W}_{g_{ij}}^l) \cdot \mathbf{q}_{ij} + \mathbf{n}_i^l \cdot \bar{\mathbf{w}}_{ij}^l \; . \tag{5.7}$$

Equation (5.7) together with the matrices defined in Eq. (5.5) represents the normal gap distance between two points p_i and p_j in terms of the generalized coordinate vectors of both bodies. However, this equation may be easily extended for the case of multiple contacts between bodies i and j or for multiple contacts of many bodies in multibody systems. For consideration of n_c contact pairs between planar bodies i and j, the gap distances vector $\mathbf{g}_{N_{ij}}$ is a $n_c \times 1$ vector. For this case, Eq. (5.7) can be rearranged in the form

$$\mathbf{g}_{N_{ij}} = \left[\begin{array}{c} g_{N_{ij}}^1 \\ \vdots \\ g_{N_{ij}}^{n_c} \end{array} \right] = \underbrace{\left[\begin{array}{c} \mathbf{n}_i^1 \cdot \mathbf{W}_g^1 \\ \vdots \\ \mathbf{n}_i^{n_c} \cdot \mathbf{W}_g^{n_c} \end{array} \right]_{ij}}_{\mathbf{W}_{g_{ij}}} \cdot \mathbf{q}_{ij} + \underbrace{\left[\begin{array}{c} \mathbf{n}_i^1 \cdot \bar{\mathbf{w}}^1 \\ \vdots \\ \mathbf{n}_i^{n_c} \cdot \bar{\mathbf{w}}^{n_c} \end{array} \right]_{ij}}_{\bar{\mathbf{w}}_{ij}} . \tag{5.8}$$

Following the same notation, a general relation for all possible contact pairs between n_b bodies in the multibody systems may be obtained. Here the general gap distance vector

for all these contact pairs is denoted by $\mathbf{g}_N$ which has to be formulated in terms of the vector $\mathbf{q}$ summarizing the system generalized coordinates of all bodies as

$$\mathbf{g}_N = \mathbf{W}_g \cdot \mathbf{q} + \bar{\mathbf{w}} \ . \tag{5.9}$$

Now, having this relationship for gap distances between possible contact pairs, one can judge whether there exist any contact between bodies or not. When, for example, the l^{th} component of $\mathbf{g}_{N_{ij}}$ has a positive value, $g^l_{N_{ij}} > 0$, it means that the l^{th} contact pair is not active. Consequently, when $g^l_{N_{ij}} = 0$ this contact becomes active and, therefore, for preventing any penetration normal contact forces must be applied at the corresponding contact points.

5.2 Frictionless Impact on Position Level

In this section, first the frictionless impact problem is considered and then will be extended to the frictional case in Section 5.3. The formulation begins by describing the generalized coordinates vector $\mathbf{q}$ in terms of the normal contact forces $\boldsymbol{\lambda}_N$. Substituting this relation in Eq. (5.9) leads to a formulation between $\mathbf{g}_N$ and $\boldsymbol{\lambda}_N$. Finally, the LCP can be formulated based on this relationship and Signorini's conditions.

5.2.1 Impact Forces and Equations of Motion

Equation (4.12) can be rewritten considering only the normal contact forces as

$$\mathbf{M}_c \cdot \ddot{\mathbf{q}}_c = \mathbf{h}_c + \underbrace{\begin{bmatrix} \mathbf{W}_N \\ \mathbf{0} \end{bmatrix}}_{\mathbf{W}_c} \cdot \boldsymbol{\lambda}_N \quad \rightarrow \quad \mathbf{M}_c \cdot \ddot{\mathbf{q}}_c = \mathbf{h}_c + \mathbf{W}_c \cdot \boldsymbol{\lambda}_N \ . \tag{5.10}$$

Suppose that there is no dependent constraint in the system and so, $\mathbf{M}_c$ is a regular matrix

$$\ddot{\mathbf{q}}_c = \mathbf{M}_c^{-1} \cdot (\mathbf{h}_c + \mathbf{W}_c \cdot \boldsymbol{\lambda}_N) \ . \tag{5.11}$$

By splitting the matrix $\mathbf{M}_c^{-1}$ in two submatrices $\widetilde{\mathbf{M}}_q$ and $\widetilde{\mathbf{M}}_\lambda$ according to the dimensions of $\mathbf{q}$ and $\boldsymbol{\lambda}_C$, one may write the following equation, see Eq. (3.6),

$$\ddot{\mathbf{q}}_c = \begin{bmatrix} \ddot{\mathbf{q}} \\ \boldsymbol{\lambda}_C \end{bmatrix} = \begin{bmatrix} \widetilde{\mathbf{M}}_q \\ \widetilde{\mathbf{M}}_\lambda \end{bmatrix} \cdot (\mathbf{h}_c + \mathbf{W}_c \cdot \boldsymbol{\lambda}_N) \quad \rightarrow \quad \ddot{\mathbf{q}} = \widetilde{\mathbf{M}}_q \cdot (\mathbf{h}_c + \mathbf{W}_c \cdot \boldsymbol{\lambda}_N) \ . \tag{5.12}$$

Now, the generalized accelerations $\ddot{\mathbf{q}}$ as a function of the Lagrange multipliers $\boldsymbol{\lambda}_N$ denoting the normal contact forces have been obtained.

5.2.2 Construction of the Complementarity Relations

In order to reach an LCP formulation of the impact problem the generalized coordinates as a function of $\boldsymbol{\lambda}_N$ are required. This can be done by integrating Eq. (5.12). Since the normal contact forces $\boldsymbol{\lambda}_N$ are unknown, a special numerical algorithm based on different integration approaches may be utilized. This algorithm is presented here for some common numerical integration approaches.

The Explicit Euler Approach

As a starting point for demonstrating the basic idea, the simplest numerical integration approach is chosen. Although this approach is not a suitable method for integration of multibody systems and has some stability problems, due to its simplicity it can be supposed to be a first choice for trying to formulate the generalized coordinates as a function of the unknown normal contact forces. Later, some more sophisticated integration approaches will be used for this purpose.

By denoting the time interval between steps $n-1$ and n with the step size Δt_n, one can write the positions and velocities of step n in terms of the values of step $n-1$

$$\mathbf{q}_n = \mathbf{q}_{n-1} + \Delta t_n \dot{\mathbf{q}}_{n-1}, \qquad \dot{\mathbf{q}}_n = \dot{\mathbf{q}}_{n-1} + \Delta t_n \ddot{\mathbf{q}}_{n-1} \ . \tag{5.13}$$

After changing the index n to $n-1$ in the right hand side equation and inserting in the first equation one obtains

$$\mathbf{q}_n = \mathbf{q}_{n-1} + \Delta t_n \dot{\mathbf{q}}_{n-2} + \Delta t_n^2 \ddot{\mathbf{q}}_{n-2} \ . \tag{5.14}$$

Changing the index n to $n-1$ in the left hand side relation of Eq. (5.13) and substituting in Eq. (5.14) yields

$$\mathbf{q}_n = \mathbf{q}_{n-2} + 2\Delta t_n \dot{\mathbf{q}}_{n-2} + \Delta t_n^2 \ddot{\mathbf{q}}_{n-2} \ . \tag{5.15}$$

Then, one can rewrite Eq. (5.12) for step $n-2$ and substitute it in Eq. (5.15) to reach

$$\begin{aligned} \mathbf{q}_n &= \underbrace{(\Delta t_n^2 \widetilde{\mathbf{M}}_{q_{n-2}} \cdot \mathbf{W}_{c_{n-2}})}_{\mathbf{W}_{q_{n-2}}} \cdot \boldsymbol{\lambda}_{N_{n-2}} + \underbrace{(\mathbf{q}_{n-2} + 2\Delta t_n \dot{\mathbf{q}}_{n-2} + \Delta t_n^2 \widetilde{\mathbf{M}}_{q_{n-2}} \cdot \mathbf{h}_{c_{n-2}})}_{\mathbf{w}_{q_{n-2}}} \\ &= \mathbf{W}_{q_{n-2}} \cdot \boldsymbol{\lambda}_{N_{n-2}} + \mathbf{w}_{q_{n-2}} \ . \end{aligned} \tag{5.16}$$

From Eq. (5.16) and after changing the index n to $n+2$, the vector $\mathbf{q}_{n+2}$ can be substituted in the normal gap distance vector $\mathbf{g}_{N_{n+2}}$ of step $n+2$ from Eq. (5.9) yielding

$$\mathbf{g}_{N_{n+2}} = \underbrace{\mathbf{W}_{g_{n+2}} \cdot \mathbf{W}_{q_n}}_{(\mathbf{W}_{gq})_{n+2}} \cdot \boldsymbol{\lambda}_{N_n} + \underbrace{(\mathbf{W}_{g_{n+2}} \cdot \mathbf{w}_{q_n} + \bar{\mathbf{w}}_{n+2})}_{(\mathbf{w}_{gq})_{n+2}} = (\mathbf{W}_{gq})_{n+2} \cdot \boldsymbol{\lambda}_{N_n} + (\mathbf{w}_{gq})_{n+2} \ . \tag{5.17}$$

This equation relates the normal contact forces $\boldsymbol{\lambda}_{N_n}$ and normal gap distances $\mathbf{g}_{N_{n+2}}$. In other words, in this formulation the normal contact forces of each step will affect the

normal gap distances of two later steps. Now, having Eq. (5.17) and considering the complementarity conditions of Eq. (5.1) in the general form for all contacts one may write the following LCP for the impact problem

$$\mathbf{g}_{N_{n+2}} = (\mathbf{W}_{gq})_{n+2} \cdot \boldsymbol{\lambda}_{N_n} + (\mathbf{w}_{gq})_{n+2} \ , \quad \text{with} \quad \mathbf{g}_{N_{n+2}} \geq \mathbf{0} \ , \quad \boldsymbol{\lambda}_{N_n} \geq \mathbf{0} \ , \quad \mathbf{g}_{N_{n+2}} \cdot \boldsymbol{\lambda}_{N_n} = 0 \ . \tag{5.18}$$

Remarks: Equation (5.18) formulates the normal gap distances of the step $n+2$ and the normal contact forces of two steps before as an LCP. In fact, this property is the result of the explicit Euler integration approach which demonstrates the effect of applied forces including contact forces on the generalized coordinates of two later integration steps. The key idea of this approach may be explained using Eq. (5.18) and Figure 5.2.

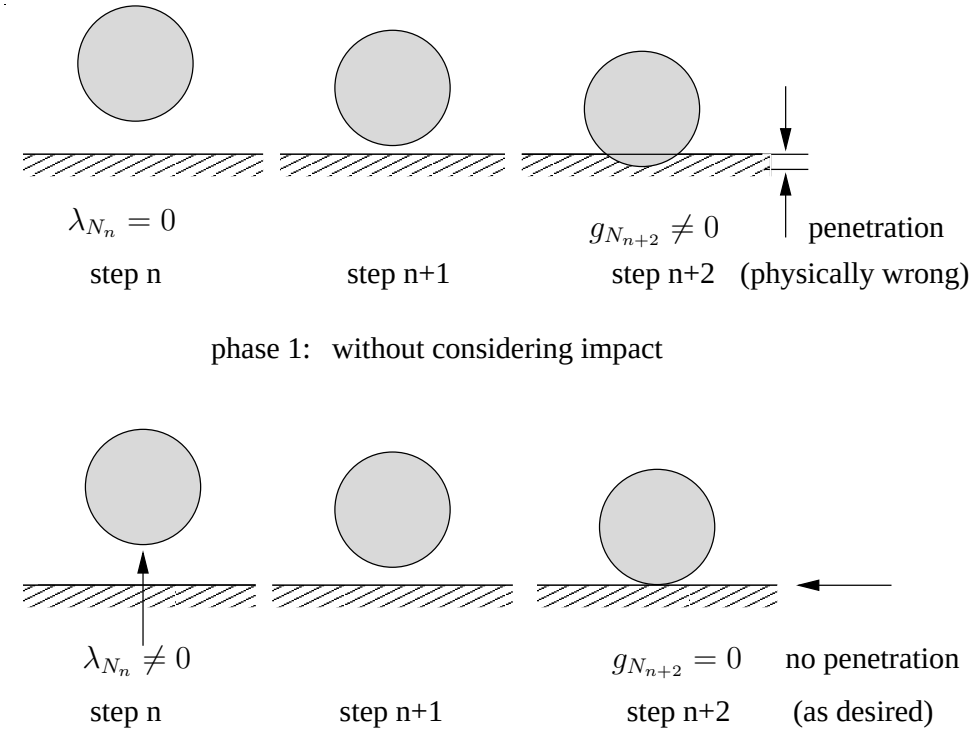

Figure 5.2: The effect of λ_{N_n} on the normal gap distance $g_{N_{n+2}}$ from the explicit Euler approach

Assume the simple example of impact between a disk and a foundation. Also assume that the integration process is at step n. For this step of phase 1 in Figure 5.2, the disk has no contact with the foundation. Having the positions and velocities of the disk at this step one can find out that without applying a force, the disk will experience penetration at step $n+2$. Now, the goal is to prevent penetration at step $n+2$. Therefore, a normal (pre-)contact force may be applied to the disk at step n to bring the disk into the no-penetration situation at step $n+2$ according to phase 2. Although the disk is not yet

in contact with the foundation at step n, this approach applies a normal contact force already at this step. This fact arises directly from the property of the explicit Euler approach since in this approach, the contact forces will affect the generalized coordinates of two integration steps later.

The required normal contact force for obtaining zero penetration can be calculated by solving the LCP of Eq. (5.18). For this simple case where one deals with one contact, after setting the normal gap distance to zero in Eq. (5.18), $g_{N_{n+2}} = 0$, the required normal contact force is simply calculated from $\lambda_{N_n} = -w_{gq}/W_{gq}$. In this relation, the parameter w_{gq} has a negative value which denotes the negative penetration in the absence of contact force for the phase 1. Also, the parameter W_{gq} must be a positive quantity which implies that the positive contact force reduces the penetration by balancing the term $W_{gq}\lambda_N$ with w_{gq}. Consequently, λ_N takes a positive value and together with the zero gap distance fulfills the linear complementarity condition of Eq. (5.18).

The 4^{th} Order Explicit Runge-Kutta Approach

The formulation presented based on the explicit Euler will not be used for actual computations since it is not accurate enough. Instead, the approach based on the 4^{th} order explicit Runge-Kutta approach can be a suitable condidate for this purpose.

The task here is to reach an analytical formulation of the generalized coordinates vector $\mathbf{q}_{n+1}$ of step $n+1$ as a function of normal contact forces $\boldsymbol{\lambda}_{N_n}$. Assume that the integration process is at step n and the generalized coordinates and generalized velocities of the system are known from the previous integration step. Equation (5.12) can be rewritten for step n

$$\ddot{\mathbf{q}}_n = \widetilde{\mathbf{M}}_{q_n} \cdot (\mathbf{h}_c + \mathbf{W}_c \cdot \boldsymbol{\lambda}_N)_n \ . \tag{5.19}$$

Since the numerical 4^{th} order Runge-Kutta approach requires four evaluations of the above equation in order to proceed from step n to $n+1$, the same strategy may be followed manually to obtain an analytical formulation of the vector $\mathbf{q}_{n+1}$ in terms of $\boldsymbol{\lambda}_{N_n}$. This can be done by successive evaluations and substitutions of the vector $\mathbf{q}$ for several stages of the 4^{th} order Runge-Kutta. Following such a strategy after some manipulations yields the required formula, see Appendix 8,

$$\mathbf{q}_{n+1} = \underbrace{\frac{\Delta t_n^2}{6}\sum_{j=1}^{3}(\widetilde{\mathbf{M}}_{q_j} \cdot \mathbf{W}_{c_j})_n}_{\mathbf{W}_{q_n}} \cdot \boldsymbol{\lambda}_{N_n} + \underbrace{(\mathbf{q}_n + \Delta t_n \dot{\mathbf{q}}_n + \frac{\Delta t_n^2}{6}\sum_{j=1}^{3}(\widetilde{\mathbf{M}}_{q_j} \cdot \mathbf{h}_{c_j})_n)}_{\mathbf{w}_{q_n}} \ , \tag{5.20}$$

where the index n is used for the n^{th} integration step, Δt_n is the integration step size and $\widetilde{\mathbf{M}}_{q_j}, \mathbf{W}_{c_j}$ and $\mathbf{h}_{c_j}$ $(j = 1, 2, 3)$ arise from the equations of motion but are evaluated at the first three stages of the 4^{th} order Runge-Kutta method. This equation is analog to Eq.

(5.16) but in this case the vector $\mathbf{q}_{n+1}$ is affected by $\boldsymbol{\lambda}_{N_n}$ from previous step. Substituting this equation in Eq. (5.9) leads to the relation of $\mathbf{g}_{N_{n+1}}$ and $\boldsymbol{\lambda}_{N_n}$

$$\mathbf{g}_{N_{n+1}} = \underbrace{\mathbf{W}_{g_{n+1}} \cdot \mathbf{W}_{q_n}}_{(\mathbf{W}_{gq})_{n+1}} \cdot \boldsymbol{\lambda}_{N_n} + \underbrace{(\mathbf{W}_{g_{n+1}} \cdot \mathbf{w}_{q_n} + \bar{\mathbf{w}}_{n+1})}_{(\mathbf{w}_{gq})_{n+1}} = (\mathbf{W}_{gq})_{n+1} \cdot \boldsymbol{\lambda}_{N_n} + (\mathbf{w}_{gq})_{n+1} \ . \quad (5.21)$$

In the next step, following the same procedure as implemented for the explicit Euler, one can get the following LCP for impact problem

$$\mathbf{g}_{N_{n+1}} = (\mathbf{W}_{gq})_{n+1} \cdot \boldsymbol{\lambda}_{N_n} + (\mathbf{w}_{gq})_{n+1} \ , \quad \text{with} \quad \mathbf{g}_{N_{n+1}} \geq \mathbf{0} \ , \quad \boldsymbol{\lambda}_{N_n} \geq \mathbf{0} \ , \quad \mathbf{g}_{N_{n+1}} \cdot \boldsymbol{\lambda}_{N_n} = 0 \ . \quad (5.22)$$

Based on the implementation of the Runge-Kutta approach, the normal gaps $\mathbf{g}_{N_{n+1}}$ may be adapted by the normal contact forces $\boldsymbol{\lambda}_{N_n}$ of one step before. Figure 5.3 shows this property.

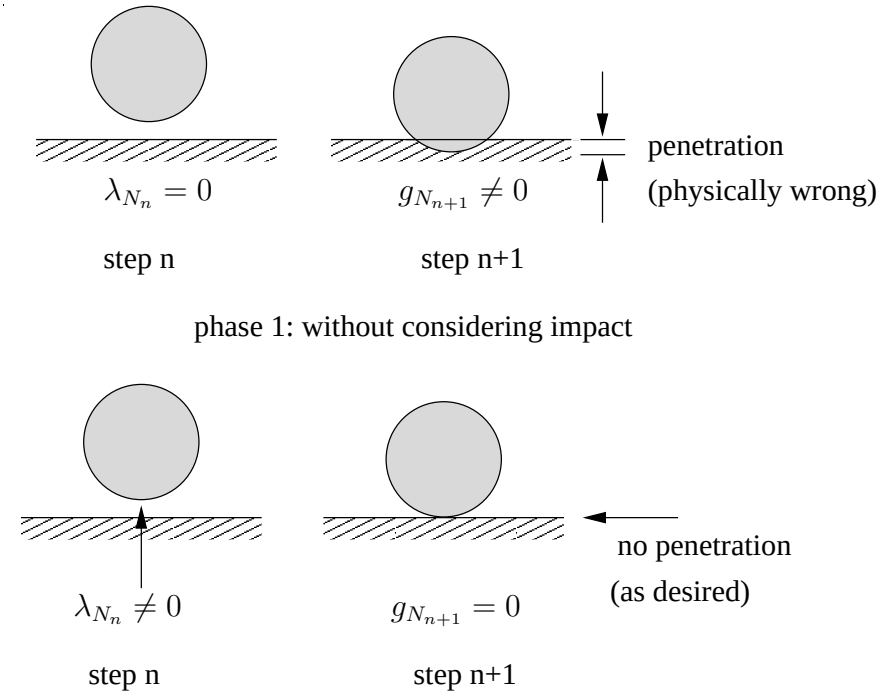

Figure 5.3: The effect of λ_{N_n} on the normal gap distance $g_{N_{n+1}}$ from the 4^{th} order explicit Runge-Kutta approach

The 5^{th} Order Implicit Runge-Kutta Approach: RADAU5

As another possibility, one can obtain the required relation between $\mathbf{q}_{n+1}$ and $\boldsymbol{\lambda}_{N_n}$ from the RADAU5 approach which is an implicit 5^{th} order Runge-Kutta method, see e.g. [38, 59].

This task has been done in Appendix 8 for which the following relation is obtained

$$\mathbf{q}_{n+1} = \mathbf{W}_{q_n} \cdot \boldsymbol{\lambda}_{N_n} + \mathbf{w}_{q_n} \ , \tag{5.23}$$

where

$$\begin{aligned}
\mathbf{W}_{q_n} = \Delta t_n^2 \Big(& \gamma_1\beta_{11} \left(\widetilde{\mathbf{M}}_{q_1} \cdot \mathbf{W}_{c_1}\right)_n^{k-1} + \gamma_1\beta_{12} \left(\widetilde{\mathbf{M}}_{q_2} \cdot \mathbf{W}_{c_2}\right)_n^{k-1} + \gamma_1\beta_{13} \left(\widetilde{\mathbf{M}}_{q_3} \cdot \mathbf{W}_{c_3}\right)_n^{k-1} + \\
& \gamma_2\beta_{21} \left(\widetilde{\mathbf{M}}_{q_1} \cdot \mathbf{W}_{c_1}\right)_n^{k-1} + \gamma_2\beta_{22} \left(\widetilde{\mathbf{M}}_{q_2} \cdot \mathbf{W}_{c_2}\right)_n^{k-1} + \gamma_2\beta_{23} \left(\widetilde{\mathbf{M}}_{q_3} \cdot \mathbf{W}_{c_3}\right)_n^{k-1} + \\
& \gamma_3\beta_{31} \left(\widetilde{\mathbf{M}}_{q_1} \cdot \mathbf{W}_{c_1}\right)_n^{k-1} + \gamma_3\beta_{32} \left(\widetilde{\mathbf{M}}_{q_2} \cdot \mathbf{W}_{c_2}\right)_n^{k-1} + \gamma_3\beta_{33} \left(\widetilde{\mathbf{M}}_{q_3} \cdot \mathbf{W}_{c_3}\right)_n^{k-1} \Big) \ , \\
\mathbf{w}_{q_n} = \mathbf{q}_n \ & + \Delta t_n \ \dot{\mathbf{q}}_n \left(\gamma_1 + \gamma_2 + \gamma_3\right) \ + \\
& \Delta t_n^2 \Big(\gamma_1\beta_{11} \left(\widetilde{\mathbf{M}}_{q_1} \cdot \mathbf{h}_{c_1}\right)_n^{k-1} + \gamma_1\beta_{12} \left(\widetilde{\mathbf{M}}_{q_2} \cdot \mathbf{h}_{c_2}\right)_n^{k-1} + \gamma_1\beta_{13} \left(\widetilde{\mathbf{M}}_{q_3} \cdot \mathbf{h}_{c_3}\right)_n^{k-1} + \\
& \gamma_2\beta_{21} \left(\widetilde{\mathbf{M}}_{q_1} \cdot \mathbf{h}_{c_1}\right)_n^{k-1} + \gamma_2\beta_{22} \left(\widetilde{\mathbf{M}}_{q_2} \cdot \mathbf{h}_{c_2}\right)_n^{k-1} + \gamma_2\beta_{23} \left(\widetilde{\mathbf{M}}_{q_3} \cdot \mathbf{h}_{c_3}\right)_n^{k-1} + \\
& \gamma_3\beta_{31} \left(\widetilde{\mathbf{M}}_{q_1} \cdot \mathbf{h}_{c_1}\right)_n^{k-1} + \gamma_3\beta_{32} \left(\widetilde{\mathbf{M}}_{q_2} \cdot \mathbf{h}_{c_2}\right)_n^{k-1} + \gamma_3\beta_{33} \left(\widetilde{\mathbf{M}}_{q_3} \cdot \mathbf{h}_{c_3}\right)_n^{k-1} \Big) \ .
\end{aligned} \tag{5.24}$$

The superscript $k-1$ is served for the quantities of one iteration before the final successful iteration counter k of its corresponding integration step n. The new parameters β and γ arise directly from the RADAU5 integration formula. At each time step n the iteration is followed untill convergence after k iterations. Then, the associated quantities of the $(k-1)^{th}$ iteration step are used in Eq. (5.23).

5.3 Frictional Impact

In order to consider friction, the formulation presented for normal impact in Section 5.2 may be appended to the formulation of tangential contact forces developed for continual contact in Chapter 4. The key issue behind this approach arises from the fact that in the case of flexible bodies, the behavior of impact in the tangential direction is similar to that of the continual contact for a short period of time. However, it is obvious that this assumption is valid only for impact analysis of flexible bodies and in the case of rigid bodies impact analysis, these two events must be distinguished.

Once again the equations of motion for the general case of frictional impact are considered as

$$\mathbf{M}_c \cdot \ddot{\mathbf{q}}_c - \mathbf{h}_c - \begin{bmatrix} \mathbf{W}_N + \mathbf{W}_G \cdot \boldsymbol{\mu}_G & \mathbf{W}_H \\ \mathbf{0} & \mathbf{0} \end{bmatrix} \cdot \begin{bmatrix} \boldsymbol{\lambda}_N \\ \boldsymbol{\lambda}_H \end{bmatrix} = \mathbf{0} \ . \tag{5.25}$$

This equation extends Eq. (5.10) by considering the effect of friction forces. By separating the tangential contact forces to sliding forces $\mathbf{W}_G \cdot \boldsymbol{\mu}_G \cdot \boldsymbol{\lambda}_N$ and sticking forces $\mathbf{W}_H \cdot \boldsymbol{\lambda}_H$

and supposing $\boldsymbol{\lambda}_H = \boldsymbol{\lambda}_H^{(+)} - \boldsymbol{\lambda}_H^{(-)}$ for sticking contact forces, one can rewrite Eq. (5.25), see [106],

$$\mathbf{M}_c \cdot \ddot{\mathbf{q}} = \mathbf{h}_c + \underbrace{\left[\begin{array}{c|c|c} \mathbf{W}_N + \mathbf{W}_G \cdot \boldsymbol{\mu}_G & \mathbf{W}_H & -\mathbf{W}_H \\ \mathbf{0} & \mathbf{0} & \mathbf{0} \end{array}\right]}_{\mathbf{W}_{NHc}} \cdot \underbrace{\left[\begin{array}{c} \boldsymbol{\lambda}_N \\ \boldsymbol{\lambda}_H^{(+)} \\ \boldsymbol{\lambda}_H^{(-)} \end{array}\right]}_{\boldsymbol{\lambda}} , \tag{5.26}$$

where $\mathbf{W}_G$ and $\mathbf{W}_H$ are matrices extracted from the matrix $\mathbf{W}_T$ and correspond to the sliding and sticking contacts, respectively, and $\boldsymbol{\mu}_G$ is a diagonal matrix of friction coefficients. At this point, the generalized accelerations are extracted from this relation in the same manner as was performed previously for frictionless impact in Eq. (5.12)

$$\ddot{\mathbf{q}}_c = \left[\begin{array}{c} \ddot{\mathbf{q}} \\ \boldsymbol{\lambda}_C \end{array}\right] = \left[\begin{array}{c} \widetilde{\mathbf{M}}_q \\ \widetilde{\mathbf{M}}_\lambda \end{array}\right] \cdot (\mathbf{h}_c + \mathbf{W}_{NHc} \cdot \boldsymbol{\lambda}) \quad \rightarrow \quad \ddot{\mathbf{q}} = \widetilde{\mathbf{M}}_q \cdot (\mathbf{h}_c + \mathbf{W}_{NHc} \cdot \boldsymbol{\lambda}) \, . \tag{5.27}$$

In the next step and based on this notation, Eq. (5.20) is modified for considering friction forces

$$\mathbf{q}_{n+1} = \underbrace{\frac{\Delta t_n^2}{6} \sum_{j=1}^{3} (\widetilde{\mathbf{M}}_{q_j} \cdot \mathbf{W}_{NHc_j})_n}_{\mathbf{W}_{q_n}} \cdot \boldsymbol{\lambda}_n + \underbrace{(\mathbf{q}_n + \Delta t_n \dot{\mathbf{q}}_n + \frac{\Delta t_n^2}{6} \sum_{j=1}^{3} (\widetilde{\mathbf{M}}_{q_j} \cdot \mathbf{h}_{c_j})_n)}_{\mathbf{w}_{q_n}} \, . \tag{5.28}$$

Similarly, one may modify the formulation developed from the RADAU5 method, Eq. (5.23), but at the moment only the above equation based on the explicit Runge-Kutta approach is considered. Now, the generalized coordinates and accelerations may be written together from Eqs. (5.28) and (5.27), respectively,

$$\left[\begin{array}{c} \mathbf{q} \\ \ddot{\mathbf{q}} \end{array}\right] = \left[\begin{array}{c} \mathbf{W}_q \\ \widetilde{\mathbf{M}}_q \cdot \mathbf{W}_{NHc} \end{array}\right] \cdot \boldsymbol{\lambda} + \left[\begin{array}{c} \mathbf{w}_q \\ \widetilde{\mathbf{M}}_q \cdot \mathbf{h}_c \end{array}\right] \, . \tag{5.29}$$

The procedure is followed by considering the second equation of Eq. (4.10) for sticking contacts illustrated by index H in Eq. (5.26)

$$\underbrace{\left[\begin{array}{c} \ddot{\mathbf{g}}_H \\ -\ddot{\mathbf{g}}_H \end{array}\right]}_{\ddot{\mathbf{g}}_{HG}} = \underbrace{\left[\begin{array}{c} \mathbf{W}_H^T \\ -\mathbf{W}_H^T \end{array}\right]}_{\mathbf{W}_{HG}^T} \cdot \ddot{\mathbf{q}} + \underbrace{\left[\begin{array}{c} \mathbf{w}_H^T \cdot \dot{\mathbf{q}} \\ -\mathbf{w}_H^T \cdot \dot{\mathbf{q}} \end{array}\right]}_{\mathbf{w}_{HG}} \, . \tag{5.30}$$

The sliding contacts have already been taken into account from the Coulomb friction law. Equation (5.30) together with Eq. (5.9) can be written in the following matrix form

$$\left[\begin{array}{c} \mathbf{g}_N \\ \ddot{\mathbf{g}}_{HG} \end{array}\right] = \left[\begin{array}{cc} \mathbf{W}_g & \mathbf{0} \\ \mathbf{0} & \mathbf{W}_{HG}^T \end{array}\right] \cdot \left[\begin{array}{c} \mathbf{q} \\ \ddot{\mathbf{q}} \end{array}\right] + \left[\begin{array}{c} \bar{\mathbf{w}} \\ \mathbf{w}_{HG} \end{array}\right] \, . \tag{5.31}$$

The generalized coordinates and accelerations can be substituted from Eq. (5.29) yielding

$$\underbrace{\begin{bmatrix} \mathbf{g}_N \\ \ddot{\mathbf{g}}_{HG} \end{bmatrix}}_{\mathbf{g}_M} = \underbrace{\begin{bmatrix} \mathbf{W}_g \cdot \mathbf{W}_q \\ \mathbf{W}_{HG}^T \cdot \widetilde{\mathbf{M}}_q \cdot \mathbf{W}_{NHc} \end{bmatrix}}_{\mathbf{W}_{gqc}^T} \cdot \boldsymbol{\lambda} + \underbrace{\begin{bmatrix} \mathbf{W}_g \cdot \mathbf{w}_q + \bar{\mathbf{w}} \\ \mathbf{W}_{HG}^T \cdot \widetilde{\mathbf{M}}_q \cdot \mathbf{h}_c + \mathbf{w}_{HG} \end{bmatrix}}_{\mathbf{w}_{gqc}} . \tag{5.32}$$

However, this equation cannot be used in this form and has to be transformed to an LCP by introducing some dummy parameters, as was mentioned for continual contact formulation in Chapter 4. The final form of the complementarity equations based on the introduced notation and according to the above mentioned points is

$$\begin{bmatrix} \mathbf{g} \\ \boldsymbol{\lambda}_{H_0} \end{bmatrix} = \begin{bmatrix} \mathbf{W}_{gqc}^T & \mathbf{I}^T \\ \mathbf{N}_H - \mathbf{I} & \mathbf{0} \end{bmatrix} \cdot \begin{bmatrix} \boldsymbol{\lambda} \\ \mathbf{z} \end{bmatrix} + \begin{bmatrix} \mathbf{w}_{gqc} \\ \mathbf{0} \end{bmatrix} ,$$
$$\begin{bmatrix} \mathbf{g} \\ \boldsymbol{\lambda}_{H_0} \end{bmatrix} \geq \mathbf{0} , \qquad \begin{bmatrix} \boldsymbol{\lambda} \\ \mathbf{z} \end{bmatrix} \geq \mathbf{0} , \qquad \begin{bmatrix} \mathbf{g} \\ \boldsymbol{\lambda}_{H_0} \end{bmatrix} \cdot \begin{bmatrix} \boldsymbol{\lambda} \\ \mathbf{z} \end{bmatrix} = 0 . \tag{5.33}$$

Here, the parameters $\boldsymbol{\lambda}_{H_0}, \mathbf{N}_H, \mathbf{I}$ and $\mathbf{z}$ are chosen in the same way as [106] and have the same meaning. Only the vector $\mathbf{g}$ has different interpretation and can be represented as

$$\mathbf{g} = \begin{bmatrix} \mathbf{g}_N^T & (\ddot{\mathbf{g}}_{HG}^+)^T & (\ddot{\mathbf{g}}_{HG}^-)^T \end{bmatrix}^T , \tag{5.34}$$

where $\ddot{\mathbf{g}}_{HG}^+$ and $\ddot{\mathbf{g}}_{HG}^-$ correspond to $\ddot{\mathbf{g}}_H^+$ and $\ddot{\mathbf{g}}_H^-$ from [106], respectively. These parameters are used in order to formulate the complementarity form of the equations in such a way to handle switching between sliding and sticking cases of contact. Maybe it is also important to point out that the required LCPs for normal and tangential directions must be considered only for their corresponding active contact pairs.

5.4 Impact Formulation on Velocity Level

As another possibility to formulate impact of planar flexible bodies one may also write the normal contact law on velocity level by considering velocity of normal gaps between active contact points, $\dot{\mathbf{g}}_N$, instead of normal gap distances, see Eq. (3.15),

$$\dot{\mathbf{g}}_N \geq \mathbf{0} , \qquad \boldsymbol{\lambda}_N \geq \mathbf{0} , \qquad \dot{\mathbf{g}}_N \cdot \boldsymbol{\lambda}_N = 0 . \tag{5.35}$$

The relation between $\dot{\mathbf{g}}_N$ and $\dot{\mathbf{q}}$ is written as the extention of Eq. (4.4) by including all potential contact points

$$\dot{\mathbf{g}}_N = \mathbf{W}_N^T \cdot \dot{\mathbf{q}} . \tag{5.36}$$

One can use the 4^{th} order explicit Runge-Kutta method but this time a relation between $\dot{\mathbf{q}}$ and $\boldsymbol{\lambda}$ is required. This desired relation based on the notation used in Section 5.3 reads

as, see Appendix 8,

$$\dot{\mathbf{q}}_{n+1} = \left(\frac{\Delta t_n}{6}(\widetilde{\mathbf{M}}_{q_1} \cdot \mathbf{W}_{NHc_1} + \widetilde{\mathbf{M}}_{q_4} \cdot \mathbf{W}_{NHc_4})_n + \frac{\Delta t_n}{3}\sum_{j=2}^{3}(\widetilde{\mathbf{M}}_{q_j} \cdot \mathbf{W}_{NHc_j})_n \right) \cdot \boldsymbol{\lambda}_n + \left(\dot{\mathbf{q}}_n + \frac{\Delta t_n}{6}(\widetilde{\mathbf{M}}_{q_1} \cdot \mathbf{h}_{c_1} + \widetilde{\mathbf{M}}_{q_4} \cdot \mathbf{h}_{c_4})_n + \frac{\Delta t_n}{3}\sum_{j=2}^{3}(\widetilde{\mathbf{M}}_{q_j} \cdot \mathbf{h}_{c_j})_n \right) . \quad (5.37)$$

The parameters in this equation have the same meaning as mentioned for Eq. (5.28) but their evaluation at each of the four stages of the Runge-Kutta method is required. Formulation of the LCP is simply done by substituting $\dot{\mathbf{q}}$ from this relation in Eq. (5.36) and following the same manner as was followed in Section 5.3. It is noticeable that the formulation on velocity level is only applicable for closed contacts for both frictionless and frictional cases.

5.5 Implemented Algorithm

In this section, the necessary steps for building and solving the linear complementarity problem associated with an impact problem of planar flexible bodies are explained. Similar to the previous chapter, the linear complementarity problem is solved by the PATH solver which is an algorithm for mixed complementarity problems, see [28] and [42]. The following algorithm has to be followed untill the end of simulation:

start
- initialize the generalized coordinates $\mathbf{q}_1$ and velocities $\dot{\mathbf{q}}_1$
- set $\boldsymbol{\lambda}_0 = \mathbf{0}, tol = 1e-6, k_{max}$ =maximum number of iterations
- initialize the step counter $n = 1$
- find active normal contact pairs $g_{N_l} \leq 0$
- find active sticking contact pairs $|\dot{g}_{T_l}| \leq tol$

while $(t < t_{end})$
- initialize the contact force from the previous time step $\boldsymbol{\lambda}_n = \boldsymbol{\lambda}_{n-1}$
- initialize the iteration counter $k = 1$ and iteration error $err = 1.0$

while $(err > tol, k < k_{max})$
- calculate new $\mathbf{q}_{n+1}$ and $\dot{\mathbf{q}}_{n+1}$ utilizing a suitable integration approach
- build the required quantities for normal as well as sliding contacts
- build the required quantities for sticking contacts
- generate and solve the LCP of Eq. (5.33) for unknowns $\mathbf{g}_{n+1}^{k+1}$ and $\boldsymbol{\lambda}_n^{k+1}$
- calculate the error $err = |(\|\boldsymbol{\lambda}_{N_n}^{k+1}\| - \|\boldsymbol{\lambda}_{N_n}^{k}\|)| + |(\|\boldsymbol{\lambda}_{H_n}^{k+1}\| - \|\boldsymbol{\lambda}_{H_n}^{k}\|)|$
- initialize the contact force for the next iteration $\boldsymbol{\lambda}_n^{k+1} = \boldsymbol{\lambda}_n^{k}$
- increase the iteration counter $k = k + 1$

end while

- proceed to the next time step $t_{n+1} = t_n + \Delta t_n$ and increase the step counter $n = n+1$

end while

end

Remarks: In this algorithm the second iteration is needed since matrix $\mathbf{W}_{g_{n+1}}$ in Eq. (5.21) depends on the generalized rotational coordinates of the integration step $n+1$. These coordinates depend on the unknown normal contact forces $\boldsymbol{\lambda}_{N_n}$ as well. Therefore, one needs an iteration to substitute the values of $\boldsymbol{\lambda}_{N_n}$ from the previous time step and to solve the LCP iteratively to find the correct values of $\boldsymbol{\lambda}_{N_n}$.

In the case that the error does not decrease below *tol* within k_{max} iterations, the values of the contact forces associated with the last iteration step are taken as the contact forces of that integration step and are used as initial values for the iteration of the next integration step. However, the experience from different simulations shows that convergence is reached just after several iterations if a suitable time step is chosen.

Maybe it is important to emphasize that the simulations can be done by using any suitable numerical integration approach like RADAU5 or Newmark methods. However, the formulations presented in Section 5.2.2 based on the explicit Euler, the 4^{th} order explicit Runge-Kutta and RADAU5 methods are just used to obtain an analytical formulation between $\mathbf{g}_N$ and $\boldsymbol{\lambda}_N$ and not for the main integration processes to proceed to the next time step. In other words, the approach presented here consists of two integrations: one is the main integration to proceed from the step n to $n+1$ and another one is responsible for calculating the normal gap distances vector as a function of normal contact forces.

Another important feature of the presented approach for **frictionless impact** is that the collission detection step is done automatically as the result of the LCP. For example, in the case of impact analysis between two bodies i and j in Figure 5.1, suppose that each discretized body consists of surface nodes. Then, the relation of $\mathbf{g}_N$ in Eq. (5.9) must include the possible connections between surface nodes of one body with the surfaces of another body if no previously chosen slidelines can be used. As the result of the LCP, the presented approach returns zero contact forces for the non-active contact pairs and non-zero contact forces for the active contact pairs. However, writing the relation of $\mathbf{g}_N$ between all possible contact pairs can tremendously increase the computational effort required for building and solving the LCP and, therefore, it is not recommended when dealing with systems including many bodies with a large number of surface nodes. In such situations, any standard collision detection may be utilized to capture the active contact points and then, the normal gap distances vector can be formulated only for these possible contact situations.

The complementarity conditions used here in order to formulate this approach for impact analysis are also valid for continual contact. Therefore, this approach may also be used as a general approach including continual contact and impact. In this way, it will eliminate the necessity of switching between continual contact and impact formulations.

In spite of these advantages, the formulation presented in Chapter 4, see also [31, 34], is preferred for continual contact case since it will have less difficulties in generating the linear complementarity equations compared to the approach for impact analysis.

5.6 Numerical Examples

For validation and checking the accuracy of the results of the presented approach, three classical examples of impacting bodies are simulated and the results are given here. In the first example, the frictionless impact problem between two elastic disks is modeled through two different approaches of LCP and FEM. In the second example, the frictionless impact of an elastic block on a rigid foundation is investigated. In the last example, frictional impact of ten identical elastic blocks is considered.

Example 1: Impact of Two Identical Elastic Disks

The problem of frictionless impact between two identical elastic disks is considered, see Figure 5.4. The goal is to implement the formulations of impact on position and velocity level. For building the model of the elastic disks and generating the equations of motion based on the impact formulation as an LCP, a certain number of eigenmodes among the 1580 modes of the FEM model is chosen and the necessary quantities are written in a standard input data (SID) file, see Chapter 2. For consideration of energy dissipation during impact, the natural damping model of the FEMBS interface of SIMPACK is used.

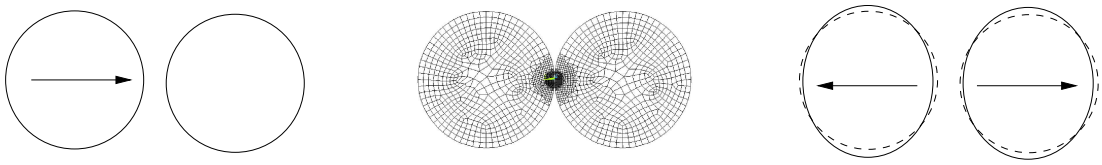

Figure 5.4: Impact of two elastic disks.

For simulation of this academic test example, the left disk has an approaching initial velocity of 0.5 m/s while the right disk is initially at rest. The quantities $\rho = 10$ kg/m^2 and $\nu = 0.3$ for areal density and Poisson's ratio are used. First, two soft elastic disks with Young's modulus $E = 2e6$ Pa are considered. In a second simulation, the Young's modulus $E = 2e8$ Pa is considered for both disks. The results of the first simulation are depicted in Figure 5.5. Here, the results are shown from the explicit Runge-Kutta method on position level with $pos_{explicit}$, the implicit Runge-Kutta method on position level with $pos_{implicit}$ and the explicit Runge-Kutta on velocity level with $vel_{explicit}$.

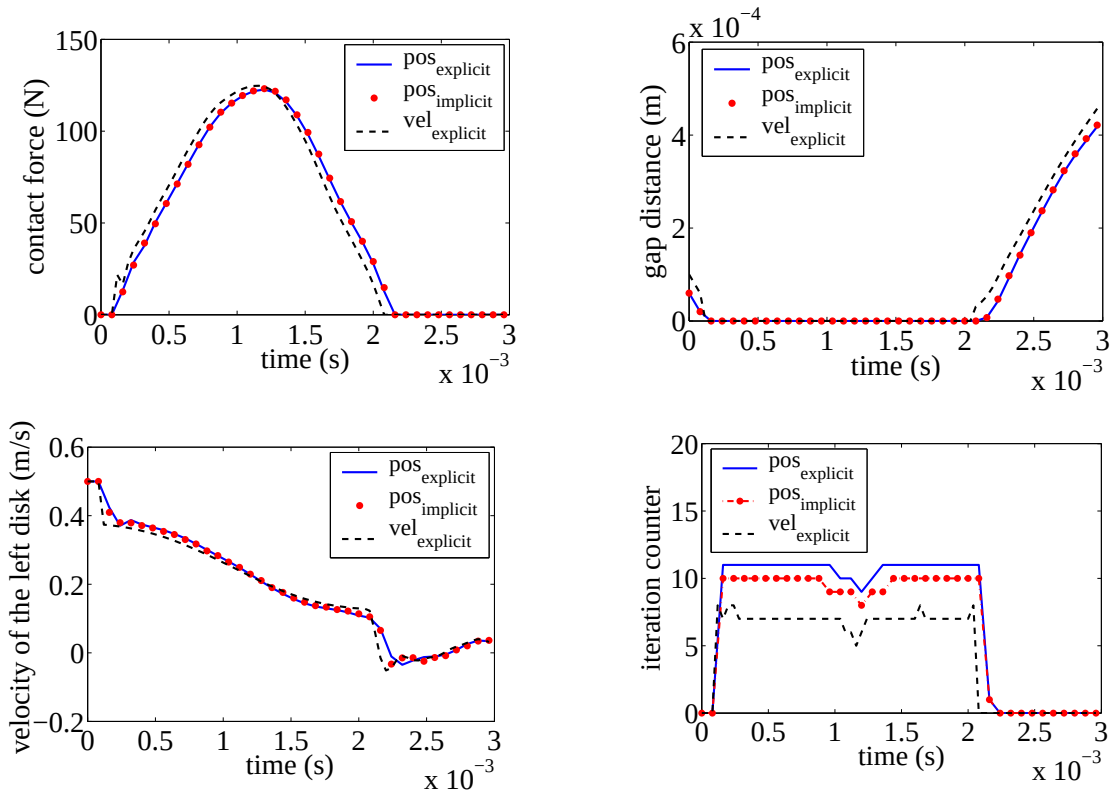

Figure 5.5: Contact simulation of two identical elastic disks for $E = 2e6$ Pa using 55 modes

As it can be seen, the explicit and implicit Runge-Kutta approaches on position level deliver the same results for contact forces and kinematic quantities like gap distance and disk velocities. To get such results, the explicit approach requires less computation time in spite of the fact that it needs more iterations. The right-down illustration in Figure 5.5 shows the required iterations for evaluation of the contact forces based on the algorithm presented in Chapter 5 and must be distinguished from the usual iteration included in the implicit Runge-Kutta approach. The results from the explicit Runge-Kutta approach on velocity level shows also a good agreement with the results from the approach on position level.

For the second simulation of this example with $E = 2e8$ Pa one observes that for stiff planar deformable bodies, which behave more closely to rigid bodies, the results of this approach using 55 modes differ from the results of FEM. The second simulation is also performed for higher number of eigenmodes, 100 and 200, for both elastic disks. The results depicted in Figure 5.6 show the expected fact that with increasing number of eigenmodes, the results of the presented approach on both position and velocity level approach the precise results of FEM for stiff planar deformable bodies provided that a proper number of eigenmodes of the FEM model is chosen for building the reduced model. This fact is not surprising since in the case of dealing with impact of stiff deformable bodies, the higher eigenmodes will be excited and, therefore, their proper selection is necessary to get realistic behavior after impact.

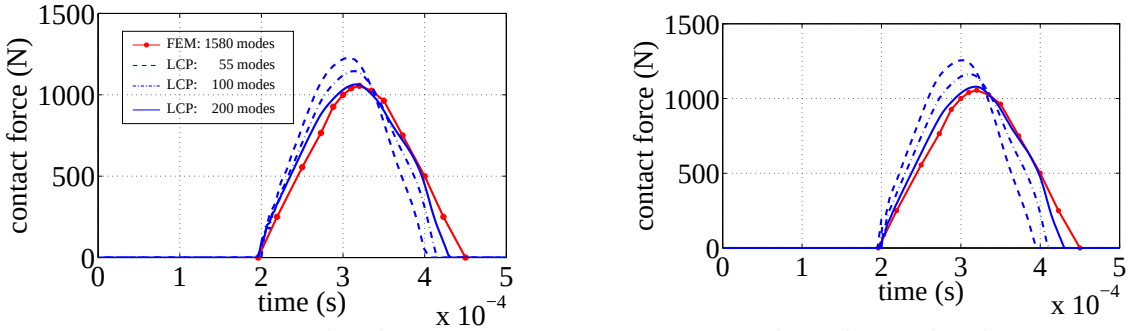

a: position level b: velocity level

Figure 5.6: Impact force for $E = 2e8$ Pa

For investigating the efficiency of both approaches, the CPU time needed for impact analysis of stiff elastic disks (simulation 2) is determined. It is noticeable that for each number of eigenmodes and for each approach there is a region of optimal time step which is to be chosen for integration. Selection of higher values leads to increasingly worse results with the possibility of getting singular matrices while smaller values result in impact forces with oscillatory behavior. The CPU times and the optimal time step for both formulations on position and velocity level are depicted in Figure 5.7.

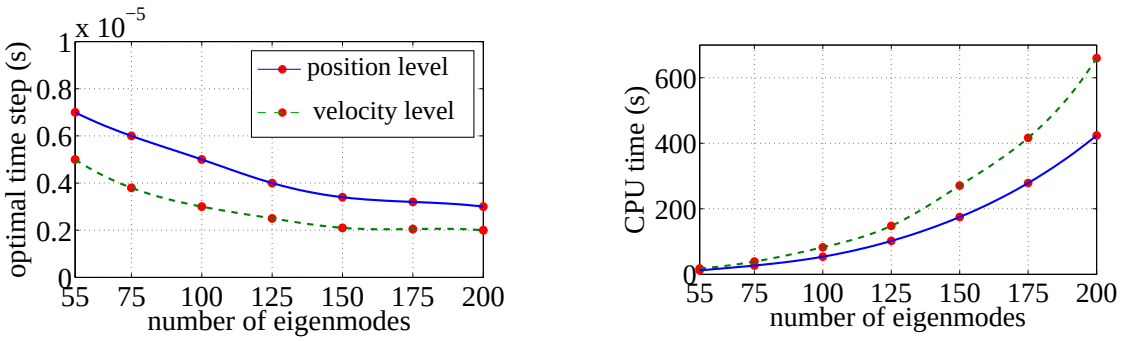

Figure 5.7: Optimal time step and CPU time for a different number of eigenmodes from the formulation on position and velocity level

The results at the evaluated number of eigenmodes for this simulation are marked with circles. Then, using a spline interpolation one can evaluate approximately the optimal time step of the integration for the required number of eigenmodes. It can clearly be seen that the position level formulation requires higher step sizes and lower CPU times when compared with the velocity level formulation for the same number of eigenmodes. Since the depicted impact forces in Figure 5.6 show the same behavior for both formulations, one concludes that the formulation on position level is computationally more efficient than the formulation on velocity level and can be chosen as a reliable approach for impact

analysis of planar deformable bodies in multibody systems provided that an optimal time step is chosen and, additionally, a proper number of eigenmodes is included.

In Figure 5.8 the percentage of dissipated total energy of the system during impact for different natural damping factors and number of eigenmodes is illustrated. In fact, both plots imply the same results but the percentage of dissipated total energy has been shown once versus natural damping for different number of eigenmodes, and once versus number of eigenmodes for different natural damping factors to clearly depict the effect of each parameter separately on the amount of dissipated total energy.

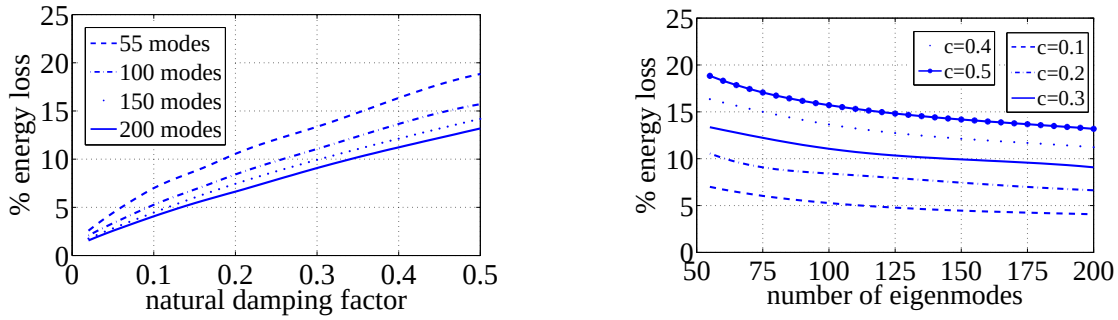

Figure 5.8: Percentage of energy loss for different number of eigenmodes and damping factors

It is seen that selection of a higher number of eigenmodes leads to the lower energy dissipation. It can be interpreted based on the fact that the higher number of modes allows a better adjustment of the shape of the elastic disks, so that collisions become effectively softer, see also [53]. It is also noticeable that for small values of the damping factor, the amount of dissipated energy for different number of modes varies slightly. However, by increasing the damping factor, the difference between the amount of dissipated energy is intensified. It means that for a higher number of eigenmodes, a higher percentage of the absorbed energy during the compression phase of impact is released during the expansion phase of impact. In other words, the amount of released energy during the expansion phase of impact increases as a higher number of eigenmodes is considered.

Example 2: Frictionless Impact of an Elastic Block

An elastic block and a rigid foundation are depicted in Figure 5.10. The interest in this example is to simulate the elastic block when it leaves the curved part and experiences the impact. In this example, the elastic block is initially at rest and starts to slide on the foundation due to gravity. Therefore, firstly it experiences a sliding motion with continual contact conditions. After awhile, it leaves the curved part of the foundation and looses the contact with the foundation at around $t = 3$ s. From the beginning untill

this time, the simulation has been done using the approach presented in Chapter 4 for continual contact of flexible bodies. Now, from this time untill the end of simulation, the presented approach for impact analysis is used to handle the impact conditions. Then, at $t = 3.6$ s node 1 and after awhile node 4 come in contact with the horizontal part of the foundation. Due to the effect of high normal contact forces, the elastic block separate from the foundation at node 1. Finally, the elastic block follows a sliding motion untill the end of the simulation. Some results of this simulation are depicted in Figure 5.9. The left side of this figure shows the trajectory of the block reference coordinate system at node 4. The variations of the elastic coordinates are shown in the right side of Figure 5.9 versus time.

For simulation of this academic test example, the same material properties and initial conditions as the example of Section 4.4 are used.

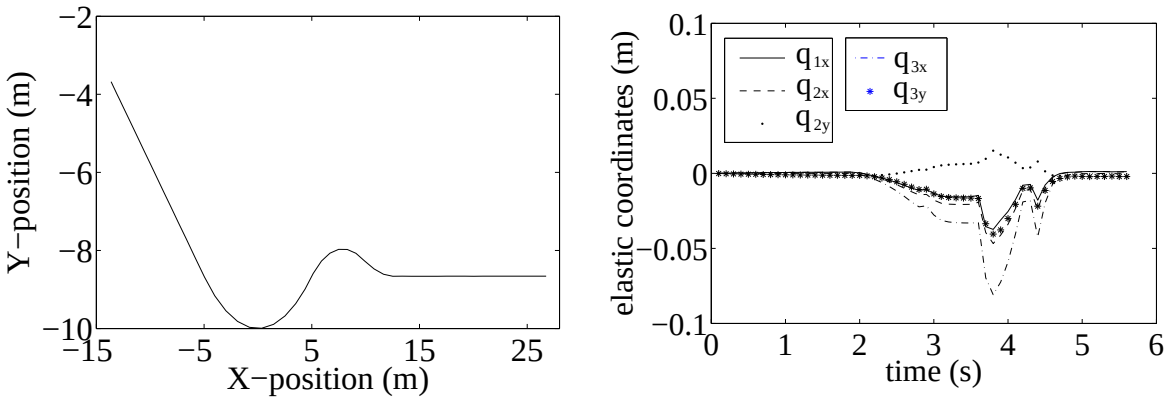

Figure 5.9: Trajectory of the block reference coordinate system and variations of the elastic coordinates

Example 3: Frictional Impact of Identical Elastic Blocks

An example of ten identical elastic rectangular blocks which topple down consecutively is considered, see Figure 5.11. For further use, let us number them from 1 to 10 starting from left to the right hand side. At first, all blocks are at rest on the rigid foundation with equal distances. Then, the first block on the left hand side follows a rotational motion with $\omega = 4$ rad/s and hits the second block. This event will repeat sequentially for the other blocks and after awhile the elastic block 10 will topple down over the rigid foundation. Hence, one can investigate the effect of impact with friction between planar elastic blocks.

For simulation of this test example, following values for the material and geometry of each elastic block have been used:

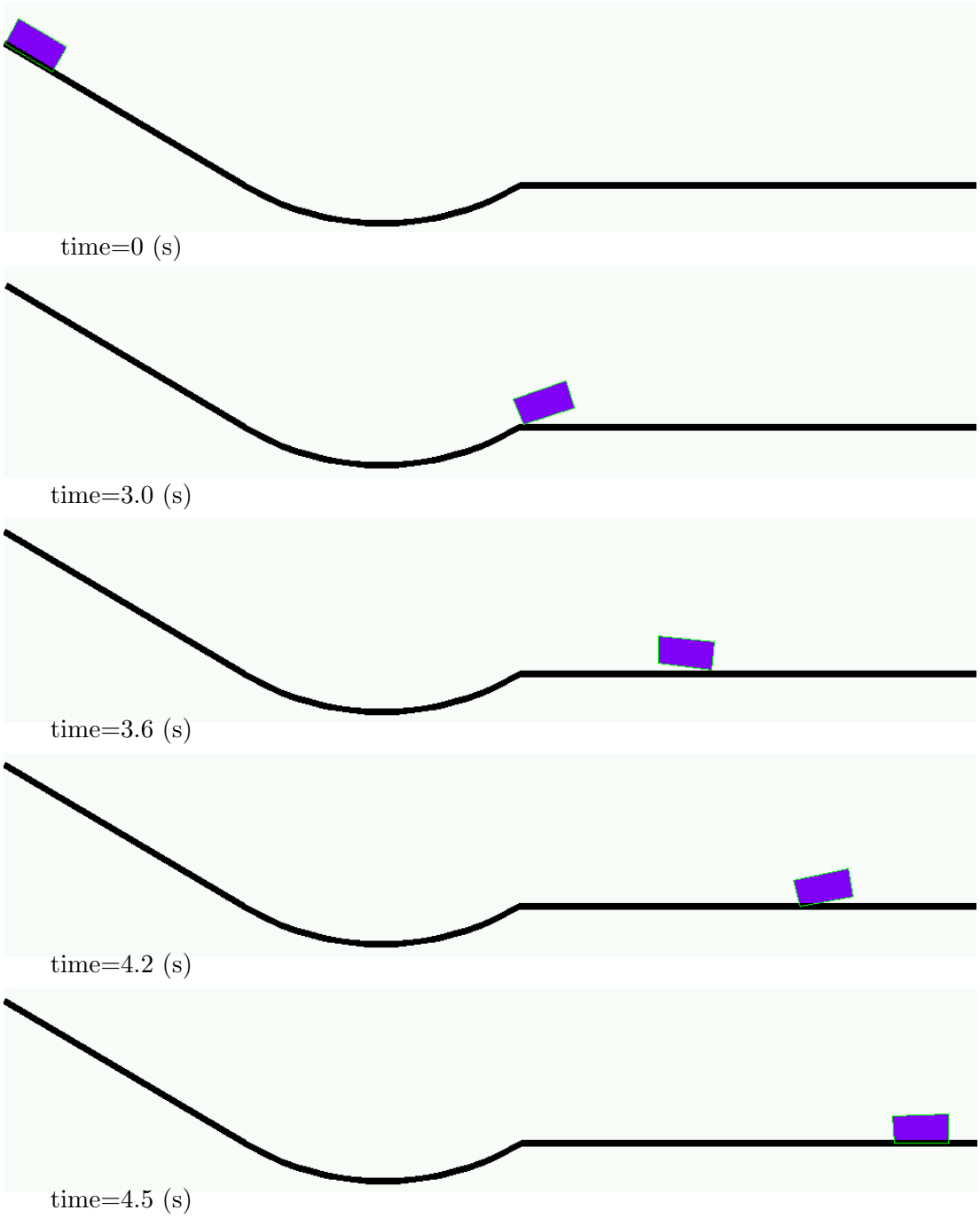

Figure 5.10: Continual contact and impact of the elastic block

material: $E = 2500$ N/m, $\nu = 0.3$, $\mu = 0.25$, $M = 4$ kg ,

geometry: $H = 1$ m, $L = 0.3$ m,

where E is the areal Young's modulus, ν is the Poisson's ratio, μ is the friction coefficient, M is the mass, H is the height and L is the length. Figure 5.12 shows the rotation angle and Y-position of the reference frame of the elastic blocks during simulation. The reference

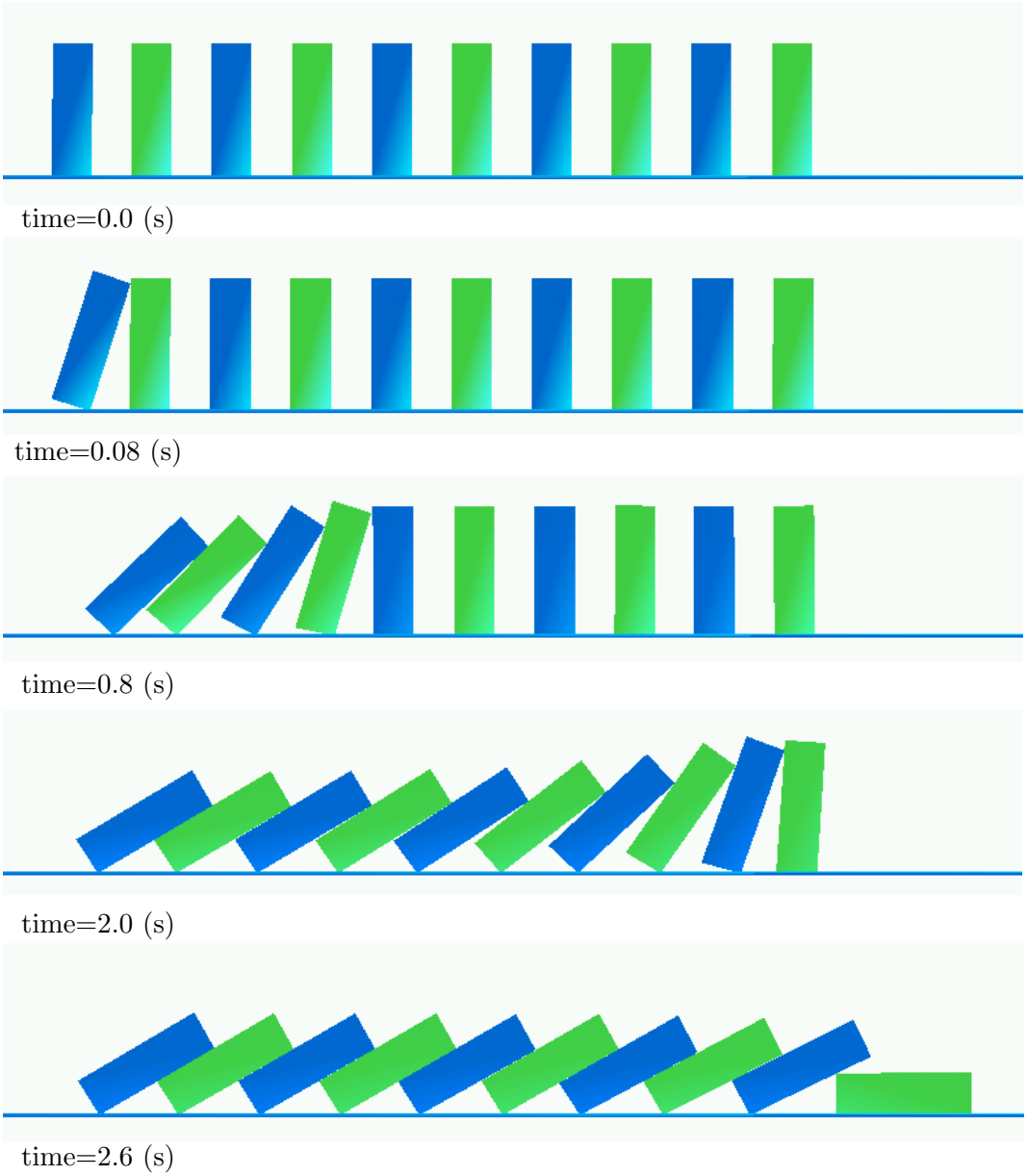

Figure 5.11: Impact between ten identical elastic rectangular blocks

frame is depicted in Figure 4.2. From the variation of both parameters, the impact instance of each elastic block can be clearly seen. The point in which all graphs intersect corresponds to the time that all the elastic blocks have almost the same rotation angle. It is also clear that finally the elastic block 10 topples down over the rigid foundation and, therefore, its rotation angle is about $-\frac{\pi}{2}$ rad at the end of the simulation.

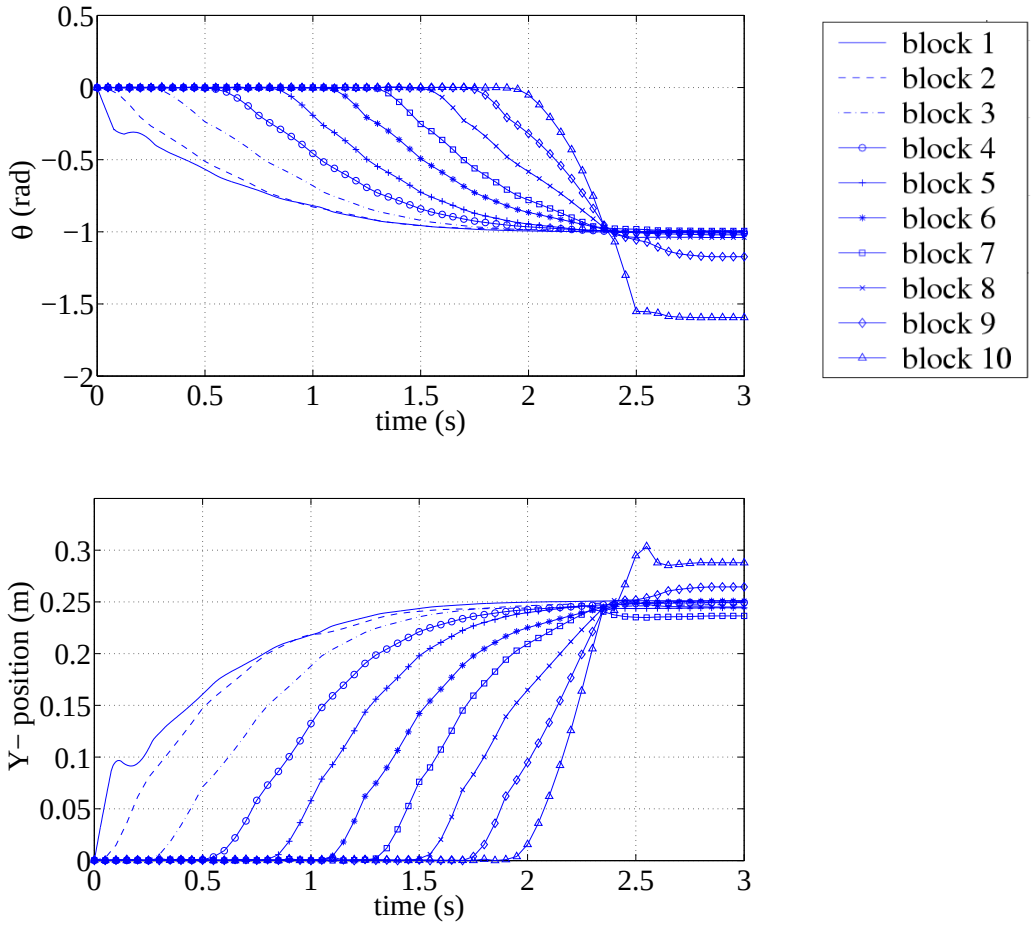

Figure 5.12: Rotation angle and Y-position of the reference frame of the elastic blocks

Chapter 6

Contact and Impact of Spatial Flexible Bodies: PCM Approach

In Chapters 4 and 5, the continual contact and impact of planar flexible bodies in multibody systems were formulated as linear complementarity problems. For the case of dealing with general spatial flexible bodies, an approach is presented in this chapter which is based on another category of contact modeling approach different from what presented for planar case. As the source of this approach, the original code by Hippmann [66, 67, 68] is used which was developed as a Polygonal Contact Model (PCM) for rigid bodies contact and it is extended and changed so that flexible bodies can be considered, too, see also [32, 33].

6.1 PCM: General Overview and Fundamentals

PCM as an algorithm of the compliance surface class is based on the following characteristics:

- A polygonal surface description is chosen for geometry description of contacting bodies. Polygonal surfaces that PCM uses must not contain duplicated vertices and their polygons have to be oriented suitably. In the case of quadrilaterals and pentagons, PCM converts them into two and three triangular polygons, respectively.

- Contact forces are modeled based on the elastic foundation model.

Contact modeling in PCM consists of three basic steps. In the following, a brief explanation of each step is given.

6.1.1 Collision Detection in PCM

PCM implements an exact and efficient algorithm based on bounding volumes (BV) hierarchies. The idea behind this approach is to approximate the geometries of colliding bodies with bounding volumes to avoid as many intersection tests as possible. The most well-known methods that can be mentioned are Octrees [99], k-d trees [62], BSP-trees [96], sphere trees [71], oriented bounding boxes (OBB) [56], axis aligned bounding boxes [62], [63], box trees [9] and DOP trees [64]. The collision detection process is done at each time step and checks if two surfaces intersect for a given relative position and orientation. The BV trees are created only once for every surface during preprocessing based on the axis aligned bounding box approach (AABB). PCM follows the top-down approach and starts to create the BV tree from the root element and splits it up into two sub-volumes and follows this procedure to the leaf elements.

In order to split up the BVs, at first the axis direction in which the BVs have the largest volume expansion is chosen. After selecting this axis, PCM uses a list of all triangles which is sorted by the barycenter positions with respect to this axis. Then, construction of the left and right BVs (BV1 and BV2) will be started from both sides of the parent BV. The child BVs 1 and 2 of the two very outer triangles initialize the subdivision of the parent BV. The first and the last one of the remaining triangles are processed gradually as follows: In a test, the volume increases are calculated for both possibilities, e.g. if the triangle would be added to BV1 and on the other hand to BV2. Then, PCM chooses the child BV which leads to the lower increase. This is repeated for all triangles of the parent BV. So the child BVs grow until they divide the included surface parts in two. Figure 6.1 shows the creation process of BV tree for a helical spring model.

The collision detection starts with a collision test of the root elements of BV trees of the two objects. If an intersection is detected the procedure has to be followed recursively to check their children for intersection otherwise the current BV pairs and all their children are excluded from further evaluation. As inputs the bounding volumes A and B are given. At the beginning PCM checks if these BVs include child BVs:

- If both, A and B, include child BVs, all possible combinations of these children are checked for collisions. For all pairs which are found to intersect, the whole algorithm recursively calls itself.

- If not, both are leaves of their BV trees. In this case their included polygons are checked for intersection. If any intersection is found, it is known that the surfaces collide. Otherwise this branch of the recursive algorithm is terminated.

- If only one of them is a leaf, PCM implements BV-Checks with all children of the other one. Again the algorithm is called recursively if the BVs collide.

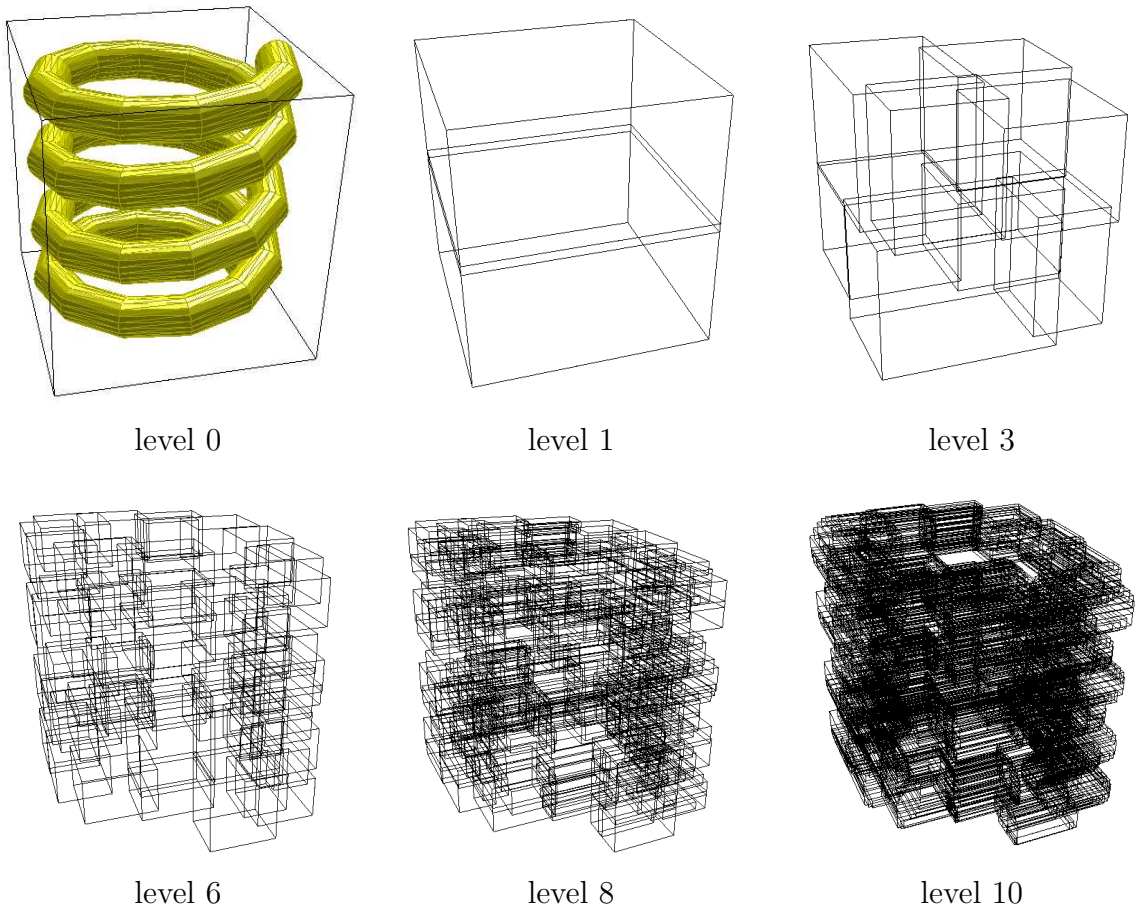

Figure 6.1: Several different levels of the BVs creation

This algorithm considerably speeds up the intersecting polygons search of two polygonal surfaces because the costly intersection test of two polygons can be avoided for most of the possible combinations.

6.1.2 Contact Element Generation

PCM approximates the contact patches by some contact elements, calculates the contact force of each contact element and sums them up to determine the total contact force and torque applied to the contacting bodies. In other words, contact elements are discretized areas of contact region for which contact forces are calculated. In doing so, PCM performs two basic steps for generation of contact elements based on the results that the collision detection step returns as output: construction of intersection polygons and determination of active areas and contact elements.

The collision detection returns the indices of intersected triangles and all the intersected lines in irregular order. The first line of the intersected lines is chosen. Then PCM implements a test in which the distances between the end points of the selected line and

the end points of all the other lines are measured. If the minimum is close to zero, then, the corresponding line is taken as the second line of the intersected polygon. Otherwise either it belongs to another intersection polygon or will be added to the current intersection polygon later on. This procedure is followed until all the intersected lines are tested and the intersection polygons are constructed.

In the next step a boundary representation data structure is utilized to determine the active areas. This type of data structure namely Doubly Connected Edge Lists (DCEL) [160] is generated during the preprocessing stage.

During the contact element generation step, for each master triangle its corresponding slave triangles are found and based on these triangles, the magnitude of penetration is determined. At last, the position of the contact element which represents the reference position of the resulting contact force of contact element is calculated.

6.1.3 Determination of Contact Forces and Torques

The contact force of each contact element consists of two normal and tangential force components. The normal force calculation is done by determination of the elastic and damping shares. The elastic share is described by

$$F_{e_k} = c_l A_{a_k} \delta_k \ , \tag{6.1}$$

where c_l is the combined layer stiffness calculated from the layer stiffnesses of two contacting bodies, A_{a_k} is area of the contact element and δ_k is penetration. Here, the indices 'e' for elastic, 'l' for layer, 'n' for normal direction and 'k' for the k^{th} contact element are used. Let us consider two contacting bodies i and j with the layer stiffnesses c_{l_i} and c_{l_j}, the Poisson's ratios ν_i and ν_j, the Young's moduli E_i and E_j and the elastic layer thicknesses b_i and b_j, respectively. Then, the relation of the combined layer stiffness c_l reads as

$$c_l = \frac{c_{l_i} c_{l_j}}{c_{l_i} + c_{l_j}} \ , \tag{6.2}$$

where

$$c_{l_i} = \frac{E_i(1-\nu_i)}{b_i(1+\nu_i)(1-2\nu_i)} \ , \qquad c_{l_j} = \frac{E_j(1-\nu_j)}{b_j(1+\nu_j)(1-2\nu_j)} \ . \tag{6.3}$$

The damping share of the normal contact force is determined by

$$F_{d_k} = \begin{cases} d_l A_{a_k} v_{n_k} & \text{for } \delta_k \geq \delta_d \ , \\ d_l A_{a_k} v_{n_k} \dfrac{\delta_k}{\delta_d} & \text{for } \delta_k < \delta_d \ . \end{cases} \tag{6.4}$$

Here d_l is the areal layer damping factor, v_{n_k} is the normal component of the relative velocity of contacting bodies at the contact element position and δ_d is a given transition depth.

The total normal contact force is determined by its elastic and damping shares

$$F_{n_k} = \begin{cases} F_{e_k} + F_{d_k} & \text{for } F_{e_k} + F_{d_k} > 0 \ , \\ 0 & \text{for } F_{e_k} + F_{d_k} \leq 0 \ . \end{cases} \tag{6.5}$$

The tangential contact force is determined based on the magnitude of the normal contact force and the tangential component of relative velocity

$$F_{t_k} = \begin{cases} \mu F_{n_k} & \text{for } v_{t_k} \geq v_\epsilon \ , \\ \mu F_{n_k} \dfrac{v_{tk}}{v_\epsilon}(2 - \dfrac{v_{t_k}}{v_\epsilon}) & \text{for } v_{t_k} < v_\epsilon \ , \end{cases} \tag{6.6}$$

where μ is the friction coefficient, F_{n_k} is the magnitude of normal contact force and v_ϵ is a so-called friction switch velocity as a small limit for the slip velocity v_t.

The total contact force $\mathbf{F}_k$ of a contact element is given by its normal and tangential components

$$\mathbf{F}_k = F_{n_k}\mathbf{n}_k + F_{t_k}\mathbf{t}_k \ . \tag{6.7}$$

The resulting torque vector $\mathbf{T}_k$ is then calculated from $\mathbf{F}_k$ and the contact element position. Finally, the forces and torques of all contact elements of that body are summed up to calculate the total contact force and torque of contacting bodies

$$\mathbf{F} = \sum_k \mathbf{F}_k \ , \qquad \mathbf{T} = \sum_k \mathbf{T}_k \ . \tag{6.8}$$

6.2 Extension of PCM for Contact of Flexible Bodies

There are some basic restrictions that must be overcome so that the contact modeling of flexible bodies would be possible too. Therefore, substantial modifications are implemented to the following parts of the algorithm.

6.2.1 Data Object Modification

During the preprocessing step PCM reads the input file of each body surface geometry in the format of a wave front object file [147]. In the case of identical surfaces, PCM reads the input file of these surfaces only once and so, for all identical surfaces the information of body surfaces is stored once. Therefore, the first step in the extension of PCM for flexible bodies contact modeling is the modification of handling and data structures in order to separate data of contact surfaces at different body positions. The surface data object of each body consists of three basic parts as shown in Figure 6.2.

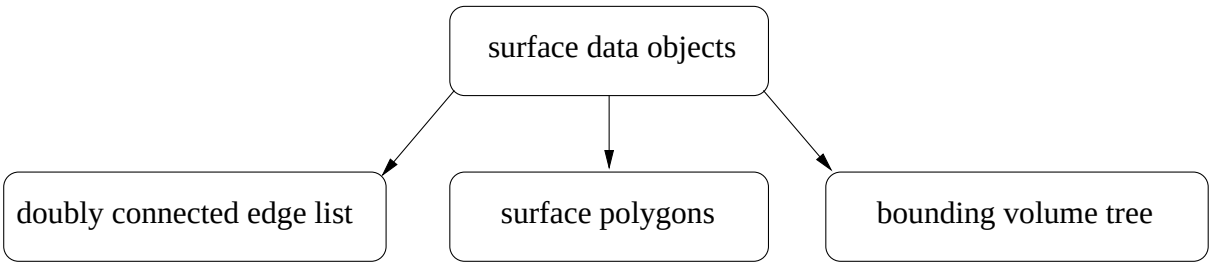

Figure 6.2: Three parts of the PCM surface data object

6.2.2 Updating Geometry of Elastic Bodies

PCM makes use of constant positions and orientations of the surface polygons of rigid bodies only once when generating BV trees during pre-processing. For flexible bodies at each time step the new surface geometry has to be calculated. In order to update geometry of flexible bodies, it is sufficient to calculate the new vertex positions of the polygonal surface with respect to the reference marker of the surface in which the vertex positions are given.

6.2.3 Updating Bounding Volume Trees

In the case of rigid bodies, it is sufficient to create BV trees only once and reuse them during simulation but for flexible bodies the limits of bonding volumes are not constant anymore and at each time step the collision detection needs to have updated values of the bounding volumes limits.

In order to find the new limits of the bounding volumes, one idea could be to rebuild the whole BV tree at each time step. However, it seems that this idea is not good since rebuilding the whole BV trees is computationally costly and not even necessary. In contrast, updating the whole BV tree can be used because it does not make a big difference to which one of two adjacent BVs a certain triangle belongs. Updating the BV limits means to keep the BVs but move and expand them so that they still include their polygons. The main idea is that one can easily update the limits of a non-leaf element by updating its children's BVs. So, one has to evaluate the current position of each triangle only once and to compare two values per limit for the non-leaf elements. This procedure can be done by a recursive function to be called once for the root element:

```
- if element == leaf
   - get vertex coordinates of included polygon
   - update min/max limits
- else
```

```
   - call this routine for child 1
   - call this routine for child 2
   - get min/max limits of children
   - update min/max limits
- end
```

For one example the simulation times in the cases of rebuilding and updating BV trees are as follows:

```
creation of the BV trees only once at preprocessing:  CPU time =  65.144(s)
updating the limits of BV trees at each time step:    CPU time =  76.055(s)
rebuilding the whole BV trees at each time step:      CPU time = 600.373(s)
```

As it can be seen, updating the limits of BV trees at each time step does not require much higher computational effort when compared with the creation of the BV trees only once at preprocessing. On the other hand, rebuilding the whole BV trees at each time step imposes prohibitive computational effort and, therefore, its practical implementation seems to be neither possible nor necessary.

6.2.4 Recalculating Normal Vectors, Areas and Barycenters

These parameters are accessed multiple times for active triangles at each time step of simulation. Therefore, in order to accelerate the procedure of recalculation, cache arrays are needed to store the data after the first access and to be reset before each evaluation of equations of motion. The idea which is used in doing so is to create an access function with these properties:

- calculate, update and return the normal vector, area and barycenter positions of all active triangles when called the first time,
- just read and return the data in successive calls.

This idea has been implemented by an additional flag per vertex which says if that parameter (normal vector, area or barycenter position of the current active triangle) is already available and is reset at the beginning of each function evaluation.

6.2.5 Modification of Relative Velocities

In order to calculate the contact force of each contact element, its relative velocity has to be taken into account. The relative velocity of a contact element is a relationship which describes the velocity of one point of body F relative to the velocity of one point of body

E at the contact element position C_k, see Figure 6.3, in the coordinate system of M_e (marker *from*). In the case of rigid bodies this velocity consists of two parts:

1. the relative velocity between M_f and M_e ($\mathbf{v}_{M_eM_f}$),
2. the relative velocity between one point of body F at the contact element position and M_f.

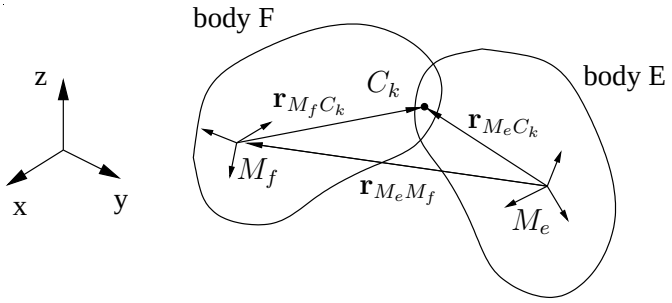

Figure 6.3: Contact element position

Therefore, the relative velocity vector is written as the summation of both parts

$$\mathbf{v}_k = \mathbf{v}_{M_eM_f} + \boldsymbol{\omega}_{M_eM_f} \times (\mathbf{r}_{M_eC_k} - \mathbf{r}_{M_eM_f}) \ . \tag{6.9}$$

Vector $\boldsymbol{\omega}_{M_eM_f}$ describes the angular velocity of marker M_f represented in the marker frame M_e when obsereved from the origin of marker M_e, i.e. it denotes the angular velocity of marker M_f relative to the marker M_e. When calculating the relative velocity of contact elements in flexible bodies, two other velocities have to be taken into account in addition to the velocities written in Eq. (6.9)

1. the relative velocity between C_k as a point of body E and M_e ($\mathbf{v}_{C_kM_e}$) in the coordinate system of marker M_e,
2. the relative velocity between C_k as a point of body F and M_f ($\mathbf{v}_{C_kM_f}$) in the coordinate system of marker M_e.

In the case of rigid bodies these two velocities vanish due to the rigidity. These relative velocities have to be calculated and considered in Eq. (6.9)

$$\mathbf{v}_k = (\mathbf{v}_{C_kM_f} - \mathbf{v}_{C_kM_e}) + \mathbf{v}_{M_eM_f} + \boldsymbol{\omega}_{M_eM_f} \times (\mathbf{r}_{M_eC_k} - \mathbf{r}_{M_eM_f}) \ . \tag{6.10}$$

For each contact element the corresponding master and slave triangles are found and then, their corresponding relative velocities are calculated. At first the relative velocity $\mathbf{v}_{C_kM_e}$ between the contact position element C_k and marker M_e is to be found. In doing so, its

corresponding triangle of surface E is found and then, the relative translational velocities ($\mathbf{v}_{v_{1e}M_e}$, $\mathbf{v}_{v_{2e}M_e}$, $\mathbf{v}_{v_{3e}M_e}$) and rotational velocities ($\boldsymbol{\omega}_{v_{1e}M_e}$, $\boldsymbol{\omega}_{v_{2e}M_e}$, $\boldsymbol{\omega}_{v_{3e}M_e}$) between the vertices v_{1e}, v_{2e}, v_{3e} and marker M_e in the coordinate system of marker M_e are calculated by utilizing a SIMPACK access function. The relative velocity $\mathbf{v}_{C_kM_e}$ is written as

$$\mathbf{v}_{C_{ki}M_e} = \mathbf{v}_{v_{ie}M_e} + \boldsymbol{\omega}_{v_{ie}M_e} \times \mathbf{r}_{v_{ie}C_k} \ , \qquad i = 1, 2, 3 \ , \tag{6.11}$$

where $\mathbf{r}_{v_{ie}C_k}$ is the distance between C_k and v_{ie}. Finally, the relative velocity $\mathbf{v}_{C_kM_e}$ is calculated as the mean value of $\mathbf{v}_{C_{k1}M_e}$, $\mathbf{v}_{C_{k2}M_e}$ and $\mathbf{v}_{C_{k3}M_e}$

$$\mathbf{v}_{C_kM_e} = \frac{1}{3}(\mathbf{v}_{C_{k1}M_e} + \mathbf{v}_{C_{k2}M_e} + \mathbf{v}_{C_{k3}M_e}) \ . \tag{6.12}$$

The relative velocity between contact element position and marker M_f is determined in the same manner when its corresponding triangle of surface F is found. To do so, the relative translational velocities ($\mathbf{v}_{v_{1f}M_f}$, $\mathbf{v}_{v_{2f}M_f}$, $\mathbf{v}_{v_{3f}M_f}$) and rotational velocities ($\boldsymbol{\omega}_{v_{1f}M_f}$, $\boldsymbol{\omega}_{v_{2f}M_f}$, $\boldsymbol{\omega}_{v_{3f}M_f}$) between the vertices v_{1f}, v_{2f}, v_{3f} and marker M_f in the coordinate system of marker M_f are calculated. The relative velocity $\mathbf{v}_{C_kM_f}$ is given as

$$\mathbf{v}_{C_{ki}M_f} = \mathbf{v}_{v_{if}M_f} + \boldsymbol{\omega}_{v_{if}M_f} \times \mathbf{r}_{v_{if}C_k} \ , \qquad i = 1, 2, 3 \ , \tag{6.13}$$

where $\mathbf{r}_{v_{if}C_k}$ is the distance between C_k and v_{if}. The relative velocity $\mathbf{v}_{C_kM_f}$ is calculated as the mean value of $\mathbf{v}_{C_{k1}M_f}$, $\mathbf{v}_{C_{k2}M_f}$ and $\mathbf{v}_{C_{k3}M_f}$ which are represented in the coordinate system of marker M_e

$$\mathbf{v}_{C_kM_f} = \frac{1}{3}\mathbf{A}_{M_eM_f} \cdot (\mathbf{v}_{C_{k1}M_f} + \mathbf{v}_{C_{k2}M_f} + \mathbf{v}_{C_{k3}M_f}) \ , \tag{6.14}$$

where $\mathbf{A}_{M_eM_f}$ is the transformation matrix from coordinate system of M_f to the coordinate system of marker M_e. The relative velocities $\mathbf{v}_{C_kM_e}$ and $\mathbf{v}_{C_kM_f}$ can now be considered in Eq. (6.10).

6.2.6 Modification of Contact Forces and Torques

In the case of rigid bodies, for each contact pairing E and F the resulting contact forces and torques are calculated for body E at the position of M_f. This procedure is not valid anymore for flexible bodies and the effect of each contact element force and torque has to be taken into account separately. Each contact element force must be applied to the barycenter of the corresponding master and slave triangles. The contact element forces and their corresponding torques are distributed and applied to the markers located at the vertices. In order to apply contact forces and torques to the vertices instead of barycenters, linear interpolation has been utilized to distribute the contact element forces and torques to the vertices of the master and slave triangles. Figure 6.4 shows a triangulated surface for which the force vector $\mathbf{F}$ applied to an arbitrary point inside the triangle surface.

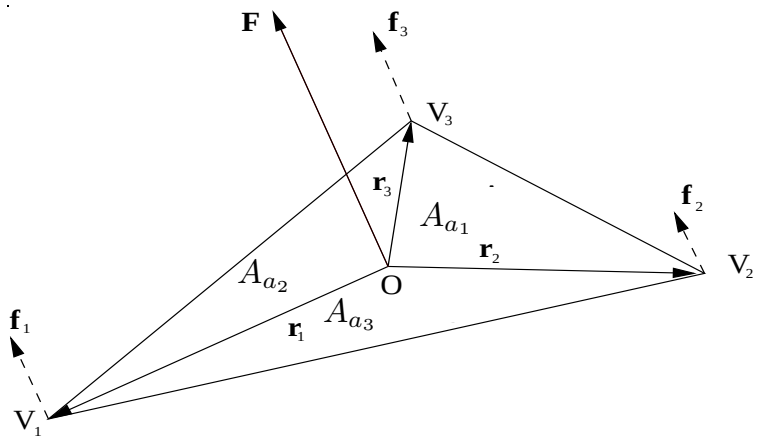

Figure 6.4: Distribution of contact element force on the vertices

After distributing the force vector $\mathbf{F}$ to the vertices, three force vectors $\mathbf{f}_1$, $\mathbf{f}_2$ and $\mathbf{f}_3$ are obtained. These three vectors have the same direction as force vector $\mathbf{F}$. This is just an assumption in order to change the indeterminate problem of force distribution to a determinate one. The force vectors $\mathbf{f}_1$, $\mathbf{f}_2$ and $\mathbf{f}_3$ must fulfill some conditions. The first condition states that their summation is equal to the original force vector $\mathbf{F}$

$$\mathbf{F} = \mathbf{f}_1 + \mathbf{f}_2 + \mathbf{f}_3 \ . \tag{6.15}$$

The second condition imposes the concept of linear interpolation. Each vector of $\mathbf{f}_1$, $\mathbf{f}_2$ and $\mathbf{f}_3$ takes a certain percentage of the primary contact force vector $\mathbf{F}$

$$\mathbf{f}_1 = w_1\mathbf{F} \ , \qquad \mathbf{f}_2 = w_2\mathbf{F} \ , \qquad \mathbf{f}_3 = w_3\mathbf{F} \ ,$$

where w_1, w_2 and w_3 are weighting factors corresponding to the position vectors $\mathbf{r}_1$, $\mathbf{r}_2$ and $\mathbf{r}_3$. They are selected in such a way to fulfill the condition

$$w_1 + w_2 + w_3 = 1 \ , \quad \text{with} \quad w_1 = \frac{|\mathbf{r}_2 \times \mathbf{r}_3|}{2A_a} \ , \quad w_2 = \frac{|\mathbf{r}_1 \times \mathbf{r}_3|}{2A_a} \ , \quad w_3 = \frac{|\mathbf{r}_1 \times \mathbf{r}_2|}{2A_a} \ .$$

where A_a is area of the triangle, see Figure 6.4,

$$A_a = A_{a_1} + A_{a_2} + A_{a_3} = \frac{1}{2}(|\mathbf{r}_2 \times \mathbf{r}_3|) + (|\mathbf{r}_1 \times \mathbf{r}_3|) + (|\mathbf{r}_1 \times \mathbf{r}_2|) \ . \tag{6.16}$$

The value of each weighting factor w_i is 1 at its corresponding vertex and is 0 at the other vertices

$$\begin{cases} \text{if } |\mathbf{r}_1| = 0 \Rightarrow w_1 = 1, \ w_2 = 0, \ w_3 = 0 \ , \\ \text{if } |\mathbf{r}_2| = 0 \Rightarrow w_1 = 0, \ w_2 = 1, \ w_3 = 0 \ , \\ \text{if } |\mathbf{r}_3| = 0 \Rightarrow w_1 = 0, \ w_2 = 0, \ w_3 = 1 \ . \end{cases} \tag{6.17}$$

In this way for any point inside the triangle $w_1 + w_2 + w_3 = 1$ and the force vector $\mathbf{F}$ is distributed in the right way. Distribution of the contact element torque vector is done in the same way as contact element force vector $\mathbf{F}$. The distributed forces and torques have to be applied to the system at the position of their corresponding vertices.

6.3 Numerical Examples

As a proof of concept and implementation, some examples of contact modelling between rigid and flexible objects are given. In these examples, animation of contact modelling shows the effect of implemented modifications.

Example 1: Contact of a Rigid Sphere and an Elastic Beam

In this example the effect of contact between a rigid sphere and an elastic beam on the updating the bounding volumes of the elastic beam is shown, see Figure 6.5. After contact, the bounding volume limits of the beam body are changed and are adjusted in order to be compatible with the current shape of the elastic beam. The new bounding volume boxes are shown in Figure 6.5. All bounding boxes are axis aligned to the surfaces reference frame. Therefore, the limits of each bounding box are set in such a way that they contain all its corresponding polygons. This example shows how the BV boxes are constructed in the case of elastic bodies in order to be used for the detection of collisions.

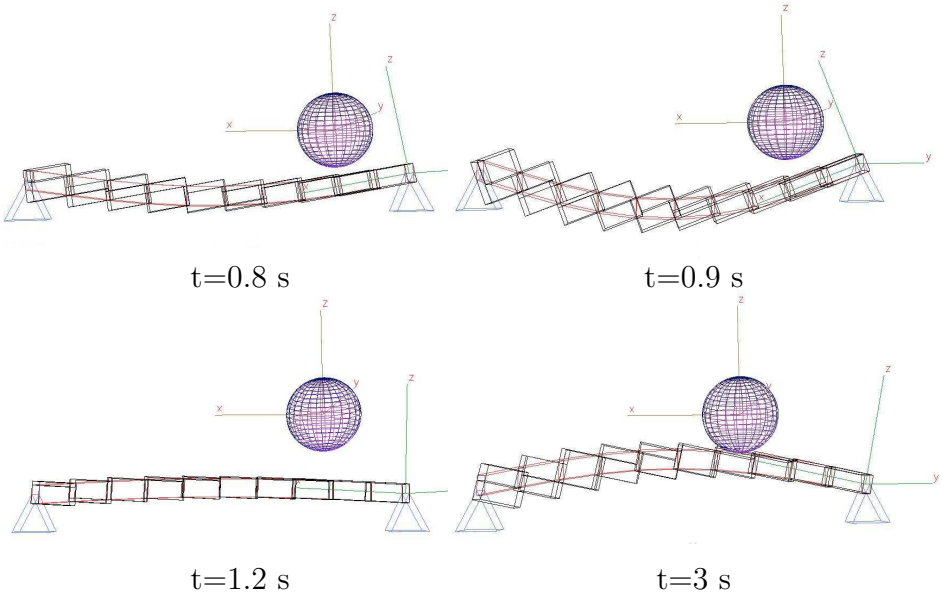

Figure 6.5: Bounding boxes after contact

In another simulation, the rigid sphere rolls from one side of the elastic beam to the other side, see Figure 6.6. As the sphere moves toward the mid-point of the beam, the deflection of the mid-point takes larger values. After leaving this point the elastic beam recovers its initial shape. This example clearly shows the effect of updating the BV limits of the beam during the simulation since the vertical position of the sphere is adjusted according to the current shape of the beam.

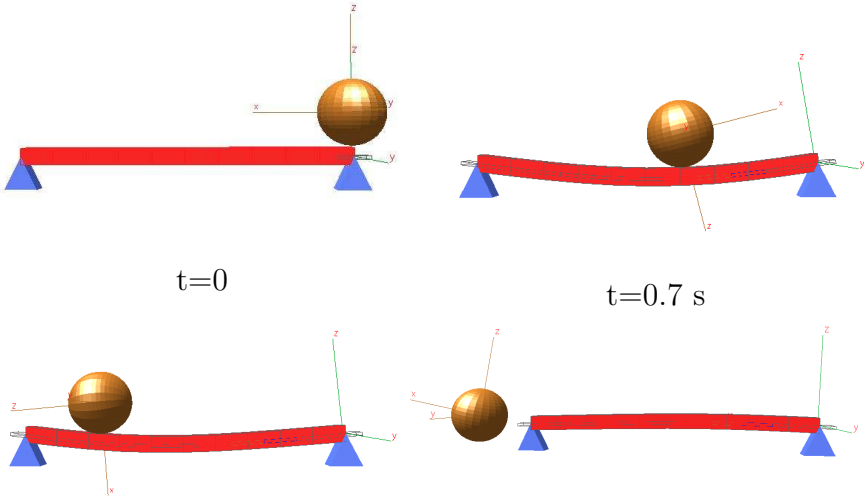

Figure 6.6: Rolling contact of a rigid sphere and an elastic beam

As a comparison between the cases in which the beam is considered as a rigid and an elastic body, the following results show the effect of updating the BV trees on the simulation time:

```
rigid beam contact for 2.5(s) :      CPU time =  9.985(s)
elastic beam contact for 2.5(s) :    CPU time = 55.843(s)
```

It can be seen that updating the BV trees as the major source of computational effort increases the CPU time considerably.

Example 2: Contact between Elastic Beams

Two parallel clamped beams are fixed at one side and are free at the other side. A rigid sphere moves toward the upper elastic beam and due to the contact and the induced motion, later a second contact between the two elastic beams occurs, see Figure 6.7. At $t = 0.53\ s$ the first contact between the sphere and the upper beam occurs. The last figure at $t = 0.75\ s$ shows contact of two elastic beams. Figure 6.8 shows the vertical deflection of the end point of the elastic beams. The oscillatory motion of the elastic beams before contact and due to gravity is also seen.

As an investigation of the effect of collision detection of flexible bodies on the simulation time another simulation without considering contact has been done. In this case, the rigid sphere doesn't have any contact with the upper beam and so, two elastic beams oscillate due to the gravity without having any contact with each other. The CPU times for both simulations are:

```
Simulation for 2(s)  without contact:      CPU time =  1.240(s)
```

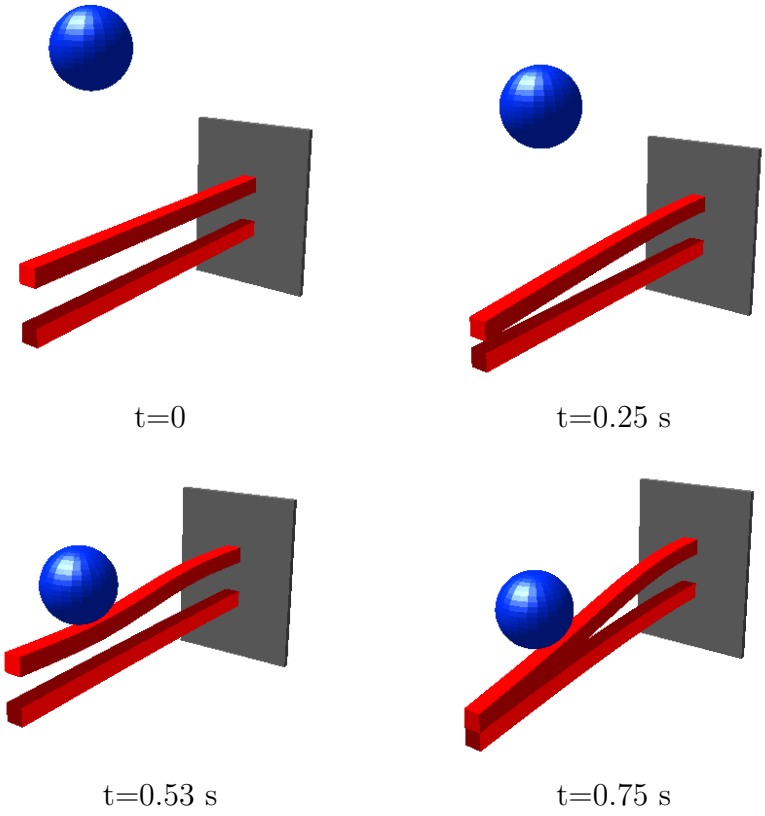

Figure 6.7: Contact modelling of two elastic beams

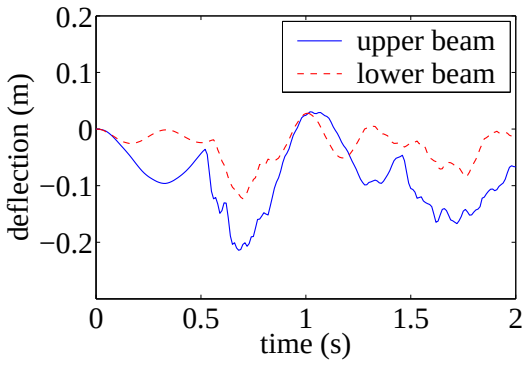

Figure 6.8: Vertical deflection of the end point of the elastic beams

```
Simulation for 2(s)  with contact:          CPU time = 41.817(s)
```

The big difference between both cases shows clearly the required computational effort for the collision detection.

Example 3: Contact in a Flexible Spring

A mechanical spring has become a non-replaceable component of mechanical systems which is distorted under load and recovers its original shape when released after being

deflected. It is used for different functions, e.g., to deflect or distort under load, to absorb energy, to support moving bodies, to isolate vibration or to control a load or a torque. The most common type of spring elements are the cylindrical helical compression springs which are wound or constructed to oppose spring compression along the axis of winding, see Figure 6.9. They can be wound in constant or variable pitch along their length. Each cylindrical helical compression spring element can be defined based on the dimension parameters like mean diameter of coil D, wire diameter d, free length h, solid length s, number of active coils n and stiffness K (which is also mainly known as spring rate). The free length is defined as the overall length of a spring in the unloaded position while the solid length is the length of a compressed spring in which under sufficient load each coil comes into contact with its adjacent coils. The stiffness is described as the necessary amount of static load p to achieve unit deflection δ

$$K = \frac{p}{\delta} = \frac{Gd^4}{8D^3n} \ , \tag{6.18}$$

where G is the shearing modulus of elasticity [139].

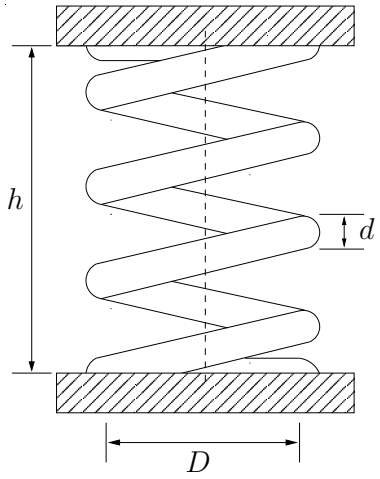

Figure 6.9: Cylindrical helical compression spring

Although in many applications of helical compression springs, they do not reach the solid length, there exist some applications in which spring coils partially or fully come into contact and, therefore, the dynamics of spring is dominated by contact. In such situations consideration of contact becomes essential and one has to calculate the resulting contact forces between contacted coils by performing a contact modeling. Here, a model of a helical compression spring under a compression load is considered. The contact situation is simulated based on the extended version of PCM for contact of flexible bodies.

Model Description

A model of a compression spring with given values of Table 6.1 is considered.

Table 6.1: Parameters of the spring model

coil diameter D	15 mm	number of active coils n	3.5
wire diameter d	2 mm	Young's modulus E	$210 \cdot 10^9$ Pa
free length h	14 mm	shearing modulus G	$79.3 \cdot 10^9$ Pa
solid length s	8 mm	Poisson's ratio ν	0.3

Construction of the model is first followed in ANSYS by generating the nodes on the mean line of the spring. For this purpose, a discretized model in which each coil is divided equally to 20 segments (which means 21 cross sections) is assumed. Then, each two successive nodes are connected with a beam element. By performing a modal analysis one gets the required data for FEMBS interface, see Section 2.4.2. Finally, one generates an SID file which can be imported later in SIMPACK to complete the model of a flexible spring. For setting contact force elements in PCM, one needs further discretization of the wire cross section. Here, the wire cross section is divided to 20 radial sections. In this way, each complete coil would consist of 420 surface nodes on each one a marker has to be attached for further recalculation of the geometry due to deformations during simulation. Figure 6.10 shows a discretized model of the spring.

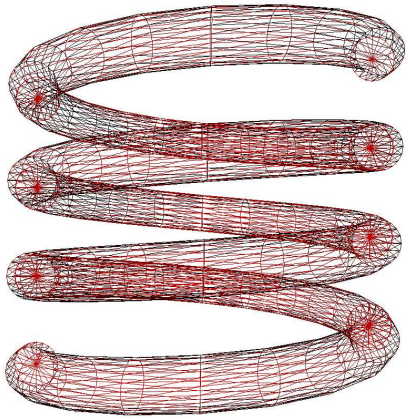

Figure 6.10: Discretized model of the spring

In order to check the created spring model in SIMPACK, a test simulation is performed. For this purpose, the spring is loaded with a rigid bulk mass of 4 kg from the top to calculate the static deflection. The mass is chosen in such a way that no coil of the spring comes in contact with its adjacent coil. The simulation result is depicted in Figure 6.11. As one can observe, the load mass oscillates untill it reaches the static condition. The final deflection is simply calculated from the subtraction of the initial and final positions of the load mass which is about 2.9 mm. The spring stiffness calculated from this simulation is consequently $k = 13.531 \cdot 10^3$ N/m. On the other hand, one calculates the theoretical spring stiffness from Eq. (6.18) using values of Table 6.1 which results in

$K = 13.426 \cdot 10^3$ N/m. By comparing these two values, one concludes that the created reduced spring model in SIMPACK preserves the theoretical model well. In the last step of the model setting, the PCM contact force elements have to be defined between adjacent coils. Furthermore, PCM performs a general collision detection between the corresponding coils of each contact element during simulation and calculates the resulting contact forces.

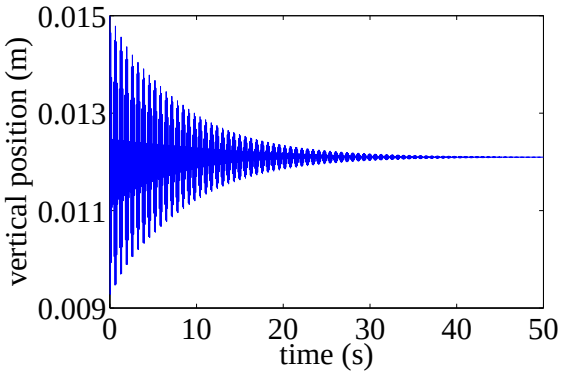

Figure 6.11: Test simulation for checking the model

Simulation Results

The contact simulation of the flexible spring model has been done for 0.4 s. The spring model consists of three full coils and one half coil on the top, see Figure 6.10. Let us number the full coils from 1 to 3 starting from bottom of the spring to the top. For contact simulation of the spring model three force elements may be considered between the body fixed markers of the successive coils: the first force element between coils 1 and 2, the second force element between coils 2 and 3 and finally, the third force element between coil 3 and the half coil.

Following values are used for parameters of the force elements: the elastic layer thickness $b = 5$ mm, the areal damping factor $d_l = 3000$ Ns/m^3, the friction coefficient $\mu = 0.2$ and the friction switch velocity $v_\epsilon = 0.001$ m/s. The spring is loaded with a rigid bulk mass of 6.5 kg aligned with the center line of the spring coils (the dashed line shown in Figure 6.9) and attached at the half coil on the top. The animation of the spring model is illustrated for some simulation times in Figure 6.12. The spring reaches the solid length at $t = 0.049$ s.

Figure 6.13 shows the vertical displacement of three different points of the spring model: the position of the bulk mass, the end point of the half coil (on the top of the spring) and the first point of the half coil where coil 3 and the half coil are connected. As it can be seen, the bulk mass stops the downward motion when the spring reaches the solid length at $t = 0.049$ s for the first time. During the simulation, the spring reaches the solid length further at $t = 0.175$ s. After the second contact at this time, the spring

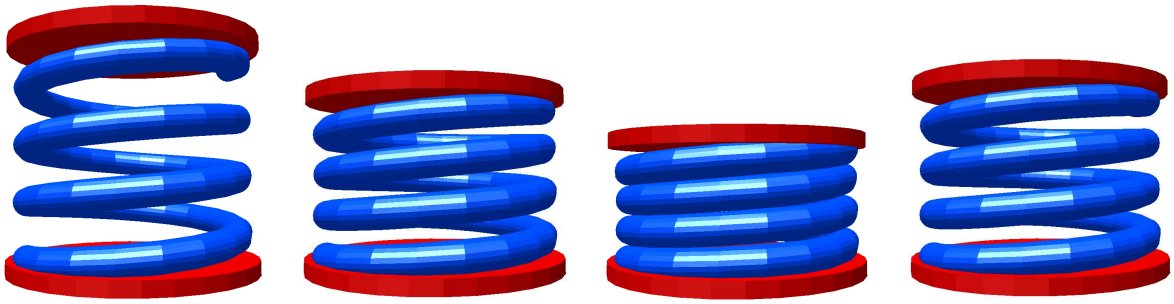

t=0 t=0.032 s t=0.049 s t=0.075 s

Figure 6.12: Contact modeling of the flexible spring

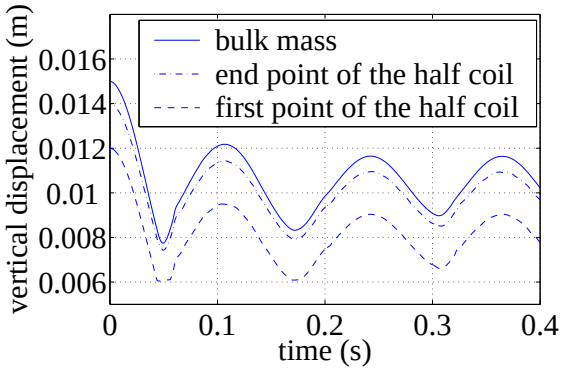

Figure 6.13: Vertical displacement of three different points of the spring model

reaches to a minimum length at $t = 0.31$ s but no contact occurs. An interesting point regarding the vertical displacement of the selected points is the peak of the displacement after each contact. The difference between the initial position at $t = 0$ and the first peak at $t = 0.105$ s shows the effect of damping at contact area. For the second contact, the effect of damping is diminished and, therefore, the second peak at $t = 0.24$ s is much closer to the first peak when compared with the difference between the initial position and the first peak. Since no further contact occurs, the third peak at $t = 0.36$ s is almost at the same level as the second one. Based on this observation, the effect of material damping compared with the damping at contact area is negligible.

Figure 6.14 shows the number of bounding volume (BV) and triangle collision tests for three force elements during the collision detection process. The number of collision tests increases when the coils are close to each other and they may come in contact further. This situation is clearly seen for both the number of BV and triangle collision tests for the first and the second contacts at $t = 0.049$ s and $t = 0.175$ s, respectively. The third peak corresponds to the minimum length of the spring at $t = 0.31$ s as described in Figure 6.13. Since this situation is not a contact, the number of collision tests at this time is lower

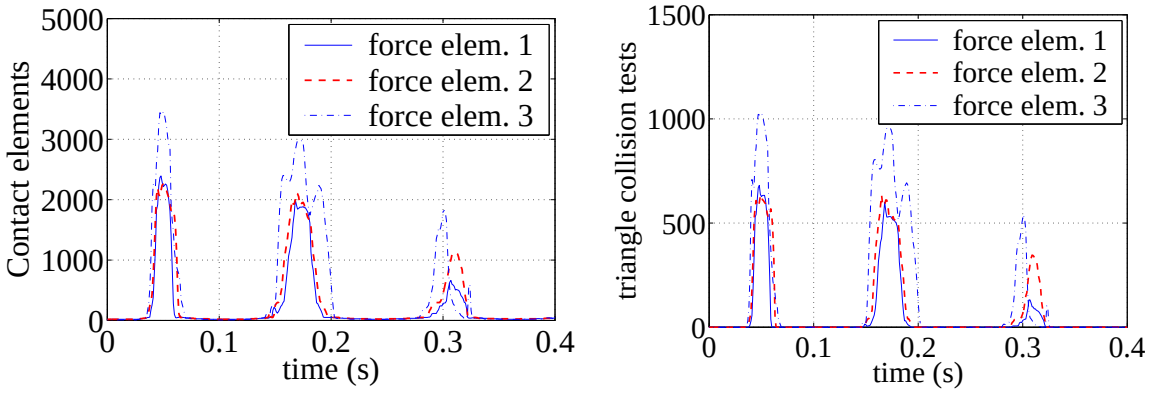

Figure 6.14: Number of BV and triangle collision tests

than those which correspond to the first and the second contacts. It is also noticeable that the number of triangle collision tests decreases when compared with the number of BV collision tests. This point implies that all the closing BVs are not necessarily in contact and, therefore, the triangle collision test is performed only for the contacting BVs. Another interesting point is the similarity of the variations form of the number of BV and triangle collision tests for all three force elements. This point is expected since by increasing/decreasing the number of BV collision tests, the number of the corresponding triangle collision tests increases/decreases, too.

Figure 6.15 shows the overall and closer views of the number of active contact elements and their corresponding contact patch areas as the result of collision between coils. It can be seen that only the first and the second peaks of the triangle collision tests in Figure 6.14 result in contact and the third peak does not lead to any contact. As another point, one observes a similar form of variations of both parameters. Based on this fact, one may claim that the contact elements of each force element have almost the same area.

As the result of contact, contact pressures are applied at the position of contact elements. Figure 6.16 shows the maximum contact pressure of contact elements for each force element. Their values for all force elements at the first contact are much higher than the corresponding values of the second contact. In practice, such high contact pressures which arise from the small contact areas and high contact forces yield the plastic deformation of spring coils at contact region.

Efficiency and computational effort

The simulation of the spring model is performed using the DASSL integrator with step size and order control. The DASSL is an implicit integrator of the category of the backward differentiation formulas (BDF) for stiff multibody systems. For the integrator parameters, the following values are chosen: maximum step size 0.001 s, initial step size 0.001 s,

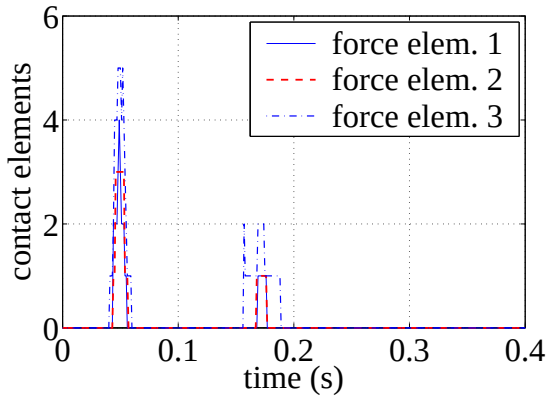

a: overall view

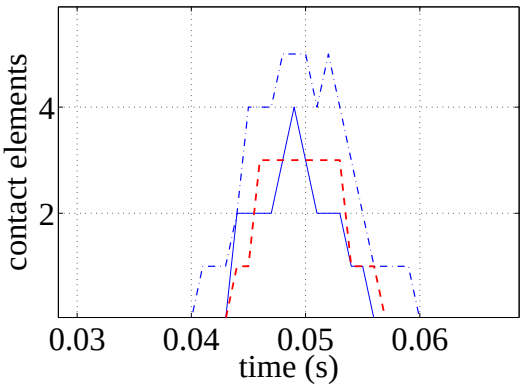

b: closer view

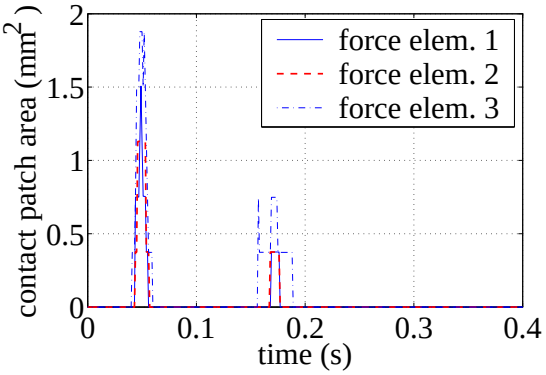

a: overall view

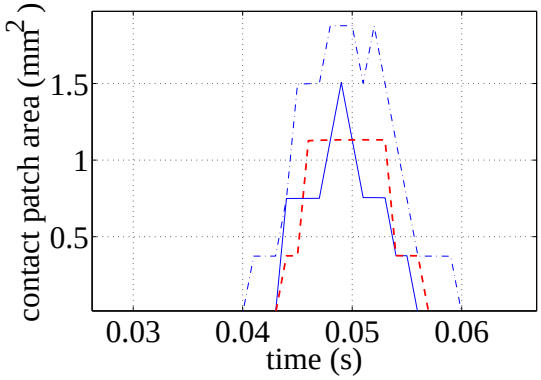

b: closer view

Figure 6.15: Number of contact elements and their corresponding contact patch areas

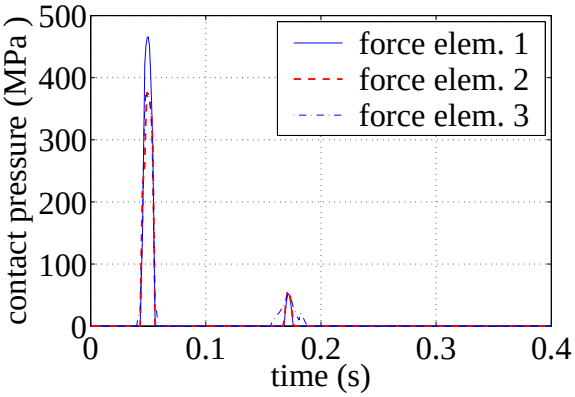

a: overall view

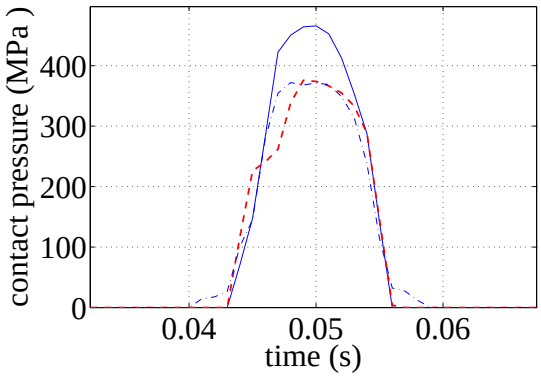

b: closer view

Figure 6.16: Maximum contact pressure

maximum order 5 and tolerance 0.0001.

Figure 6.17 illustrates the step size and order of the integration during simulation. The step size is kept constant at its predefined maximum value of 0.001 s when the coils are not close to each other. However, when the coils are approaching each other and the system becomes very stiff, the step size is decreased. This situation at contact times is very clear.

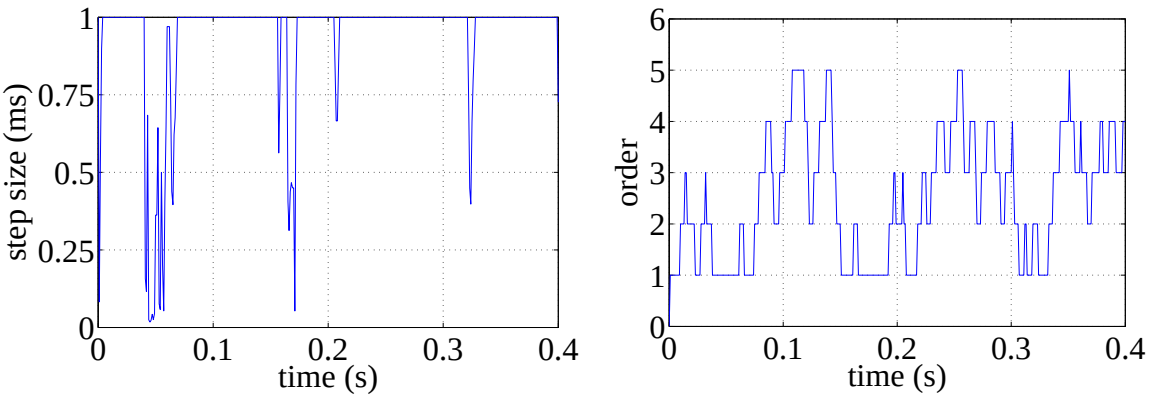

Figure 6.17: Step size and order of the integration

The value of the integrator order is variable between 1 and 5. An interesting point regarding the order change is that the order decreases with decreasing the step size. This situation occurs when the system experiences a non-smooth behavior and, therefore, the integrator cannot use the information of the previous steps. On the other hand, when the step size takes its predefined maximum value, i.e. the system behavior is smooth, the order increases.

The CPU time of collision detection and total CPU time of contact calculation process for three force elements are depicted in Figures 6.18, 6.19 and 6.20. As it can be seen, one observes a feasible CPU time only for the case of potential contacts when the coils are close to each other. For the other periods of simualtion, the CPU time is close to zero.

The contact calculation process consists of collision detection, construction of intersection polygons and generation of contact elements. By comparing the CPU times, one recognizes that for each force element, the CPU time of collision detection is almost the same as the total CPU time of contact calculation process. This fact clarifies that the major computational effort of the contact calculation process is the collision detection which itself is composed of updating the BV trees and finding the contact between the updated BVs.

As the last variable, an interesting parameter for the efficiency of the simulation is considered. A real time factor of the simulation is introduced by dividing the required total

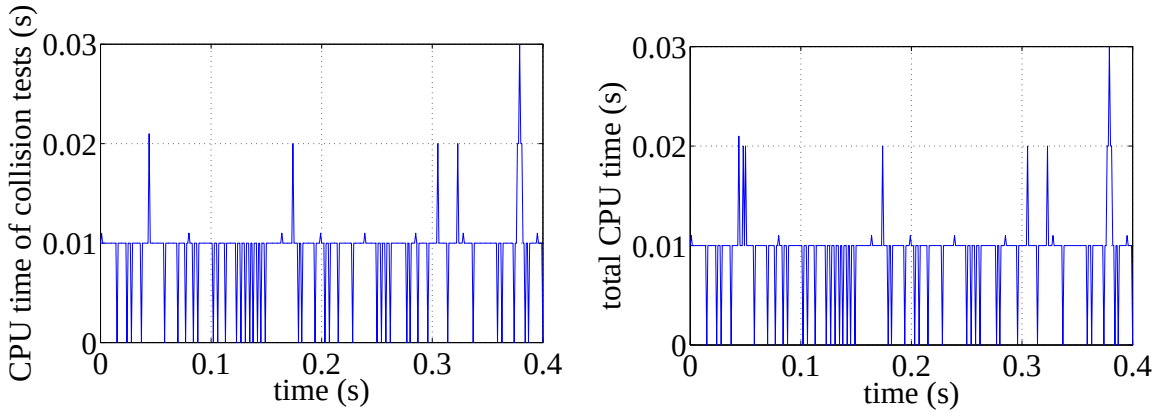

Figure 6.18: CPU time of collision detection and total CPU time for force element 1

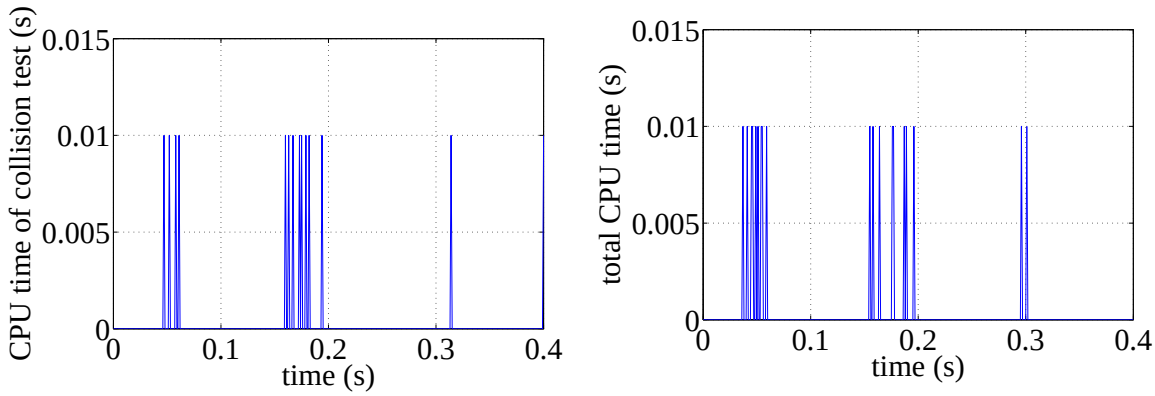

Figure 6.19: CPU time of collision detection and total CPU time for force element 2

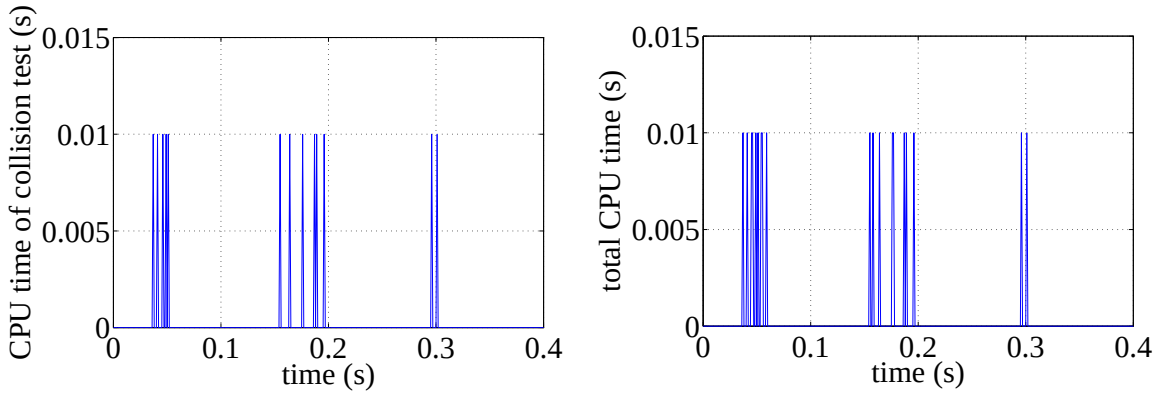

Figure 6.20: CPU time of collision detection and total CPU time for force element 3

CPU time at each time step by the corresponding time step size

$$\tau = \frac{\Delta t_{CPU}}{\Delta t_{integration}} \ . \tag{6.19}$$

The real time factor of the spring model simulation has been calculated and the result

has been shown in Figure 6.21.

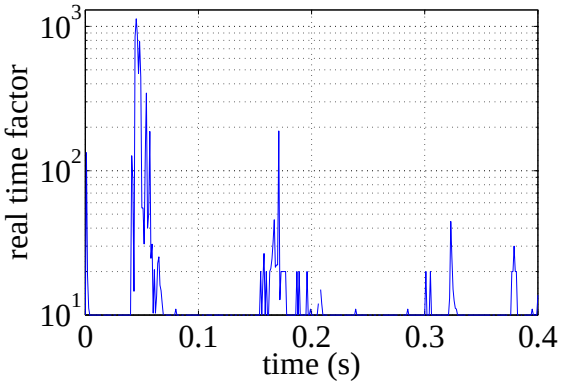

Figure 6.21: Real time factor of the simulation

Its value increases rapidly during contact. For this simulation, the maximum value reaches 1000 which can be supposed as a very desirable value when dealing with contact of flexible bodies with fine discretization of body surfaces. However, depending on the assigned values for parameters of force elements, this factor can increase tremendously. In addition, selection of non-realistic values can lead to the wrong results of simulation.

Chapter 7

Rigid-Elastic Modeling of Gear Wheels in Multibody Systems

In many applications in mechanical engineering, gear wheels are used to transmit power between rotating shafts. Therefore, the ability to incorporate them into multibody systems and to simulate contact between them has become an essential topic in multibody dynamics.

Contact modeling of gear wheels has some special difficulties which arise, e.g., from the nonlinear behavior of tooth stiffness, backlash, gear geometric parameters, see e.g. [75, 76, 143]. There exist researches which focus on modeling of meshing gear wheels using analytical approaches, see e.g. [75, 87, 88]. In most of these contributions, the equation of motion for one gear pair is formulated. These formulations are basically functions of the gear geometry and some material parameters like stiffness and damping coefficients. For simplicity, contact between each gear pair is modeled through a spring-damper element which acts tangentially to the base circle of each meshing gear. In using such formulations, some important features of contact of gear wheels, such as the effect of involute meshing teeth, nonstandard teeth or multiple contact are often not taken into account and, therefore, they cannot be used for the general case of contact between gear wheels. Instead, numerical approaches can handle realistic cases of contact modeling with all difficulties involved by introducing effective parameters which have a great effect on the dynamical behavior.

The numerical approaches based on FEM establish a powerful tool for contact modeling of gear wheels. However, FEM needs very long simulation times. In such situations, multibody dynamics can often be used to efficiently model the contact of gear pairs with acceptable accuracy and considerably less computational effort compared to the FEM.

Numerical approaches based on multibody dynamics rely on different techniques [104]. The simplest level of modeling deals with simulation of only one torsional degree of free-

dom (DOF) of each gear wheel. In this level, one focuses on torsional vibration of meshing gears and no other vibrations can be considered. Some prior approaches have focused on the modeling of a single gear mesh interface [102]. The next level of complexity considers all six DOFs of each free gear body and is an extension of the one torsional DOF model. These six DOFs per gear wheel models can be achieved by introducing appropriate spring-damper elements in bearings. A six DOFs rigid body model for gear wheels was introduced in [75]. Later, in [16] a six DOFs gear mesh interface model was presented that can be employed in dynamic analysis of internal and external spur and helical gears. This formulation is an extention of the prior work in [15] and the work described in [102]. In [138] the methodology and the results of a multibody model of multi-mesh transmission systems were summarized. The authors have used a rigid body gear with the assumption of time-dependent and distributed gear mesh stiffness. Finally, further extension of multibody models to a combined MBS-FEM model is considered where certain components are modeled by finite element models instead of fully rigid bodies. A combined model of FEM and MBS was developed in [3, 4] to incorporate a spatially varying mesh stiffness. A brief survey of different researches on contact modeling of multi-mesh geared systems can be found in [138].

This chapter starts with a brief explanation of the approach used in [91] for contact modeling of meshing rigid gear wheels. Then, an extension of this approach is implemented by introducing elastic elements between the teeth and the gear body. Due to the effect of contact forces relevant deformations occur in meshing teeth and, therefore, it is required for a high quality of the analysis to introduce some elasticities in the model of meshing gear wheels. The approach presented here has been implemented for contact modeling of spur and helical gears and can probably with some modifications also be used for contact modeling of bevel gears.

7.1 Contact Modeling of Rigid Gear Wheels

The approach presented in [91] is a force element which takes the geometry, initial rotational angle and rotational velocity of meshing gears as input and calculates forces and moments acting on gear wheels as output. In this implementation, all geometric features of the involute tooth are considered. This force element is connected between two body fixed markers located on the axis of rotation of gear wheels. It takes into account some important features like: involute meshing teeth, spur and helical gear trains, backlash and addendum modification, tip relief factor, changes in axes distance, relative axial movement of gear pairs and parabolic behavior of tooth stiffness.

The algorithm and implementation of [91] is based on three main steps. First a brief description of each step is given before the modifications and extensions are introduced.

7.1.1 Calculation of Basic Parameters

Due to the nature of contact in geared systems and the special geometry of gear wheels, various parameters including geometric and material properties have to be considered. One of the geometric parameters related to the involute tooth shape is the involute parameter. The profile of a gear tooth is shaped as an involute curve to minimize wear, vibration and noise and to maximize the efficiency of power transmission. According to Figure 7.1, the involute parameter can be determined from, see [88],

$$\theta(\alpha) = \mathrm{inv}(\alpha) = \tan(\alpha) - \alpha \ . \tag{7.1}$$

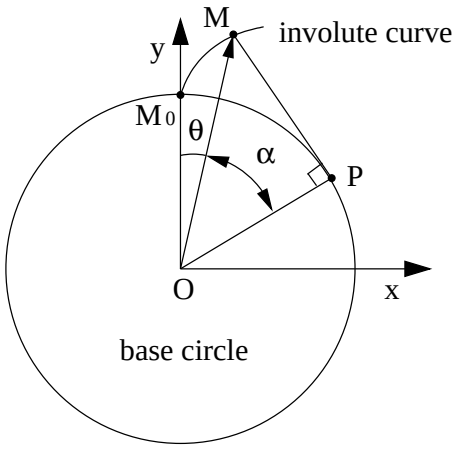

Figure 7.1: Definition of the involute function $\theta(\alpha)$

Point M in this figure is an arbitrary point on the involute curve and the length of line PM is equal to the length of the arc PM_0. Determination of α can be done by solving the nonlinear equation

$$\tan(\alpha) - \alpha - \mathrm{inv}(\alpha) = 0 \ . \tag{7.2}$$

The solution of this equation can be obtained, e.g., by a Newton-Raphson iteration using as initial value

$$\alpha_{\mathrm{initial}} = \sqrt[3]{3\theta} \ . \tag{7.3}$$

The involute parameter is used in the calculation of backlash and addendum modification in nonstandard gears. In the case of nonstandard gear wheels, the nominal transverse working pressure angle α_t cannot be used anymore and an actual working pressure angle α_v has to be used instead. The following relationship holds between α_t and α_v according to [91]

$$\mathrm{inv}(\alpha_v) = \mathrm{inv}(\alpha_t) + 2\frac{x_1 + x_2}{n_{th1} + n_{th2}} \tan(\alpha_t) \ , \tag{7.4}$$

where x_1 and x_2 are shift factors and n_{th1} and n_{th2} are the teeth numbers of gear 1 and 2, respectively. The relation of the true distance a_v of gear centers in terms of the nominal center distance a_0 can be written as

$$a_v = a_0(1 + \frac{x_1 + x_2}{n_{th1} + n_{th2}}) \ . \tag{7.5}$$

The amount of circumferential backlash depending on teeth geometry can be expressed in terms of the involute functions $\text{inv}(\alpha_w)$ and $\text{inv}(\alpha_v)$ and the tooth clearance factor, for details see [91, 97]. The true transverse working pressure angle α_w is obtained based on the base circle radii r_{b1} and r_{b2} and the actual center distance a_w

$$\alpha_w = \arc\cos(\frac{r_{b1} + r_{b2}}{a_w}) \ . \tag{7.6}$$

Backlash is one of the most important factors which can considerably affect the dynamical behavior of meshing gear wheels by leading to loss of contact between contacting teeth and causing vibration. Therefore, the backlash and its effect on the rotation of gear pairs must be considered. In practice, there are different approaches for the measurement of backlash, e.g. described in [113, 131, 132]. In this work, as one can see in the next section, the detection of collision between possible contacting teeth is based on the amount of backlash.

For calculation of the meshing stiffness of gear pairs, the geometric overlap ratio of meshing teeth has to be considered. In doing so, a parabolic stiffness behavior along the line of action is adopted. By introducing the gear stiffness ratio and using some geometric and material properties, the maximum and minimum value of the gear stiffness can be calculated

$$c_{max} = 14 \cdot 10^9 \frac{E}{2.1 \cdot 10^{11}} bs \ , \qquad c_{min} = k c_{max} \ , \tag{7.7}$$

where E is the mean value of Young's modulus of the gear bodies, b is the effective face width of meshing gears, s is the shape factor and k is the stiffness ratio. Later, these values will be used to determine the correct amount of stiffness based on a parabolic stiffness behavior, see [97].

Calculation of the contact region from the path of contact is done through the contact ratio parameter. In doing so, first the lengths of recess g_{a1} and g_{a2} for both gears 1 and 2 are obtained

$$g_{a1} = \sqrt{{r_{a1}}^2 - {r_{b1}}^2} - r_{p_1} \sin\alpha_w \ , \qquad g_{a2} = \sqrt{{r_{a2}}^2 - {r_{b2}}^2} - r_{p_2} \sin\alpha_w \ , \tag{7.8}$$

where r_{a1} and r_{a2} are radii of addendum circles and r_{p_1} and r_{p_2} are radii of pitch circles corresponding to gears 1 and 2, respectively. Then, by dividing by the base pitch p_b and adding them, the total transverse contact ratio ϵ_α will be determined

$$\epsilon_\alpha = \frac{g_{a1} + g_{a2}}{p_b} \ . \tag{7.9}$$

In the case of helical gears the overlap ratio ϵ_β has to be considered too

$$\epsilon_\beta = \frac{b \tan |\beta|}{m_t \pi} \ , \tag{7.10}$$

where β is the helix angle and m_t is the transverse module. Therefore, the total transverse contact ratio is the sum

$$\epsilon = \epsilon_\alpha + \epsilon_\beta \ . \tag{7.11}$$

The above mentioned parameters were just the most important ones and have been explained only briefly. One can find more details about the necessary parameters for contact modeling of geared systems in [91] or in books like [88, 97].

7.1.2 Calculation of Contact Geometry

In order to calculate the position of contact points of meshing teeth as well as the amount of elastic penetration, geometric relationships which utilize appropriate theories have to be used. Consequently, costly and complex contact point search algorithms can be avoided. First of all, the center line crossing through the center points of the gear pairs is chosen as the measurement reference for the contact point angles. Then, as illustrated in Figure 7.2, the teeth of the gears 1 and 2 whose left flanges are closer to this line are considered. The angles ϕ_1 and ϕ_2 associated with these flanges are determined. Then, the amount of relative turn angle related to gear 2 in terms of ϕ_1 and ϕ_2 can be written as

$$\Delta\phi = \phi_2 + |\frac{n_{th1}}{n_{th2}}|\phi_1 \ . \tag{7.12}$$

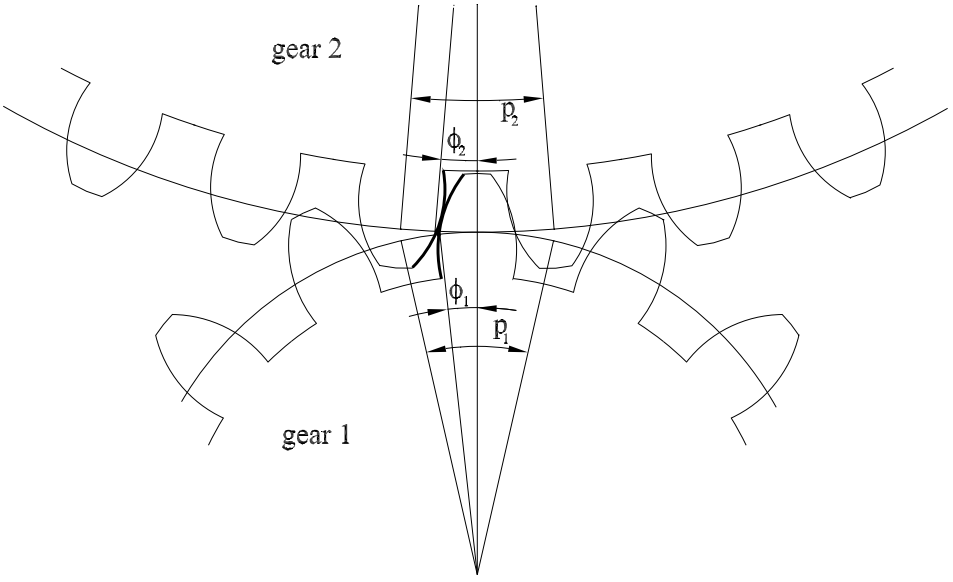

Figure 7.2: Left hand side flanges of gears 1 and 2 inside central borders

In this relation n_{th1} and n_{th2} are the teeth numbers of gears 1 and 2, respectively. At this point, let us call this relative turn angle the central relative turn angle since according to the above explanation, it corresponds to the tooth profiles of gears 1 and 2 which are located in the central borders. By comparing the central turn angle with the circumferential backlash ϕ_b one can find out whether there is contact between the meshing teeth of gears 1 and 2

```
if |Δφ| ≤ φb
    no flange contact
else
    if Δφ > φb
        left hand side contact: angle of attack has a negative sign
    else
        right hand side contact: angle of attack has a positive sign
    end
end
```

The first *if* statement checks for flange contact and the second one checks for the left or right hand side contact cases. If any central contact is found, then, the contact of neighboring teeth inside the contact region will be checked too by considering the contact ratio. Therefore, by following this algorithm all possible multiple contacts including left and right hand side contacts will be found. It is noticeable that for calculation of real penetration the difference between the amount of circumferential backlash and the central relative turn angle must be considered. In doing so, the final value $\Delta\phi$ has to be modified as follows

$$\begin{cases} \text{if } \Delta\phi > \quad \phi_b & \rightarrow & \Delta\phi_{new} = \Delta\phi - \phi_b \ , \\ \text{if } \Delta\phi < -\phi_b & \rightarrow & \Delta\phi_{new} = \Delta\phi + \phi_b \ , \\ \text{if } \phi_b \geq \Delta\phi \geq -\phi_b & \rightarrow & \text{no contact} \ . \end{cases} \tag{7.13}$$

Based on the amount of central relative turn angle, the penetration for each contact will be calculated and used for determination of applied contact forces as described in the next section.

7.1.3 Determination of Contact Forces and Resulting Torques

The contact force calculated here is based on the penalty method. It uses spring and damper elements located on teeth surfaces in order to apply appropriate forces according to the amount of penetration and relative velocities in the normal and tangential directions.

First, for both left and right hand side contacts, the central contact is considered. Then, all other possible contacts of neighboring teeth are found. The location and angle of each

contact situation have to be considered. Also, the relative velocities between meshing teeth in the normal and tangential directions for each contact situation related to gear 2 are calculated

$$v_n = \Delta\omega r_{b2} \ , \qquad v_{ti} = (|\omega_1| + |\omega_2|)\theta_i r_{p2} \ , \qquad i = 1, \ldots, k \ . \tag{7.14}$$

In the first relation, v_n is the relative normal velocity at the contact points and is identical for all contacts, $\Delta\omega$ is the relative angular velocity related to gear 2, see Eq. (7.12), and r_{b2} is the base circle radius of gear 2. The second equation holds for the relative tangential velocity at all k contacts and is a relation between angular velocities ω_1 and ω_2 of both gears, the angle of contact θ_i and the pitch circle radius r_{p_2} of gear 2. The relative tangential velocity with the constant coefficient of friction which is given at the beginning will be used to determine a variable coefficient of friction μ_i on the meshing teeth surfaces.

In the next step, the amount of penetration δ_i for each contact is determined. Then, the normal contact forces F_{ni} can be written as

$$F_{ni} = K_i\delta_i + D_i v_n \ , \qquad i = 1, \ldots, k \ , \tag{7.15}$$

where K_i and D_i are the stiffness and damping coefficients, respectively. By using the amount of normal contact force and the friction coefficient μ_i of teeth surfaces at contact points, tangential contact forces are calculated as

$$F_{ti} = \mu_i F_{ni} \ , \qquad i = 1, \ldots, k \ . \tag{7.16}$$

The total contact force vector $\mathbf{F}_i$ at each contact point can be obtained as the projection of normal and tangential contact forces to the x, y and z directions of the reference coordinate system

$$\mathbf{F}_i = \begin{bmatrix} F_{xi} \\ F_{y_i} \\ F_{zi} \end{bmatrix} = \begin{bmatrix} (F_{ni}\cos\alpha_n - F_{ti}\sin\alpha_n)\cos\beta \\ F_{ni}\sin\alpha_n + F_{ti}\cos\alpha_n \\ F_{ni}\cos\alpha_n\sin\beta \end{bmatrix} \ , \qquad i = 1, \ldots, k \ , \tag{7.17}$$

where α_n is the normal working pressure angle at the pitch point and β is the helix angle of the meshing gears. The resulting torques $\mathbf{T}_i$ corresponding to each contact can now be calculated. Finally, the total contact force and contact torque vectors are determined by summing up the vectors $\mathbf{F}_i$ and $\mathbf{T}_i$.

7.2 Extension of Rigid Gears through Introducing Tangentially Movable Teeth

In this approach, the tangentially movable teeth and the body of each gear wheel are still rigid but they are connected to each other by elastic elements. This approach is

especially well-suited for multibody systems since it is a compromise between a totally rigid model and a fully elastic model allowing the simulation of large motions with many revolutions while still important elasticities are considered. What follows is a description of the required steps for this extension.

7.2.1 Introducing Teeth Coordinates as New Force States

Tangential displacements of the teeth will be described through additional rotational coordinates which can be supposed as states assigned internally to the force elements, see [129]. Therefore, corresponding to each tooth, an independent rotational coordinate is introduced. Each coordinate is measured from the reference position of the corresponding tooth. Figure 7.3 shows an illustration of a gear wheel with rotational coordinate ϕ of the gear body and rotational coordinate S_1 of the first tooth which is the angle between the reference position and the displaced position of the tooth. The positive value of S_1 is a clockwise rotation similar to what is shown for angle ϕ. The teeth can move only tangentially with respect to the gear body and there is no movement feasible in radial direction.

7.2.2 Placement of Elastic Elements

In order to restrict the movement of the teeth relative to the gear body and to model teeth elasticities, identical elastic elements including parallel spring-damper combinations are considered between the teeth and the gear body. Unfortunately, there is not yet a fully developed theory for determining the spring stiffness and damper coefficient without additional pre-computations. Therefore, they have to be identified once in advance from a numerical reference computation using an FEM program. Having a gear wheel model, first a semi-elastic FEM model has to be created. In this semi-elastic model, the gear body is meshed with at least one rigid element and the teeth are meshed using elastic elements. Then, the rotation of the gear body is fixed and an arbitrary external force has to be applied to the flange surface of one arbitrary tooth tangential to the base circle of the gear wheel. By dividing the amount of applied force by displacement or velocity of the tooth, the appropriate spring stiffness and damping coefficient can be obtained, respectively.

The equation of motion of each tooth in terms of the spring stiffness K_e and damping coefficient D_e of the elastic elements can be written as

$$m_{th} r_d^2 \ddot{S}_i = K_e r_d^2 (\phi - S_i) + D_e r_d^2 (\omega - \dot{S}_i) + T_i \ , \qquad i = 1, \ldots, n_{th} \ , \tag{7.18}$$

where m_{th} is the mass of each single tooth, r_d is the dedendum circle radius of the gear wheel, ϕ and ω are the rotational position and velocity of the gear body, T_i is the contact

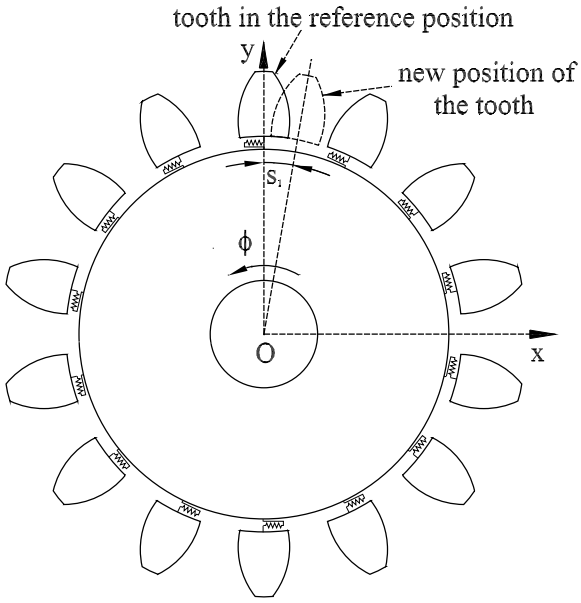

Figure 7.3: Model of a gear wheel considering elastic elements between the teeth and the gear body

torque applied to the tooth i, n_{th} is the total teeth number, and S_i, $\dot{S}_i$ and $\ddot{S}_i$ are the rotational position, velocity and acceleration of the tooth i, respectively.

7.2.3 Modified Contact Search Algorithm

In the case of contact between two meshing teeth of rigid gears, the contact point moves along the contact line. The contact region on this line is located between two points which are the intersections of the line of action with addendum circles of the meshing gears. In the presented approach, it is supposed that this condition is still fulfilled and although the meshing teeth can rotate a little with respect to the gear body, the contact point is located on the contact line. This assumption is valid since in the presented model the contact is between two involute teeth with feasible positions.

The algorithm of contact search described in Section 7.1.2 for rigid gears cannot be followed in the same way for the case when the teeth can move tangentially with respect to the gear body. Therefore, it is essential to utilize a modified algorithm which can handle this situation appropriately and can identify the contacts correctly.

In contact of gear wheels both cases of left hand and right hand side contact can happen simultaneously. Therefore, the presented algorithm at each time step will search for contacts on both lines of action of the left and right hand side flanges separately. For convenience, let us call these lines of action the left and right lines of action. The main successive steps of this algorithm for finding the contacts between the meshing gears 1

and 2 can be summarized briefly as follows:

1. Considering gear 1, the tooth whose left hand side flange is located within $-p_1/2$ and $+p_1/2$ has to be found, see Figure 7.2. This tooth can be supposed to be the central tooth of the contact region.

2. The neighboring teeth whose left hand side flanges are located inside the contact region have to be found.

3. Corresponding to these teeth of gear 1, the teeth of gear 2 whose left hand side flanges are close are considered.

4. The angle and position of the intersection point of these flanges including the teeth flange of gears 1 and 2 with the left line of action are calculated.

5. Corresponding to each probable contact, the relative turn angle $\Delta\phi_i$ related to gear 2 is calculated
$$\Delta\phi_i = \theta_{2i} + \theta_{1i}\frac{r_{1i}}{r_{2i}} , \qquad i = 1, \ldots, n_c , \tag{7.19}$$
where θ_{1i} and r_{1i} are the angle and position of the intersection points of gear 1, θ_{2i} and r_{2i} have the same meaning but they are related to gear 2 and n_c is the number of probable contacts. Later, the values of $\Delta\phi_i$ have to be checked against the amount of circumferential backlash in order to find if the teeth of gears 1 and 2 have contact in these probable contacts.

6. The above mentioned steps have to be repeated for the right hand side flanges of gears 1 and 2.

In the next step, based on the amount of relative turn angle $\Delta\phi$ corresponding contact forces will be determined.

7.2.4 Modification of Contact Forces and Torques

Since in the presented modeling strategy the teeth are connected to the gear body with elastic elements, the effect of elastic elements has to be considered. This procedure can be explained as follows:

1. Suppose that one tooth of gear 1 is in contact with another tooth of gear 2 and assume that the amount of contact force is obtained as the force vector $\mathbf{F}$ with components F_x, F_y in the gear plane and F_z normal to the gear plane. The corresponding angle and position of this contact point related to gear 1 are θ_1 and r_1, respectively. Then, one can project the F_x and F_y components to the two components F_{n1} normal and F_{t1} tangential to the dedendum circle of gear 1. In fact,

F_{n1} is aligned to the line connecting the center of gear 1 to the contact point and towards this point and F_{t1} is perpendicular to F_{n1}. These projections for gear 1 can be written as

$$F_{n1} = -F_x \sin\theta_1 + F_y \cos\theta_1 \ , \qquad F_{t1} = -F_x \cos\theta_1 - F_y \sin\theta_1 \ . \tag{7.20}$$

2. The resulting torque of the tangential force F_{t1} for this tooth is calculated. This torque may not be applied to the gear body directly and instead, has to be applied to the corresponding teeth of gear 1. This point is considered in Eqs. (7.18) in the term T_i.

3. The amount of tangential force F_{te1} arising from the elastic element connecting this tooth to the gear body is determined as

$$F_{te1} = K_e r_{d1}^2(\phi_1 - S_1) + D_e r_{d1}^2(\omega_1 - \dot{S}_1) \ , \tag{7.21}$$

where S_1 and $\dot{S}_1$ are the rotational position and velocity of this tooth, respectively.

4. By projecting the forces F_{n1} and F_{te1} to the x and y directions and summing them with considering the component F_z of the force vector $\mathbf{F}$, the applied force arising from the considered tooth of gear 1 can be obtained. The corresponding torque applied to gear 1 which arises from F_{te1} has to be determined, too.

5. By following the same procedure for the other teeth, calculating applied forces and torques and summing them, the total force and torque applied to gear 1 are calculated. It is noticeable that for the teeth which are not in contact with any other tooth, only the steps 3 and 4 have to be repeated. All these steps must be followed for gear 2, too.

Following the above mentioned modifications, the effect of elastic elements on contact forces and torques will be taken into account correctly.

7.3 Numerical Examples

In the first example, the results of the new approach and the FEM are compared for one side flange contact between two spur gears. The results of this example are investigated in order to judge whether the additional effort of the new approach is justified by an improvement of the obtainable results. For getting a sound feeling of control for the effect of considering the elastic elements on the rotation of meshing gears, in the second example the contact between two spur gears with the possibility of multiple contacts simulated from both approaches, i.e. the fully rigid modeling approach of [91] and the new approach, which is implemented based on the original code of [91], is investigated. The third example clarifies the possibility of applying the new developed approach for a practical case such as a gearbox.

Example 1: One Side Flange Contact between Two Spur Gears

The contact between the left hand side flanges of central meshing teeth of two spur gears is investigated by three different methods: the fully rigid modeling approach, the new approach and a full FEM simulation. It is supposed that the right hand side flanges cannot exert any contact force. Since only one contact situation and a very short period of time is considered, one can clearly see that considering elastic elements between the teeth and the gear body leads to the contact force closer to the accurate results of FEM.

In Table 7.1 the geometric and material properties of the gears of this example are summarized. Only their mass moment of inertia around the corresponding rotation axes are different. The joints of both gears are the revolute joints with initial angular velocities of $\omega_1 = 1.745$ rad/s and $\omega_2 = 0$. In this simulation, the stiffness coefficient $K_e = 2 \cdot 10^9$ N/m and damping coefficient $D_e = 2 \cdot 10^5$ Ns/m have been used.

Table 7.1: Geometric and material properties of spur gears in the second example

teeth number n_{th}	97	addendum coefficient	1.0
shift factor x	0	dedendum coefficient	1.0315
moment of inertia of gear 1 $I_{1_{zz}}$	2.27 kgm^2	face width b	0.05 m
moment of inertia of gear 2 $I_{2_{zz}}$	4.1 kgm^2	shape factor s	0.85
normal module m_n	0.006 m	tip relief factor	0
normal pressure angle α_n	20 deg	Poisson's ratio ν	0.3
Young's modulus E	$2.1 \cdot 10^{11}$ N/m^2	friction coefficient μ	0
normal backlash factor	0	teeth stiffness ratio	0.8

The illustrated results of FEM in the Figures 7.4 and 7.5 are extracted from a detailed model described by Ziegler in [162]. In these figures the solid lines correspond to FEM, dashed lines to the rigid modeling approach and point-dashed lines to the new approach. Since the amount of normal contact force in the rigid modeling approach is higher than that of the FEM, the duration of contact will be shorter. However, in the new approach by choosing the appropriate values for stiffness and damping coefficients, the amount of normal contact force will be close to that of the FEM and, therefore, the contact duration will improve too.

As a comparison between the computational effort of these three different approaches, the CPU time for simulation of $0.001s$ is reported as follows:

```
fully rigid modeling approach:  CPU time = 0.2 s
new approach:                   CPU time = 2.0 s
fully FEM approach:             CPU time = 10 hours
```

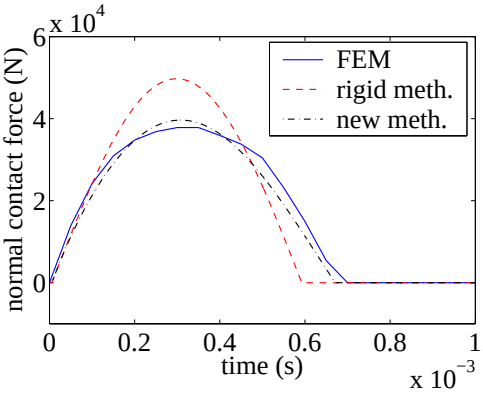

Figure 7.4: Normal contact force obtained from three different approaches

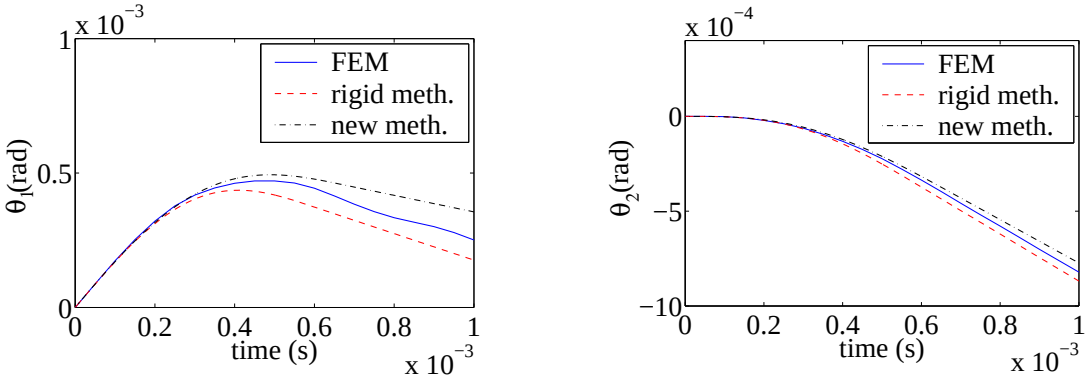

a: rotation angle of gear 1

b: rotation angle of gear 2

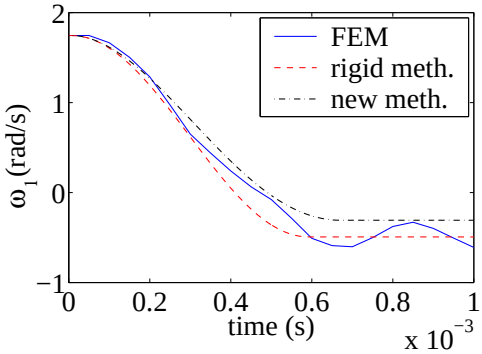

c: angular velocity of gear 1

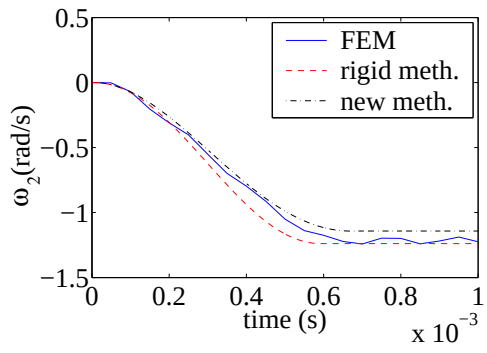

d: angular velocity of gear 2

Figure 7.5: Kinematic quantities obtained from three different approaches

The difference between the computational effort of FEM and the other two approaches is dramastic. The FEM simulation done in [162] is for the case of fully transient modeling of elastic gear wheels and no modal reduction techniques has been used and, therefore, the simulation time is very high. Of course with utilizing reduced models of gear wheels the simulation time will decrease considerably but still will be very high compared to the other two approaches. It can also be seen that the new approach will not need prohibitively more computational effort compared to the rigid modeling and can be used for simulation of contact of multibody geared systems over a long period of simulation time.

Example 2: Contact Modeling of Spur Gears

Tangentially movable teeth and the used simple model of teeth elasticities can significantly affect the dynamic behavior of rotating meshing gears. Since in the approach used in [91] gear wheels are modeled as fully rigid bodies, sudden left and right hand side contacts can occur. This sequence of contacts will also cause high resulting forces and torques in the bearings on which the meshing gears are mounted as we will see in the results of this example.

For indicating the effect of considering the elastic elements on the rotation of meshing gears, contact of two spur gears is investigated through the fully rigid approach in the implementation of [91] and the new approach. Some geometric and material properties of the meshing gears of this example are summarized in Table 7.2. In this example, the rheonomic joint of the driver gear (gear 1) has a constant angular velocity of $\omega_1 = 0.5$ rad/s while the revolute joint of the driven gear (gear 2) has zero initial angular velocity $\omega_2 = 0$.

Table 7.2: Geometric and material properties of the spur gears in the first example

teeth number of the gear 1 n_{th1}	14	addendum coefficient	1.0
teeth number of the gear 2 n_{th2}	39	dedendum coefficient	1.05
moment of inertia of gear 1 $I_{1_{zz}}$	$0.367 \cdot 10^{-3}$ kgm^2	face width b	0.02 m
moment of inertia of gear 2 $I_{2_{zz}}$	$2.214 \cdot 10^{-2}$ kgm^2	shape factor s	1
normal module m_n	0.005 m	tip relief factor	0
normal pressure angle α_n	20 deg	Poisson's ratio ν	0.3
Young's modulus E	$2.1 \cdot 10^{11}$ N/m^2	friction coefficient μ	0
normal backlash factor	0.008	teeth stiffness ratio	0.8

Depicted in Figure 7.6 are some kinematic and kinetic quantities of the driven gear 2 obtained from the fully rigid modeling approach. These illustrated parameters show clearly that at the beginning, the left and right hand side contacts occur frequently. After awhile, the rotation of this gear becomes smoother and, therefore, the amount of applied force and torque decreases.

In Figure 7.7 one can see the corresponding results obtained from the new approach for two different sets of stiffness and damping coefficients. It should be emphasized that in this comparison it is not intended to identify the correct values of K_e and D_e as described in Section 7.2.2, but to study the the effect of the elastic elements on the rotation of meshing gears. For the first case the stiffness coefficient $K_{e_1} = 5.6 \cdot 10^7$ N/m and damping coefficient $D_{e_1} = 10^4$ Ns/m have been chosen. The results shown in Figures 7.7a to 7.7d correspond to this case. Compared to the results shown in Figure 7.6 the

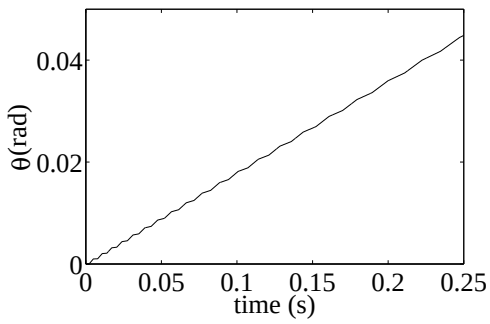

a: rotation angle of gear 2

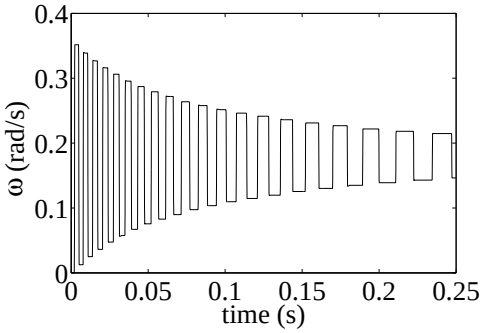

b: angular velocity of gear 2

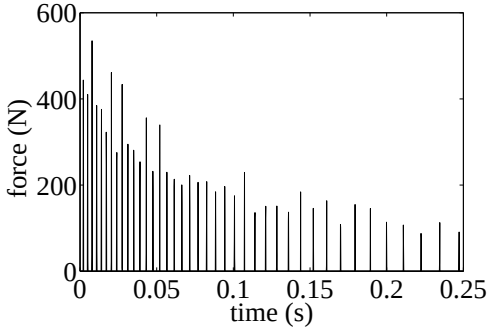

c: absolute value of applied force on gear 2

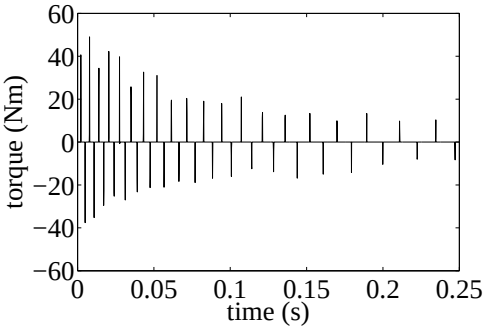

d: resulting torque of gear 2

Figure 7.6: Simulation results for gear 2 obtained from the rigid modeling approach

number of contacts decreases considerably. This point is expected since after the first contact, the time needed for the second contact will be longer compared to the fully rigid modeling approach. Therefore, the driven gear 2 will follow a monotonous rotation and the variations in the resulting force and torque will be smaller.

One can expect that with increasing the stiffness and damping coefficients of the elastic elements, the results will approach to the results of the fully rigid modeling approach. This case has also been checked by choosing higher values of the stiffness coefficient $K_{e_2} = 3.6 \cdot 10^9$ N/m and the damping coefficient $D_{e_2} = 10^5$ Ns/m. The corresponding results are depicted in Figures 7.7e to 7.7h. It is also concluded that the sequence of sudden left and right hand side contacts in fully rigid modeling approach results in higher values of contact forces. On the other hand, introducing tooth elasticities can influence the resulting contact forces. Small values of the stiffness and damping coefficients result in the lower number of contacts and lower contact forces while higher values increase the number of contacts and contact forces.

Example 3: Simulation of a Gearbox Model

Figure 7.8 shows a model of a gearbox used to transfer power from the engine to the rear wheels of a car. This model consists of 12 helical gears named from G_1 to G_{12} that are

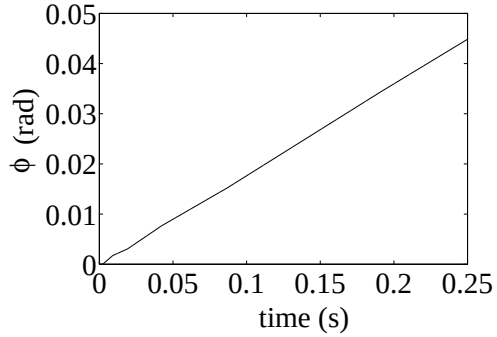

a: rotation angle of gear 2

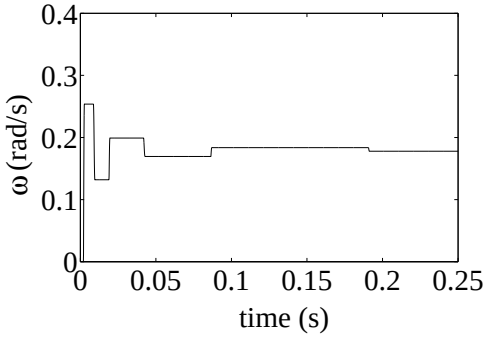

b: angular velocity of gear 2

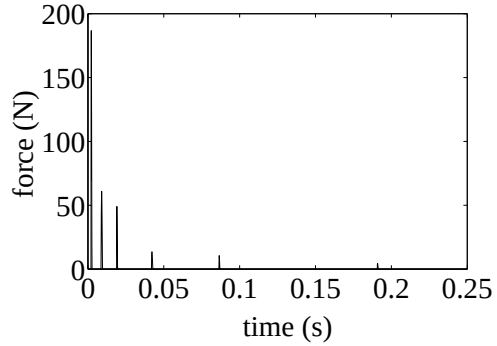

c: absolute value of applied force on gear 2

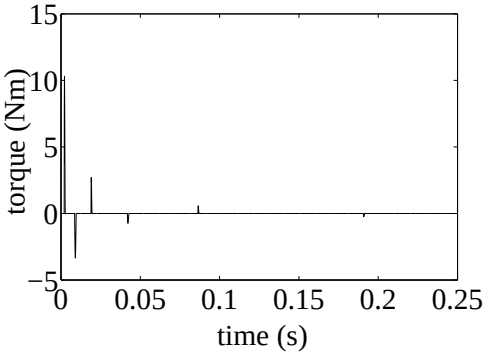

d: resulting torque of gear 2

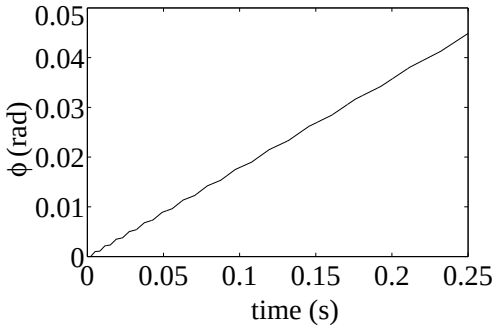

e: rotation angle of gear 2

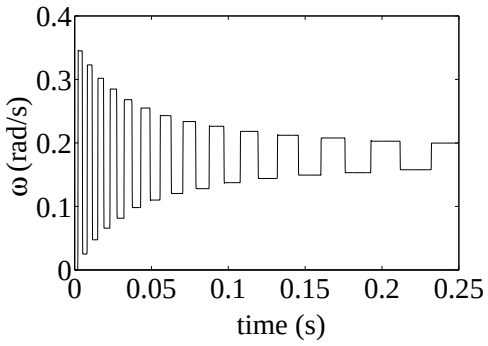

f: angular velocity of gear 2

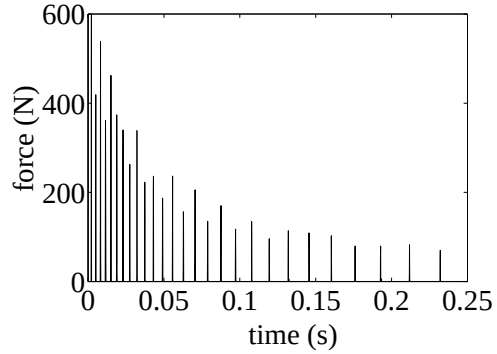

g: absolute value of applied force on gear 2

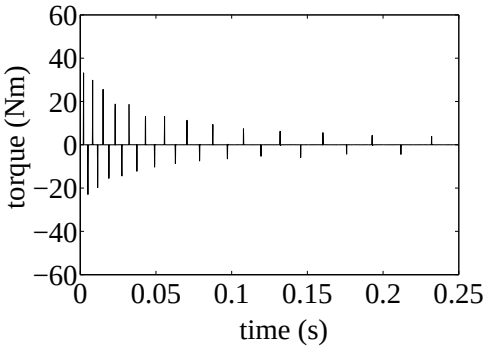

h: resulting torque of gear 2

Figure 7.7: Simulation results for gear 2 obtained from the new approach for two different sets of stiffness and damping coefficients (a-d for K_{e_1} and D_{e_1}, e-h for K_{e_2} and D_{e_2})

mounted on four shafts. The arrangement of these four shafts and gear pairs are clearly shown in Figure 7.8. The first gear pair is the driving pair D and includes the gear G_1 mounted on the driving shaft (input) and the gear G_2 of the transmission shaft.

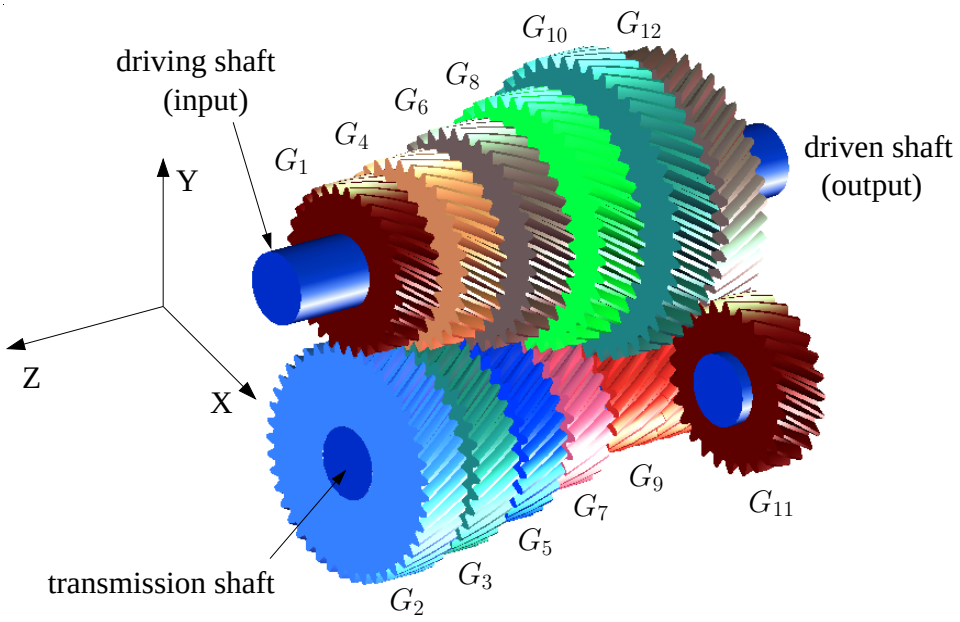

a: perspective view

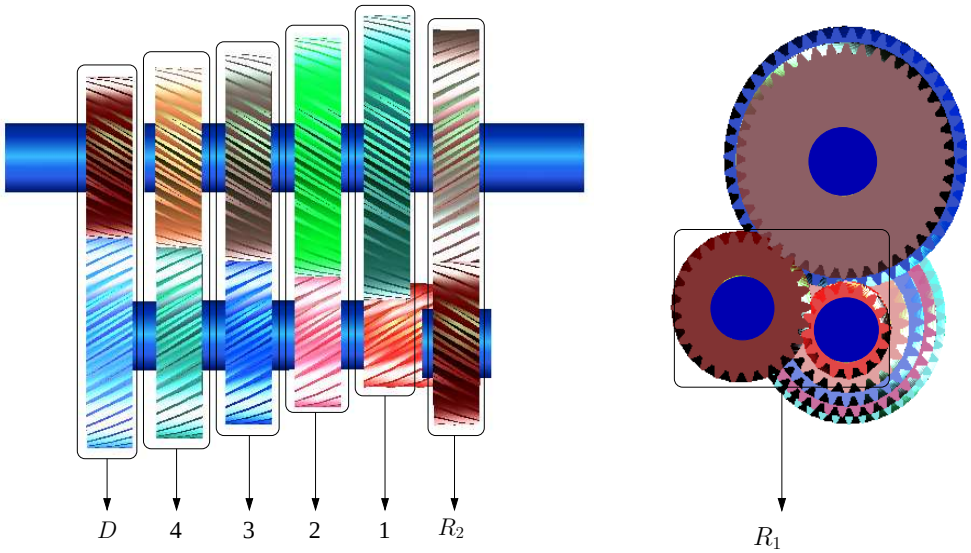

b: front view c: rear view

Figure 7.8: A gearbox model in three different views

Then, gear pairs 1 to 4 are being used to be able to transfer four different powers depending on the corresponding gear ratio. The gear pair 1 transfers the highest torque compared to the other gear pairs. The gear pairs R_1 and R_2 are also considered to reverse the rotation of the output shaft, opposite to the direction of input shaft through the gear

G_{11}. In order to be able to activate a required gear pair, the other gear pairs have to be deactivated in order to avoid locking of the gearbox. However, it is important to point out that although the deactivated gears are not engaged directly for power transmission, they are rotated by their pairing gears which are fixed to their corresponding shafts. For example, for activating the gear ratio 2, the gears G_3 and G_5 of the transmission shaft have to rotate freely and instead, the gears G_2, G_7 and G_9 are rigidly fixed to this shaft. On the other hand, the gears G_4, G_6 and G_8 are fixed to the output shaft, while the gears G_{10} and G_{12} have to rotate freely without being fixed to this shaft. In this way, the power is transmitted at first from G_1 to the transmission shaft through G_2. Then G_7 will rotate G_8 and the output shaft. However, the freely mounted gears of the gear pairs 1, 3, 4, R_1 and R_2 will be rotated due to contact without having any direct effect on the power transmission. Although the power is transferred through the gear pairs D and 2, the deactivated gear pairs 1, 3, 4, R_1 and R_2 will influence a little the transferred power due to contact and inertia properties of the gears.

The values of parameters used for the simulation of this gearbox are given in Table 7.3. In this table, n_{th} is used for teeth number, I_{zz} for mass moment of inertia about rotational axis, s for shift factor, m_n for normal module and a_0 for nominal axes distance. Table 7.4 provides some other necessary parameters which have the same value for each gear.

Table 7.3: Properties of the gears in the gearbox model

gear pair	gear	n_{th}	I_{zz} (kgm^2)	x	m_n (m)	a_0 (m)
D	G_1	30	$0.833 \cdot 10^{-3}$	0.254	0.00185	0.08
	G_2	43	$2.880 \cdot 10^{-3}$	0.149		
4	G_3	37	$1.135 \cdot 10^{-3}$	0.235	0.00194	0.08
	G_4	32	$1.030 \cdot 10^{-3}$	0.299		
3	G_5	31	$0.967 \cdot 10^{-3}$	0.359	0.002	0.08
	G_6	36	$1.120 \cdot 10^{-3}$	0.357		
2	G_7	23	$0.291 \cdot 10^{-3}$	0.422	0.00209	0.08
	G_8	40	$2.010 \cdot 10^{-3}$	0.226		
1	G_9	16	$0.306 \cdot 10^{-3}$	0.149	0.00214	0.08
	G_{10}	47	$2.860 \cdot 10^{-3}$	0.149		
R_1	G_9				0.00214	0.0543
	G_{11}	26	$0.312 \cdot 10^{-3}$	0.254		
R_2	G_{11}				0.00214	0.086
	G_{12}	42	$2.201 \cdot 10^{-3}$	0.149		

As the input to the gearbox, the input torque $T_{inp} = 200$ Nm is applied clockwise to the driving shaft while the resistant output torque $T_{out} = 498.55$ Nm is applied at the

Table 7.4: Other properties of the gears in the gearbox model

normal pressure angle α_n	20 deg	face width b	0.02 m
addendum coefficient	1.1	shape factor s	0.85
dedendum coefficient	1.15	tip relief factor	0
Young's modulus E	$2.1 \cdot 10^{11}$ N/m^2	Poisson's ratio ν	0.3
normal backlash factor	0	friction coefficient μ	0
helix angle β	31.5 deg	teeth stiffness ratio	0.8

same time counterclockwise to the driven shaft. The values of these torques are chosen in such a way to be consistent with the gear ratio of the active gear pairs (D and 2). However, a consistent initial rotational velocity has to be given to each shaft as well as deactivated gears in order to let the gears rotate. Here, the driven shaft rotates with the initial rotational velocity of $\omega = 10$ rad/s. The initial rotational velocity of the other shafts may be calculated based on the gear ratio. In this case, the rigidly fixed gear wheels will follow the same initial rotational velocities as their corresponding shafts but the deactivated gears will be initially at rest.

The simulation of the gearbox model has been performed for $t = 0.01$ s using both the fully rigid modeling and the new approach to compare the results as depicted in Figures 7.9 to 7.13. In the case of the new approach, the simulation has been done twice with different damping coefficients $D_e = 5 \cdot 10^4$ Ns/m and $D_e = 1 \cdot 10^4$ Ns/m of the elastic elements. The value of the stiffness coefficient is kept constant $K_e = 5 \cdot 10^6$ N/m. As one can expect, by increasing the value of the stiffness coefficient the results of the new procedure approach to the results of the fully rigid modeling approach, as we observed in the second example. Like that example, here it is not intended to identify the correct values of K_e and D_e but to study the the effect of the elastic elements on the behavior of the gearbox system and to show the difference between the obtained applied forces on the shafts from the fully rigid modeling and the new approach.

For this simulation, the rigid approach takes about 10 s of the CPU time while the new approach needs approximately 1200 s for $D_e = 5 \cdot 10^4$ Ns/m and 2700 s for $D_e = 10^4$ Ns/m. This computational effort, however, is not unexpected since the new approach introduces additional states to consider teeth rotation relative to gear body. Therefore, this approach adds 403 additional DOFs to the gearbox model compared to the fully rigid modeling approach with 8 DOFs. As another important factor, the system of equations of motion are very stiff due to the small teeth mass and high stiffness and damping coefficients of the elastic elements. Both reasons cause the observed computational effort.

For further modifications, the new approach may be adapted to consider the elastic elements when they are needed. In other words, it considers additional DOFs and their

corresponding elastic elements only for the teeth which come into contact. However, they have to be fixed rigidly to their corresponding gear bodies after leaving the contact region and damping out their relative vibrations. In this way, nonrequired DOFs and their corresponding elastic elements will not be considered when generating equations of motion and, therefore, it will speed up the simulation time considerably.

Figures 7.9 and 7.10 illustrate the rotational velocity ω of the transmission and output shafts from both approaches during the simulation. As it can be seen, the variation of ω is high at the beginning and decreases gradually. This condition may be interpreted as a steady condition. However, one can observe that the new approach delivers a smoother rotational velocity. This effect is intensified for the lower damping coefficient since it allows larger tangential movements of the teeth relative to the gear body.

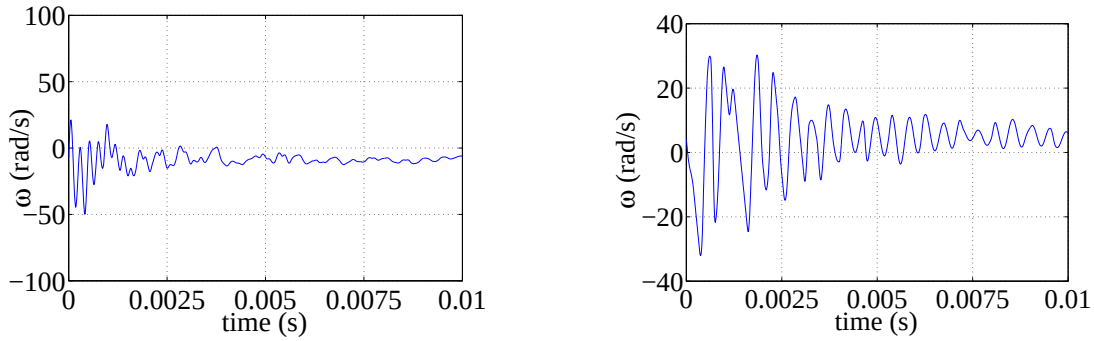

a: transmission shaft b: output shaft

Figure 7.9: Rotational velocity from the rigid approach

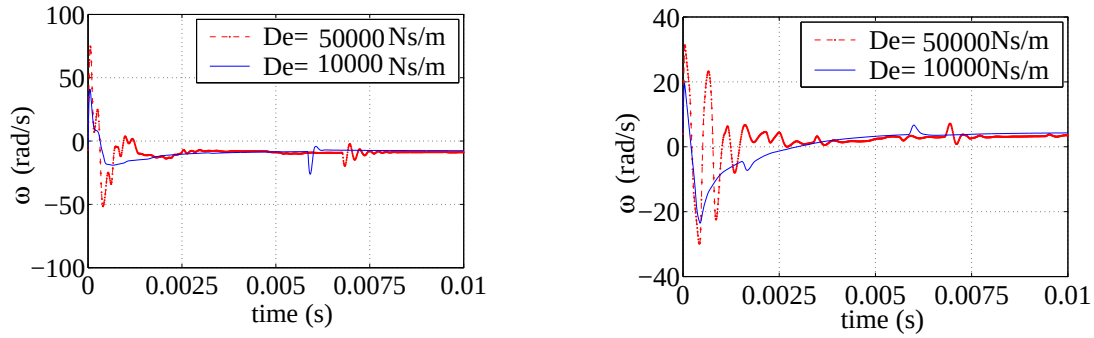

a: transmission shaft b: output shaft

Figure 7.10: Rotational velocity from the new approach

The total amount of absolute forces applied to the transmission and output shafts from both approaches are shown in Figures 7.11 and 7.12. Again, here the overall behavior of the applied forces obtained from the rigid approach is non-smooth whereas the new

approach provides applied forces with smoother behavior specially for the steady condition. It is also noticeable that the new approach for high values of stiffness and damping coefficients of the elastic elements results in higher values of applied forces at the beginning but approaches rapidly to constant values for steady condition. However, the lower damping coefficient leads to the applied forces with lower values at the beginning when it is compared to both the fully rigid modeling and the new approaches with high damping coefficient. Finally, it approaches to the same steady applied forces as for both cases.

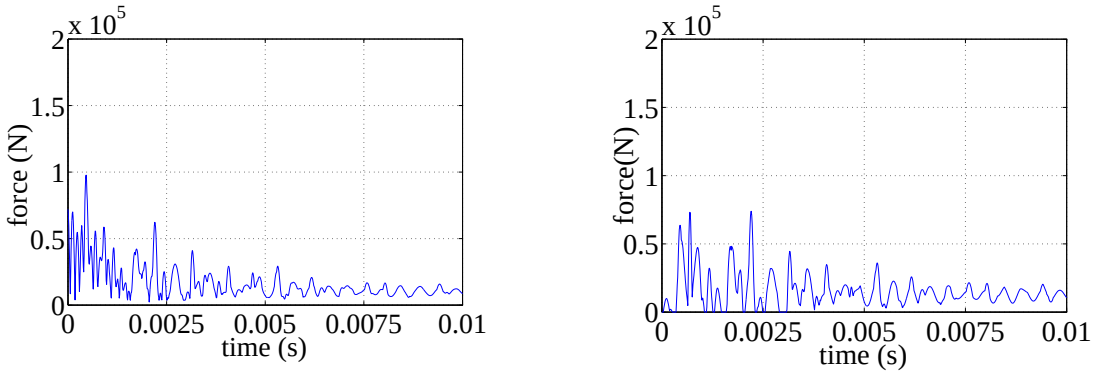

a: transmission shaft b: output shaft

Figure 7.11: Absolute applied force from the rigid approach

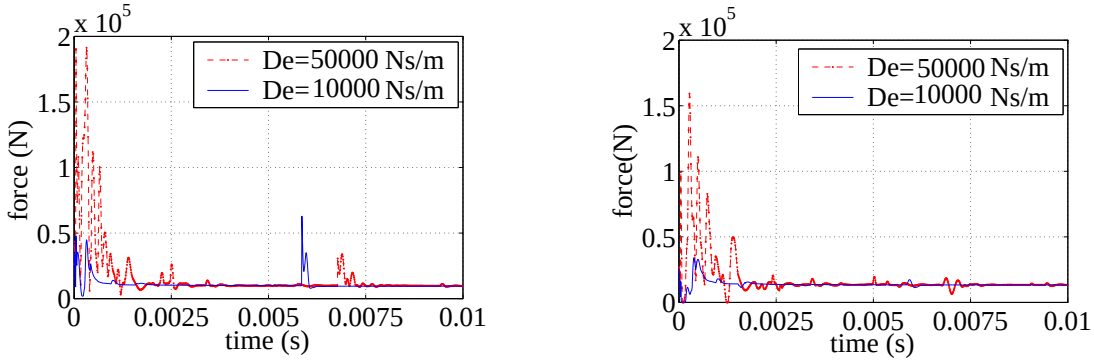

a: transmission shaft b: output shaft

Figure 7.12: Absolute applied force from the new approach

Figure 7.13 shows another property which presents the amount of energy loss consumed for rotating the deactivated gear G_3 during the simulation.

In the case of fully rigid modeling approach, the energy loss has high variations at the beginning which means that the energy is frequently interchanged between gears G_3 and G_4. Finally, its value approaches approximately to zero. In the new approach, one can observe higher amount of energy loss compared to the rigid case. This difference describes

clearly the effect of damping in the elastic elements between teeth and the gear body. Higher values of damping result in higher amount of the energy loss during simulation.

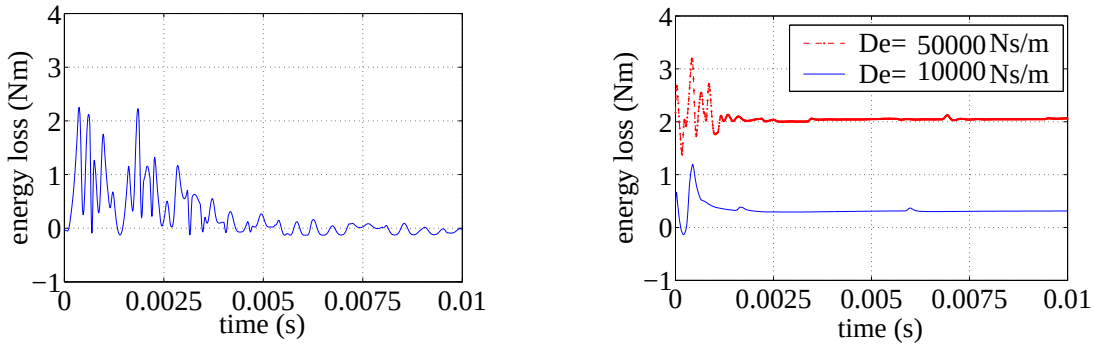

a: rigid approach b: new approach

Figure 7.13: Energy loss associated with the gear G_3

Chapter 8

Summary

This thesis is devoted to computational contact procedures in flexible multibody systems. For this purpose, first in Chapter 1 contact problems in multibody systems together with some computational procedures were briefly introduced.

Then, in Chapter 2 starting from kinematics and kinetics of rigid bodies, some basic concepts of flexible multibody dynamics including solution algorithms were explained. In this context, some common modeling strategies were briefly explained. Among all, the floating frame of reference has been used in this work to generate equations of motion. This approach is a widely-used method which introduces two kinds of variables for body reference motion and elastic deformations. Chapter 2 ended with giving some notes regarding symbolic and numerical derivation of equations of motion together with numerical integration methods.

Some of the most frequently-used formulations for incorporating the contact constraints into the governing equations of motion were introduced briefly in Chapter 3. Among them, the penalty approach, the Lagrange multipliers approach, linear complementarity problem formulations and proximal point approach were mentioned.

Contact and impact problem of planar flexible bodies in multibody systems were formulated in Chapters 4 and 5, respectively, yielding the linear complementarity problems. Such formulations are the result of other methods which mathematically give the exact solution to the contact problem and have been well established and frequently used in the context of rigid bodies contact. In contrast, they have been used comparatively rarely for flexible bodies. In Chapter 4, the available approach for planar rigid bodies [55, 106] was extended for planar flexible bodies. The major difference between both approaches was in the formulation of contact kinematics. It was formulated as an LCP constructed by following the same procedure as described in [106] for contact of rigid bodies. It was also shown that our formulation approaches the LCP formulation of [106] when the effect of deformations is ignored. It is noticeable that when dealing with spatial systems, one

formulates the contact problem as a nonlinear complementarity problem and not an LCP. Another important difference appears when friction is taken into consideration. In such a case, one has to approximate the friction cone with a polyhedral approximation model. Formulation of contact and impact of spatial rigid bodies can be found in [134] and [152].

Impact analysis was followed in Chapter 5 by formulating some other LCPs on position and velocity level. The formulations on position level for normal direction was done by imposing non-penetrability conditions through complementarity relations between normal gaps and normal impact forces. In doing so, at first kinematics of impacting bodies was described in terms of generalized coordinates. Some common integration approaches have been further used to find the required relations which represent generalized coordinates as functions of impact forces. Then, this formulation was appended to the formulation of tangential contact forces which was developed for continual contact in Chapter 4. To do so, it was assumed that the behavior of impact in tangential direction is similar to the one of the continual contact for a short period of time when dealing with flexible bodies. For the velocity level formulation of normal impact, one deals with velocity of normal gaps and the generalized velocities instead of normal gaps and the generalized coordinates.

In the case of impact, examples for both short and long impacts were considered. The results showed a good agreement between the results of our approach based on the formulations from the explicit Runge-Kutta approach on position and velocity level and also the RADAU5 approach with the results of FEM for soft planar flexible bodies. The formulation from the RADAU5 approach is computationally expensive and is not recommended for practical use. The comparison between the formulation from the explicit Runge-Kutta approach on position and velocity level showed that the formulation on position level is computationally more efficient than the formulation on velocity level. Consequently, it can be chosen as a reliable approach for impact analysis of planar deformable bodies provided that an appropriate time step is chosen.

It was shown that the formulations on both position and velocity level approach the precise results of FEM even for stiff planar deformable bodies provided that a proper number of eigenmodes of the FEM model is chosen for building the reduced model of deformable bodies. We also observed that selection of higher number of eigenmodes leads to the lower energy dissipation. Selection of higher eigenmodes allows a better adjustment of the shape of deformable bodies during impact which consequently leads to lower normal impact forces. As a result, the amount of released energy during the expansion phase of impact increases as a higher number of eigenmodes is considered.

Then, the modeling of contact and impact of spatial flexible bodies using the polygonal contact model approach was explained in Chapter 6. It was originally an algorithm of contact of spatial rigid bodies based on the surface compliance approach [68]. In Chapter 6 the extension of polygonal contact model as a general algorithm for contact of flexible bodies which establishes a more realistic modeling of many contact problems in multibody

systems was explained. The obtained results implied that the collision detection is the major source of the computation effort in polygonal contact model for contact of flexible bodies. In the current extension, updating the content of the whole bounding volume tree is done at each evaluation of the equations of motion. It can be summarized that with the extended polygonal contact model, contacts between elastic bodies can be considered at only moderate additional costs.

As an application of contact modeling in multibody systems, Chapter 7 was devoted to the subject of contact in geared systems. First, the approach for contact modeling of meshing rigid gear wheels [91] was briefly explained. Furthermore, it was extended by introducing some elastic elements between the teeth and the gear body of each gear wheel to consider partially elasticities. In the first example one side flange contact of two spur gears was simulated with FEM, the fully rigid modeling approach and the extended approach. The resulting contact force of the presented approach was closer to the accurate results of FEM compared to the fully rigid modeling procedure. For getting such results, the new procedure did not need much more computation time compared to the rigid modeling. The results of the second example showed the effect of the considered elastic elements. In the third example the possibility of applying the new developed approach for a practical case such as a gearbox was also tested.

As the further work in the context of this work following points may be mentioned:

- Regarding the presented approach in Chapter 5, the effect of considering different material damping models and proper selection of the mode shapes on the impact of stiff planar flexible bodies can be investigated.
- For contact modeling of spatial flexible bodies, some issues may be considered to make the procedure more efficient, e.g.:
  - Update of the limits of bounding volumes can be performed only for those bounding volumes which are checked for collision. This modification speeds up the bounding volume tree updating considerably and prevents unnecessary calculations.
  - A more efficient collision detection algorithm with the capability of checking the self contacts may be used.
  - Additionally, some other modifications about determination of relative velocities of contact elements and contact forces and torques can and should be implemented.
- For further modifications of the presented approach for contact modeling of meshing gear wheels in Chapter 7, following points are noticeable:
  - It may be adapted to consider the elastic elements only for the teeth which come into contact and to avoid the definition of the nonrequired DOFs and

corresponding elastic elements. After leaving the contact region and damping out the relative vibrations of these teeth, they have to be fixed rigidly to their corresponding gear bodies.

– The values of the stiffness and damping coefficients of the elastic elements for introducing the teeth elasticities have to be provided by the analyst. Since this is still under investigation and unfortunately there is not yet a simple theory for computing these values, they have to be identified once from a numerical precomputation using an FEM simulation.

Appendix

System States versus Impact Forces

The objective of this appendix is to present some relations required for formulation of linear complementarity problems on position and velocity levels for impact of planar flexible bodies in Chapter 5. These desired relations specify the dependency of the generalized coordinates and velocities on the impact forces. In following, two different approaches based on the 4^{th} order explicit Runge-Kutta and RADAU5 methods are presented.

A.1 The 4^{th} Order Explicit Runge-Kutta Method

The classical 4^{th} order explicit Runge-Kutta method is a one step method of second order which reads as

$$\mathbf{Y}_{n+1} = \mathbf{Y}_n + \Delta t_n \left(\frac{1}{6}{}^n\mathbf{k}_1 + \frac{1}{3}{}^n\mathbf{k}_2 + \frac{1}{3}{}^n\mathbf{k}_3 + \frac{1}{6}{}^n\mathbf{k}_4 \right) , \tag{A.1}$$

where $\mathbf{Y}_n$ denotes the states vector which contains the generalized coordinates and velocities

$$\mathbf{Y}_n = \begin{bmatrix} \mathbf{q}_n \\ \dot{\mathbf{q}}_n \end{bmatrix} . \tag{A.2}$$

The index n is the n^{th} integration step and Δt_n is the integration step size. The vectors ${}^n\mathbf{k}_1$, ${}^n\mathbf{k}_2$ and ${}^n\mathbf{k}_3$ are defined as

$$\begin{aligned} {}^n\mathbf{k}_1 &= \mathbf{f}\left(t_n,\ \mathbf{Y}_n\right) && , \\ {}^n\mathbf{k}_2 &= \mathbf{f}\left(t_n + \frac{\Delta t_n}{2},\ \mathbf{Y}_n + \frac{\Delta t_n}{2}\ {}^n\mathbf{k}_1\right) && , \\ {}^n\mathbf{k}_3 &= \mathbf{f}\left(t_n + \frac{\Delta t_n}{2},\ \mathbf{Y}_n + \frac{\Delta t_n}{2}\ {}^n\mathbf{k}_2\right) && , \\ {}^n\mathbf{k}_4 &= \mathbf{f}\left(t_n + \Delta t_n,\ \mathbf{Y}_n + \Delta t_n {}^n\mathbf{k}_3\right) && . \end{aligned} \tag{A.3}$$

The value of ${}^n\mathbf{k}_1$ corresponding to the first stage of integration reads as

$$ {}^n\mathbf{k}_1 = \begin{bmatrix} {}^n\dot{\mathbf{q}}_1 \\ {}^n\ddot{\mathbf{q}}_1 \end{bmatrix} = \begin{bmatrix} \dot{\mathbf{q}}_n \\ {}^n\ddot{\mathbf{q}}_1 \end{bmatrix} . \tag{A.4} $$

For the second step, one has to evaluate the following states required for ${}^n\mathbf{k}_2$ in Eq. (A.3)

$$ \begin{bmatrix} {}^n\mathbf{q}_2 \\ {}^n\dot{\mathbf{q}}_2 \end{bmatrix} = \begin{bmatrix} \mathbf{q}_n \\ \dot{\mathbf{q}}_n \end{bmatrix} + \frac{\Delta t_n}{2}\, {}^n\mathbf{k}_1 = \begin{bmatrix} \mathbf{q}_n + \dfrac{\Delta t_n}{2}\, \dot{\mathbf{q}}_n \\ \dot{\mathbf{q}}_n + \dfrac{\Delta t_n}{2}\, {}^n\ddot{\mathbf{q}}_1 \end{bmatrix} , \tag{A.5} $$

which consequently yields

$$ {}^n\mathbf{k}_2 = \begin{bmatrix} {}^n\dot{\mathbf{q}}_2 \\ {}^n\ddot{\mathbf{q}}_2 \end{bmatrix} = \begin{bmatrix} \dot{\mathbf{q}}_n + \dfrac{\Delta t_n}{2}\, {}^n\ddot{\mathbf{q}}_1 \\ {}^n\ddot{\mathbf{q}}_2 \end{bmatrix} . \tag{A.6} $$

Similarly for ${}^n\mathbf{k}_3$

$$ \begin{bmatrix} {}^n\mathbf{q}_3 \\ {}^n\dot{\mathbf{q}}_3 \end{bmatrix} = \begin{bmatrix} \mathbf{q}_n \\ \dot{\mathbf{q}}_n \end{bmatrix} + \frac{\Delta t_n}{2}\, {}^n\mathbf{k}_2 = \begin{bmatrix} \mathbf{q}_n + \dfrac{\Delta t_n}{2} \left(\dot{\mathbf{q}}_n + \dfrac{\Delta t_n}{2}\, {}^n\ddot{\mathbf{q}}_1 \right) \\ \dot{\mathbf{q}}_n + \dfrac{\Delta t_n}{2}\, {}^n\ddot{\mathbf{q}}_2 \end{bmatrix} , \tag{A.7} $$

$$ {}^n\mathbf{k}_3 = \begin{bmatrix} {}^n\dot{\mathbf{q}}_3 \\ {}^n\ddot{\mathbf{q}}_3 \end{bmatrix} = \begin{bmatrix} \dot{\mathbf{q}}_n + \dfrac{\Delta t_n}{2}\, {}^n\ddot{\mathbf{q}}_2 \\ {}^n\ddot{\mathbf{q}}_3 \end{bmatrix} , \tag{A.8} $$

and for ${}^n\mathbf{k}_4$

$$ \begin{bmatrix} {}^n\mathbf{q}_4 \\ {}^n\dot{\mathbf{q}}_4 \end{bmatrix} = \begin{bmatrix} \mathbf{q}_n \\ \dot{\mathbf{q}}_n \end{bmatrix} + \Delta t_n\, {}^n\mathbf{k}_3 = \begin{bmatrix} \mathbf{q}_n + \Delta t_n \left(\dot{\mathbf{q}}_n + \dfrac{\Delta t_n}{2}\, {}^n\ddot{\mathbf{q}}_2 \right) \\ \dot{\mathbf{q}}_n + \Delta t_n\, {}^n\ddot{\mathbf{q}}_3 \end{bmatrix} , \tag{A.9} $$

$$ {}^n\mathbf{k}_4 = \begin{bmatrix} {}^n\dot{\mathbf{q}}_4 \\ {}^n\ddot{\mathbf{q}}_4 \end{bmatrix} = \begin{bmatrix} \dot{\mathbf{q}}_n + \Delta t_n\, {}^n\ddot{\mathbf{q}}_3 \\ {}^n\ddot{\mathbf{q}}_4 \end{bmatrix} . \tag{A.10} $$

Now, based on the already obtained relations for ${}^n\mathbf{k}_j,\ j = 1, 2, 3, 4$ and using Eq. (A.1) one obtains

$$ \begin{bmatrix} \mathbf{q}_{n+1} \\ \dot{\mathbf{q}}_{n+1} \end{bmatrix} = \begin{bmatrix} \mathbf{q}_n + \Delta t_n\, \dot{\mathbf{q}}_n + \dfrac{\Delta t_n^2}{6}\ ({}^n\ddot{\mathbf{q}}_1 + {}^n\ddot{\mathbf{q}}_2 + {}^n\ddot{\mathbf{q}}_3) \\ \dot{\mathbf{q}}_n + \dfrac{\Delta t_n}{6}({}^n\ddot{\mathbf{q}}_1 + {}^n\ddot{\mathbf{q}}_4) + \dfrac{\Delta t_n}{3}({}^n\ddot{\mathbf{q}}_2 + {}^n\ddot{\mathbf{q}}_3) \end{bmatrix} . \tag{A.11} $$

At this instant, the amount of accelerations ${}^n\ddot{\mathbf{q}}_j,\ j = 1, 2, 3, 4$ can be substituted from the equations of motion, Eq. (5.27),

$$ {}^n\ddot{\mathbf{q}}_j = {}^n \left(\widetilde{\mathbf{M}}_{q_j} \cdot \mathbf{h}_{c_j} \right) + {}^n \left(\widetilde{\mathbf{M}}_{q_j} \cdot \mathbf{W}_{NHc_j} \right) \cdot \boldsymbol{\lambda}_n , \qquad j = 1, 2, 3, 4 , \tag{A.12} $$

yielding the following relation between the generalized coordinates and impact forces

$$\mathbf{q}_{n+1} = \underbrace{\frac{\Delta t_n^2}{6}\sum_{j=1}^{3}(\widetilde{\mathbf{M}}_{q_j}\cdot\mathbf{W}_{NHc_j})_n}_{\mathbf{W}_{q_n}}\cdot\boldsymbol{\lambda}_n + \underbrace{(\mathbf{q}_n + \Delta t_n\dot{\mathbf{q}}_n + \frac{\Delta t_n^2}{6}\sum_{j=1}^{3}(\widetilde{\mathbf{M}}_{q_j}\cdot\mathbf{h}_{c_j})_n)}_{\mathbf{w}_{q_n}} \ . \quad \text{(A.13)}$$

In the same manner, the relation between the generalized velocities and impact forces can be written as

$$\dot{\mathbf{q}}_{n+1} = \left(\frac{\Delta t_n}{6}(\widetilde{\mathbf{M}}_{q_1}\cdot\mathbf{W}_{NHc_1} + \widetilde{\mathbf{M}}_{q_4}\cdot\mathbf{W}_{NHc_4})_n + \frac{\Delta t_n}{3}\sum_{j=2}^{3}(\widetilde{\mathbf{M}}_{q_j}\cdot\mathbf{W}_{NHc_j})_n \right)\cdot\boldsymbol{\lambda}_n +$$
$$\left(\dot{\mathbf{q}}_n + \frac{\Delta t_n}{6}(\widetilde{\mathbf{M}}_{q_1}\cdot\mathbf{h}_{c_1} + \widetilde{\mathbf{M}}_{q_4}\cdot\mathbf{h}_{c_4})_n + \frac{\Delta t_n}{3}\sum_{j=2}^{3}(\widetilde{\mathbf{M}}_{q_j}\cdot\mathbf{h}_{c_j})_n \right) \ . \quad \text{(A.14)}$$

Maybe it is important to point out that the index $j = 1,2,3,4$ of the parameters $\widetilde{\mathbf{M}}_{q_j}, \mathbf{W}_{NH_j}$ and $\mathbf{h}_{c_j}$ in Eqs. (A.13) and (A.14) corresponds to the four stages of the 4^{th} order Runge-Kutta method, respectively. Each parameter of $\widetilde{\mathbf{M}}_{q_j}, \mathbf{W}_{NHc_j}$ and $\mathbf{h}_{c_j}$ is evaluated in the corresponding stage of the 4^{th} order Runge-Kutta method and is finally used in Eqs. (A.13) and (A.14) for calculating the required terms in those equations.

A.2 The 5^{th} Order Implicit Runge-Kutta Method: RADAU5

As another possibility, one can formulate the required relation between $\mathbf{q}$ and $\boldsymbol{\lambda}$ from the 5^{th} order implicit Runge-Kutta method for which in this work, the implicit method of RADAU5 has been served, see [38] and [59],

$$\mathbf{Y}_{n+1} = \mathbf{Y}_n + \Delta t_n \ (\gamma_1 {}^n\mathbf{k}_1 + \gamma_2 {}^n\mathbf{k}_2 + \gamma_3 {}^n\mathbf{k}_3) \ . \quad \text{(A.15)}$$

The vectors ${}^n\mathbf{k}_1$, ${}^n\mathbf{k}_2$ and ${}^n\mathbf{k}_3$ have to be evaluated in an iterative process defined as

$$\begin{aligned}
{}^n\mathbf{k}_1^{k+1} &= f\left(t_n + \alpha_1\,\Delta t_n,\ \mathbf{Y}_n + \Delta t_n\ \left(\beta_{11}{}^n\mathbf{k}_1^k + \beta_{12}{}^n\mathbf{k}_2^k + \beta_{13}{}^n\mathbf{k}_3^k\right)\right) \ , \\
{}^n\mathbf{k}_2^{k+1} &= f\left(t_n + \alpha_2\,\Delta t_n,\ \mathbf{Y}_n + \Delta t_n\ \left(\beta_{21}{}^n\mathbf{k}_1^k + \beta_{22}{}^n\mathbf{k}_2^k + \beta_{23}{}^n\mathbf{k}_3^k\right)\right) \ , \\
{}^n\mathbf{k}_3^{k+1} &= f\left(t_n + \alpha_3\,\Delta t_n,\ \mathbf{Y}_n + \Delta t_n\ \left(\beta_{31}{}^n\mathbf{k}_1^k + \beta_{32}{}^n\mathbf{k}_2^k + \beta_{33}{}^n\mathbf{k}_3^k\right)\right)
\end{aligned} \quad \text{(A.16)}$$

with the iteration counter k. The iteration process is followed till convergence based on a prescribed tolerance. In addition, the coefficients β_{mp}, α_m and γ_m for $m,p = 1,2,3$ are defined as follows, see [38] and [59],

$$\beta = \begin{bmatrix} \frac{88-7\sqrt{6}}{360} & \frac{296-169\sqrt{6}}{1800} & \frac{-2+3\sqrt{6}}{225} \\ \frac{296+169\sqrt{6}}{1800} & \frac{88+7\sqrt{6}}{360} & \frac{-2-3\sqrt{6}}{225} \\ \frac{16-\sqrt{6}}{36} & \frac{16+\sqrt{6}}{36} & \frac{1}{9} \end{bmatrix} ,$$

$$\gamma = \begin{bmatrix} \frac{16-\sqrt{6}}{36} & \frac{16+\sqrt{6}}{36} & \frac{1}{9} \end{bmatrix} , \tag{A.17}$$

$$\alpha = \begin{bmatrix} \frac{4-\sqrt{6}}{10} & \frac{4+\sqrt{6}}{10} & 1 \end{bmatrix} .$$

For the first iteration of each integration step n, the values of ${}^n\mathbf{k}_1^1$, ${}^n\mathbf{k}_2^1$ and ${}^n\mathbf{k}_3^1$ are substituted from the corresponding values from the last iteration of the previous integration step

$${}^n\mathbf{k}_j^1 = {}^{(n-1)}\mathbf{k}_j = \begin{bmatrix} {}^n\dot{\mathbf{q}}_j^1 \\ {}^n\ddot{\mathbf{q}}_j^1 \end{bmatrix} , \qquad j = 1, 2, 3 . \tag{A.18}$$

For the second iteration step, ${}^n\mathbf{k}_1^2$ reads as

$${}^n\mathbf{k}_1^2 = \begin{bmatrix} {}^n\dot{\mathbf{q}}_1^2 \\ {}^n\ddot{\mathbf{q}}_1^2 \end{bmatrix} . \tag{A.19}$$

The states needed for evaluation of ${}^n\mathbf{k}_1^2$ are written based on the first relation of Eq. (A.16) as follows

$$\begin{bmatrix} {}^n\mathbf{q}_1^2 \\ {}^n\dot{\mathbf{q}}_1^2 \end{bmatrix} = \begin{bmatrix} \mathbf{q}_n \\ \dot{\mathbf{q}}_n \end{bmatrix} + \Delta t_n \left(\beta_{11} \begin{bmatrix} {}^n\dot{\mathbf{q}}_1^1 \\ {}^n\ddot{\mathbf{q}}_1^1 \end{bmatrix} + \beta_{12} \begin{bmatrix} {}^n\dot{\mathbf{q}}_2^1 \\ {}^n\ddot{\mathbf{q}}_2^1 \end{bmatrix} + \beta_{13} \begin{bmatrix} {}^n\dot{\mathbf{q}}_3^1 \\ {}^n\ddot{\mathbf{q}}_3^1 \end{bmatrix} \right) \tag{A.20}$$

and consequently using Eq. (A.19)

$${}^n\mathbf{k}_1^2 = \begin{bmatrix} \dot{\mathbf{q}}_n + \Delta t_n \ (\beta_{11}{}^n\ddot{\mathbf{q}}_1^1 + \beta_{12}{}^n\ddot{\mathbf{q}}_2^1 + \beta_{13}{}^n\ddot{\mathbf{q}}_3^1) \\ {}^n\ddot{\mathbf{q}}_1^2 \end{bmatrix} . \tag{A.21}$$

Evaluation of ${}^n\mathbf{k}_2^2$ and ${}^n\mathbf{k}_3^2$ is carried out by following the same procedure

$${}^n\mathbf{k}_2^2 = \begin{bmatrix} {}^n\dot{\mathbf{q}}_2^2 \\ {}^n\ddot{\mathbf{q}}_2^2 \end{bmatrix} = \begin{bmatrix} \dot{\mathbf{q}}_n + \Delta t_n \ (\beta_{21}{}^n\ddot{\mathbf{q}}_1^1 + \beta_{22}{}^n\ddot{\mathbf{q}}_2^1 + \beta_{23}{}^n\ddot{\mathbf{q}}_3^1) \\ {}^n\ddot{\mathbf{q}}_2^2 \end{bmatrix} \tag{A.22}$$

and

$${}^n\mathbf{k}_3^2 = \begin{bmatrix} {}^n\dot{\mathbf{q}}_3^2 \\ {}^n\ddot{\mathbf{q}}_3^2 \end{bmatrix} = \begin{bmatrix} \dot{\mathbf{q}}_n + \Delta t_n \ (\beta_{31}{}^n\ddot{\mathbf{q}}_1^1 + \beta_{32}{}^n\ddot{\mathbf{q}}_2^1 + \beta_{33}{}^n\ddot{\mathbf{q}}_3^1) \\ {}^n\ddot{\mathbf{q}}_3^2 \end{bmatrix} . \tag{A.23}$$

The iteration process may be followed till step k in which convergence is achieved. At that instant, the corresponding state vectors ${}^n\mathbf{k}_1^k$, ${}^n\mathbf{k}_2^k$ and ${}^n\mathbf{k}_3^k$ are to be evaluated following

the same procedure as was followed for the second iteration step

$$
\begin{aligned}
{}^n\mathbf{k}_1^k &= \begin{bmatrix} {}^n\dot{\mathbf{q}}_1^k \\ {}^n\ddot{\mathbf{q}}_1^k \end{bmatrix} = \begin{bmatrix} \dot{\mathbf{q}}_n + \Delta t_n \ \left(\beta_{11}\,{}^n\ddot{\mathbf{q}}_1^{k-1} + \beta_{12}\,{}^n\ddot{\mathbf{q}}_2^{k-1} + \beta_{13}\,{}^n\ddot{\mathbf{q}}_3^{k-1}\right) \\ {}^n\ddot{\mathbf{q}}_1^k \end{bmatrix} , \qquad \text{(A.24)} \\
{}^n\mathbf{k}_2^k &= \begin{bmatrix} {}^n\dot{\mathbf{q}}_2^k \\ {}^n\ddot{\mathbf{q}}_2^k \end{bmatrix} = \begin{bmatrix} \dot{\mathbf{q}}_n + \Delta t_n \ \left(\beta_{21}\,{}^n\ddot{\mathbf{q}}_1^{k-1} + \beta_{22}\,{}^n\ddot{\mathbf{q}}_2^{k-1} + \beta_{23}\,{}^n\ddot{\mathbf{q}}_3^{k-1}\right) \\ {}^n\ddot{\mathbf{q}}_2^k \end{bmatrix} , \\
{}^n\mathbf{k}_3^k &= \begin{bmatrix} {}^n\dot{\mathbf{q}}_3^k \\ {}^n\ddot{\mathbf{q}}_3^k \end{bmatrix} = \begin{bmatrix} \dot{\mathbf{q}}_n + \Delta t_n \ \left(\beta_{31}\,{}^n\ddot{\mathbf{q}}_1^{k-1} + \beta_{32}\,{}^n\ddot{\mathbf{q}}_2^{k-1} + \beta_{33}\,{}^n\ddot{\mathbf{q}}_3^{k-1}\right) \\ {}^n\ddot{\mathbf{q}}_3^k \end{bmatrix} .
\end{aligned}
$$

The amount of accelerations ${}^n\ddot{\mathbf{q}}_1^{k-1}$, ${}^n\ddot{\mathbf{q}}_2^{k-1}$ and ${}^n\ddot{\mathbf{q}}_3^{k-1}$ can be substituted from the equations of motion, Eq. (5.27),

$$
\ddot{\mathbf{q}} = \widetilde{\mathbf{M}}_q \cdot (\mathbf{h}_c + \mathbf{W}_{NHc} \cdot \boldsymbol{\lambda}) \qquad \text{(A.25)}
$$

which yields

$$
\begin{aligned}
{}^n\ddot{\mathbf{q}}_1^{k-1} &= \left(\widetilde{\mathbf{M}}_{q_1} \cdot \mathbf{h}_{c_1}\right)_n^{k-1} + \left(\widetilde{\mathbf{M}}_{q_1} \cdot \mathbf{W}_{NHc_1}\right)_n^{k-1} \cdot \boldsymbol{\lambda}_n \ , \\
{}^n\ddot{\mathbf{q}}_2^{k-1} &= \left(\widetilde{\mathbf{M}}_{q_2} \cdot \mathbf{h}_{c_2}\right)_n^{k-1} + \left(\widetilde{\mathbf{M}}_{q_2} \cdot \mathbf{W}_{NHc_2}\right)_n^{k-1} \cdot \boldsymbol{\lambda}_n \ , \qquad \text{(A.26)} \\
{}^n\ddot{\mathbf{q}}_3^{k-1} &= \left(\widetilde{\mathbf{M}}_{q_3} \cdot \mathbf{h}_{c_3}\right)_n^{k-1} + \left(\widetilde{\mathbf{M}}_{q_3} \cdot \mathbf{W}_{NHc_3}\right)_n^{k-1} \cdot \boldsymbol{\lambda}_n \ .
\end{aligned}
$$

For obtaining the required relation between $\mathbf{q}_{n+1}$ and the impact forces $\boldsymbol{\lambda}_n$, the generalized coordinates and velocities of the step $n+1$ are written from Eq. (A.15)

$$
\begin{bmatrix} \mathbf{q}_{n+1} \\ \dot{\mathbf{q}}_{n+1} \end{bmatrix} = \begin{bmatrix} \mathbf{q}_n \\ \dot{\mathbf{q}}_n \end{bmatrix} + \Delta t_n \ \left(\gamma_1 \ {}^n\mathbf{k}_1^k + \gamma_2 \ {}^n\mathbf{k}_2^k + \gamma_3 \ {}^n\mathbf{k}_3^k\right) \ . \qquad \text{(A.27)}
$$

This equation together with Eqs. (A.24) and (A.26) yields

$$
\mathbf{q}_{n+1} = \mathbf{W}_{q_n} \cdot \boldsymbol{\lambda}_n + \mathbf{w}_{q_n} \ , \qquad \text{(A.28)}
$$

where

$$
\begin{aligned}
\mathbf{W}_{q_n} = \Delta t_n^2 \Big(& \gamma_1\beta_{11}\left(\widetilde{\mathbf{M}}_{q_1} \cdot \mathbf{W}_{NHc_1}\right)_n^{k-1} + \gamma_1\beta_{12}\left(\widetilde{\mathbf{M}}_{q_2} \cdot \mathbf{W}_{NHc_2}\right)_n^{k-1} + \gamma_1\beta_{13}\left(\widetilde{\mathbf{M}}_{q_3} \cdot \mathbf{W}_{NHc_3}\right)_n^{k-1} \\
& + \gamma_2\beta_{21}\left(\widetilde{\mathbf{M}}_{q_1} \cdot \mathbf{W}_{NHc_1}\right)_n^{k-1} + \gamma_2\beta_{22}\left(\widetilde{\mathbf{M}}_{q_2} \cdot \mathbf{W}_{NHc_2}\right)_n^{k-1} + \gamma_2\beta_{23}\left(\widetilde{\mathbf{M}}_{q_3} \cdot \mathbf{W}_{NHc_3}\right)_n^{k-1} \\
& + \gamma_3\beta_{31}\left(\widetilde{\mathbf{M}}_{q_1} \cdot \mathbf{W}_{NHc_1}\right)_n^{k-1} + \gamma_3\beta_{32}\left(\widetilde{\mathbf{M}}_{q_2} \cdot \mathbf{W}_{NHc_2}\right)_n^{k-1} + \gamma_3\beta_{33}\left(\widetilde{\mathbf{M}}_{q_3} \cdot \mathbf{W}_{NHc_3}\right)_n^{k-1}\Big) \ , \\
\mathbf{w}_{q_n} = \mathbf{q}_n \ & + \Delta t_n \ \dot{\mathbf{q}}_n \left(\gamma_1 + \gamma_2 + \gamma_3\right) \ + \\
\Delta t_n^2 \Big(& \gamma_1\beta_{11}\left(\widetilde{\mathbf{M}}_{q_1} \cdot \mathbf{h}_{c_1}\right)_n^{k-1} + \gamma_1\beta_{12}\left(\widetilde{\mathbf{M}}_{q_2} \cdot \mathbf{h}_{c_2}\right)_n^{k-1} + \gamma_1\beta_{13}\left(\widetilde{\mathbf{M}}_{q_3} \cdot \mathbf{h}_{c_3}\right)_n^{k-1} + \\
& \gamma_2\beta_{21}\left(\widetilde{\mathbf{M}}_{q_1} \cdot \mathbf{h}_{c_1}\right)_n^{k-1} + \gamma_2\beta_{22}\left(\widetilde{\mathbf{M}}_{q_2} \cdot \mathbf{h}_{c_2}\right)_n^{k-1} + \gamma_2\beta_{23}\left(\widetilde{\mathbf{M}}_{q_3} \cdot \mathbf{h}_{c_3}\right)_n^{k-1} + \\
& \gamma_3\beta_{31}\left(\widetilde{\mathbf{M}}_{q_1} \cdot \mathbf{h}_{c_1}\right)_n^{k-1} + \gamma_3\beta_{32}\left(\widetilde{\mathbf{M}}_{q_2} \cdot \mathbf{h}_{c_2}\right)_n^{k-1} + \gamma_3\beta_{33}\left(\widetilde{\mathbf{M}}_{q_3} \cdot \mathbf{h}_{c_3}\right)_n^{k-1}\Big) \ .
\end{aligned}
\qquad \text{(A.29)}
$$

As it can be seen, the generalized coordinates of step $n+1$ are affected by the impact forces at step n. The presented relation in Eq. (A.28) is more sophisticated and needs much effort when it is compared with the corresponding relation obtained from the explicit Runge-Kutta method in Eq. (A.13). The index $j = 1, 2, 3$ of the parameters $\widetilde{\mathbf{M}}_{q_j}, \mathbf{W}_{NHc_j}$ and $\mathbf{h}_{c_j}$ in the relations mentioned above corresponds to three stages of the RADAU5 method.

Bibliography

[1] Agrawal, O.P.; Shabana, A.A.: Application of Deformable-Body Mean Axis to Flexible Multibody System Dynamics. *Computer Methods in Applied Mechanics and Engineering*, Vol. 56, pp. 217–245, 1986.

[2] Alart, P.; Curnier A.: A Mixed Formulation for Frictional Contact Problems Prone to Newton Like Solution Methods. *Computer Methods in Applied Mechanics and Engineering*, Vol. 92, pp. 353–375, 1991.

[3] Amirouche, F.M.L.; Shareef, N.H.; Xie, M.: Dynamic Analysis of Flexible Gear Trains/Transmissions: An Automated Approach. *Machinery Dynamics and Element Vibrations*, Vol. 36, pp. 257–262, 1991.

[4] Amirouche, F.M.L.: *Computational Methods in Multibody Dynamics*, Prentice Hall, Englewood Cliffs, 1992.

[5] Anitescu, M.; Potra, F.A.: A Constraint-Stabilized Time-Stepping Approach for Rigid Multibody Dynamics with Joints, Contact and Friction. *International Journal for Numerical Methods in Engineering*, Vol. 55, pp. 753–784, 2002.

[6] Anitescu, M.; Hart, G.D.: A Time-Stepping Method for Stiff Multibody Dynamics with Contact and Friction. *International Journal for Numerical Methods in Engineering*, Vol. 60, pp. 2335–2371, 2004.

[7] Antoulas, A.C.; Sorensen, D.C.; Gugercin, A.: Approximation of Large-Scale Dynamical Systems: An Overview. *Technical Report*, Rice University, Houston, 2001, URL: http://www-ece.rice.edu/∼aca/mtns00.pdf.

[8] Bakr, E.M.; Shabana, A.A.: Effect of Geometric Elastic Nonlinearities on the Impact Response of Flexible Multibody Systems. *Journal of Sound and Vibration*, Vol. 112, pp. 415–432, 1987.

[9] Barequet, G.; Chazelle, B.; Guibas, L.J.; Mitchell, J.S.B.; Tal, A.: BOXTREE: A Hierarchical Representation for Surfaces in 3D. *Computer Graphics Forum*, Vol. 15, pp. 387–396, 1996.

[10] Bathe, K.; Chaudhary, A.: A Solution Method for Planar and Axisymmetric Contact Problems. *International Journal for Numerical Methods in Engineering*, Vol. 21, pp. 65–88, 1985.

[11] Bathe, K.J.: *Finite Element Procedures*. Prentice Hall, Englewood Cliffs, 1996.

[12] Bauchau, O.A.: On the Modeling of Friction and Rolling in Flexible Multibody Systems. *Multibody Systems Dynamics*, Vol. 3, pp. 209–239, 1999.

[13] Bauchau, O.A.; Bottasso, C.L.; Trainelli, L.: Robust Integration Schemes for Flexible Multibody Systems. *Computer Methods in Applied Mechanics and Engineering*, Vol. 192, pp. 395–420, 2003.

[14] Belytschko, T.; Hsieh, B.J.: Nonlinear Transient Finite Element Analysis with Convected Coordinates. *International Journal for Numerical Methods in Engineering*, Vol. 7, pp. 255–271, 1973.

[15] Blankenship, G.W.; Singh, R.: A Comparative Study of Selected Gear Mesh, Force Interface Dynamic Models. *ASME* 6^{th} *International Power Transmission and Gearing Conference*, DE-43-1, pp. 137–146, 1992.

[16] Blankenship, G.W.; Singh, R.: A New Gear Mesh Interface Dynamic Model to Predict Multi-Dimensional Force Coupling and Excitation. *Mechanism and Machine Theory*, Vol. 30, pp. 43–57, 1995.

[17] Bremer, H.; Pfeiffer, F.: *Elastische Mehrkörpersysteme* (in German). Teubner, Stuttgart, 1992.

[18] Brenan, K.E.; Campbell, S.L.; Petzold, L.R.: *Numerical Solution of Initial-Value Problems in Differential-Algebraic Equations*. SIAM, Classics in Applied Mathematics, Philadelphia, Second Edition, 1996.

[19] Byrne, G.D.; Hindmarsh, A.C.: Stiff ODE Solvers: A Review of Current and Coming Attractions. *Journal of Computational Physics*, Vol. 70, pp. 1–62, 1987.

[20] Canavin, J.R.; Likins, P.W.: Floating Reference Frames for Flexible Spacecraft. *Journal of Spacecraft and Rockets*, Vol. 14, pp. 724–732, 1977.

[21] Cetinkunt, S.; Book, W.J.: Symbolic Modeling of Flexible Manipulators. *Proceedings of IEEE, International Conference on Robotics and Automation*, pp. 2074–2080, 1987.

[22] Chaudhary, A.: A Solution Method for Static and Dynamic Analysis of Three-Dimensional Contact Problems with Friction. *Journal of Computers and Structures*, Vol. 24, pp. 855–873, 1986.

[23] Chung, J.; Hulbert, G.M.: A Time Integration Algorithm for Structural Dynamics with Improved Numerical Dissipation: The Generalized-α Method. *Journal of Applied Mechanics*, Vol. 60, pp. 371–375, 1993.

[24] Clough, R.W.: The Finite Element Method in Plane Stress Analysis. *Proceedings of the 2nd ASCE Conference on Electronic Computation*, Pittsburgh, 1960.

[25] Cottle, R.W.; Pang, J.S.; Stone, R.E.: *The Linear Complementarity Problem*, Academic Press, Boston, 1992.

[26] Dias, J.M.P.; Pereira, M.S.: Dynamics of Flexible Mechanical Systems with Contact-Impact and Plastic Deformations. *Nonlinear Dynamics*, Vol. 8, pp. 491–512, 1995.

[27] Dietz, S.; Wallrapp, O.; Wiedemann, S.: Nodal vs. Modal Representation in Flexible Multibody System Dynamics. *Proceedings of Multibody Dynamics*, Ambrosio, J.A.C. (ed), IDMEC/IST, Lisbon, Portugal, July 1-4, 2003.

[28] Dirske P.S.; Ferris M.C.: The PATH Solver: A Non-Monotone Stabilization Scheme for Mixed Complementarity Problems. *Optimization Methods and Software*, Vol. 5, pp. 123–156, 1995.

[29] Eberhard. P.: *Kontaktuntersuchungen durch hybride Mehrkörpersystem/Finite Elemente Simulationen* (in German). Shaker Verlag, Aachen, 2000.

[30] Eberhard, P.; Schiehlen, W.: Computational Dynamics of Multibody Systems: History, Formalisms, and Applications. *Journal of Computational and Nonlinear Dynamics*, Vol. 1, pp. 1–12, 2006.

[31] Eberhard, P.; Ebrahimi, S.: On the Use of Linear Complementarity Problems for Contact of Planar Flexible Bodies. *Proceedings of the ECCOMAS Thematic Conference on Multibody Dynamics*, Goicolea, J.M.; Cuadrado, J.; Garcia Orden, J.C. (eds), Spain, 2005.

[32] Ebrahimi, S.; Eberhard, P.: Polygonal Contact Model for Elastic Bodies. *Internal Report* No.140, University of Stuttgart, Institute of Engineering and Computational Mechanics, 2004.

[33] Ebrahimi, S.; Hippmann, G.; Eberhard, P.: Extension of the Polygonal Contact Model for Flexible Multibody Systems. *International Journal of Applied Mathematics and Mechanics*, Vol. 1, pp. 33–50, 2005.

[34] Ebrahimi, S.; Eberhard, P.: Contact of Planar Deformable Bodies Using a Linear Complementarity Formulation. *PAMM Proceedings in Applied Mathematics and Mechanics*, Vol. 5, pp. 197–198, 2005.

[35] Ebrahimi, S.; Eberhard, P.: Rigid-Elastic Modeling of Gear Wheels in Multibody Systems. *Multibody System Dynamics*, Vol. 16, pp. 55–71, 2006.

[36] Ebrahimi, S.; Eberhard, P.: A Linear Complementarity Formulation on Position Level for Frictionless Impact of Planar Deformable Bodies. *ZAMM Zeitschrift für Angewandte Mathematik und Mechanik*, Vol. 86, pp. 807–817, 2006.

[37] Ebrahimi, S.; Eberhard, P.: Frictional Impact of Planar Deformable Bodies. *IUTAM Symposium on Multiscale Problems in Multibody System Contacts*, Eberhard, P. (ed), pp. 23–32, Springer, Dordrecht, 2007.

[38] Eich-Soellner, E.; Führer, C.: *Numerical Methods in Multibody Dynamics*. B.G. Teubner, Stuttgart, 1998.

[39] Escalona, J.L.; Sany, J.R.; Shabana, A.A.: On the Use of the Restitution Condition in Flexible Body Dynamics. *Nonlinear Dynamics*, Vol. 30, pp. 71–86, 2002.

[40] Feeny, B.; Guran, A.; Hinrichs, N.; Popp, K.: A Historical Review on Dry Friction and Stick-Slip Phenomena. *Applied Mechanics Review*, Vol. 51, pp. 321–341, 1998.

[41] *FEMBS User Manual*. Intec GmbH, Wessling, Germany, 2003.

[42] Ferris, M.C.; Munson, T.S.: Interface to PATH 3.0: Design, Implementation and Usage. *Computational and Applied Optimization*, Vol. 12, pp. 207–227, 1999.

[43] Fichera, G.: Sul Problema Elastostatico di Signorini Con Ambigue condizioni al Ritorno (in Italian). *Rend. Accad. Naz.* Lincei, Vol. 34, pp. 138–142, 1963.

[44] Fisette, P.; Samin, J.C.; Willems, P.W.: Contribution to Symbolic Analysis of Deformable Multibody Systems. *International Journal of Numerical Methods in Engineeirng*, Vol. 32, pp. 1621–1635, 1991.

[45] Fisette, P; Jhonson, D.A.; Samin, J.C.: A Fully Symbolic Generation of the Equations of Motion of Multibody Systems Containing Flexible Beams. *Computer Methods in Applied Mechanics and Engineering*, Vol. 142, pp. 123–152, 1997.

[46] Fisette, P.; Postiau, T.; Sass, L.; Samin, J.C.: Fully Symbolic Generation of Complex Multibody Models. *Mechanics of Structures and Machines*, Vol. 30, pp. 31–82, 2002.

[47] Förg, M.; Pfeiffer, F.; Ulbrich, H.: Simulation of Unilateral Constrained Systems with Many Bodies. *Multibody System Dynamics*, Vol. 14, pp. 137–154, 2005.

[48] Funk, K.; Pfeiffer, F.: A Time-Stepping Algorithm for Stiff Mechanical Systems with Unilateral Contacts. *PAMM Proceedings in Applied Mathematics and Mechanics*, Vol. 2, pp. 228–229, 2003.

[49] Galin, L. A.: *Contact Problems in the Theory of Elasticity* (in Russian). Gostekhizdat, Moscow-Leningrad, 1953 (English translation by Moss, H. edited by Sneddon, I.N., North Carolina State College, Departments of Mathematics and Engineering Research, 1961).

[50] Geradin, M.; Cardona, A.; Doan, D.B.; Duysens, J.: Finite Element Modeling Concepts in Multibody Dynamics. *Computer-Aided Analysis of Rigid and Flexible Mechanical Systems*, Pereira, M.S.; Ambrosio, J.A.C. (eds), Kluwer Academic Publishers, Dordrecht, pp. 233–284, 1994.

[51] Geradin, M.; Rixen, D.: *Mechanical Vibrations: Theory and Applications to Structural Dynamics*. Wiley & Sons, New York, 1998.

[52] Geradin, M.; Cardona, A.: *Flexible Multibody Dynamics: A Finite Element Approach*. Wiley & Sons, New York, 2001.

[53] Gerl, F.; Zippelius, A.: Coefficient of Restitution for Elastic Disks. *Physical Review E*, Vol. 59, pp. 2361–2372, 1999.

[54] Gladwell, G.M.L.: *Contact Problems in the Classical Theory of Elasticity*. Alphen aan den Rijn: Sijthoff and Noordhoff, 1980.

[55] Glocker, C.: *Dynamik von Starrkörpersystemen mit Reibung und Stössen* (in German). Dissertation, VDI Fortschritt-Berichte, Reihe 18, Nr. 182, VDI-Verlag, Düsseldorf, 1995.

[56] Gottschalk, S.; Lin, M.; Manocha, D.: OBB-Tree: A Hierarchical Structure for Rapid Interference Detection. *SIGGRAPH 96 Conference Proceedings*, Rushmeier, H. (ed), pp. 171–180, 1996.

[57] Greenwood, J.A.; Williamson, J.B.P.: Contact of Nominally Flat Surfaces. *Proceedings of the Royal Society of London*, Series A, Vol. 295, pp. 300–319, 1966.

[58] Grimme, E.J.: Krylov Projection Methods for Model Reduction. PhD Thesis, University of Illinois, Urbana, 1997.

[59] Hairer, E.; Wanner, G.: *Solving Ordinary Differential Equations II: Stiff and Differential-Algebraic Problems*. Springer, Berlin, 1996.

[60] Haug, E.J.; Wu, S.C.; Yang, S.M.: Dynamics of Mechanical Systems with Coulomb Friction, Stiction, Impact and Constraint Addition-Deletion, Part I: Theory. *Mechanism and Machine Theory*, Vol. 21, pp. 401–4 06, 1986.

[61] Haug, E.J.: *Computer-Aided Kinematics and Dynamics of Mechanical Systems: Basic Methods*. Allyn and Bacon, Boston, 1989.

[62] Held, M.; Klosowski, J.T.; Mitchell, J.S.B.: Evaluation of Collision Detection Methods for Virtual Reality Fly-Throughs. *Proceedings of the 7^{th} Canadian Conference on Computational Geometry*, Gold, C.; Robert, J.M. (eds), pp. 205–210, 1995.

[63] Held, M.; Klosowski, J.T.; Mitchell, J.S.B.: Speed Comparison of Generalized Bounding Box Hierarchies. *Technical Report*, Department of Applied Mathematics, SUNY Stony Brook, 1995.

[64] Held, M.; Klosowski, J.T.; Mitchell, J.S.B.: Real-Time Collision Detection for Motion Simulation within Complex Environments. *SIGGRAPH 96 Visual Proceedings*, Blau, B.; Dodsworth, C.; Branagan, L.; Ippolito, J.; Musgrave, K.; Waggenspackpp, W. (eds). 151, New Orleans, 1996.

[65] Hertz, H.: Über die Berührung fester elastischer Körper (in German). *Journal für die reine und angewandte Mathematik*, Vol. 92, pp. 156–171, 1882.

[66] Hippmann, G.: An Algorithm for Compliant Contact between Complex Shaped Surfaces in Multibody Dynamics. *Proceedings of the ECCOMAS Thematic Conference on Multibody Dynamics*, Ambrosio, J.A.C. (ed), Portugal, 2003.

[67] Hippmann, G.: An Algorithm for Compliant Contact between Complexly Shaped Bodies. *Multibody System Dynamics*, Vol. 12, pp. 345–362, 2004.

[68] Hippmann, G.: *Modellierung von Kontakten komplex geformter Körper in der Mehrkörperdynamik* (in German). Dissertation, Reihe: DLR-IB, Nr. 515-04-35, 2004.

[69] Hilber, H.M.; Hughes, T.J.R.; Taylor, R.L.: Improved Numerical Dissipation for Time Integration Algorithms in Structural Dynamics. *Earthquake Engineering and Structural Dynamics*, Vol. 5, pp. 283–292, 1977.

[70] Hunt, K.H.; Grossley, F.R.E.: Coefficient of Restitution Interpreted as Damping in Vibroimpact. *ASME Journal of Applied Mechanics*, Vol. 97, pp. 440–445, 1975.

[71] Hubbard, P.M.: Interactive Collision Detection. *IEEE Symposium on Research Frontiers in Virtual Reality*, pp. 24–31, 1993.

[72] Huston, R.L.: *Multibody Dynamics*. Butterworth-Heinemann, Boston, 1990.

[73] Huston, R.L.; Wang, Y.: Flexibility Effects in Multibody Systems. *Computer-Aided Analysis of Rigid and Flexible Mechanical Systems*, Pereira, M.S.; Ambrosio, J.A.C. (eds), Kluwer Academic Publishers, Dordrecht, pp. 351–376, 1994.

[74] Johnson, K.L.: *Contact Mechanics*. Cambridge University Press, Cambridge, 1985.

[75] Kahraman, A.; Singh, R.: Non-linear Dynamics of a Spur Gear Pair. *Journal of Sound and Vibration*, Vol. 142, pp. 49–75, 1990.

[76] Kahraman, A.; Singh, R.: Interaction between Time-varying Mesh Stiffness and Clearance Non-linearities in a Geared System. *Journal of Sound and Vibration*, Vol. 146, pp. 135–156, 1991.

[77] Kalker, J.J.: *Three-Dimensional Elastic Bodies in Rolling Contact*. Kluwer Academic Publishers, Dordrecht, 1990.

[78] Kane, T.R.; Ryan, R.R.; Banerjee, A.K.: Dynamics of a Cantilever Beam Attached to a Moving Base. *AIAA Journal of Guidance, Control, and Dynamics*, Vol. 10, pp. 139–151, 1987.

[79] Khulief, Y.A.; Shabana, A.A.: Dynamic Analysis of Constrained System of Rigid and Flexible Bodies with Intermittent Motion. *Journal of Mechanism, Transmission and Automation in Design*, Vol. 108, pp. 38–45, 1986.

[80] Khulief, Y.A.; Shabana, A.A.: Dynamics of Multibody Systems with Variable Kinematic Structure. *ASME Journal of Machines, Transmission and Automated Design*, Vol. 108, pp. 167–175, 1986.

[81] Khulief, Y.A.; Shabana, A.A.: A Continuous Force Model for the Impact Analysis of Flexible Multibody Systems. *Mechanism and Machine Theory*, Vol. 22, pp. 213–224, 1987.

[82] Kim, J.; Kwak, B.M.: Dynamic Analysis of Two-Dimensional Frictional Contact by Linear Complementarity Problem Formulation. *International Journal of Solids and Structures*, Vol. 30, pp. 4605–4624, 1996.

[83] Kwak, B.M.: Complementarity Problem Formulation of Three-Dimensional Frictional Contact. *Journal of Applied Mechanics*, Vol. 58, pp. 134–140, 1991.

[84] Lankarani, H.M.; Nikravesh, P.E.: A Contact Force Model with Hysteresis Damping for Impact Analysis of Multibody Systems. *ASME Journal of Mechanical Design*, Vol. 112, pp. 369–376, 1990.

[85] Lankarani, H.M.; Nikravesh, P.E.: Continuous Contact Force Models for Impact Analysis in Multibody Systems. *Nonlinear Dynamics*, Vol. 5, pp. 193–207, 1994.

[86] Leine, R.I.; Glocker, C.: A Set-Valued Force Law for Spatial Coulomb-Contensou Friction. *European Journal of Mechanics A/Solids*, Vol. 22, pp. 193–216, 2001.

[87] Litak, G.; Friswell, M.I.: Dynamics of a Gear System with Faults in Meshing Stiffness. *Nonlinear Dynamics*, Vol. 41, pp. 415–421, 2005.

[88] Litvin, F.L.; Fuentes, A.: *Gear Geometry and Applied Theory*, Cambridge University Press, Cambridge, 2004.

[89] Lötstedt, P.: Coulomb Friction in Two-Dimensional Rigid Body Systems. *ZAMM Zeitschrift für Angewandte Mathematik und Mechanik*, Vol. 61, pp. 605–615, 1981.

[90] Magnus, K. (ed): *Dynamics of Multibody Systems*. Springer, Berlin, 1978.

[91] Mauer, L.: Force Element 225 Gear Wheel. *Internal Report*, Intec GmbH, Wessling, Germany, 2005.

[92] Mavroudakis, B.; Eberhard, P.: Analysis of Alternative Front Suspension Systems for Motorcycles. *Proceedings XIX IAVSD*, Milano, 2005.

[93] Meirovitch, L.; Kwak, M.K.: Convergence of the Classical Rayleigh Ritz Method and the Finite Element Method. *AIAA Journal*, Vol. 28, pp. 1509–1516, 1990.

[94] Melzer, F.: Symbolic Computations in Flexible Multibody Systems. *Nonlinear Dynamics*, Vol. 9, pp. 147–163, 1996.

[95] Muth, B.; Müller, M.K.; Eberhard, P.; Luding, S.: Contacts between Many Bodies. *Machine Dynamics Problems*, Vol. 28, pp. 101–114. 2004.

[96] Naylor, B.; Amatodes, J.A.; Thibault, W.: Merging BSP Trees Yields Polyhedral Set Operations. *Computational Graphics*, Vol. 24, pp. 115–124, 1990.

[97] Niemann, G.; Winter, H.: *Maschinenelemente 2* (in German). Springer, Berlin, 1989.

[98] Nikravesh, P.E.: *Computer-Aided Analysis of Mechanical Systems*. Prentice Hall, Engelwood Cliffs, 1988.

[99] Noborio, H.; Fukuda, S.; Arimoto, S.: Fast Interference Check Method Using Octree Representation. *Advanced Robotics*, Vol. 3, pp. 193–212, 1989.

[100] Nour-Omid, B.; Wriggers, P.: A Note on the Optimum Choice of Penalty Parameters. *Communications in Applied Numerical Methods*, Vol. 3, pp. 581–585, 1987.

[101] Oden, J.T.; Martins, J.A.C.: Models and Computational Methods for Dynamic Friction Phenomena. *Computer Methods in Applied Mechanics and Engineering*, Vol. 52, pp. 527–634, 1985.

[102] Özgüven, H.N.; Houser, D.R.: Mathematical Models Used in Gear Dynamics - A Review. *Journal of Sound and Vibration*, Vol. 121, pp. 383–411, 1988.

[103] Pang, J.S.; Trinkle, J.: Complementarity Formulations and Existence of Solutions of Dynamic Multi-Rigid-Body Contact Problems with Coulomb Friction. *Mathematical Programming*, Vol. 73, pp. 199–226, 1996.

[104] Peeters, J.; Vandepitte, D.; Sas, P.: Flexible Multibody Model of a Three-Stage Planetary Gearbox in a Wind Turbine. *ISMA: International Conference on Noise and Vibration Engineering*, Leuven, Belgium, pp. 3923–3942, 2004.

[105] Pereira, M.S.; Nikravesh, P.: Impact Dynamics of Multibody Mechanical Systems with Frictional Contact Using Joint Coordinates and Canonical Equations of Motion. *Nonlinear Dynamics*, Vol. 9, pp. 53–71, 1996.

[106] Pfeiffer, F.; Glocker, C.: *Multibody Dynamics with Unilateral Contacts*, Wiley & Sons, New York, 1996.

[107] Pfeiffer, F.: The Idea of Complementarity in Multibody Dynamics. *Archive of Applied Mechanics*, Vol. 72, pp. 807–816, 2003.

[108] Rankin, C.C.; Brogan, F.A.: An Element Independent Corotational Procedure for the Treatment of Large Rotations. *ASME Journal of Pressure Vessel Technology*, Vol. 108, pp. 165–174, 1986.

[109] Rockafellar, R.T.: *Convex Analysis*. Princeton University Press, New Jersey, 1970.

[110] Rockafellar, R.T.: Augmented Lagrangian and Applications of the Proximal Point Algorithm in Convex Programming. *Mathematics of Operations Research*, Vol. 1, pp. 97–116, 1976.

[111] Ryu, J.; Kim, S.S.; Kim, S.S.: A General Approach to Stress Stiffening Effects on Flexible Multibody Systems. *Mechanics of Structures and Machines*, Vol. 22, pp. 157–180, 1994.

[112] Sany, J.R.; Shabana, A.A.: On the Use of the Momentum Balance in the Impact Analysis of Constrained Elastic Systems. *Journal of Vibration and Acoustics*, Vol. 112, pp. 119–126, 1990.

[113] Sarkar, N.; Ellis, R.E.; Moore, T.N.: Backlash Detection in Geared Mechanisms: Modeling, Simulation, and Experimentation. *Mechanical Systems and Signal Processing*, Vol. 11, pp. 391–408, 1997.

[114] Schiehlen, W.; Rauh, J.: Modeling of Flexible Multibeam Systems by Rigid-Elastic Superelements. *Revista Brasiliera de Ciencias Mecanicas*, Vol. 8, pp. 151–163, 1986.

[115] Schiehlen, W. (ed): *Multibody Systems Handbook*, Springer Verlag, New York, 1990.

[116] Schiehlen, W.: Multibody System Dynamics: Roots and Perspectives. *Multibody System Dynamics*, Vol. 1, pp. 149–188, 1997.

[117] Schwertassek, R.; Wallrapp, O.: *Dynamik flexibler Mehrkörpersysteme* (in German). Vieweg Verlag, Wiesbaden, 1999.

[118] Schwertassek, R.; Wallrapp, O.; Shabana, A.A.: Flexible Multibody Simulation and Choice of Shape Functions. *Nonlinear Dynamics*, Vol. 20, pp. 361–380, 1999.

[119] Seifried, R.; Schiehlen, W.; Eberhard, P.: Numerical and Experimental Evaluation of the Coefficient of Restitution for Repeated Impacts. *International Journal of Impact Engineering*, Vol 32, pp. 508–524, 2005.

[120] Shabana, A.A.: Finite Element Incremental Approach and Exact Rigid Body Inertia. *ASME Journal of Mechanical Design*, Vol. 118, pp. 171–178, 1996.

[121] Shabana, A.A.: Flexible Multibody Dynamics: Review of Past and Recent Developments. *Multibody System Dynamics*, Vol. 1, pp. 189–222, 1997.

[122] Shabana, A.A.: Computer Implementation of the Absolute Nodal Coordinates Formulation for Flexible Multibody Dynamics. *Journal of Nonlinear Dynamics*, Vol. 16, pp. 293–306, 1998.

[123] Shabana, A.A.: *Computational Dynamics*. John Wiley & Sons, New York, 2001.

[124] Shabana, A.A.: *Dynamics of Multibody Systems*. Third Edition, Cambridge University Press, Cambridge, 2005.

[125] Signorini, A.: Sopra akune questioni di elastostatica (in Italian). *Societa Italiana per Il Progresso delle Scienze*, Atti., 1933.

[126] Simeon, B.: Stiff Solvers and Model Reduction in Flexible Multibody Systems. *ZAMM Zeitschrift für Angewandte Mathematik und Mechanik*, Vol. 78, pp. 1079–1083, 1998.

[127] Simeon, B.: Numerical Analysis of Flexible Multibody Systems. *Multibody Systems Dynamics*, Vol. 6, pp. 305–325, 2001.

[128] Simo, J.C.; Vu-Quoc, L.: On the Dynamics of Flexible Beams Under Large Overall Motions-The Planar Case: Part I. *ASME Journal of Applied Mechanics*, Vol. 53, pp. 849–854, 1986.

[129] *Simpack User Routine Manual: User Routines-Force and Control Elements*. Intec GmbH, Wessling, Germany, 2003.

[130] Song, P.; Pang, J.S.; Kumar, V.: A Semi-Implicit Time-Stepping Model for Frictional Compliant Contact Problem. *International Journal for Numerical Methods in Engineering*, Vol. 60, pp. 2231–2261, 2004.

[131] Stein, J.L.; Wang, C.H.: Automatic Detection of Clearance in Mechanical Systems: Theory and Simulation. *Proceedings of the 1995 American Control Conference on Automatic Control*, Vol. 3, Seattle, Washington, pp. 1737–1745, 1995.

[132] Stein, J.L.; Wang, C.H.: Automatic Detection of Clearance in Mechanical Systems: Experimental Validation. *Journal of Mechanical Systems and Signal Processing*, Vol. 10, pp. 395–412, 1996.

[133] Stewart, D.E.; Trinkle, J.C.: An Implicit Time-Stepping Scheme for Rigid Body Dynamics with Inelastic Collisions and Coulomb Friction. *International Journal for Numerical Methods in Engineering*, Vol. 39, pp. 2673–2691, 1996.

[134] Stiegelmeyr, A.: *Zur numerischen Berechnung strukturvarianter Mehrkörpersysteme* (in German). Dissertation, Reihe 18, Nr. 271, VDI-Verlag, Düsseldorf, 2001.

[135] Studer, C.; Glocker, C.: Simulation of Non-Smooth Mechanical Systems with Many Unilateral Constraints. *Proceedings of ENOC Fifth Euromech Nonlinear Dynamics Conference*, van Campen D. (ed), Eindhoven, 2005.

[136] Turner, M.J.; Clough, R.W.; Martin, H.C.; Topp, L.J.: Stiffness and Deflection Analysis of Complex Structures. *Journal of the Aeronautical Sciences*, Vol. 23, pp. 805–823, 1956.

[137] Villmagne, C.; Skelton, R.E.: Model Reduction Using a Projection Formulation. *International Journal of Control*, Vol. 46, pp. 2141–2169, 1987.

[138] Vinayak, H.; Singh, R.; Padmanabhan, C.: Linear Dynamic Analysis of Multi-Mesh Transmissions Containing External, Rigid Gears. *Journal of Sound and Vibration*, Vol. 185, pp. 1–32, 1995.

[139] Wahl, A.M.: *Mechanical Springs*. Second Edition, McGraw-Hill, New York, 1963.

[140] Wallrapp, O.: Standard Input Data of Flexible Members for Multibody System Codes. *Advanced Multibody System Dynamics-Simulation and Software Tools*, Schiehlen, W. (ed), Kluwer Academic Publishers, pp. 445–450, 1993.

[141] Wallrapp, O.: Standardization of Flexible Body Modeling in Multibody System Codes, Part I: Definition of Standard Input Data. *Mechanics of Structures and Machines*, Vol. 22, pp. 283–304, 1994.

[142] Wallrapp, O.: Flexible Multibody Dynamics with Space Flight Applications Using SIMPACK. *Workshop on Flexible Multibody Dynamics*, FHM, 2006, http://www.fh-muenchen.de/fb06/professoren/wallrapp/d_wallrapp_o.html.

[143] Warminski, J.; Litak, G.; Szabelski, K.: Dynamic Phenomena in Gear Boxes. *Applied Nonlinear Dynamics and Chaos of Mechanical Systems with Discontinuities*, Vol. 28, pp. 177–206, 2000.

[144] Wasfy, T.M.: Modeling Contact/Impact of Flexible Manipulators with a Fixed Rigid Surface. *Proceedings of IEEE International Conference on Robotics and Automation*, Japan, pp. 621–626, 1995.

[145] Wasfy, T.M.; Noor, A.K.: Computational Procedure for Simulating the Contact/Impact Response in Flexible Multibody Systems. *Computer Methods in Applied Mechanics and Engineering*, Vol. 147, pp. 153–166, 1997.

[146] Wasfy, T.M.; Noor, A.K.: Computational Strategies for Flexible Multibody Systems. *ASME Applied Mechanics Reviews*, Vol. 56, pp. 553–613, 2003.

[147] *Wavefront object file specification:*
http://www710.univ-lyon1.fr/∼jciehl/Public/utiles/maya_obj_spec.pdf.

[148] Wehage, R.A.; Haug, E.J.: Dynamic Analysis of Mechanical Systems with Intermittent Motion. *ASME Journal of Mechanical Design*, Vol. 104, pp. 778–784, 1982.

[149] Winfrey, R.C.: Elastic Link Mechanism Dynamics. *ASME Journal of Engineering for Industry*, Vol. 93, pp. 268–272, 1971.

[150] Wittenburg, J.: *Dynamics of Systems of Rigid Bodies*. Teubner, Stuttgart, 1977.

[151] Wösle, M.; Pfeiffer, F.: Dynamics of Multibody Systems Containing Dependent Unilateral Constraints with Friction. *Journal of Vibration and Control*, Vol. 2, pp. 161–192, 1996.

[152] Wösle, M.: *Dynamik von räumlichen strukturvarianten Starrkörpersystemen* (in German). Dissertation, VDI Fortschritt-Berichte, Reihe 18, Nr. 213, VDI-Verlag, Düsseldorf, 1997.

[153] Wriggers, P.; Simo, J.C.; Taylor, R.L.: Penalty and Augmented Lagrangian Formulation for Contact Problems. *Proceedings of NUMETA Conference*, Balkema, Rotterdam, 1985.

[154] Wriggers, P.: Finite Element Algorithms for Contact Problems. *Archives of Computational Methods in Engineering*, Vol. 2, pp.1–49, 1995.

[155] Wriggers, P.: *Computational Contact Mechanics*. John Wiley & Sons, Chichester, 2002.

[156] Wu, S.C.; Yang, S.M.; Haug, E.J.: Dynamics of Mechanical Systems with Coulomb Friction, Stiction, Impact and Constraint Addition-Deletion, Part II: Planar Systems. *Mechanism and Machine Theory*, Vol. 21, pp. 407–416, 1986.

[157] Wu, S.C.; Yang, S.M.; Haug, E.J.: Dynamics of Mechanical Systems with Coulomb Friction, Stiction, Impact and Constraint Addition-Deletion, Part III: Spatial Systems. *Mechanism and Machine Theory*, Vol. 21, pp. 417–425, 1986.

[158] Wu, S.C.; Haug, E.J.: A Substructure Technique for Dynamics of Flexible Mechanical Systems with Contact/Impact. *Journal of Mechanical Design*, Vol. 112, pp. 390–398, 1990.

[159] Yoo, W.S.; Park, S.J.; Dmitrochenko, O.N.; Pogorelov, D.Y.: Verification of Absolute Nodal Coordinate Formulation in Flexible Multibody Dynamics via Physical Experiments of Large Deformation Problems. *Journal of Computational and Nonlinear Dynamics*, Vol. 1, pp. 81–93, 2006.

[160] Zachmann, G.: *Exact and Fast Collision Detection*. Diploma Thesis, Department of Computer Science, Darmstadt University of Technology, 1994.

[161] Zakhariev, E.V.: A Numerical Method for Multibody System Frictional Impact Simulation. *Proceedings of ASME 2001 DETC*, Paper No. DETC2001/VIB-21367, Pittsburgh, 2001.

[162] Ziegler, P.; Eberhard, P.; Schweizer, B.: Simulation of Impacts in Geartrains Using Different Approaches. *Archive of Applied Mechanics*, Published Online, http://www.springerlink.com/content/l51m813tp7888501, 2006.

Notation

In this part, the basic symbols and parameters used in this thesis are explained. Here, only the main ones are mentioned and the intermediately defined symbols are ignored.

$\mathbf{a}$	acceleration vector
a_0	nominal center distance
a_v, a_w	true and actual center distances
b	elastic layer thickness, ffective face width of meshing gears
c_l	combined layer stiffness
$c_{min,max}$	minimum and maximum values of gear stiffness
d	deflection, wire diameter of a spring
$\mathbf{d}_{ee}$	damping matrix associated with the elastic coordinates
d_l	areal layer damping factor
e	coefficient of restitution
$\mathbf{e}_{1,2,3}$	axes of a reference coordinate system with unit lengths
$\mathbf{f}_i$	force vector at vertex i of a polygonal surface
g	gap distance
g_a	length of recess of a gear
$\mathbf{g}$	gap distances vector
h	layer thickness, free length of a spring
$\mathbf{h}$	vector of internal, external and Coriolis forces
$\mathbf{h}_d$	vector of internal damping forces
$\mathbf{h}_s$	vector of internal elastic forces
k	counter, gear stiffness ratio
k_{max}	maximum number of iterations
$\mathbf{k}_{ee}$	stiffness matrix associated with the elastic coordinates
l	contact number
m	unit of length: meter
$\mathbf{m}$	components of mass matrix
m_n, m_t	normal and transverse modules
m_{th}	mass of each single gear tooth
n	integration step, number of active coils of a spring
$\mathbf{n}$	normal vector
n_b	number of bodies

n_c	number of contacts
n_{th}	teeth numbers of a gear
p_b	base pitch
$\mathbf{q}$	generalized coordinates
$\mathbf{q}_e$	elastic coordinates
$\mathbf{q}_r$	reference coordinates
r	position variable, positive scale factor
$\mathbf{r}$	position vector given in the inertial frame
r_a, r_d	radius of addendum and dedendum circles
r_b, r_p	radius of base and pitch circles
s	shape factor of a gear, unit of time: second, solid length of a spring
t	time
$\mathbf{t}$	tangential vector
$\mathbf{u}$	position vector in the current configuration given in the inertial frame
$\bar{\mathbf{u}}$	position vector in the current configuration given in the body reference frame
$\mathbf{u}_0$	position vector in the undeformed configuration given in the inertial frame
$\mathbf{u}_e$	vector of elastic displacements
$\bar{u}_{0x}$,$\bar{u}_{0y}$	x and y components of the vector $\bar{\mathbf{u}}_0$
$\mathbf{v}$	velocity vector
v	vertex
v_n, v_t	normal and tangential components of relative velocity
v_ϵ	friction switch velocity
w	weighting factor
x_i	shift factor of the gear i
$\mathbf{A}$	transformation matrix
A_a	area
$\mathbf{C}_N, \mathbf{C}_T$	convex sets of admissible normal and tangential contact forces
D	damping coefficient, core diameter of a spring
$\mathbf{D}$	general damping matrix
D_e	damping coefficient of elastic elements between teeth and gear body
E	Young's modulus
$\mathbf{E}$	elastic constants matrix
F	contact force
$\mathbf{F}$	vector of contact forces
$\mathbf{F}_C$	vector of generalized contact forces
F_e	spring force
F_d	damping force
F_n, F_t	normal and tangential components of contact force
$\mathbf{F}_p$	vector of external point forces
$\mathbf{F}_s$	vector of surface forces per unit area

$\mathbf{F}_v$	vector of volume forces per unit volume
$\mathbf{G}$	transformation matrix between derivatives of Euler parameters and Euler angles
H	height
I_N	set of active contacts
$\mathbf{I}$	identity matrix
$\mathbf{I}_{zz}$	moment of inertia around z axes
K	stiffness coefficient
$\mathbf{K}$	general stiffness matrix
K_e	spring stiffness of elastic elements between teeth and gear body
L	length
M	mass, marker
$\mathbf{M}$	mass matrix
$\mathbf{M}_c$	general mass matrix
$\mathbf{M}_p$	vector of external point moments
N	shape function, unit of force: Newton
O	origin of a coordinate system
$\mathbf{Q}_Q$	quadratic velocity vector (generalized Coriolis forces)
$\mathbf{Q}_C$	vector of generalized constraint forces
$\mathbf{Q}_D$	vector of generalized damping forces
$\mathbf{Q}_E$	vector of generalized external forces
$\mathbf{Q}_S$	vector of generalized elastic forces
$\mathbf{R}$	position vector of the body reference coordinate system
$\mathbf{S}$	shape function matrix corresponding to the translational coordinates
S_i	rotational state of the tooth i
T	kinetic energy, contact torque
$\mathbf{T}$	vector of contact torques
V	volume of a body
$\mathbf{W}_N$	transformation matrix of contact forces from normal to generalized directions
$\mathbf{W}_T$	transformation matrix of contact forces from tangential to generalized directions
$\mathbf{Y}$	vector of system states
α	first constant parameter of the Rayleigh damping, inclination angle
α_n, α_t	normal and nominal transverse working pressure angles
α_v	actual working pressure angle
α_w	true transverse working pressure angle
β	second constant parameter of the Rayleigh damping, helix angle of a helical gear
β_{ij}	coefficients in the RADAU5 integration method
γ_i	coefficients in the RADAU5 integration method
$\boldsymbol{\gamma}$	right hand side of the acceleration of constraints
δ	penetration
δ_d	transition depth

$\delta\mathbf{D}$	differential operator
δW	virtual work
$\delta\boldsymbol{\theta}_e$	vector of total virtual rotation angles of the body at a point
$\delta\boldsymbol{\theta}$	vector of virtual rotation angles of the body reference frame
$\delta\boldsymbol{\theta}_{r/e}$	vector of virtual rotation angles with respect to the body reference frame
ϵ	penalty factor, total overlap ratio
ϵ_α	total transverse contact ratio
ϵ_β	overlap ratio
$\boldsymbol{\varepsilon}$	strain tensor
$\boldsymbol{\varepsilon}_v$	strain vector
ζ	hysteresis damping factor
θ	rotation angle, involute parameter
$\theta_{0,1,2,3}$	Euler parameters
$\boldsymbol{\theta}$	vector of rotation angles
$\boldsymbol{\lambda}$	Lagrange multipliers for contact forces
$\boldsymbol{\lambda}_C$	Lagrange multipliers for constraint forces
$\boldsymbol{\lambda}_N, \boldsymbol{\lambda}_T$	Lagrange multipliers for normal and tangential contact forces
μ	coefficient of friction
$\boldsymbol{\mu}_G$	matrix of friction coefficients
ν	Poisson's ratio
ξ	damping ratio
ρ	body density
τ	real time factor
ϕ	turn angle
ϕ_b	circumferential backlash
ω	angular velocity, frequency
$\boldsymbol{\omega}$	angular velocity vector given in the inertial frame
$\bar{\boldsymbol{\omega}}$	angular velocity vector given in the body reference frame
$\widetilde{\boldsymbol{\omega}}$	skew symmetric matrix of $\boldsymbol{\omega}$
Γ_C	contact surface
Δt	time step
$\Delta\phi$	relative turn angle
$\Delta\omega$	relative angular velocity
$\boldsymbol{\Lambda}$	impulse
$\boldsymbol{\Phi}$	constraint equations
$\boldsymbol{\Phi}_\mathbf{q}$	Jacobian matrix of constraints
$\boldsymbol{\Psi}$	shape function matrix corresponding to the rotation angles
$\boldsymbol{\Omega}$	contact constraints
err	error
tol	tolerance